

#### 4.1.1.1 Total System Performance Assessment Methods and Objectives

TSPA is a systematic analysis that synthesizes information (data, analyses, and expert judgment) about the site and region with the design attributes of the engineered barriers of the repository system. As defined in 10 CFR 63.2 (66 FR 55732),

Performance assessment means an analysis that:

- (1) Identifies the features, events and processes (except human intrusion) and sequences of events and processes (except human intrusion) that might affect the Yucca Mountain disposal system and their probabilities of occurring during 10,000 years after disposal;
- (2) Examines the effects of those features, events, and processes and sequence of events and processes upon the performance of the Yucca Mountain disposal system; and
- (3) Estimates the dose incurred by the reasonably maximally exposed individual, including the associated uncertainties, as a result of releases caused by all significant features, events, and processes, and sequences of events and processes weighted by their probability of occurrence.

Features are the physical components of the total repository system, including both the natural system (e.g., the geologic setting) and the engineered system (e.g., the waste package). Processes typically act more or less continuously on the features; for example, moisture flow through the geologic materials and corrosion of the waste package. Events also act on the features but at discrete times. Examples include seismic and volcanic events.

The TSPA approach and models are designed to address the processes that could lead to release and migration of radionuclides, and the radiological consequences to potential human receptors. The approach is intended to provide a transparent analysis of the geologic repository in terms of the performance of the natural and engineered barriers over long periods of time.

40 CFR Part 197 provides that the DOE and NRC should determine compliance with the radiation protection standard of 40 CFR 197.20 based on the mean of the distribution of the highest doses resulting from the performance assessment. In the background information accompanying their final rule (66 FR 32074, p. 32125), the EPA noted that they believe that a thorough assessment of repository performance should examine the full range of reasonably foreseeable conditions and processes. However, they also stated that quantitative estimates of repository performance should not be dominated by unrealistic or extreme situations or assumptions. Therefore, the EPA believed the use of the mean was reasonable but still conservative. They further noted that the use of the mean was consistent with the literal mathematical interpretation of the term "reasonable expectation" and with the approach used to certify Waste Isolation Pilot Plant.

During their consideration of the appropriate performance measure, the EPA evaluated other possible measures, such as the median value of the distribution, or more extreme measures, such as the 95<sup>th</sup> or 99<sup>th</sup> percentile. Their analysis showed that the use of either the mean or the median was reasonably conservative because both are influenced by the high exposure estimates, without reflecting only the high dose results.

Although the EPA selected the mean for the compliance determination, both the EPA and NRC provide that the DOE consider the uncertainties inherent in performance assessment results. One way that the DOE's method addresses this concern is by presenting and analyzing the full range of doses resulting from the performance assessment. In addition, the DOE has performed numerous sensitivity and uncertainty analyses to characterize

the properties and processes that are particularly important to dose calculations.

The TSPA described briefly in Section 4.4 and in more detail in *Total System Performance Assessment for the Site Recommendation (CRWMS M&O 2000a)*, Volume 2 of *FY01 Supplemental Science and Performance Analyses (BSC 2001b)*, and *Total System Performance Assessment—Analyses for Disposal of Commercial and DOE Waste Inventories at Yucca Mountain—Input to Final Environmental Impact Statement and Site Suitability Evaluation (Williams 2001a)* examines the performance of the potential repository for a broad range of potential subsurface and surface conditions (e.g., hydrologic, geologic, climatic, and biosphere) and evaluates potential radiation doses to future generations. The radiation protection standards that would apply to the postclosure performance of a Yucca Mountain repository are found in regulations promulgated by the EPA (40 CFR 197.20, 197.25, and 197.30) and the NRC (10 CFR 63.113(b), (c), and (d) [66 FR 55732]). Specific technical requirements for a comprehensive TSPA are prescribed in the NRC regulation, 10 CFR Part 63.

The TSPA method requires evaluation of postclosure performance of the Yucca Mountain disposal system where there is no human intrusion into the repository. The final regulations also require evaluation of the performance of the system where there is human intrusion, in accordance with NRC regulations. The TSPA evaluation method in both cases is the same, except that the TSPA method for human intrusion provides prescribed assumptions about the human intrusion scenario (10 CFR 63.322 [66 FR 55732]).

Human intrusion refers to inadvertent intrusion into the repository as a result of exploratory drilling for groundwater. Limited intrusion means a single borehole that penetrates the repository and the underlying groundwater aquifer.

To present the assessment results transparently, the first case (without human intrusion) is further subdivided into:

- A nominal scenario composed of the likely FEPs representing the most plausible evolution of the repository system, without the occurrence of unlikely disruptive FEPs
- Disruptive scenarios that include unlikely FEPs that could diminish the waste isolation capability of the repository system (e.g., igneous activity).

The result of a TSPA analysis is a distribution (range) of possible outcomes of future performance. Because of the probabilistic nature of the method, TSPA results can capture and display much of the uncertainty associated with complex models and unknown future conditions. For this reason, however, the results should be regarded as indicative of future performance, not as predictive in a precise way.

The TSPA methodology (i.e., approach and models) described in this report is the culmination of research and development conducted over more than a decade. Moreover, reviews of previous TSPAs by internal and external professional organizations have been invaluable in enhancing the rigor of the approach and guiding the improvements of the models. Most notably, important advances in the TSPA methodology have been made in response to review comments from:

- Nuclear Waste Technical Review Board (NWTRB 1998; NWTRB 1999a; NWTRB 2000)
- Total System Performance Assessment Peer Review Panel (Budnitz et al. 1999)
- NRC staff (Paperiello 1999)
- State of Nevada consultants and other independent expert review groups.

The TSPA methodology used for this report is very similar to that used in the compliance certification application for the Waste Isolation Pilot Plant

(DOE 1996a, Section 6.1; Helton, Anderson et al. 1999), a bedded salt repository in southern New Mexico. The Waste Isolation Pilot Plant was certified by the EPA in 1998 and began receiving and disposing of transuranic nuclear waste in March 1999. The TSPA approach is also similar to approaches adopted by other countries currently conducting detailed siting studies for potential geologic repositories (NEA 1991; Thompson 1999). In addition, the computer techniques used in TSPAs to address uncertainties are rooted in the probabilistic risk assessment method applied in the safety assessments for commercial nuclear reactors (Rechard 1999).

#### 4.1.1.2 Treatment of Uncertainty in the Performance Assessment

Inherent uncertainties will exist in any projections of the future performance of a deep geologic repository. These uncertainties must be addressed in a way that is both clear and understandable to ensure technical credibility and sound decision-making and must be reduced or eliminated if important. Most, but not all, of those uncertainties can be quantified and addressed in the TSPA; examples include:

- Potential changes in climate, seismicity, and other processes, such as coupled thermal-hydrologic-chemical processes, over the compliance period for geologic disposal (i.e., 10,000 years)
- Variability and lack of knowledge of the properties of geologic media over large spatial scales of the hydrogeologic setting (e.g., the flow path from the repository to a point of compliance)
- Incomplete knowledge about the long-term material behavior of engineered components (e.g., corrosion of metals over many thousands of years).

Both the EPA and the NRC have recognized that uncertainty about the future performance of the repository will remain even after site characterization is complete. In the licensing context, both EPA

regulations at 40 CFR 197.14 and NRC regulations at 10 CFR 63.304 (66 FR 55732) have incorporated "reasonable expectation" as the standard for the NRC to determine whether the DOE complies with EPA and NRC regulations. Characteristics of reasonable expectation include that it:

- Requires less than absolute proof because absolute proof is impossible to attain for disposal due to the uncertainty of projecting long-term performance
- Accounts for the inherently greater uncertainties in making long-term projections of the performance of the Yucca Mountain disposal system
- Does not exclude important parameters from assessments and analyses simply because they are difficult to precisely quantify to a high degree of confidence
- Focuses performance assessments and analyses upon the full range of defensible and reasonable parameter distributions rather than only upon extreme physical situations and parameter values.

There are a number of ways to accommodate or address uncertainty in analyses of performance. The methods employed for the TSPA models include:

- Definition of parameter probability distributions
- Representation of spatial and temporal variability
- Definition of data bounds or conservative estimates
- Formulation and evaluation of alternative models permitted by current state of knowledge
- FEPs screening (screening out certain aspects from consideration because of low probability or consequence).

Whether uncertainties are incorporated quantitatively through probabilistic distributions, or by developing "conservative" or "bounding" estimates, it is important to define and document assumptions on how uncertainties are treated in performance analyses. Clear documentation of the rationale for the assumptions in the models will enable others to understand and evaluate their adequacy. For the total system model to be transparent and defensible, the selection of each probability distribution must also be defensible. In some instances, the insufficient information that exists on the subsystem model is so complex that a probability distribution cannot be defined defensibly. In these instances, conservative or bounding approaches are taken.

Individual sources of uncertainties may be either quantified or unquantified. Quantified uncertainty consists of those sources of uncertainties that can be and have been explicitly (i.e., mathematically) represented and evaluated through a probabilistic performance analysis. Unquantified uncertainties are those that are recognized but are not well suited for direct evaluation through a probabilistic analysis.

As described in Section 4.4.1.2, many uncertainties have been quantified and incorporated directly into the TSPA models. The analyses done to address quantified uncertainties in the TSPA-SR model include a variety of sensitivity studies that address how total system performance might be affected if individual or groups of processes or parameters differed significantly from the way they were represented in the TSPA-SR model. These are described further in Section 4.4.5 and in *Total System Performance Assessment for the Site Recommendation* (CRWMS M&O 2000a). Additional uncertainties have been identified, analyzed, and quantified in *FY01 Supplemental Science and Performance Analyses* (BSC 2001a; BSC 2001b). These analyses are described, as appropriate, throughout Section 4.

As noted by the National Research Council (1990, p. 13) and others, there are residual uncertainties with deep geologic disposal that cannot easily be quantified and incorporated into performance analyses. Nevertheless, their potential impact must be,

to the extent practicable, addressed and, if important, mitigated to provide confidence in postclosure performance. Examples of residual uncertainties associated with geologic disposal that are difficult to quantify include:

- The potential for currently unknown processes to affect performance
- The possibility that incompletely characterized processes have been incorporated in the TSPA in a manner that results in the underestimation of radionuclide releases; examples of incompletely characterized processes include thermal, chemical, hydrologic, and mechanical processes that are coupled in complex ways that cannot be completely tested at the scale of a repository, as well as processes that are difficult to observe and test, such as colloidal transport of radionuclides
- Uncertainty associated with the projections of engineered barrier performance over 10,000 years based on data from short-term (e.g., several years) laboratory testing
- Uncertainty associated with the large spatial scale of the three-dimensional groundwater flow system, which makes it difficult to characterize flow paths and processes.

The DOE has made a substantial effort to identify, characterize, and mitigate the potential impacts of residual uncertainties that could significantly affect long-term performance. Where practicable, additional tests have been conducted to collect information that would provide insight to analysts. For example, the DOE, along with Nye County and the National Park Service, is continuing research on the regional groundwater system. The program includes cooperative and joint analysis of soil, rock, and water samples provided by Nye County, which is drilling additional boreholes to characterize the saturated zone as part of its review of the project.

To address uncertainties associated with coupled thermal-hydrologic-geochemical processes, the DOE has performed numerous tests that were not

envisioned when site characterization began. Where additional testing was not feasible (e.g., it is not possible to run tests over the same time period as the repository must perform) or of limited benefit (e.g., no amount of excavation or drilling could completely characterize the natural system), modelers used conservative assumptions to "bound" their analyses of uncertain processes. To do this, they have incorporated assumptions in their models that represent the observed range of properties and processes and that also include parameter values or processes likely to result in calculated dose assessments that are greater than actual dose. The DOE has also used empirical observations and qualitative lines of evidence from natural analogues to address uncertainties (see Section 4.1.2).

In some cases, more than one conceptual model may be consistent with available data and observations; if so, the analysis of uncertainty includes the identification of the basis for model selection. In the absence of definitive data sets or compelling technical arguments for any specific conceptual model, analyses or sensitivity studies may be performed to test whether the selection of a given model is likely to substantially affect analyses of system performance. When model uncertainty is unavoidable, analysts may develop simplified performance models for use in TSPA that reflect the range of outcomes predicted by more detailed and specific conceptual models. The selection of models, model parameters, and scenarios of potential future behavior are described in *Total System Performance Assessment for the Site Recommendation* (CRWMS M&O 2000a) and its supporting documents, as well as in *FY01 Supplemental Science and Performance Analyses* (BSC 2001a; BSC 2001b) and *Total System Performance Assessment—Analyses for Disposal of Commercial and DOE Waste Inventories at Yucca Mountain—Input to Final Environmental Impact Statement and Site Suitability Evaluation* (Williams 2001a).

In addition, consistent with the postclosure safety case described in Section 4.1.3, the DOE has implemented a safety margin/defense-in-depth approach to the design of repository facilities. This approach mitigates some of the residual uncertainties by providing additional confidence in the

performance of the total system. The iterative approach to characterization and testing, design, and performance analysis remains a fundamental part of the DOE approach in evaluating whether Yucca Mountain is a safe site to host a repository.

One disadvantage of an approach that combines both conservative and representative parameter distributions is that it is difficult to assess the extent to which the total system results are conservative or realistic. More realistic representations may be drawn from literature data, analogue systems or processes, and the technical judgment of the broader scientific and engineering community. In addition, the DOE initiated several activities to improve the treatment of uncertainty in current models. These are described in *FY01 Supplemental Science and Performance Analyses* (BSC 2001a; BSC 2001b). These activities:

- Identified and evaluated the degree of conservatism introduced by current approaches, quantified key unquantified uncertainties, and characterized the effect of explicitly quantifying ranges of possible parameters
- Developed alternative representations of key unquantified uncertainties and evaluated the impact on TSPA results
- Considered the uncertainties associated with alternative models into which assumptions or conservatisms were introduced when they were abstracted for use in the TSPA, in addition to assumptions and conservatisms in the process model
- Developed more realistic representations of models and parameters, based on all available information and the scientific judgment of individuals who are experts in the appropriate disciplines
- Developed, for each model in the TSPA, alternate lines of evidence, such as additional analogues and defense in depth, that are less dependent on the TSPA computational tool than those given in *Repository Safety Strategy: Plan to Prepare the Safety Case to Support Yucca Mountain Site Recommendation*

*tion and Licensing Considerations (CRWMS M&O 2001a).*

This approach provides recommendations for consistent treatment of uncertainties, which will lead to a more rigorous treatment of the different types of uncertainty. It will also lead to a more transparent description of uncertainties in the process models and in the overall system models.

**4.1.1.3 Explicit Consideration of Disruptive Processes and Events that Could Affect Repository Performance**

Most of this report, as well as the *Total System Performance Assessment for the Site Recommendation (CRWMS M&O 2000a)*, the *FY01 Supplemental Science and Performance Analyses (BSC 2001a; BSC 2001b)*, the *Total System Performance Assessment—Analyses for Disposal of Commercial and DOE Waste Inventories at Yucca Mountain—Input to Final Environmental Impact Statement and Site Suitability Evaluation (Williams 2001a)*, and associated documentation, focuses on the processes that are expected to operate in and near the repository over time (e.g., water flow, the effects of heat on conditions near waste packages, and the slow degradation of the engineered barrier system). Because of the time frames involved, however, it is also important for analysts to understand the safety consequences of unexpected events or behavior. Consequently, the performance analysis also describes explicitly how disruptive events (i.e., possible but unlikely events that could negatively affect performance) and alternative models of processes could affect the performance of the total system. This thorough consideration of what could go wrong, how wrong the models could be, and what the effect of inaccuracy in the models would be is a key element of the postclosure safety case.

A comprehensive set of potentially disruptive events, ranging from meteor or comet impacts to unexpected flooding of the repository, has been identified and evaluated. Similarly, a wide variety of potentially harmful processes, such as unanticipated failure of the waste packages and damage to repository systems by seismic activity, have been identified and evaluated. Section 4.3 describes the

identification and screening of these potentially adverse processes and events. Depending on the results of this analysis, the events and processes have been treated in one of three ways:

1. Events or processes with very low probabilities (e.g., less than 1 chance in 10,000 of occurring in 10,000 years, such as meteor impacts) or very small consequences (e.g., potential radionuclide releases much lower than regulatory standards) have been screened out and not analyzed further.
2. Events or processes that have probabilities greater than 1 chance in 10,000 of occurring in 10,000 years (e.g., intrusive igneous activity), have been included in the performance assessment probabilistically—that is, the consequence of each event is weighted by its probability of occurrence.
3. Events or processes expected to occur during the period of regulatory compliance, such as climate change or ground shaking associated with earthquakes, are included directly in models of the performance of the repository.

The potential consequences of each event and process considered in the performance assessment models are analyzed. These analyses are summarized in Section 4.2, which considers alternative models of subsystem processes that could affect performance, and Section 4.3, which considers specific events or processes that are not part of nominal site behavior. Section 4.4.5 also describes a number of sensitivity studies that enable analysts to assess the importance of alternative models or unexpected events on total system performance.

Many different events and processes have been considered to assess whether they might have the potential to disrupt repository performance. Examples of potential events considered include:

- The potential for future volcanism near the repository

- The potential for future seismic activity near the repository
- The potential for future human intrusion into the repository
- The potential for climate change in the region of the repository
- The potential for criticality to occur during the postclosure period.

Climate change and cladding damage caused by earthquake ground motion is directly incorporated into the nominal case performance analyses (CRWMS M&O 2000c) because climate change and seismic activity are expected to occur during the period of regulatory compliance.

Many other events and processes have been considered but screened out because their impacts are so inconsequential that inclusion in the TSPA-SR is not warranted. Examples include the potential for future rises in the water table that could inundate the repository and the potential for nuclear criticality in spent nuclear fuel after repository closure. These examples are discussed in Section 4.3.

It is not possible to foresee every event or process that could affect the potential repository. However, by recognizing and explicitly analyzing all identified events and processes that could affect repository performance, the DOE has provided a sound basis for evaluating the performance of the repository system.

#### 4.1.2 Observations from Natural and Man-Made Analogues

An alternative means of analyzing the reliability of repository performance models is by comparing them with natural or anthropogenic (man-made) analogues. As defined in this report, analogues are systems in which processes similar to those that could occur in a nuclear waste repository have occurred over long time periods (decades to millennia) and large spatial scales (up to tens of kilometers) not suited to laboratory or field experiments. The concept of geologic disposal is based

on an analogue observation that certain geologic environments have intrinsic properties that contribute to the isolation of waste and will continue to do so for a long time. Analogue studies can also help scientists understand how specific repository systems might behave by allowing them to compare possible future behavior with the known past behavior of an analogue system. A variety of specific analogue sites are described throughout Section 4.2, including several in settings that provide insight into the flow of water in the unsaturated zone, as described in Section 4.2.1.2.13.

For example, observations of the hydrologic behavior of ancient man-made tunnels and natural caves can provide relevant information about water seepage into mined openings in an unsaturated zone over thousands of years. Similarly, observations of the past migration of radioactive contaminants in groundwater in similar environments can provide insight into the possible future transport of radionuclides away from a repository. Such information can be obtained from both natural analogues (e.g., natural deposits of uranium and other minerals) or from anthropogenic analogues (e.g., the Nevada Test Site, Hanford, or the Idaho National Engineering and Environmental Laboratory), where the movement of radionuclides in groundwater caused by past releases is currently being monitored. The archaeological and historical record can also provide qualitative information on the degradation of materials that may be relevant to the performance of the repository (e.g., the preservation of materials in Egyptian pyramids and tombs more than 5,000 years old).

The value of natural analogues is not restricted to locations that may mimic aspects of repository behavior. The study of natural analogues is an intrinsic part of scientific studies, particularly in the earth sciences. For example, in order to undertake studies of basaltic volcanism in the vicinity of the Yucca Mountain site, an investigator must be versed in basaltic volcanism and especially in basaltic volcanism in the southern Great Basin. All other known occurrences of basaltic volcanism become, to some degree, natural analogues for volcanism near Yucca Mountain. Each occurrence can tell the investigator something about the mech-

anisms and controls on volcanic episodes. The overall understanding of volcanic processes gained from regional studies provides a basis for analyzing trends and patterns in the Yucca Mountain area that are essential to evaluating the possibility that future volcanic events could occur and affect a repository. In fact, it would be impossible to understand basaltic volcanism as a site characterization issue without recourse to natural analogues. One of the fundamental tasks for the investigator is to recognize and appreciate the value of the information offered by this kind of analogue study.

The scientific community has endorsed the use of analogues as a means of assessing the potential future performance of systems, components, and processes related to nuclear waste disposal (Chapman and Smellie 1986). The National Academy of Sciences/National Research Council (National Research Council 1990) and the NRC (10 CFR 63.101(a)(2) [66 FR 55732]) have also encouraged analogue studies.

There are no close analogues to a total repository system at Yucca Mountain. Nevertheless, studies of a variety of analogues can and have been used to assess how well repository models represent processes known to be important to performance, as well as the magnitude and duration of the phenomena. Analogue information has also been used (1) to evaluate the validity of extrapolating from short-term field-scale experiments to longer time scales in which field-scale experiments are impractical and (2) to add confidence when spatially extrapolating processes studied at laboratory and intermediate-scale experiments to tests at larger spatial scales. Knowledge gained from natural analogues has helped refine performance assessment model assumptions and parameter ranges and has improved the robustness and consistency of process models.

Given the imprecise nature of the information gained from investigations of similar, but not identical, processes and sites, analogue studies alone cannot prove that process or total system performance models are valid in a strict sense. However, natural analogue observations can confirm that a model takes into account the relevant processes in

appropriate ways. In this way, the analogues can build confidence in models of future behavior. This is consistent with the expectations of NRC regulations in 10 CFR 63.101(a)(2) (66 FR 55732), which state: "Demonstrating compliance will involve the use of complex predictive models that are supported by limited data from field and laboratory tests, site-specific monitoring, and natural analog studies that may be supplemented by prevalent expert judgment."

Throughout this report and its supporting documents, numerous analogues are analyzed to provide information on processes that may affect both engineered and natural system features of a geologic repository at Yucca Mountain. Specific examples of relevant analogues are presented in Table 4-1. Additional discussion of analogues is provided as appropriate throughout Sections 4.2 and 4.3, which discuss in greater detail the understanding of the Yucca Mountain site. Although the direct applicability of the analogues for each process model varies, the analogue observations generally suggest that the conceptual and numerical models that form the basis for analyses of repository performance are reasonable to conservative. For many of the analogues, a large body of literature exists.

#### **4.1.3 Use of Defense in Depth and Safety Margin to Increase Confidence in System Performance**

The extensive testing program at Yucca Mountain and the thorough assessments of the future performance of the potential repository do not "prove," in the usual sense of the word, that the potential repository will be safe. To provide additional assurance of long-term safety, the third major element of the postclosure safety case relies on a complementary, but less analytical, approach that is based on engineering principles that have a proven track record for safety. These principles are known as "safety margin" (or design margin) and "defense in depth."

Safety margin refers to the standard engineering practice of including safety factors on the performance of engineered components to account for uncertainty and variability in material, fabrication,

Table 4-1. Process Models and Natural Analogues

| Process Model   | Feature, Event, or Process                            | Model Parameter   | Information from Analogues   |  |
|---|---|---|--|--|
| UZ Flow and Transport                                       | Climate   | Range of climate conditions   | Paleoclimate studies in Great Basin provide bounds on precipitation and temperature expected under wetter future climate scenarios.  |  |
|   | Infiltration  | Range of infiltration values  | Infiltration at Yucca Mountain, determined by models, is within range of measured infiltration rates in Negev Desert, Israel.  |  |
|   | Seepage into drifts                                   | Drift seepage model; effect of discrete fractures   | Excavations worldwide in arid environments (e.g., Altamira, Spain; Amman, Jordan) show high seepage thresholds. At Rainier Mesa, Nevada, tunnel in welded tuff above perched water zone shows no seepage. Tunnel in zeolites below perched water experiences seepage. Very limited seepage occurs at Hell's Half Acre, Idaho, 1 m below a monitored overhang in fractured tuff.  |  |
|   | Coupled processes: effects on UZ flow                 | UZ flow and transport, THC processes  | Magma intrusions, such as sill at Palute Ridge, Nevada, and Grants Ridge, New Mexico, as well as lava flow contact at Banco Bonito, New Mexico, show extent of alteration effects at temperatures greater than 100°C is less than 1 m from contact; fracture sealing has occurred in welded rhyolitic tuff in Yellowstone geothermal field.  |  |
|   | Coupled processes: thermal-mechanical effects         | Rockfall size distributions and thermal-mechanical effects  | Measured thermal-mechanical stress at Krasnoyarsk-26, Russia, is small over 50-year operation period of underground nuclear reactor (temperatures less than 100°C).  |  |
|   | Moisture, temperature, and chemistry on drip shield   | Mineral reaction rates and assemblages in near-field  | Geothermal fields (e.g., Wairakei, New Zealand; Yellowstone, Wyoming), and Yucca Mountain as self-analogue, predict mineral assemblage similar to syngenetic alteration at Yucca Mountain; mineral precipitation kinetics is faster in field than in laboratory tests.   |  |
|   | Moisture, temperature, and chemistry on waste package | Same as for drip shield, with addition of drip shield for protection  | Potential drip shield analogue at Japanese archaeological site.  |  |
|   | UZ flow and transport: advective pathways             |   | (1) UZ flow; effects of transient flow   | (1) Box Canyon (Idaho National Engineering and Environmental Laboratory) analogue in fractured basalt shows little effect from transient flow. |
|   |   |   | (2) Effect of water table rise   | (2) Records associated with historical earthquakes in Nevada show water table rise is limited to about 5 m and is transient.                   |
|   | UZ flow and transport: sorption and matrix diffusion  | UZ flow and transport   | Sorption of uranium takes place in fracture-coating minerals in rhyolitic tuff at Peña Blanca, Mexico, where matrix diffusion is minor; Peña Blanca has experienced only minor transport of uranium daughter products over 300,000 years. Trace metals at Santorini, Greece, were transported less than 5 m in rhyolitic tuff over 3,000 years.  |  |
| UZ flow and transport: colloid-facilitated transport        | UZ flow and transport                                 | Idaho National Engineering and Environmental Laboratory may be an analogue for colloid transport.   |  |  |
| Coupled processes: effects on UZ transport                  | UZ flow and transport; THC processes                  | Clay mineral alteration assemblages produced by THC processes in high-silica rocks at Oklo, Gabon, and Cigar Lake, Canada, are effective in sequestering radionuclides. |  |  |
| Waste Package, Waste Form, and Engineered Barrier Processes | Performance of waste package barriers                 | Degradation of steel alloys and cladding  | Meteorites with high nickel/iron content have higher rate of preservation than those with low nickel/iron ratio; meteorites, iron nails, and other iron artifacts are better preserved in the presence of a corrosion crust; eskolaite for chromate ( $Cr_2O_3$ ); rare earth phosphates as analogue to gadolinium phosphate ( $GdPO_4$ ) (neutron absorber); stability of the mineral josephinite, a natural iron-nickel alloy. |  |
|   | Commercial spent nuclear fuel waste form performance  | Chemical alteration of uranium dioxide and secondary mineral formation  | Uraninite alteration at Nopal I in Peña Blanca, Mexico, produces the same mineral assemblage as in laboratory tests of spent fuel degradation.   |  |

Table 4-1. Process Models and Natural Analogues (Continued)

| Process Model   | Feature, Event, or Process   | Model Parameter  | Information from Analogues   |
|---|--|--|--|
| Waste Package, Waste Form, and Engineered Barrier Processes (continued) | DOE spent nuclear fuel, plutonium disposition waste form performance | Chemical alteration of uranium and secondary mineral formation                       | Natural plutonium has remained unfractionated from uranium at Poços de Caldas, Brazil, for more than 100,000 years.  |
|   | High-level waste glass waste form performance                        | Stability of glasses   | In the absence of radiation, devitrification of volcanic glasses (basaltic and rhyolitic) and manufactured uranium-bearing glasses is too slow to be significant to a repository.  |
|   | Dissolved radionuclide concentration limits                          | Solubility of waste form   | (Solubility limiting conditions not usually observed through analogues.)   |
|   | In-package radionuclide transport                                    | Radiolysis, sequestration in secondary minerals                                      | At Oklo, Gabon, radiolysis caused reduction of iron and oxidation of uranium, followed by sequestration of uranium and fission products in clays and iron oxides.  |
|   | Performance of cements   | Effects of materials on performance  | Maqarin, Jordan, provides data on thermodynamic stability of natural cement minerals and interaction with groundwater. Krasnoyarsk, Russia, provides data on stability of cement minerals under THC conditions. Microbes are instrumental in attacking cement at New Zealand geothermal sites. Roman concretes varied in stability with dependence on composition of contact material. |
|   | Performance of getter (sorptive materials in backfill)               | Effects of materials on performance  | Clay minerals are instrumental in sequestering radionuclides at Cigar Lake, Canada, and have preserved ancient wood fiber at Dunarobba Forest, Italy.  |
| SZ Flow and Transport   | SZ flow and transport—advective pathways                             | Transverse and longitudinal dispersion   | Contaminant plumes at DOE and EPA sites (e.g., Hanford) can be used to determine the limits of dispersion in a particular substrate.   |
|   | SZ flow and transport—sorption and matrix diffusion                  | Sorption coefficient in alluvium, importance of matrix diffusion                     | Sorption coefficient tested at Nevada Test Site. Matrix diffusion plays strong role at Poços de Caldas, Brazil; Alligator Rivers, Australia; Oklo, Gabon; Palmottu, Finland; Cigar Lake, Canada. Fracture pathways play a role in transport at Palmottu; Poços de Caldas; and Alligator Rivers.  |
|   | SZ flow and transport—colloid-facilitated transport                  | Colloidal transport in SZ  | Filtration of colloids is effective at El Berrocal, Spain; Poços de Caldas, Brazil; Alligator Rivers, Australia; and Cigar Lake, Canada.   |
| Biosphere   | Biosphere transport and uptake                                       | Plant uptake of radionuclides  | High uranium concentrations found in green plants near ore bodies at Poços de Caldas, Brazil, and Peña Blanca, Mexico.   |
| Potentially Disruptive Events   | Volcanism  | Eruptive frequency, location, and intensity  | Nevada-California-Arizona provide eruptive histories of similar basalt fields.   |
|   | Seismicity   | Frequency of event, extent and location of fault rupture, intensity of ground motion | Nevada-California historic earthquakes provide database for predictions.   |
|   | Criticality  | Probability and consequence of criticality   | Occurred at Oklo 2 billion years ago and lasted several hundred thousand years; studies have determined which radionuclides remained in the ore body, which ones were transported, and to what distances.  |
|   | Water table rise   | Probability and consequence of water table rise                                      | Travertine Point calcite and silica deposits provide insight into the origin of surficial deposits at Yucca Mountain.  |

NOTES: THC = thermal-hydrologic-chemical; UZ = unsaturated zone; SZ = saturated zone. Sources: CRWMS M&O 2000bp; Stuckless 2000; CRWMS M&O 2000b, Section 13.

and use. These safety factors are typically expressed as a ratio of the calculated level of performance to an allowable or laboratory measured level of performance. They are developed to ensure that the component or system has ample reserve performance capability. A simple example of a safety factor would be the limiting of the stress in a component to a fraction of what would cause failure. The safety margin is then the reserve strength over and above what would actually be applied. A Yucca Mountain-specific example of safety margin is the design and selection of the waste package material. The assumed corrosion resistance of Alloy 22, used in the outer shell of the waste packages, was decreased (or the corrosion rate was increased) over the laboratory values to account for potential environmental conditions. The corrosion rate of Alloy 22 was increased by 2.5 times to address potential heat-accelerated corrosion and an additional 2.0 times to address potential microbial corrosion.

The defense-in-depth approach (or reliance on multiple system attributes) complements design margin in that it provides a method of ensuring overall performance if one or more components of the repository system fail to perform as expected. Defense in depth is provided by having safety

components that do not share common failure modes. In other words, the processes or conditions (such as the geochemical environment) that might cause a degradation of performance of one component of the design will not similarly affect other components. In a repository, defense in depth is provided by the attributes of both the natural barriers and the engineered barrier system.

The safety margin/defense-in-depth approach is not specifically required by the regulations for a repository. However, the NRC regulation (10 CFR Part 63 [66 FR 55732]) does contain statements that are based on a similar philosophy, adapted to the long-term requirements for postclosure safety. 10 CFR 63.113(a) provides that a repository include multiple barriers, consisting of both natural barriers and an engineered barrier system.

At Yucca Mountain, the potential geologic repository system would contain several different barriers. As defined in 10 CFR 63.2 (66 FR 55732), a barrier is any material, structure, or feature that prevents or substantially reduces the rate of movement of water or radioactive material from the Yucca Mountain repository to the accessible environment. Table 4-2 presents a summary

**Table 4-2. Identification of Natural and Engineered Barriers at Yucca Mountain**

| Barrier  | Barrier Function  |
|--|---|
| Surficial soils and topography   | Reduce the amount of water entering the unsaturated zone by surficial processes (e.g., precipitation lost to runoff, evaporation, and plant transpiration).   |
| Unsaturated rock layers overlying the repository and host unit   | Reduce the amount of water reaching the repository by subsurface processes (e.g., lateral diversion and flow around emplacement drifts).  |
| Drip shield above the waste packages   | Prevent water contacting the waste package and waste form by diverting water flow around the waste package.   |
| Waste package  | Prevent water from contacting the waste form for thousands of years.  |
| Spent fuel cladding  | Delay and/or limit liquid water contacting spent nuclear fuel after waste packages have degraded.   |
| Waste form   | Prevent liquid water from contacting waste as a result of elevated temperatures in the commercial spent nuclear fuel waste package; limit radionuclide release rates as a result of intrinsic low leach rates of DOE high-level radioactive waste glass form. |
| Drift invert below the waste package   | Limit transport into the host rock.   |
| Unsaturated rock layers below the repository   | Delay radionuclide movement to the groundwater aquifer because of water residence time, matrix diffusion, and/or sorption.  |
| Volcanic tuff and alluvial deposits below the water table (flow path extending from below the repository to point of compliance) | Delay radionuclide movement to the receptor location because of water residence time, matrix diffusion, and/or sorption; decrease radionuclide concentrations by passive mixing.  |

of the natural and engineered barriers present at Yucca Mountain, along with a brief description of their intrinsic and intended functions for the design analyzed in this section. An analysis of each barrier's contribution to performance is presented in Section 4.5.

Implementation of the safety margin/defense-in-depth approach has resulted in several improvements in the repository design since the design described in 1998 in the Viability Assessment (VA) (DOE 1998). Examples include:

- Modification of the waste package design to place the corrosion-resistant Alloy 22 layer on the outside. Having the corrosion-resistant layer outside provides sufficient margin that performance assessments indicate complete containment (in the absence of unlikely disruptive processes) of nuclear wastes throughout the period of regulatory compliance.
- Evaluating thermal loading strategies that may reduce the complexity of coupled processes in the near-field zone and simultaneously maximizes the redirection of water away from the repository drifts.
- Adding drip shields to the engineered barrier design to minimize the potential for dripping water to contact the waste packages (and waste form).

More detailed descriptions of the barriers and their performance functions are summarized in Section 4.5. Additional information is available in Volume 2 of *Repository Safety Strategy: Plan to Prepare the Safety Case to Support Yucca Mountain Site Recommendation and Licensing Considerations* (CRWS M&O 2001a) and *Total System Performance Assessment for the Site Recommendation* (CRWS M&O 2000a) as well as *FY01 Supplemental Science and Performance Analyses* (BSC 2001a; BSC 2001b) and *Total System Performance Assessment—Analyses for Disposal of Commercial and DOE Waste Inventories at Yucca Mountain—Input to Final Environmental Impact Statement and Site Suitability Evaluation* (Williams 2001a).

#### 4.1.4 Mitigation of Uncertainties by Selection of a Thermal Operating Mode

One way of mitigating the uncertainties in modeling long-term repository performance is to operate the repository so the temperature of the host rock stays below the boiling point of water. Uncertainties in thermally driven processes are of special interest because of their complexity and because the current modeling approach may mask the importance of thermal effects on performance. Two key uncertainties about thermal effects on potential repository performance are (1) the way coupled processes in the mountain will respond to the heat generated by emplaced waste and (2) the long-term performance of waste package materials in the potential repository environment.

In the models and design described in this report, uncertainties related to the higher-temperature operating mode have been recognized and addressed. Since the VA, the design has evolved to include a thermal management strategy that limits the region of rock with temperatures above the boiling point of water, along with other features (such as drip shields) that mitigates uncertainty. Current models attempt to capture the remaining uncertainties well enough to understand their impacts; however, the DOE has considered additional options for mitigation. In particular, the performance characteristics of lower-temperature operating mode concepts such as those described in Section 2.1 have been investigated in *FY01 Supplemental Science and Performance Analyses* (BSC 2001a; BSC 2001b) and *Total System Performance Assessment—Analyses for Disposal of Commercial and DOE Waste Inventories at Yucca Mountain—Input to Final Environmental Impact Statement and Site Suitability Evaluation* (Williams 2001a).

Because uncertainties due to thermally induced coupled processes cannot be eliminated through additional testing, the DOE's approach is to consider options for mitigating thermal uncertainties by lowering temperatures in the emplacement drifts and on the waste package surface. Keeping the host rock temperature below boiling may reduce uncertainties associated with coupled processes (Anderson et al. 1998, p. 18; Cohon

1999). In addition, uncertainties in localized corrosion rates may be mitigated by avoiding the conservatively defined window of increased susceptibility by keeping the temperature of the waste package below 85°C (185°F) or the relative humidity in the emplacement drifts below 50 percent. Section 2.1 provides additional discussions of lower-temperature operating modes.

#### **4.1.5 Performance Confirmation, Postclosure Monitoring, and Site Stewardship**

The EPA, NRC, and DOE have recognized that some uncertainty about repository performance cannot be eliminated. Furthermore, the DOE understands that ensuring public safety requires continued site stewardship, including a program for evaluating new information discovered during the construction and operation phases. Therefore, the final component of the postclosure safety case is a program of performance confirmation, monitoring, and site stewardship that accomplishes several goals related to the DOE's obligation to protect public health and safety and the environment. The program addresses 10 CFR Part 63 (66 FR 55732) Subpart F provisions for performance confirmation to ensure consistency with license specifications after waste emplacement and before permanent closure. The program also includes activities necessary for the DOE to provide postclosure oversight, as specified by Section 801(c) of the Energy Policy Act of 1992 (Public Law No. 102-486), and post-permanent closure monitoring, consistent with 10 CFR 63.51(a)(2). Specifically, the DOE will continue to observe and test the performance of the repository during and after waste emplacement and will maintain the integrity and security of the repository through a variety of institutional controls. The DOE will also continue to participate in research on geologic disposal, in cooperation with other international programs. These activities will ensure that any new information discovered at Yucca Mountain (or elsewhere) that is relevant to future repository decisions is considered appropriately.

The performance confirmation program is the most important monitoring activity. NRC regulations provide for performance confirmation to continue

for at least 50 years after the initiation of waste emplacement. The DOE will continue its performance confirmation program until the repository is permanently closed. The amount of information collected during this period may be more relevant for long-term analyses of the repository than any experiment or test that could be conducted now or in the near future. Any decision to close the repository would be based on the increased understanding and confidence derived from decades of testing and observation.

The performance confirmation program will provide data on the actual performance of the key natural and engineered systems and components of the repository as conditions evolve. The program will also provide data to confirm (after repository construction and operation) that subsurface conditions encountered, and any changes in those conditions during repository construction and waste emplacement, are consistent with the expected performance of the repository. A primary goal of the program will be to confirm, through observation, monitoring, and analysis, that the repository is performing in a manner that will contain and isolate waste.

As described in Section 4.6, the performance confirmation program will monitor the processes important to future waste isolation in the repository. Examples include the flow of water past and near the repository, the geochemical environment in and near emplaced waste, coupled thermal-hydrologic-chemical-mechanical processes, and the performance characteristics of engineered materials in the repository environment (e.g., drip shield and waste package degradation). In addition to technical monitoring of the performance of the site, the DOE will maintain the security and integrity of the site throughout the performance confirmation period and beyond as required by the Energy Policy Act of 1992, Section 801(c) (Public Law No. 102-486). A program will be developed to prevent any human activity, including deliberate or inadvertent human intrusion, that could affect engineered or geologic barriers.

Section 122 of the NWSA (42 U.S.C. 10142) requires the DOE to maintain the ability to retrieve any and all emplaced wastes "for any reason

pertaining to the public health and safety, or the environment, or for the purpose of permitting the recovery of the economically valuable contents of such spent fuel" prior to closure. For example, if it were learned from the monitoring program that an engineered barrier had been damaged, the waste packages could be removed and repairs could be made, as necessary.

NRC regulations (10 CFR Part 63 [66 FR 55732]) anticipate that the repository could be closed as early as 50 years after initial waste receipt. Closing the repository would involve the sealing of shafts, ramps, exploratory boreholes, and other underground openings. These actions would discourage any human intrusion into the repository and prevent water from entering through these openings. If a decision to close the repository were made, the DOE would still be responsible for a program of site stewardship under the Energy Policy Act of 1992 (Public Law No. 102-486).

At the surface, all radiological areas would be decontaminated, all structures removed, and all wastes and debris disposed at approved sites. All disturbed areas would be restored as close as practicable to their preconstruction condition.

NRC regulations (10 CFR Part 63 [66 FR 55732]) require the DOE to submit a plan for postclosure monitoring with any application to close the repository. The DOE has also committed to maintain security and continue monitoring at the Nevada Test Site for the foreseeable future. A network of permanent monuments and markers would be erected around the site to warn future generations of the presence and nature of the buried waste. Detailed records of the repository would be placed in the archives and land records of local, state, and federal government agencies and archives elsewhere in the world that future generations would be likely to consult. These records would identify the location and layout of the repository and the nature and hazard of the waste it contains.

#### **4.2 DESCRIPTION OF SITE CHARACTERIZATION DATA AND ANALYSES RELATED TO POSTCLOSURE SAFETY**

This section discusses the data obtained during site characterization activities, as well as analyses of the safety of a potential Yucca Mountain repository. The DOE planned and conducted its site characterization program to collect data about the site and about those physical and chemical processes that would affect the ability of the repository system to isolate waste.

Section 1.3 presented a brief summary of the geology of Yucca Mountain based on the results of site investigations. It provided a framework for the descriptions of the repository and waste package designs contained in Sections 2 and 3. In this section, the results of studies focused on the characteristics and potential future behavior of the repository system are presented in additional detail. The discussion is organized to provide a description of the major processes that control the waste isolation capability of the potential repository. As shown schematically in Figure 4-2, Section 4.2 describes in sequence the data and analyses relevant to the processes that affect the movement of water through Yucca Mountain and relevant to the potential for that water to contact and mobilize radionuclides. Disruptive events could potentially affect these processes and, therefore, also need to be considered. The data and analyses related to potential disruptive events are presented in Section 4.3, and the combined analysis of the potential performance of the repository is summarized in Section 4.4.

The processes pertinent to performance include those physical processes that control the movement of water, beginning with precipitation as rain and snow at the surface, followed by infiltration into the mountain, flow through the unsaturated zone to the potential repository level, flow from the repository level to the saturated zone, and from there to the accessible environment. At the repository level, water moving past the engineered barriers would be affected by the physical and chemical processes associated with the decay heat and could interact with waste packages and waste forms. These

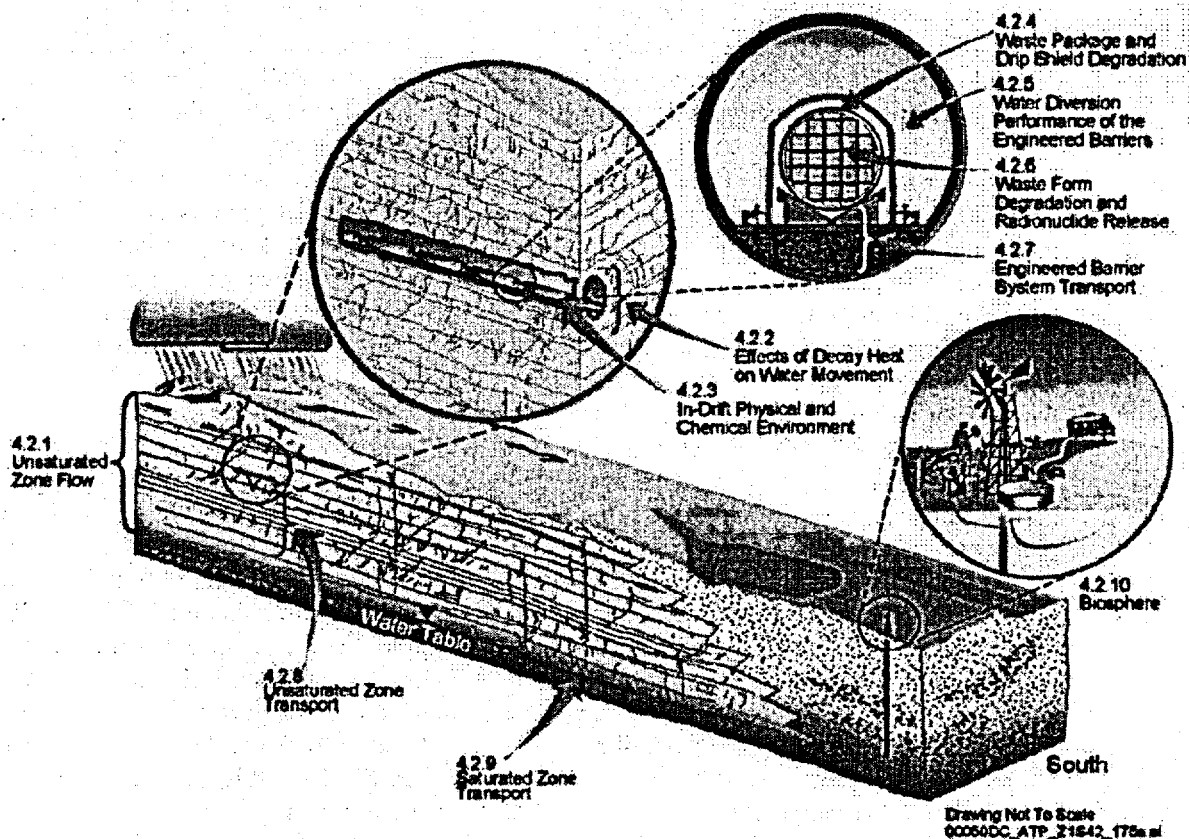


Figure 4-2. Schematic Illustration of the Ten General Processes Considered and Modeled for Total System Performance Assessment

These ten highlighted processes roughly correspond to the ten sections in Section 4.2, as indicated.

processes could lead to the mobilization of radionuclides. Eventually, the water could move out of the repository horizon and further downward through the unsaturated zone. Subsequently, it could move into the saturated zone, where it could be transported to the accessible environment where humans could be exposed.

The data collected during site characterization have been used to develop conceptual and numerical models of the hydrologic, geochemical, thermal, and mechanical processes that will determine how a repository at Yucca Mountain may behave over the next 10,000 years. These process models have, in turn, been used to develop a TSPA model that has been used to assess quantitatively the potential for radionuclide releases to the public and, consequently, the safety of the Yucca Mountain site.

**Attributes Important to Long-Term Performance**—The potential repository system can be described in terms of five key attributes that would be important to long-term performance: (1) limited water entering waste emplacement drifts; (2) long-lived waste package and drip shield; (3) limited release of radionuclides from the engineered barriers; (4) delay and dilution of radionuclide concentrations by the natural barriers; and (5) low peak mean annual dose considering potentially disruptive events. These attributes are summarized below. The first four reflect the interactions of natural barriers and the engineered barriers in prolonging the containment of radionuclides within the repository and limiting their release. The fifth attribute reflects the likelihood that disruptive events would not affect repository performance over 10,000 years.

- 1. Limited Water Entering Emplacement Drifts**—The climate at Yucca Mountain is dry and arid, with precipitation averaging about 190 mm (7.5 in.) per year. Little of this precipitation percolates into the mountain; nearly all of it (above 95 percent) either runs off or is lost to evaporation, limiting the amount of water available to seep into emplacement drifts. For the higher-temperature operating mode described in this report, a thermal management strategy was developed that would take advantage of the heat of the emplaced wastes to drive water away from the emplacement drifts. The heat generated by the waste would dry out the rock surrounding the drift and decrease the amount of water available to contact the waste packages until the wastes have cooled substantially. Drainage of water in the rock pillars between drifts would be encouraged by keeping much of the pillar rock between the drifts below the boiling temperature of water. As long as the drift walls remained at temperatures above the boiling point of water, there would be no liquid water in the emplacement drifts and very little in the nearby rock. Even after the drift walls cooled below the boiling point of water, the residual heat would increase evaporation in and near emplacement drifts, thereby continuing to limit the amount of water present in the rocks adjacent to waste packages. In lower-temperature operating modes, the waste packages would be exposed to water earlier. Because the rock would eventually cool in any operating mode, there does not appear to be a significant difference in the amount of water to which the waste packages would eventually be exposed.

Over the range of operating modes, the design also takes advantage of the mechanical and hydrologic processes that divert water around emplacement drift openings in the unsaturated zone. Because of capillary forces, water flowing in narrow fractures tends to remain in the fractures rather than flow into large open-

ings, such as drifts. If any water reaches an emplacement drift, it could flow down the drift wall to the floor and drain without contacting the drip shield or the waste packages (however, in taking a more conservative approach in modeling, this potential process is not included in the models). Thus, the natural and engineered features of a repository in the unsaturated zone will combine to limit the potential for water to enter the emplacement drifts.

- 2. Long-Lived Waste Package and Drip Shield**—To further reduce the possibility of water contacting waste, the DOE has designed a robust, dual-wall waste package with an outer cylinder of corrosion-resistant material, Alloy 22. Alloy 22 was selected because it will remain stable in the geochemical environment that would be expected in a repository at Yucca Mountain. In the operating mode described in this report, the repository environment would be warm, with temperatures at the waste package surface initially rising above the boiling point of water. Waste package surface temperatures are expected to gradually decrease to below boiling after a period of hundreds to thousands of years, depending on the waste package's location within the repository layout, spatial variation in the infiltration of water at the ground surface, and variability in the heat output of individual waste packages.

Chemically, the environment is expected to be near-neutral pH (mildly acidic to mildly alkaline) and mildly oxidizing. Because most corrosion would occur only in the presence of water and because highly corrosive chemical conditions are not expected, both the titanium drip shield and the Alloy 22 outer barrier of the waste package are expected to have long lifetimes in an unsaturated zone repository. In lower-temperature operating modes, the waste packages would be exposed to water earlier.

- 3. Limited Release of Radionuclides from the Engineered Barriers**—Because of the characteristics of the natural system, the drip shields, and the waste packages, scientists do not expect water to come into contact with the waste forms for over 10,000 years. Even if water were to penetrate a breached waste package before 10,000 years, several characteristics of the waste form and the repository would limit radionuclide releases. First, because of the warm temperatures, much of the water that penetrates the waste package will evaporate before it can dissolve or transport radionuclides. Neither spent nuclear fuel nor glass waste forms will dissolve rapidly in the expected repository environment. Further, a large majority of the radionuclide inventory is insoluble in the geochemical environment expected within the repository. Although the performance of the cladding (metallic outer sheath of a fuel element) as a barrier may vary because of possible degradation, it is expected to limit contact between water and waste. The component of the engineered barrier system below the waste package, called the invert, contains crushed tuff that would also limit the transport of radionuclides into the host rock.
  - 4. Delay and Dilution of Radionuclide Concentrations by the Natural Barriers**—Eventually, the engineered barrier systems in the repository are expected to degrade, and small amounts of water may contact waste. Even then, features of the geologic environment and the repository system will help decrease radionuclide migration to the accessible environment and slow it by hundreds to thousands of years. Processes that could be important to the movement of radionuclides include sorption, matrix diffusion, dispersion, and dilution. Rock units in both the unsaturated zone and the saturated zone at Yucca Mountain contain minerals that can adsorb many types of radionuclides (i.e., radionuclides would attach to and collect on the mineral surfaces). As water flows through fractures, dissolved radionuclides can diffuse into and out of the pores of the rock matrix, increasing both the time it takes for radionuclides to move from the repository and the likelihood that radionuclides will be exposed to sorbing minerals. Dispersion and dilution will occur naturally as potentially contaminated groundwater flows and mixes with other groundwater and lowers the concentration of contaminants.
  - 5. Low Mean Annual Dose Considering Potentially Disruptive Events**—Yucca Mountain provides an environment in which hydrogeologic conditions important to waste isolation (e.g., a thick unsaturated zone with low rates of water movement) have not changed very much for at least hundreds of thousands of years. Analysts have identified and evaluated a wide variety of potentially disruptive processes and events that could affect the performance of the design and operating mode described in this report. These range from extremely unlikely events, such as meteor impacts, to events that are likely to occur, such as regional climate change. Although the probability of volcanic activity in or near the potential repository is low, volcanic activity was a consideration in TSPA in the disruptive scenario case. Performance assessment results to date show that potentially disruptive events are not likely to compromise the performance of the repository, and the probability-weighted mean dose for an igneous disruption is low.
- Table 4-3 shows the relationship between the key attributes of the site and the physical barriers that comprise the repository system, the processes important to waste isolation, and the descriptions presented in Sections 4.2.1 through 4.2.10 and in Section 4.3. The table is based on similar information developed and presented in *Repository Safety Strategy: Plan to Prepare the Safety Case to Support Yucca Mountain Site Recommendation and Licensing Considerations* (CRWMS M&O 2001a)

Table 4-3. Correlation of Key Attributes of Yucca Mountain, Barriers to Radionuclide Release, and Processes Important to Performance, with Reference to Where Descriptions of the Processes can be Found in this Report and Process Model Reports

| Key Attributes of System   | Barrier: Function   | Processes Affecting Repository Performance   | S&ER Section   | PMR  |
|--|---|--|--|--|
| Limited Water Entering Emplacement Drifts  | Surficial soils and topography: Reduce the amount of water entering the unsaturated zone by surficial processes   | Climate  | Section 4.2.1  | UZ Flow and Transport (CRWMS M&O 2000c)  |
|  |   | Net infiltration   |  |  |
|  | Unsaturated rock layers overlying the repository: Reduce the amount of water reaching the repository by subsurface processes  | Unsaturated zone flow  | Section 4.2.1  | UZ Flow and Transport (CRWMS M&O 2000c)  |
|  |   | Seepage into emplacement drifts  |  |  |
|  |   | Coupled thermal effects on unsaturated zone flow and seepage   | Section 4.2.2  | Near-Field Environment (CRWMS M&O 2000a); UZ Flow and Transport (CRWMS M&O 2000c)                |
| Long-Lived Waste Package and Drip Shield   | Drip shield above the waste packages: Prevent water from contacting the waste package and waste form by diverting water flow.   | In-drift physical and chemical environments  | Section 4.2.3  | Near-Field Environment (CRWMS M&O 2000a); EBS Degradation, Flow and Transport (CRWMS M&O 2000as) |
|  |   | Drip shield degradation and performance  | Section 4.2.4  | Waste Package Degradation (CRWMS M&O 2000n)  |
|  | Waste package degradation and performance   |  |  |  |
|  | Waste package: Prevent water from contacting the waste form for thousands of years  | In-drift water movement and moisture distribution  | Section 4.2.5  | EBS Degradation, Flow and Transport (CRWMS M&O 2000as)   |
| Limited Release of Radionuclides from the Engineered Barriers  | Spent fuel cladding: Delay and/or limit liquid water contacting spent nuclear fuel after waste packages have degraded   | Cladding degradation and performance   | Section 4.2.6  | Waste Form Degradation (CRWMS M&O 2000bm)  |
|  |   | Radionuclide inventory   | Section 4.2.6  | Waste Form Degradation (CRWMS M&O 2000bm)  |
|  | In-package environments   |  |  |  |
|  | Commercial SNF and DOE SNF degradation and performance  |  |  |  |
|  | DOE HLW degradation and performance   |  |  |  |
|  | Dissolved radionuclide concentrations   |  |  |  |
|  | Colloid-associated radionuclide concentrations  |  |  |  |
|  | Waste form: Limit liquid water contacting waste during the period when temperatures are elevated and limit radionuclide release rates as a result of low solubilities and leach rates           | In-package radionuclide transport  |  |  |
| Invert below the waste packages: Limit transport of radionuclides out of the engineered barrier system | Engineered barrier system transport, inverts, degradation and performance   | Section 4.2.7  | EBS Degradation, Flow and Transport (CRWMS M&O 2000as) |  |
| Delay and Dilution of Radionuclide Concentrations by the Natural Barriers                              | Unsaturated rock layers below the repository: Delay and reduce the concentration of radionuclides in the groundwater aquifer because of water residence time, matrix diffusion, and/or sorption | Unsaturated zone radionuclide transport (advective pathways; colloid transport and retardation; dispersion)  | Section 4.2.8  | UZ Flow and Transport (CRWMS M&O 2000c)  |
|  |   | Saturated zone radionuclide transport (advective pathways; colloid transport and retardation; dispersion; dilution)  | Section 4.2.9  | SZ Flow and Transport (CRWMS M&O 2000bn)   |
|  | Volcanic tuff and alluvial deposits below the water table: Delay radionuclide movement to the receptor location by water residence time, matrix diffusion, and/or sorption                      | Dilution   | Section 4.2.10   | Biosphere (CRWMS M&O 2000bo)   |
| Low Mean Annual Dose Considering Potentially Disruptive Events   | N/A (Disruptive processes and events act on the barriers listed above).   | Probability and consequences of volcanic eruption (characteristics and effects of eruption, atmospheric transport);<br>Probability and consequences of igneous intrusion (characteristics and effects of igneous intrusion);<br>Probability and consequences of seismic events;<br>Probability and consequences of other disruptive events;<br>Biosphere dose conversion factors | Section 4.3  | Disruptive Events (CRWMS M&O 2000f)  |

NOTES: EBS = engineered barrier system; HLW = high-level radioactive waste; N/A = not applicable; PMR = process model report; S&ER = Yucca Mountain Science and Engineering Report; SNF = spent nuclear fuel; SZ = saturated zone; UZ = unsaturated zone.

and the *Total System Performance Assessment for the Site Recommendation* (CRWMS M&O 2000a). The table incorporates the results of lower-temperature operating mode evaluations (BSC 2001b). In addition to the information presented in these sources, Table 4-3 relates the key attributes and processes to the natural and engineered barriers that would contribute to waste isolation at Yucca Mountain. The last column of the table also lists process model reports that contain more detailed descriptions of the processes summarized here and included in the TSPA. The column showing the processes important to repository performance is not intended to be comprehensive: it is presented at a summary level. More detailed definitions of the proposed repository system and relevant specific processes are included in the individual sections that follow.

**Organization of Section 4.2**—As organized below, and shown in Figure 4-2, the total system consists of numerous interdependent subsystems that are described in ten subsections, as follows:

- Section 4.2.1 describes the data and analyses relevant to the movement of water in the unsaturated zone and describes the development of process models related to the potential movement of water into the repository.
- Section 4.2.2 describes the data and analyses related to the effects of decay heat on the movement of water through the unsaturated zone.
- Section 4.2.3 describes information that provides the basis for the DOE's understanding of the physical and chemical environment within the repository drifts, which influences the expected lifetimes of the drip shields and waste packages.
- Section 4.2.4 summarizes the data and evaluations that support models of the degradation of drip shields and waste packages, which will affect the lifetimes of the engineered barrier system.
- Section 4.2.5 describes the information that supports the analysis of the performance of engineered barriers in diverting water away from the waste package. After the eventual degradation of the waste packages, and in the presence of liquid water, it would be possible for chemical reactions to occur to mobilize radionuclides within the waste packages.
- Section 4.2.6 describes the experimental data and analyses of the chemical and hydrologic processes within the breached waste packages that would result in the release of radionuclides from the waste form.
- Section 4.2.7 describes information related to the potential transport of mobilized radionuclides through the engineered barriers.
- Section 4.2.8 describes the data and analyses related to the potential flow and transport of radionuclides through the unsaturated zone.
- Section 4.2.9 describes potential flow and transport in the saturated zone.
- Section 4.2.10 describes the biosphere model used to model the uptake and biological consequences of released radionuclides that eventually reach the human environment.

Within each of these sections, a similar internal organization is used to present the DOE's understanding of the key processes and to present the data and analyses that provide the basis for that understanding. Each discussion includes:

1. A summary description of how each process would operate in a potential repository
2. A description of the investigations, tests, and other data (including analogue information) that provide the technical basis for the DOE's understanding
3. A description of the conceptual and numerical models that have been developed to allow the DOE to assess potential future performance, including specific

information about the sources and treatment of uncertainties, alternative models, and model calibration and validation

4. A description of how the conceptual and numerical models have been abstracted (or represented) in the TSPA-SR (CRWMS M&O 2000a).

#### 4.2.1 Unsaturated Zone Flow

This section summarizes the current understanding of water movement (i.e., percolation flux) through the unsaturated zone and into a repository (i.e., seepage into drifts) at Yucca Mountain. Fluid flow through the unsaturated zone at Yucca Mountain is described at length in *Unsaturated Zone Flow and Transport Model Process Model Report* (CRWMS M&O 2000c, Sections 3.2 to 3.4 and 3.6 to 3.9), which is supported by 24 detailed analysis model reports. *Yucca Mountain Site Description* (CRWMS M&O 2000b, Sections 8.2 to 8.10) also provides a comprehensive summary of investigations performed to characterize flow and seepage in the unsaturated zone. Figure 4-3 shows the relationships between the main unsaturated zone processes, with those relevant to unsaturated zone flow highlighted.

The primary purpose of *Unsaturated Zone Flow and Transport Model Process Model Report* (CRWMS M&O 2000c) is to develop models for the TSPA that evaluate the postclosure performance of the unsaturated zone. *Unsaturated Zone Flow and Transport Model Process Model Report* supplies to the TSPA (1) ambient and predicted (i.e., future) three-dimensional flow fields based on different climate states and infiltration scenarios and (2) seepage rates into potential waste emplacement drifts. The flow fields are used directly in TSPA calculations of transport, while the seepage rates are used to calculate distributions of the fraction of waste packages in contact with seepage water and the volumetric flow rate to a waste package segment, taking into account possible flow focusing effects from site scale to drift scale (see Section 4.2.1.4).

As noted in Section 4.1.4, the DOE is evaluating the possibility of mitigating uncertainties in

modeling long-term repository performance by operating the design described in this report at lower temperatures. Some analyses described in this section have been updated and expanded to capture the features and processes relevant to operating the design at lower temperatures. The updated analyses are described in Volume 2, Section 4 of *FY01 Supplemental Science and Performance Analyses* (BSC 2001b).

##### 4.2.1.1 Conceptual Basis

On the most fundamental level, the important factors affecting unsaturated groundwater flow at Yucca Mountain are climate and rock hydrologic properties. Derived from these two basic components are estimates of percolation flux and seepage into potential waste emplacement drifts, both of which are key unsaturated zone processes.

Located in southern Nevada, one of the most arid regions of the United States, Yucca Mountain is underlain by a thick unsaturated zone (CRWMS M&O 2000c, Section 3.2.1). A dry climate and a deep water table are considered favorable characteristics for waste isolation. In a desert environment, the total amount of available water is small. The potential repository would be designed to complement the hydrologic environment by diverting the small flow of water that does occur away from the waste packages. Multiple natural and engineered barriers are expected to limit contact between water and waste forms, and retard radionuclide migration. The climate data and unsaturated zone characteristics are discussed in Sections 4.2.1.2.1 and 4.2.1.2.2, respectively.

The major components of the unsaturated zone and the emplacement drifts that affect water movement are illustrated in Figure 4-4. Water movement starts with rainfall in the arid environment, which is subject to runoff, evaporation, and plant uptake, such that much of the rainfall never reaches the potential repository host rock units. The infiltration of water that penetrates into the rock units of the unsaturated zone is redistributed by flow processes in the fractured and faulted, welded and nonwelded tuff layers. When percolating water encounters an underground drift, much of it will be diverted by

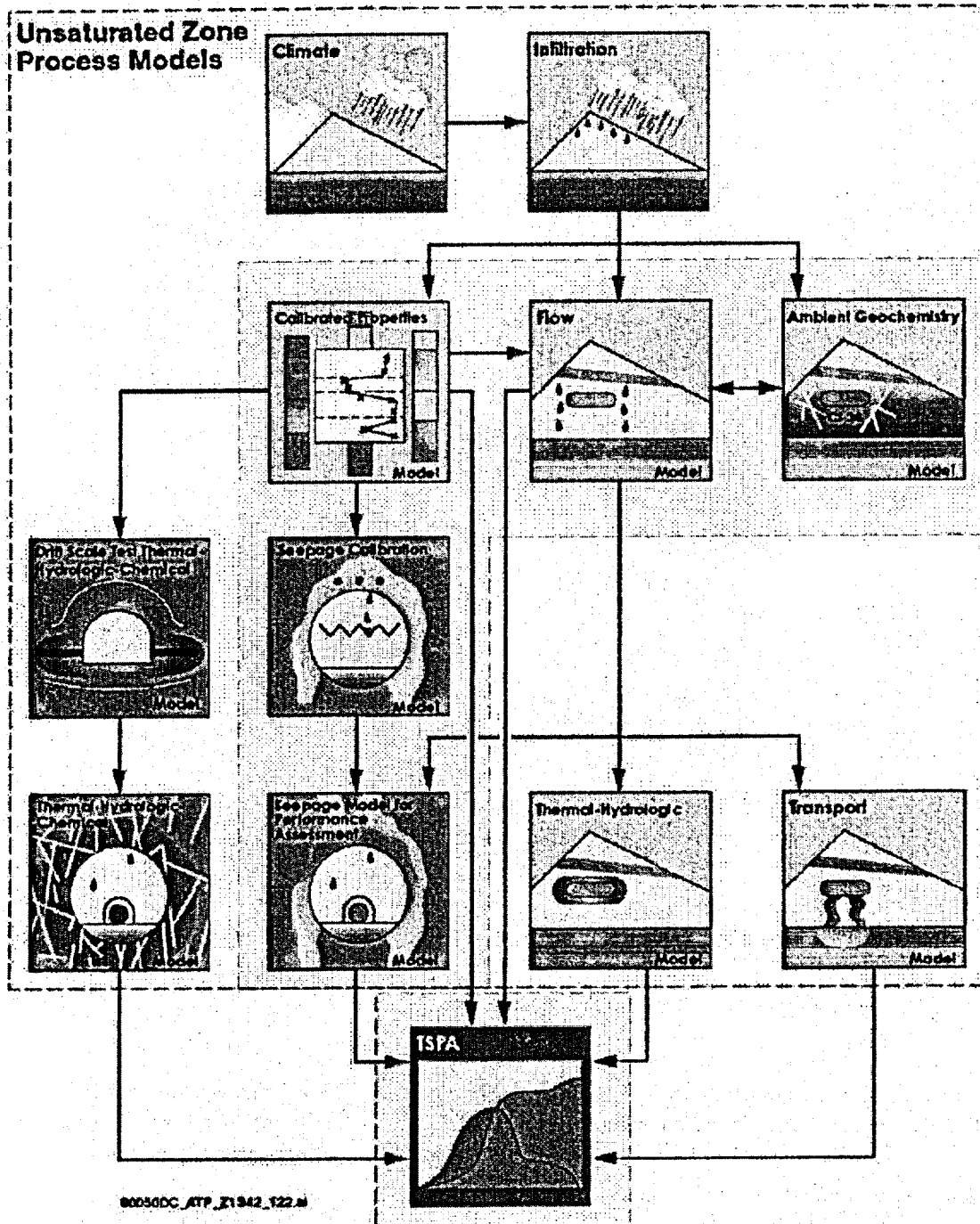


Figure 4-3. Main Models Included in the Unsaturated Zone Process Model Report, Their Interrelations, and Their Connections to Total System Performance Assessment  
Models relevant to this section are highlighted with a cream-colored background. Source: CRWMS M&O 2000c, Figure 1-2.

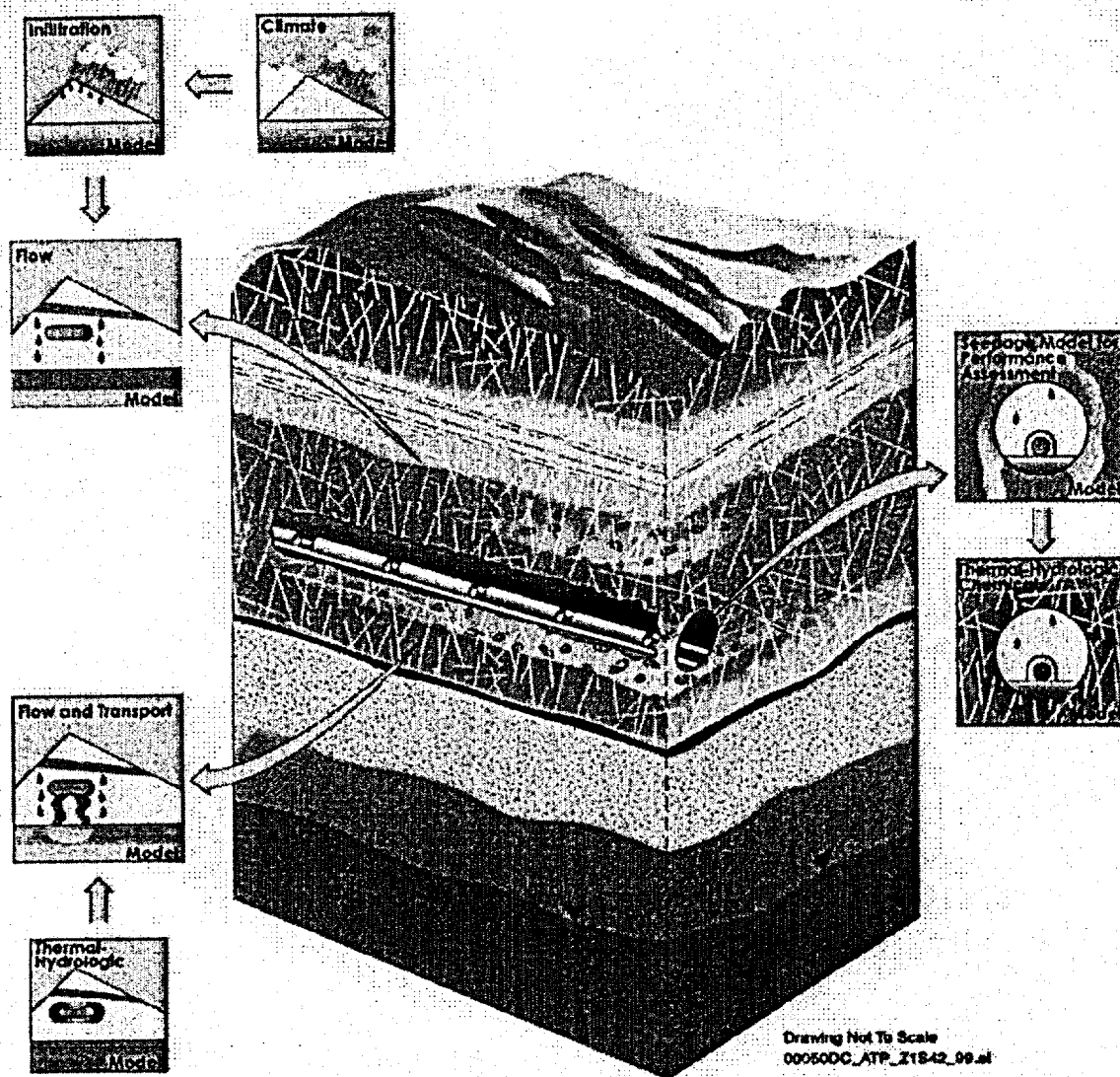


Figure 4-4. Schematic Block Diagram Showing Major Unsaturated Zone Flow Processes Above, Within, and Below Repository Emplacement Drifts

capillary barrier mechanisms around the opening and never contact the engineered barriers within.

Major issues related to unsaturated zone flow processes include:

- Climate and infiltration
- Fracture flow versus matrix flow within major hydrogeologic units
  - Flow above the potential repository

- Flow below the potential repository, including the formation and hydrologic significance of perched water

- Fracture-matrix interaction
- Effects of major faults
- Seepage into drifts.

Using these major issues as subheadings, a summary of the current conceptual understanding of unsaturated zone flow beneath Yucca Mountain

is first presented. Following this summary are subsections that describe the data supporting the conceptual understanding of flow in the unsaturated zone (Section 4.2.1.2), the development and integration of numerical process models based on the conceptual interpretation of the available data (Section 4.2.1.3), and how the results of unsaturated zone numerical modeling studies have been abstracted for the TSPA (Section 4.2.1.4).

#### 4.2.1.1.1 Climate and Infiltration

Climate is defined by the variation of meteorological conditions (such as temperature, pressure, humidity, precipitation rate and prevailing winds) over time. At Yucca Mountain, climate is important because it provides the boundary conditions for the hydrologic system—specifically, the amount of water available at the surface. Estimates of the precipitation rate and temperature taken from climate models have been used as information to determine the net infiltration of water into Yucca Mountain and the percolation flux at the repository horizon. Percolation flux within the unsaturated zone, governed by climate and rock hydrogeologic properties, is a key process affecting seepage in waste emplacement drifts and transport of radioactive particles below the repository. Three representative climates are forecast to occur within the next 10,000 years (i.e., the period of regulatory compliance): the modern (present-day) climate, a monsoon climate, and a glacial-transition climate (USGS 2000a, Section 6.6). Beyond 10,000 years, the TSPA-SR extends the glacial-transition climate for base-case simulations and includes a revised long-term climate model in a sensitivity study, as discussed in Section 4.4.2.4 (CRWMS M&O 2000a, Section 3.2.1.2) and Volume 1, Section 3.3.1 of *FY01 Supplemental Science and Performance Analyses* (BSC 2001a).

Net infiltration refers to the penetration of liquid water through the ground surface and to a depth where it can no longer be removed by evaporation or transpiration by plants. Net infiltration is the source of groundwater recharge and water percolation at the potential repository horizon; it provides the water for flow and transport mechanisms that could move radionuclides from the potential repository to the water table. The overall framework of

the conceptual model for net infiltration is based on the hydrologic cycle. Important processes that affect net infiltration include precipitation (rain and snow), runoff and run-on (flow of surface water off one place and onto another), evaporation, transpiration, and moisture redistribution by flow in the shallow subsurface (USGS 2000b, Section 6.1.3). Infiltration is temporally and spatially variable because of the nature of the storm events that supply precipitation and because of variation in soil cover and topography (CRWMS M&O 2000bq, Section 6.1.1). Surficial soils and topography are considered part of the natural barrier system because they reduce the amount of water entering the unsaturated zone by surficial processes (e.g., precipitation lost to runoff, evaporation, and plant transpiration) (Table 4-2). Net infiltration rates are believed to be high on sideslopes and ridge tops where bedrock is exposed and fracture flow in the bedrock is able to move liquid water away from zones of active evaporation (Flint, L.E. and Flint 1995, p. 15).

Within the limits of extant monitoring data, significant net infiltration occurs only every few years under the present climate (CRWMS M&O 2000bq, Section 6.1.1). In these years, the amount of net infiltration still varies greatly, depending on storm amplitude, duration, and frequency. In very wet years, net infiltration pulses into Yucca Mountain may occur over a period of a few hours to a few days. A detailed discussion of net infiltration processes can be found in *Simulation of Net Infiltration for Modern and Potential Future Climates* (USGS 2000b) and in Volume 1, Section 3.3.1 of *FY01 Supplemental Science and Performance Analyses* (BSC 2001a).

#### 4.2.1.1.2 Fracture Flow and Matrix Flow within Major Hydrogeologic Units

An early conceptual hydrologic model of unsaturated flow at Yucca Mountain, developed by Montazer and Wilson (1984), identified five major hydrogeologic units within the unsaturated zone. From the land surface to the water table, these units are the Tiva Canyon welded (TCw), the Paintbrush nonwelded (PTn), the Topopah Spring welded (TSw), the Calico Hills nonwelded (CHn), and the Crater Flat undifferentiated (CFu) units. Table 4-4

Table 4-4. Major Hydrogeologic Unit, Lithostratigraphic Unit, Detailed Hydrogeologic Unit, and Unsaturated Zone Model Layer Nomenclatures

| Major Hydrogeologic Unit           | Lithostratigraphic Unit     |                     | Detailed Hydrogeologic Unit    | Unsaturated Zone Model Layer |               |
|------------------------------------|-----------------------------|---------------------|--------------------------------|------------------------------|---------------|
| Tiva Canyon welded (TCw)           | Tiva Canyon Tuff            | Tp1c                | CCR, CUC                       | tcw11                        |               |
|                                    |                             | Tp1p                | CUL, CW                        | tcw12                        |               |
|                                    |                             | Tp1pv3              | CMW                            | tcw13                        |               |
|                                    |                             | Tp1pv2              |                                |                              |               |
|                                    |                             | Tp1pv1              | CNW                            | ptn21                        |               |
| Paintbrush nonwelded (PTR)         | Bedded Tuff                 | Tp1b4               | BT4                            | ptn22                        |               |
|                                    | Yucca Mountain Tuff         | Tpy                 | TPY                            | ptn23                        |               |
|                                    |                             |                     | BT3                            | ptn24                        |               |
|                                    | Bedded Tuff                 | Tp1bt3              | TPP                            | ptn25                        |               |
|                                    | Pah Canyon Tuff             | Tpp                 |                                |                              |               |
|                                    | Bedded Tuff                 | Tp1bt2              |                                |                              |               |
|                                    | Topopah Spring welded (TSw) | Topopah Spring Tuff | Tp1tv3                         | BT2                          | ptn26         |
|                                    |                             |                     | Tp1tv2                         |                              |               |
|                                    |                             |                     | Tp1tv1                         | TC                           | tsw31         |
|                                    |                             |                     | Tp1tm                          | TR                           | tsw32         |
| Tp1tl                              |                             |                     | TUL                            | tsw33                        |               |
| Tp1tpul                            |                             |                     |                                |                              |               |
| Tp1tpmn                            |                             |                     | TMN                            | tsw34                        |               |
| Tp1tpl                             |                             |                     | TLL                            | tsw35                        |               |
| Tp1tpin                            |                             |                     | TM2 (upper 2/3)                | tsw36                        |               |
|                                    |                             |                     | TM1 (lower 1/3)                | tsw37                        |               |
| Tp1tpv3                            | PV3                         | tsw38               |                                |                              |               |
| Tp1tpv2                            | PV2                         | tsw39               |                                |                              |               |
| Calico Hills nonwelded (CHn)       | Bedded Tuff                 | Tp1bt1              | BT1 or BT1 (altered)           | ch1 (vit, zeo)               |               |
|                                    | Calico Hills Formation      | Tac                 | CHV (vitric) or CHZ (zeolitic) | ch2 (vit, zeo)               |               |
|                                    |                             |                     |                                | ch3 (vit, zeo)               |               |
|                                    |                             |                     |                                | ch4 (vit, zeo)               |               |
|                                    |                             |                     |                                | ch5 (vit, zeo)               |               |
|                                    |                             |                     |                                | ch6                          |               |
|                                    | Bedded Tuff                 | Tacbt               | BT                             | ch6                          |               |
|                                    | Prow Pass Tuff              | Tc1puv              | PP4 (zeolitic)                 | pp4                          |               |
|                                    |                             |                     | PP3 (devitrified)              | pp3                          |               |
|                                    |                             |                     | PP2 (devitrified)              | pp2                          |               |
| PP1 (zeolitic)                     |                             |                     | pp1                            |                              |               |
|                                    |                             |                     |                                | Tc1piv                       |               |
| Bedded Tuff                        | Tc1pbt                      | PP1 (zeolitic)      | pp1                            |                              |               |
| Crater Flat undifferentiated (CFu) | Bullfrog Tuff               | Tc1buv              | BF3 (welded)                   | bf3                          |               |
|                                    |                             | Tc1buc              |                                |                              |               |
|                                    |                             | Tc1bmd              |                                |                              |               |
|                                    |                             | Tc1bic              |                                |                              |               |
|                                    |                             | Tc1biv              |                                |                              |               |
| Bedded Tuff                        | Tc1bbt                      | BF2 (nonwelded)     | bf2                            |                              |               |
| Tram Tuff                          | Tctuv                       | Tctuc               | Not Available                  | tr3                          |               |
|                                    |                             | Tctmd               |                                |                              |               |
|                                    |                             | Tctic               |                                |                              |               |
|                                    |                             | Tctiv & below       |                                |                              | Not Available |

Source: CRWMS M&O 2000c, Table 3.2-2.

correlates major hydrogeologic, lithostratigraphic, and detailed hydrogeologic units with the layering scheme used in unsaturated zone modeling activities. These units are described in greater detail in the *Development of Numerical Grids for UZ Flow and Transport Modeling* (CRWMS M&O 2000br, Section 6.4.1), in the *Geologic Framework Model (GFM3.1)* (CRWMS M&O 2000bs, Section 6.4.1), and by Flint, L.E. (1998).

The texture of Yucca Mountain tuffs ranges from nonwelded to densely welded (CRWMS M&O 2000c, Section 3.2.1). Typically, the porosity and permeability of the rock mass are inversely proportional to the degree of welding, and the degree of fracturing is directly proportional to the degree of welding. The degree of welding observed in the individual tuff units is primarily controlled by their cooling history. Generally speaking, the slower a rock cools, the more densely welded the material becomes. This densely welded material (matrix) is usually quite brittle in nature and develops well-connected fracture networks. These extensive, well-connected fracture networks, in turn, provide numerous pathways for the flow of liquids and gases. Conversely, the nonwelded rocks, which experienced rapid heat dissipation, display high matrix porosity and possess few fractures. Flow through these rocks is dominated by matrix flow processes (CRWMS M&O 2000c, Section 3.3.3).

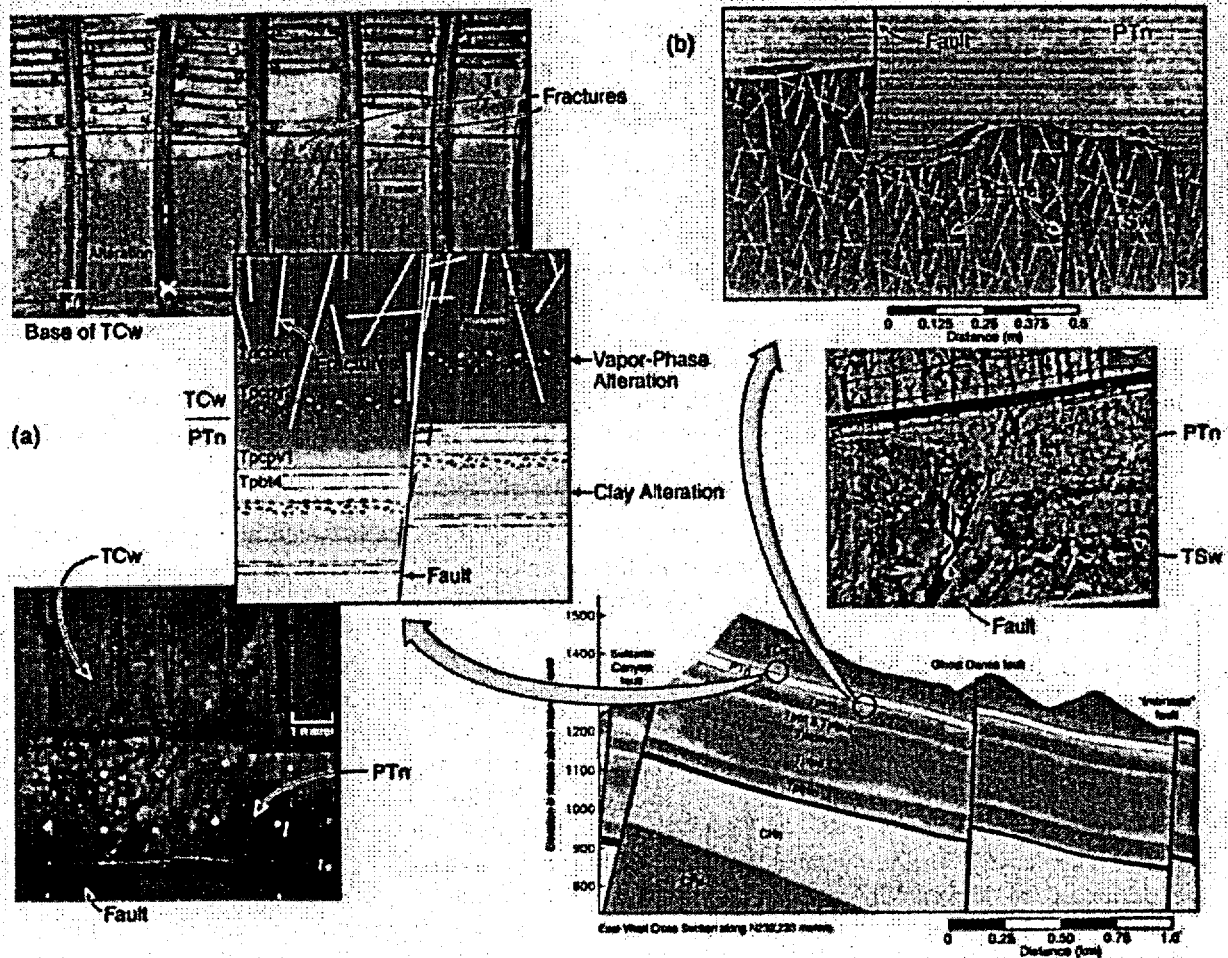
The partitioning of total flux between the fracture flow component and the matrix flow component is one of the most important processes to determine in the unsaturated zone. Percolation distribution determines the amount of water that could potentially contact the waste packages and other components of the engineered barrier system. Determination of the flow components is also important for chemical transport processes. Water flow in fractures is typically much faster than flow in the matrix, leading to much faster movements for radionuclides and other chemicals in fractures compared to the matrix (CRWMS M&O 2000c, Section 3.3.3). The characteristic flow behavior in each of the major hydrogeologic units is described in the following paragraphs.

**Flow Above the Potential Repository—The TCw** is the most prevalent hydrogeologic unit exposed at

the land surface (CRWMS M&O 2000c, Section 3.2.2.1). The unit is of variable thickness because of erosion and is composed of moderately to densely welded, highly fractured pyroclastic flow deposits of the Tiva Canyon Tuff. The high density of interconnected fractures and low matrix permeability of the unit (CRWMS M&O 2000bt, Sections 6.1 and 6.2) are considered to give rise to significant water flow in fractures and limited matrix imbibition (water flow from fractures to the matrix). Therefore, episodic infiltration pulses are expected to move rapidly through the fracture system into the underlying PTn unit with little attenuation by the matrix.

At the interface between hydrogeologic units TCw and PTn, tuffs grade downward over a few tens of centimeters from densely welded to nonwelded, accompanied by an increase in matrix porosity and a decrease in fracture frequency (Figure 4-5a) (CRWMS M&O 2000c, Section 3.2.2.1). The relatively high matrix permeabilities and porosities, and low fracture densities, of the PTn (CRWMS M&O 2000bt, Sections 6.1 and 6.2) should convert the predominant fracture flow in the TCw to dominant matrix flow within the PTn unit (CRWMS M&O 2000bq, Section 6.1). This, along with the relatively large storage capacity of the matrix resulting from its high porosity and low saturation, is expected to give the PTn significant capability to attenuate infiltration pulses and smooth areal differences in infiltration from the overlying welded unit and result in approximately steady-state water flow below the PTn. Through-going fracture networks within the PTn unit are rare and typically associated with faults (Rousseau, Kwicklis et al. 1999, pp. 53 to 54), so only a small amount of water is expected to pass through the PTn by way of fast flow paths. Recent analyses indicates that some lateral diversion on the PTn is probable (BSC 2001a, Section 3.3.3).

Conceptualization of the character of flow at the interface between the PTn and the overlying TCw for the TSPA-SR model was based on findings from estimates of flux rates in the PTn from geochemistry (Yang and Peterman 1999) and on hydrogeological properties described by Flint, L.E. (1998). The implication of that characterization was that little or no lateral flow diversion of down-



000500C\_ATP\_Z1542\_125.ai

Figure 4-5. Lithostratigraphic Transitions at the Upper and Lower Margins of the PTn Hydrogeologic Unit. (a) Photos and schematic at the TCw-PTn interface, where tuffs grade downward from densely welded to nonwelded, accompanied by an increase in matrix porosity and a decrease in fracture frequency. (b) Photo and schematic at the PTn-TSw interface, where tuffs grade downward from nonwelded to densely welded, accompanied by a decrease in matrix porosity and an increase in fracture frequency. Source: Adapted from CRVMS M&O 2000c, Figures 3.2-2 and 3.3-3.

ward percolating unsaturated zone water could be expected as a result of a contrast of hydrologic properties across this surface and its gentle dip to the east. If diversion of downward percolating water to permeable fault zones outside the potential repository footprint at that elevation occurs, it implies that water might be diverted around a repository, thus benefiting repository performance. Earlier work by Montazer and Wilson (1984) supported the conceptual model of lateral diversion on the PTn. The TSPA-SR model did not include lateral diversion on the PTn on the assumption that

if any such diversion exists, it is small and that to leave it out of the model is conservative.

Geochemical evidence collected since the conceptualization of the original TSPA-SR modeling appears to support the existence of lateral diversion in the PTn based on chloride abundance (BSC 2001a, Section 3.2.3). Recent modeling approaches that combine pneumatic data from above, below, and within the PTn, saturation and water potential data, and geochemical data were used to calibrate unsaturated characteristic parameters and to differ-

entiate alternative conceptual models (BSC 2001a, Section 3.2.3). Using a fine grid spacing, calibrated to match the chloride distributions and the estimated percolation flux data in the unsaturated zone below the PTn, supports the lateral diversion of water around a potential repository and the relatively uniform distribution of percolation flux in the deep unsaturated zone (BSC 2001a, Section 3.3.3). The PTn exhibits inhomogeneous lithologic character and distribution and some evidence, in the form of inferred occurrences of bomb-pulse chlorine-36 at depth, that fast flow paths for relatively small volumes of water may exist along faults and perhaps in zones of fracture flow focusing. In most of the region of the potential repository footprint, the PTn is expected to damp flow surges in the percolation flux rate and smooths areal differences in flow, which originate in the temporal and spatial patterns of infiltration at the surface (CRWMS M&O 2000c, Section 3.3.3.2). Smoothing of flow is supported by evenly distributed chloride mass balance data (BSC 2001a, Section 3.3.3).

Although the PTn is predominantly nonwelded, rock-hydrologic properties are highly heterogeneous because of differing depositional environments, lateral variations in welding, and the variable distribution of mineralogically altered (e.g., smectitic and zeolitic) intervals within the individual PTn subunits (CRWMS M&O 2000c, Section 3.2.2.2).

The transition from the lower PTn into the upper TSw is marked by a decrease in matrix porosity and an increase in fracture frequency (Figure 4-5b) (CRWMS M&O 2000c, Section 3.2.2.2) as the tuffs grade sharply downward from nonwelded to densely welded. These changes in porosity and fracture characteristics may create saturated conditions above this contact that could initiate fracture flow into the TSw.

Lithostratigraphic units within the TSw (including the middle nonlithophysal, lower lithophysal, and lower nonlithophysal potential repository host units) are moderately to densely welded and are primarily distinguished by the relative abundance of lithophysae (cavities formed by bubbles of volcanic gases trapped in the tuff matrix during

cooling), crystal content, mineral composition, pumice and rock fragment abundance, and fracture characteristics (CRWMS M&O 2000c, Section 3.2.2.3). Differences in lithophysal abundance and fracture characteristics are shown in Figure 4-6.

Unsaturated flow in the TSw is primarily through the fractures because of the magnitude of matrix hydraulic conductivity of the TSw relative to the estimated average infiltration rate. If the hydraulic gradient is assumed to be one (i.e., flow is vertically downward and gravity driven), the maximum matrix percolation rate is the same as the matrix hydraulic conductivity. Because the estimated matrix hydraulic conductivity of some TSw subunits is much lower than the average estimated infiltration rate (CRWMS M&O 2000bq, Section 6.1.2), the remainder of the flow must be distributed in the fracture network.

**Flow Below the Potential Repository**—Flow behavior below the TSw is important for modeling radionuclide transport from the repository horizon to the water table because transport paths follow the water flow pattern. The main hydrogeologic units below the TSw are the CHn and CFu (CRWMS M&O 2000c, Sections 3.2.2.4 and 3.2.2.5). The CHn contains primarily nonwelded layers whose initial vitric composition has been variably transformed by high and low temperature alteration to clays and zeolites. A portion of the lower half of the CHn (corresponding to the interior of the Prow Pass Tuff) is characterized by moderately welded to densely welded layers that have undergone devitrification (high-temperature conversion of glass to crystalline material). Devitrified, welded rocks show greater fracture intensity than the nonwelded layers and typically do not contain alteration minerals (Flint, L.E. 1998, p. 9). In the southern half of the potential repository footprint and to the south, a portion of the upper CHn (corresponding principally to the Calico Hills Formation, Tac) is largely unaltered (i.e., vitric). This volume of vitric material is believed to represent the part of the CHn that remained above past elevated saturated zone water levels (CRWMS M&O 2000c, Section 3.2.4).

The CFu unit (consisting of portions of the Bullfrog and Tram tuffs that occur above the water

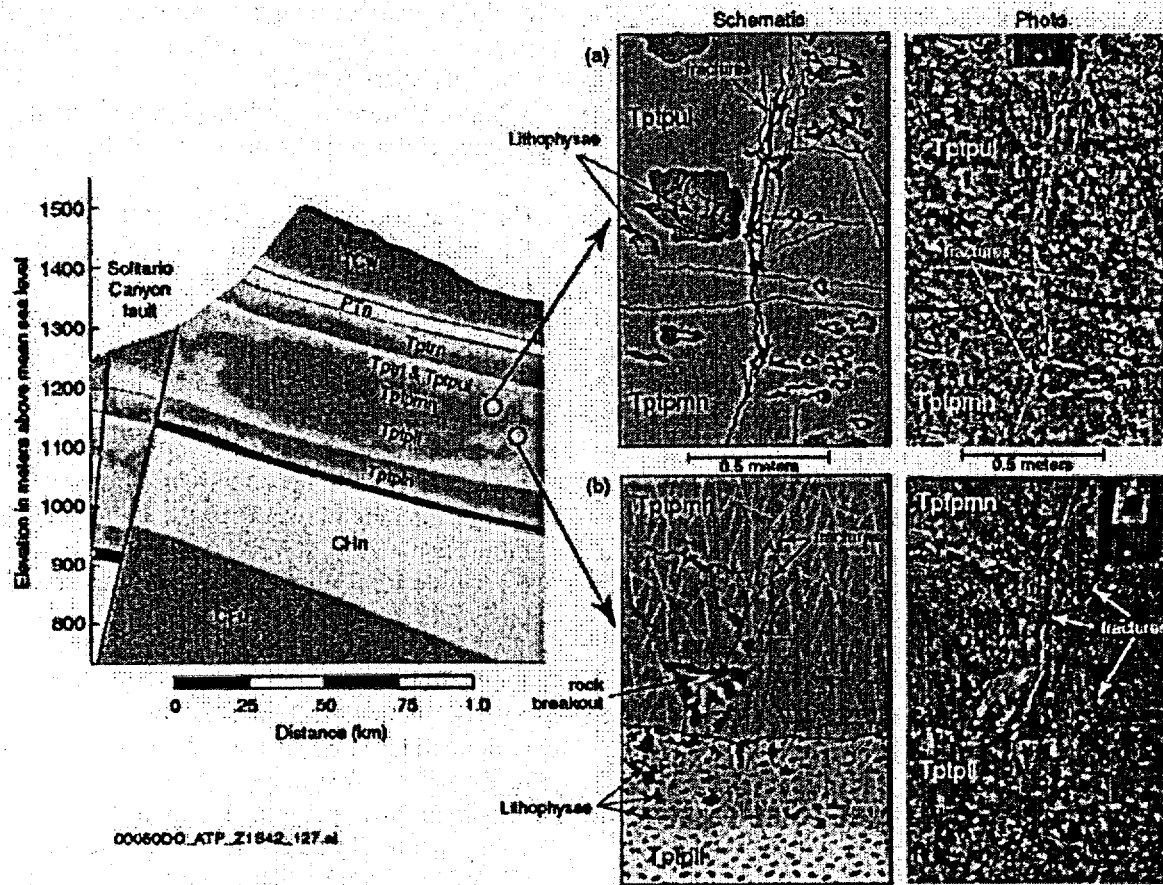


Figure 4-6. Lithophysal Transitions within the TSw Unit

(a) Photo and schematic of the contact between the upper nonlithophysal (Tptul) and the middle nonlithophysal (Tptpm) zones showing a downward decrease in lithophysal volume. (b) Photo and schematic of the contact between the middle nonlithophysal (Tptpm) and lower lithophysal (Tptpl) zones showing a downward increase in lithophysal volume. Fractures in the nonlithophysal units are generally smoother, more planar, and more continuous than fractures in the lithophysal units. Source: CRWMS M&O 2000c, Figure 3.2-4.

table) is a subset of the Crater Flat Group, which contains the Prow Pass, Bullfrog, and Tram tuffs (CRWMS M&O 2000b, Section 4.5.4.5). Lithostratigraphic units within the CFu are nonwelded to densely welded, with the nonwelded tuffs being pervasively altered to zeolites. The Prow Pass, Bullfrog, and Tram tuffs are all similar in that they each contain devitrified, densely welded interiors that grade above and below into nonwelded, zeolitically altered tuffs.

The nonwelded vitric, nonwelded zeolitic, and welded devitrified tuffs have significantly different properties and flow characteristics. The zeolitic

rocks have very low matrix permeability and slightly greater fracture permeability; therefore, a relatively small amount of water may flow through the zeolitic units (primarily through fractures), while most of the water is diverted around these low-permeability bodies (Figure 4-7b) (CRWMS M&O 2000c, Section 3.3.3.4). Conversely, vitric portions of the CHn have relatively high matrix porosity and permeability and are characterized by low fracture frequencies (similar to layers within the PTn); therefore, matrix flow dominates, and fracture flow is believed to be limited in the vitric units. Devitrified tuffs have slightly lower matrix porosities than the nonwelded tuffs and increased

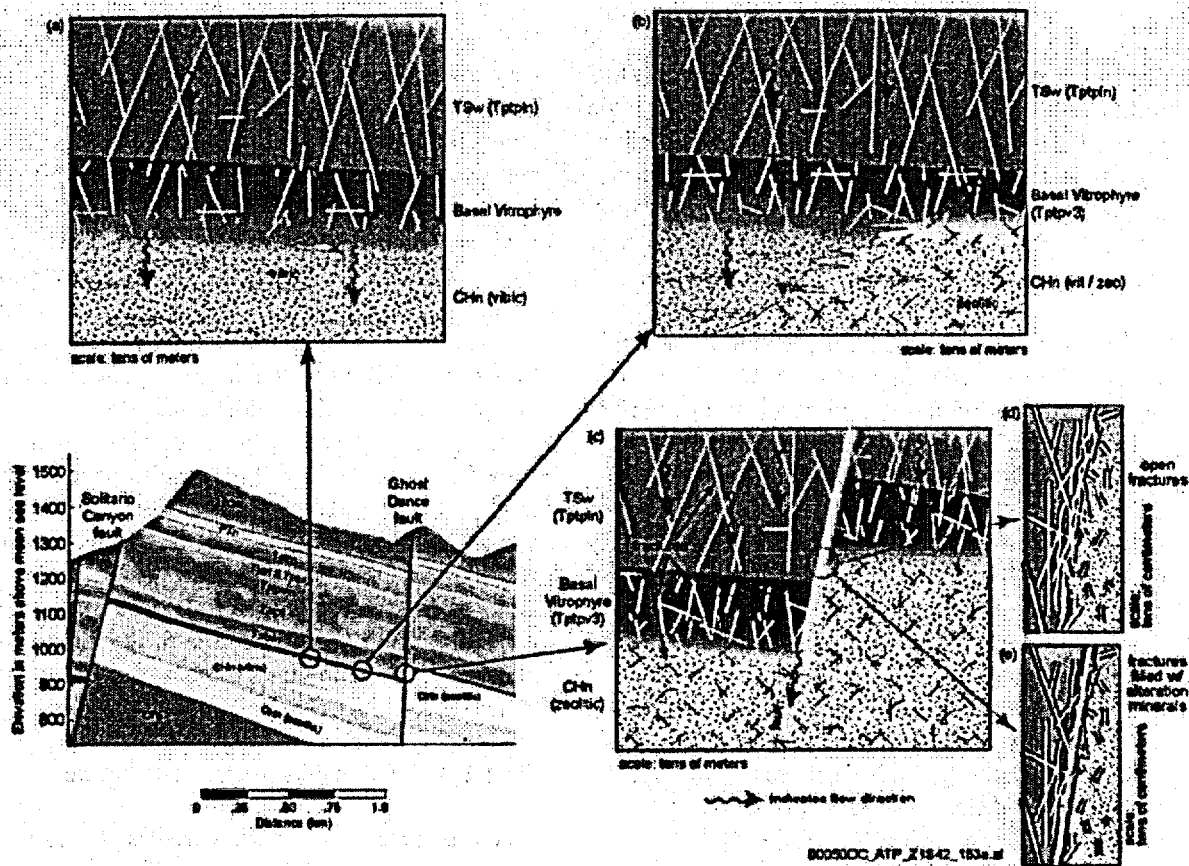


Figure 4-7. Lithostratigraphic Transitions and Flow Patterns at the TSw-CHn Interface

(a) Schematic with minimal alteration at the TSw-CHn contact showing a transition from fracture-dominated to matrix-dominated flow. (b) Schematic with variable alteration at the TSw-CHn contact showing flow diversion around zeolites. (c) Schematic with prevalent alteration at the TSw-CHn contact showing lateral flow within the perched-water body, followed by fault-dominated flow. (d) Schematic detail of open fractures, which may represent a fast flow pathway. (e) Schematic detail illustrating fractures filled by deposits of alteration minerals, which could create a flow barrier. Source: CRWMS M&O 2000c, Figure 3.2-5.

fracturing (because of increased welding), yet little or no alteration, giving them relatively higher permeabilities than the zeolitic tuffs (Flint, L.E. 1998, pp. 29 and 32).

The high storage capacity of the vitric (unaltered) CHn matrix will attenuate the rate of water movement through the unsaturated zone (Figure 4-7a). Where extensive mineralogic alteration has occurred—for example, at the TSw-CHn contact—the downward flux of water may exceed the rock's transmissive capacity, leading to ponding above the flow barrier and the formation

of perched water (Figure 4-7c). The presence of a low-permeability barrier to vertical flow can lead to lateral flow diversion, especially if the flow barrier is dipping and saturated moisture conditions (i.e., perched water bodies) exist above the barrier. Therefore, not all flow paths below the potential repository horizon are expected to be vertical. Lateral diversion of water at perching horizons may lead to flow focusing if the vertical flow barrier is intersected by a high-permeability feature, such as a fault, that could channel flow to the water table (CRWMS M&O 2000c, Sections 3.3.3.4 and 3.3.5).

#### 4.2.1.1.3 Effects of Major Faults

Different kinds of faults with varying amounts of displacement exist at Yucca Mountain (CRWMS M&O 2000c, Section 3.3.5). Fault hydrologic properties are variable and generally controlled by rock type and stratigraphic displacement. Because major faults have the potential to significantly affect the flow processes at Yucca Mountain, they are important features of the unsaturated zone.

A fault can act as a fast flow conduit for liquid water (Figure 4-7d). In this case, transient water flow may occur within a fault as a result of temporarily variable infiltration. Major faults cut through the PTn unit, possibly reducing the attenuating effect of the PTn on transient water flow. However, fast flow along major faults is expected to carry only a small amount of water and may not contribute significantly to the flow of water above the potential repository horizon in the unsaturated zone (see Section 4.2.1.3.1.1). Faults intercepting the perched water bodies, however, can correspond to significant vertical water flow if fault permeability is relatively high because of the locally saturated conditions existing in the surrounding rock (see Figure 4-7c) (CRWMS M&O 2000c, Sections 3.3.5 and 3.7.3.2).

If faults within the CHn are relatively permeable features, they may provide a direct flow pathway to the water table. This is particularly significant because radionuclides released from the potential repository could bypass zeolitic or vitric layers within the CHn unit, where they could be retarded by sorption. Conversely, faults might be considered a positive feature of the site if they divert water around waste emplacement drifts or prevent laterally flowing water from focusing at the area of waste emplacement.

Alternatively, a fault can act as a barrier for water flow (CRWMS M&O 2000c, Section 3.3.5). Where a fault zone is highly fractured, the corresponding coarse openings will create a capillary barrier for lateral flow. On the other hand, a fault can displace the surrounding geologic units such that a unit with low permeability abuts one with relatively high permeability within the fault zone. In this case, the fault will act as a permeability

barrier to lateral flow within the units with relatively high permeability. Montazer and Wilson (1984, p. 20) hypothesized that permeability would vary along faults, with higher permeability in the brittle, welded units and lower permeability in the nonwelded units where gouge or sealing material may be produced. While a fault sealed with gouge or other fine-grained material has much higher capillary suction (i.e., driving imbibition), it also has low permeability, retarding the movement of water.

Large lateral flow to the faults and/or focusing of infiltration near the fault zone on the ground surface are required to generate significant water flow in faults. Below the repository, low-permeability (zeolitic) layers in the CHn may channel some flow to faults that act as pathways to the water table. However, it is also possible that alteration of faulted rocks in the CHn and CFu causes the faults to be of low permeability (Figure 4-7e), slowing water movement from the TSw to the water table.

#### 4.2.1.1.4 Fracture-Matrix Interaction

Fracture-matrix interaction refers to flow and transport between fractures and the rock matrix (CRWMS M&O 2000c, Section 3.3.4). Owing to their different hydrologic properties, distinct flow and transport behavior occurs in each hydrogeologic unit. The extent of fracture-matrix interaction is therefore a key factor in assessing flow and transport processes in the unsaturated zone (BSC 2001a, Section 4.2.1).

#### 4.2.1.1.5 Seepage into Drifts

Potential seepage of water into waste emplacement drifts is important to the overall performance of the potential repository system. The corrosion of drip shields and waste packages, the mobilization of radioactive contaminants from breached waste packages, and the migration of radionuclides to a receptor location all depend on the distribution of water seepage into the emplacement drifts.

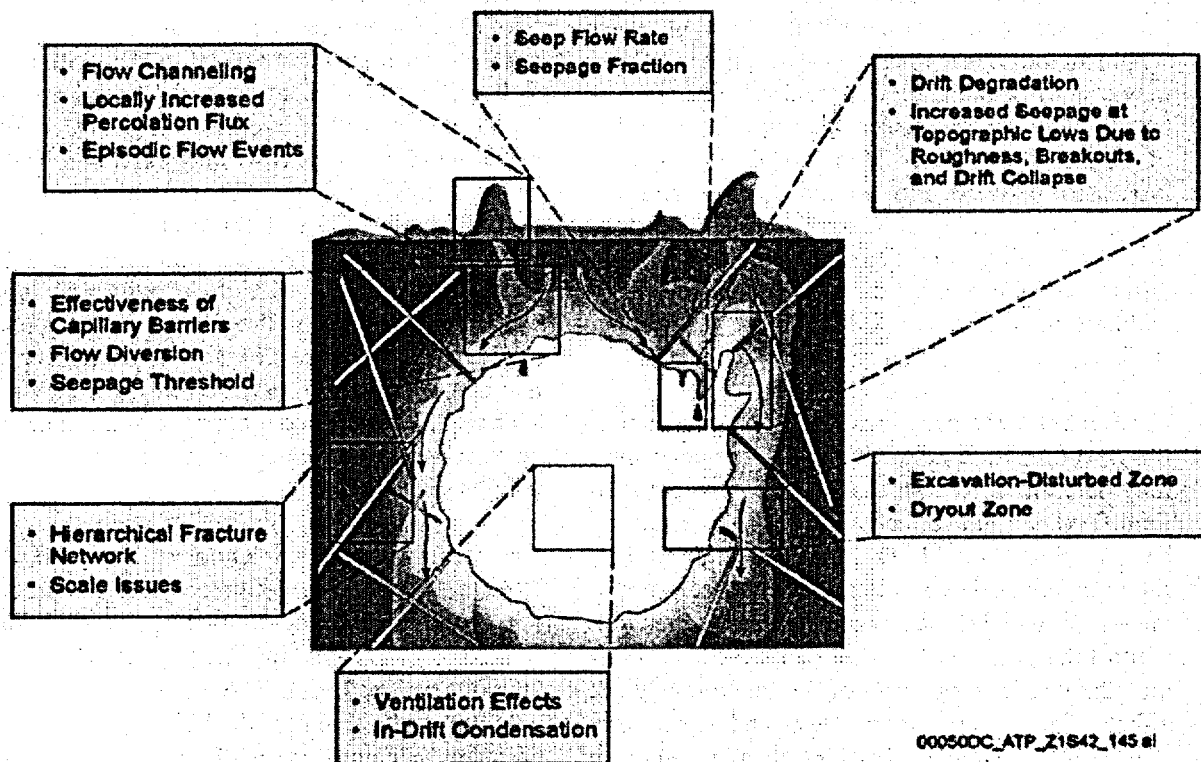
Seepage is defined as flow of liquid water into an underground opening, such as a waste emplacement drift or exploratory tunnel (CRWMS M&O

2000c, Section 3.9.1). Seepage does not include water vapor movement into openings or condensation of water vapor within openings. Seepage flux is the rate of seepage flow per unit area. The seepage percentage is the ratio of seepage flux to percolation flux in the surrounding host rock unit. Seepage threshold is defined as a critical percolation flux below which seepage into the opening is unlikely to occur. The seepage fraction is the proportion of waste packages that are located where drift seepage occurs. The drift shadow zone is a zone of reduced water saturation beneath the emplacement drift as a result of diversion of seepage around the drift opening by capillary forces.

Estimating seepage into underground openings excavated from an unsaturated fractured formation requires an understanding of processes on a wide range of scales (CRWMS M&O 2000c, Section 3.9.1). These scales range from the mountain-scale distribution of percolation flux, to the intermediate-scale channeling or dispersion of flow in an

unsaturated fracture network, to the small-scale capillary-barrier effect, to the microscale phenomena within fractures, and specifically at the drift wall. Moreover, the thermodynamic environment in the drift (temperature, relative humidity, ventilation regime, etc.) must be considered. Figure 4-8 illustrates and summarizes seepage-related processes. The factors affecting drift seepage highlighted in Figure 4-8 are outlined below.

**Capillary-Barrier Effect, Flow Diversion, and Seepage Threshold**—For unsaturated conditions, the seepage flux is expected to be less than the percolation flux because the drift opening acts as a capillary barrier (Philip et al. 1989). When percolating water encounters the opening, capillary forces retain the water in the rock, preventing it from seeping into the drift. Water accumulates in the rock around the opening, and if the rock permeability is sufficient, the water flows around the drift opening. If the incident percolation flux is very high or the rock permeability is insufficient,



000500C\_ATP\_Z1842\_145 el

Figure 4-8. Schematic of Phenomena and Processes Affecting Drift Seepage  
Source: Adapted from CRWMS M&O 2000c, Figures 3.9-1 and 3.9-3.

complete water saturation occurs in the rock above the opening, and seepage occurs. The effectiveness of the capillary barrier to seepage is determined by the capillarity of fractures surrounding the drift and by the permeability and connectivity of the fracture network in the horizontal direction (BSC 2001a, Section 4.2.2). Note that even if seepage occurs, the seepage flux is generally less than the percolation flux unless flow is focused by fractures or other features. The seepage threshold indicates whether or not water seeps into the opening for a given average percolation flux in the surrounding rock. Seepage threshold behavior is controlled by drift geometry, fracture geometry, capillary properties of fractures, and the hydrologic properties of the fracture network (BSC 2001a, Section 4.2.2).

**Distribution of Percolation Flux, Flow Channeling, and Episodic Flow**—The magnitude and spatial distribution of percolating water in the potential repository host rock is the most important factor affecting seepage. The distribution of flow channels in the fracture network and the hydrologic properties of individual flowing fractures determine how seepage occurs (CRWMS M&O 2000c, Section 3.9.1). Depending on the flow of water within an individual channel, the seepage threshold may or may not be exceeded locally. This is important because seepage is sensitive to the magnitude of the percolation flux, which is moderated by flow processes between the ground surface and the potential repository horizon. For repository thermal loading conditions, the percolation flux will include downward flow of condensed water, in addition to water that infiltrates at the ground surface.

**Hierarchical Fracture Network**—The characteristics of the fracture network affect seepage because they determine the spatial distribution of percolation flux and the effectiveness of the capillary barrier (CRWMS M&O 2000c, Section 3.9.1). Intermediate-scale characteristics (between mountain-scale and drift-scale) of the fracture network control the potential focusing of flux in the unsaturated zone. Heterogeneity of the fracture network affects local percolation flux and, therefore, seepage. The capillary-barrier effect depends on the connectivity of the fracture network near drift openings and the capillary properties of individual

fractures. Small fractures and microfractures, if interconnected, can decrease seepage because they have sufficient capillarity to hold water, but (unlike the rock matrix) sufficient permeability for flow diversion around the openings.

**Drift Opening Geometry and Rock Surface Characteristics**—The shape and size of underground openings also affects the likelihood of seepage. Partial collapse of the opening because of rockfall can affect seepage. Analytical solutions demonstrating the impact of drift geometry on seepage were developed by Philip et al. (1989). In addition, the geometry of the rock roof in drift openings and the characteristics of the rock surface control processes that could lead to dripping of seepage onto the engineered barriers below.

**Ventilation, Evaporation, and Condensation**—Until permanent closure of the potential repository, the emplacement drifts will be ventilated. The resulting temperature and humidity conditions in the drift will determine evaporation and condensation effects. Evaporation at the drift wall will generally decrease droplet formation and dripping (Ho 1997a) and create a dryout zone around the drift. When relative humidity in the drift is kept well below 100 percent by ventilation, seepage of liquid water will decrease, while water vapor movement into the drift will increase. Seepage flux and the moisture from increased vapor influx will be effectively removed by ventilation. After the thermal period, the relative humidity in emplacement drifts may be high enough to support condensation within the drift and engineered barrier system whose thermal properties are such that their temperature may be below the dew point. This would mostly occur after the diminution of all or most of the waste heat and the cessation of drift ventilation.

**Excavation-Disturbed Zone and Dryout Zone Effects**—The capillary-barrier effect that produces seepage diversion around openings occurs within a limited region around the opening (CRWMS M&O 2000c, Section 3.9.1). The extent of this zone is approximately given by the height to which water rises on account of capillarity. It is probably smaller than the zone affected by the mechanical effects of excavation; therefore, these effects may

modify seepage behavior. Thermally induced stress changes may also cause changes in fracture permeability. These stress changes are currently under investigation in field-scale thermal testing at Yucca Mountain (BSC 2001a, Section 4.3.1.5). In addition, drift ventilation and heating will produce a dryout zone with associated dissolution and precipitation of minerals (CRWMS M&O 2000c, Section 3.9.1). The consequent alteration of hydrologic properties and its extent are also under investigation (BSC 2001a, Section 4.3.5).

**Design**—The layout and design of the potential repository and the engineered barrier system affect the probability of seepage water contacting waste packages. Orientation of the emplacement drifts with respect to natural fracturing and in situ stress directions affects the hydrologic behavior of the fracture network around the openings and the potential for rockfall that changes the drift geometry (see Section 2.3.4.1). Thermal loading controls temperatures, the duration and extent of dryout associated with heating, and the potential for coupled mechanical and chemical processes that can impact hydrologic properties of the host rock.

#### 4.2.1.2 Summary State of Knowledge

Site data characterizing the ambient unsaturated system at Yucca Mountain have been collected since the early 1980s (CRWMS M&O 2000c, Section 2.1). The data are of numerous types (e.g., lithology, rock hydrologic properties, mineralogy, temperature, geochemistry, climate/infiltration) collected from surface-based activities (e.g., geologic mapping, installation of vertical boreholes) as well as subsurface mapping, sampling, and in situ testing in excavated tunnels.

Data collection has focused mainly on near-surface units down to the potential repository horizon. Site characterization data gathered from surface-based studies (including vertical boreholes and mapped pavements) represent the upper hydrogeologic units (i.e., TCw, PTn, and TSw), which are more readily accessible than the deeper units (i.e., the CHn and CFu) in the unsaturated zone. Exploratory tunnels excavated within Yucca Mountain, allowing scientists to collect large amounts of many different types of data, transect those layers

above the lowest lithostratigraphic unit within which a repository would be constructed (i.e., the lower nonlithophysal unit of the TSw).

The discussion that follows summarizes the results of studies that collected many different types of data, including:

- Climate and infiltration data
- Geologic data
- Pneumatic data
- Matrix properties
- Fracture properties
- Fault properties
- Evidence for fracture flow
- Evidence for flow attenuation in the matrix
- Field observation of fracture-matrix interaction
- Mineralogic and perched water data
- Geochemical and isotopic field measurements
- Seepage data information from studies of natural analogues to Yucca Mountain.

#### 4.2.1.2.1 Climate and Infiltration Data

The southwestern United States is characterized by dry climates with evaporation exceeding annual precipitation. The dry climates are divided into an arid (or desert) type and a semiarid (or steppe) type from annual temperature and precipitation considerations (Moran et al. 1997, pp. 438 to 443; Trewartha and Horn 1980, pp. 221 to 229). For Yucca Mountain's mean annual air temperature of approximately 17°C (63°F) (USGS 2000b, Section 6.4.2), the climate is arid if the precipitation is less than 243 mm (9.6 in.) per year and is semiarid if the precipitation is between 243 mm (9.6 in.) and 486 mm (19.1 in.) per year, based on a modified Köppen climate classification scheme (Trewartha and Horn 1980, p. 228). Seasonal variations and atmospheric conditions can be used to further modify and refine the classifications. The climate boundary definition depends on the classification scheme used and is best viewed as convenient approximation only (Trewartha and Horn 1980, p. 223).

Present day climate data have been collected in and around Yucca Mountain since 1988. The climate is

dry and arid. The average annual potential evapotranspiration rate is approximately six times greater than the average precipitation rate (USGS 2000b, Section 6.1.4). On average over the unsaturated zone flow and transport model area, Yucca Mountain receives about 190 mm (7.5 in.) of rain and snow per year; nearly all the precipitation (above 95 percent) either runs off or is lost to evaporation (USGS 2000b, Table 6-9; CRWMS M&O 2000c, Table 3.5-2). The precipitation increases with elevation, so the higher portions of the mountain receive more precipitation than adjacent valleys. Over a larger area that includes valleys and flat lands around the Yucca Mountain model area, the average precipitation value can be lower (Hevesi et al. 1994, p. 2520, Figure 1).

Yucca Mountain is located in the rain shadow caused by the Sierra Nevada and other mountain ranges, which limits the number of storms that can generate precipitation throughout the Great Basin (USGS 2000a, Section 6.1). During the winter, regional precipitation comes from the occasional intrusion of frontal storms associated with polar fronts; during the summer, precipitation comes from the regular intrusion of hot, dry, subtropical high-pressure weather systems. Local vegetation on all but the highest mountains is limited by the poor soils and the amount of available water. The vegetation that grows there typically uses most of the available precipitation that is not removed by evaporation or runoff. Therefore, infiltration of precipitation from the surface into the underlying rock is modest and commonly associated with wet years that may be linked to El Niño cycles.

The climate study also evaluated the long-term records of analogue sites, such as calcite dating data from Devils Hole (Winograd et al. 1992) and microfossil records from Owens Lake (Forester et al. 1999, pp. 14 to 18). Geological information indicates that the regional climate has changed over the past million years and that long-term average precipitation (which reflects wetter glacial and monsoonal cycles in the past) is greater than modern conditions. Future climate scenarios use available climate data from wetter analogue sites in western states (CRWMS M&O 2000b, Section 6.4; USGS 2000a, Section 6.6.2).

Studies of past climates indicate that the climate oscillates between glacial and interglacial periods. The current climate is typical of interglacial periods, although paleoclimate records suggest that the present interglacial period is hotter and drier than some earlier interglacial periods. In contrast with the current climate, periods of more extensive glaciation have dominated the long-term climate for most of the past 500,000 years. Glacial periods characterized by wetter and colder conditions than now exist have prevailed during approximately 80 percent of that time (USGS 2000a, Section 6.2).

No glaciation has occurred in the Yucca Mountain region during these glacial periods; instead, the region has experienced climates characterized by increased rainfall and cooler temperatures (USGS 2000a). During glacial periods, winter storm activity is more common because the polar front moves far south of its average present-day position. Subtropical high-pressure systems in the summer are less frequent to nonexistent. Local vegetation receives more water from the atmosphere and average air temperatures are colder, leading to lower plant uptake rates and higher soil infiltration rates than today. The primary form of annual precipitation shifts from summer rain to winter precipitation (often snow). Wetlands are common on the valley floors, and local streams are active during all or most of the year. Large closed basins, such as Owens Valley and Death Valley, contain lakes. Although glacial climates are generally characterized by cooler temperatures and higher precipitation, particular glacial periods vary. Some are relatively warm and wet, whereas others are cold and may be either wet or dry.

In *Future Climate Analysis* (USGS 2000a, Section 6.6), three climatic states are forecast: (1) the current arid climate, (2) an interglacial monsoon climate of warm but wetter conditions, and (3) a cooler, wetter, glacial-transition climate typical of glacial conditions over much of the past several hundred thousand years. Within each of these general categories, conditions may vary from year to year and over decades and centuries. Monsoon climates would vary from climates like present-day Yucca Mountain to somewhat wetter climates like Nogales, Arizona, or Hobbs, New Mexico. Glacial-transition climates would likely range from condi-

tions like the present-day central Great Basin (in central Nevada) to cooler conditions like the climate near Spokane, Washington. None of the likely future climates for Yucca Mountain is characterized by much larger annual precipitation rates at least for times on the order of 10,000 years. However, the cooler temperatures and decreased plant uptake of water would allow more water to infiltrate into Yucca Mountain during a glacial-transition climate.

The infiltration study at Yucca Mountain was initiated in 1984. To date, the infiltration study has used nearly 100 shallow boreholes located on ridgetops, on sideslopes, on stream terraces, and in/across stream channels to measure the changes in water-content profiles in response to precipitation and snowmelt events (Flint, L.E. and Flint 1995; Flint, A.L. et al. 1996, pp. 60 to 63; USGS 2000b, Sections 6.3.4 and 7.1). Weekly or monthly measurements were collected from 1984 through 1995. Four washes were instrumented for run-on and runoff measurements. Water-balance calculations from precipitation, evapotranspiration, run-on, and runoff along washes are used to derive the infiltration flux values over the ridge top, side slopes, and stream channels. Areas with exposed bedrock and no soil cover promote greater infiltration compared to areas with soil covers that have substantial storage capacity for excess water.

Deep soils and vegetation inhibit infiltration by allowing evaporation and plant transpiration to remove water. Steep slopes encourage rapid runoff, also limiting infiltration (USGS 2000b, Section 6.1.2). For these reasons, most infiltration probably occurs in areas with low slopes and relatively shallow soil cover, as is common at the higher elevations on the northern part of Yucca Mountain. Analyses of groundwater chemistry (especially oxygen and hydrogen isotopic compositions) indicate that much of the infiltration at Yucca Mountain occurs during the winter. During the cool rainy season, evaporation rates are low because of low temperatures, and low-intensity but sustained precipitation can saturate shallow soil or cover the soil with snow. Summer storms are more intense than winter rains, but higher runoff and evaporation combine to limit summer infiltration.

The infiltration distributions for different climate states are used as upper boundary conditions for the unsaturated zone flow model and TSPA models. A numerical, water-balance, infiltration model was developed for the Yucca Mountain area, including the area of the three-dimensional, site-scale unsaturated zone flow model. The infiltration model uses physiographic and hydrologic information and a daily precipitation record to calculate daily values of infiltration using a water-balance approach. The infiltration model was calibrated first by comparison to the total water-content change in the soil profile in neutron boreholes during 1984 to 1995 and then by comparison of model-simulated streamflow to discharge measures at stream-gauging sites on Yucca Mountain during 1994 to 1995 (USGS 2000b, Section 6.8.2).

The numerical infiltration model was used to simulate lower-bound, mean, and upper-bound infiltration associated with three climate scenarios determined to be pertinent to performance of the potential repository: modern, monsoon, and glacial-transition (USGS 2000b, Section 6.9). The modern, or present-day, climate conditions are expected to prevail for about the next 400 to 600 years. Monsoon climate conditions, with wetter summers than the modern climate, are expected to prevail for the following 900 to 1,400 years. Glacial-transition climate conditions, with cooler air temperatures and higher annual precipitation than the modern climate, are expected to begin in about 2,000 years and continue throughout the remainder of the 10,000-year period specified for performance analyses.

Average precipitation and average infiltration rates over the unsaturated zone flow model area are presented in Section 4.2.1.3.3. The distributions of mean present-day, monsoon, and glacial-transition infiltration are also shown in Section 4.2.1.3.1.3 in Figure 4-25.

#### 4.2.1.2.2 Geologic Data

Depth below ground surface to the water table ranges from approximately 500 to 800 m (1,600 to 2,600 ft) within the potential repository area. The higher-temperature repository layout has the waste emplacement drifts at a depth ranging from about

200 to 500 m (660 to 1,600 ft) below ground surface and between about 210 and 390 m (690 and 1,300 ft) above the water table. These distances were estimated using the *Site Recommendation Subsurface Layout* (BSC 2001d, Table V-1), topographic data from the *Geologic Framework Model (GFM 3.1)* (CRWMS M&O 2000bs, Section 4.1), and water table elevations (USGS 2000c, Table I-1; CRWMS M&O 2000g, Table 3).

Some of the most important site characterization data come from surface-based vertical boreholes. The first deep boreholes at Yucca Mountain were used to define site lithostratigraphy, to locate the water table, to collect core for rock-property analyses, and to test in situ borehole monitoring techniques. The lithostratigraphic description of the tuff units has been refined with coring, mapping, and geophysical logging data from additional surface-based boreholes and confirmed by data collected in the underground drifts (i.e., the Exploratory Studies Facility and Cross-Drift tunnels). Figure 4-9 illustrates the locations of selected deep boreholes, the underground Exploratory Studies Facility, and the Enhanced Characterization of the Repository Block (ECRB) Cross-Drift. A summary of the geology of Yucca Mountain is presented in Section 1.3.

The division of tuff units into members, zones, and subzones is based on variations in degree of welding (compaction and fusion at high temperatures), abundance of lithophysae (cavities formed by bubbles of volcanic gases trapped in the tuff matrix during cooling), depositional features, crystal content, mineral composition, pumice and rock fragment abundance, and fracture characteristics. These features of site lithostratigraphy are described by Moyer et al. (1996, pp. 7 to 54) and Buesch et al. (1996, pp. 4 to 16) and in the *Unsaturated Zone Flow and Transport Model Process Model Report* (CRWMS M&O 2000c, Section 3.2).

Early geologic mapping of Yucca Mountain was done by Scott and Bonk (1984) and was later updated and refined by Day, Potter et al. (1998) to include additional small faults at the land surface (such as the Sundance fault in the potential repository block) (Spengler et al. 1994, pp. 9 to 11). The

fracture patterns in the bedrock were also mapped in pavement studies (i.e., with thin soil covers removed) and in shallow-pit studies of fractures exposed on the pit walls. Mapping and sampling data along transects, especially along washes and valleys, together with logs and core samples from deep boreholes and regional geophysical surveys, were used to construct early stratigraphic and structural models. Current three-dimensional geologic models rely heavily on surface-based vertical boreholes, as well as the Day, Potter et al. (1998) geologic map (CRWMS M&O 2000bs, Section 4). These geologic models are used as a framework for development of numerical models for simulating unsaturated zone flow and transport processes (CRWMS M&O 2000br).

#### 4.2.1.2.3 Pneumatic Data

Several deep boreholes at Yucca Mountain have been instrumented in the unsaturated zone and continuously monitored to record changes in pneumatic pressure and gas flow with depth in response to changes in barometric pressure of the atmosphere (CRWMS M&O 2000b, Section 8.4.2). Changes in atmospheric pressure are transmitted very rapidly throughout the TCw because of its high fracture permeability. In contrast, the PTn significantly attenuates the atmospheric-pressure signal and imposes a time delay to signal arrival because of higher porosity and water content and much lower fracture density and bulk permeability than the TCw. In general, attenuation of the atmospheric-pressure signal across the TSw is negligible and pressure signals are transmitted nearly instantaneously throughout most of the entire vertical section of the TSw. Nearly all the pressure data from the TSw indicate that the fractures within the TSw apparently are very permeable and highly interconnected within both the lithophysal and nonlithophysal units. In situ pressure records indicate that essentially all of the remaining barometric signal is attenuated by the CHn, primarily due to low permeability and the presence of perched-water zones.

When the Exploratory Studies Facility was excavated, the effects on in situ pneumatic pressure were carefully monitored to determine how the overall gaseous-phase system in the unsaturated

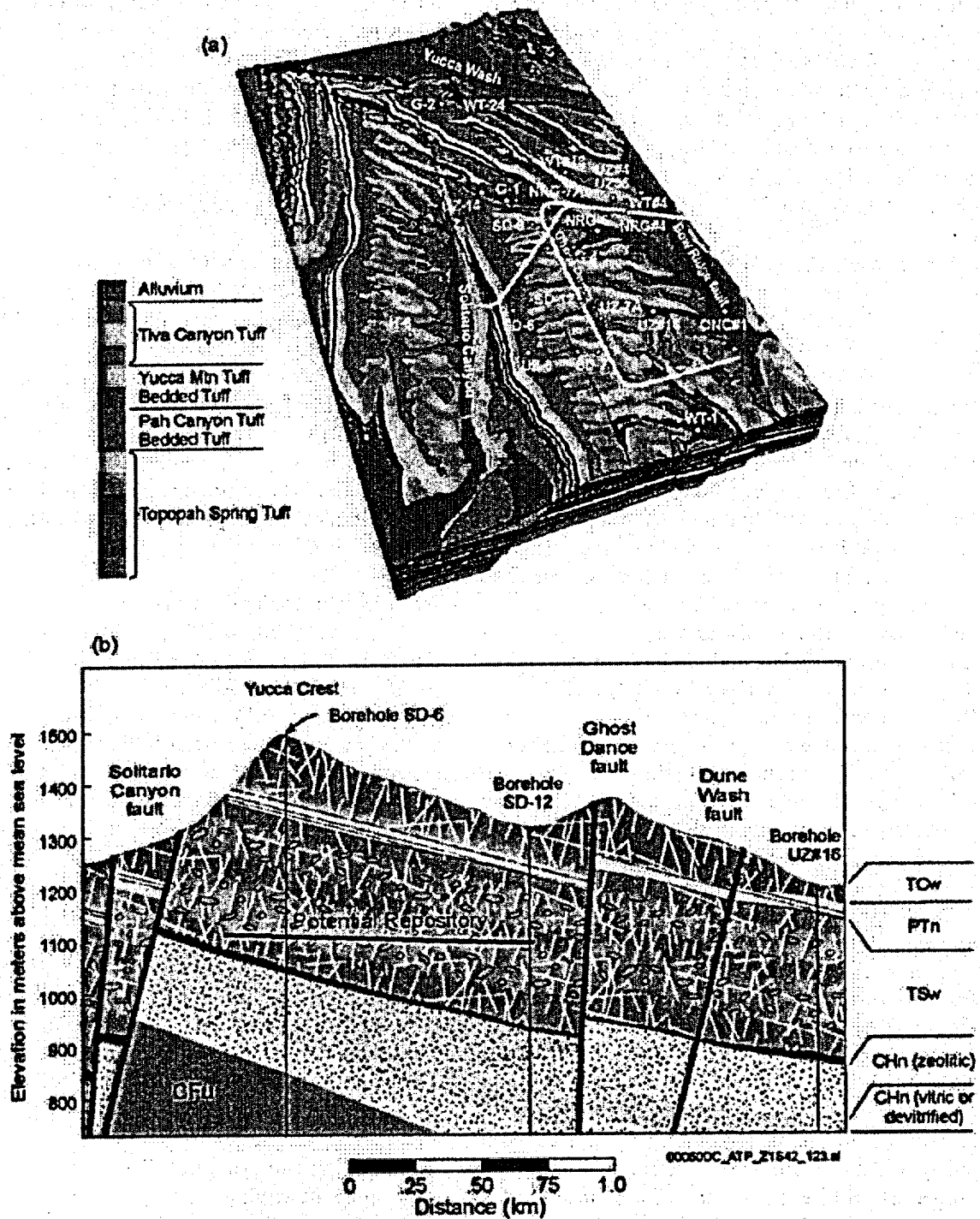


Figure 4-9. Yucca Mountain Site-Scale Geology  
(a) Three-dimensional perspective with borehole, Exploratory Studies Facility, and ECRB Cross-Drift locations.  
(b) View along an east-west cross section, showing locations of boreholes SD-6, SD-12, and UZ#16. Source: Adapted from CRWMS M&O 2000c, Figures 2.1-2 and 3.2-1.

zone was affected by direct exposure of deeply buried rock units to atmospheric pressure by way of the tunnel. Pneumatic monitoring data indicate that some faults, such as the Drill Hole Wash fault, transmit pneumatic-pressure signals over distances of several hundred meters nearly instantaneously. The data also indicate that gas-phase flow from the atmosphere into the TSw was essentially short-circuited when the Exploratory Studies Facility penetrated the PTn, locally removing this pneumatic barrier (CRWMS M&O 2000b, Section 8.4.2).

#### 4.2.1.2.4 Matrix Properties

Rock matrix hydrogeologic properties (including porosity, bulk density, particle density, water content, saturated hydraulic conductivity, moisture retention characteristics, and saturation) have been measured for several thousand core samples recovered from 8 deep boreholes and over 30 relatively shallow boreholes. The deep boreholes penetrate to at least the bottom of the TSw, while the shallow boreholes penetrate only to the top of the TSw. Collection, processing, and preliminary analyses of the core data are described by Flint, L.E. (1998). Results show that nonwelded tuffs (i.e., PTn and CHn) usually have large matrix porosities (typically 30 to 50 percent), while the densely welded tuffs (i.e., TCw and TSw) tend to have greatly reduced pore space (generally less than 15 percent matrix porosity). Because of variations in capillary strength, liquid saturations are usually lower in the nonwelded tuffs than in the welded tuffs, unless the nonwelded tuffs contain significant amounts of clay or zeolite. Mean matrix permeability ranges from about  $10^{-15}$  to  $10^{-12}$  m<sup>2</sup> ( $10^{-14}$  to  $10^{-11}$  ft<sup>2</sup>) for the unaltered nonwelded tuffs and from about  $10^{-18}$  to  $10^{-15}$  m<sup>2</sup> ( $10^{-17}$  to  $10^{-14}$  ft<sup>2</sup>) for the welded and altered (i.e., zeolitized) nonwelded tuffs.

Numerical models of flow and transport use matrix property data to estimate effective hydrogeologic properties for each layer within the model. Upscaling of rock properties (particularly permeability) from core scale to mountain scale is required for the larger, three-dimensional numerical models. Upscaling is an adjustment to the estimate of the effective property when the property data are collected on one scale but the estimate

is intended for use in simulations and predictions on a much larger scale. Additional data from in situ water potential measurements are used to estimate moisture-retention characteristics. Collection and preliminary analysis of these data are described by Rousseau, Loskot et al. (1997, Section 4.2) and Rousseau, Kwicklis et al. (1999, pp. 143 to 151).

#### 4.2.1.2.5 Fracture Properties

Fracture data are very important to the characterization of unsaturated flow at Yucca Mountain. Fracture hydrologic properties are estimated using (1) permeability data from in situ air-injection tests conducted in four surface-based boreholes and boreholes in alcoves of the Exploratory Studies Facility; (2) porosity data from gas tracer tests in boreholes in Alcove 5 of the Exploratory Studies Facility; and (3) fracture mapping from the Exploratory Studies Facility, ECRB Cross-Drift, and surface-based boreholes.

Air-injection testing is described by LeCain (1997, pp. 2 to 9; 1998, pp. 5 to 11) and Rousseau, Kwicklis et al. (1999, pp. 63 to 67) and in *In Situ Field Testing of Processes* (CRWMS M&O 2000bu, Section 6.1). The data show the TCw unit as having the highest mean fracture permeabilities (as high as  $10^{-10}$  m<sup>2</sup> or  $10^{-9}$  ft<sup>2</sup>) and the CHn as having the lowest mean fracture permeabilities (on the order of  $10^{-14}$  m<sup>2</sup> or  $10^{-13}$  ft<sup>2</sup>). Mean values of fracture permeability within PTn and TSw layers are approximately  $10^{-13}$  and  $10^{-11}$  m<sup>2</sup> ( $10^{-12}$  and  $10^{-10}$  ft<sup>2</sup>), respectively. As stated previously in this section, most data available is from testing at the upper hydrogeologic units. There are limited air-permeability data for units below the TSw. Air-permeability data for the CHn are available from a single sampled interval in borehole UE-25 UZ#16. This interval lies within a zeolitically altered portion of the upper CHn.

Detailed line surveys and full peripheral mapping of fracture networks have been conducted along the Exploratory Studies Facility and ECRB Cross-Drift by Barr et al. (1996, pp. 133 to 135) and Albin et al. (1997, Appendix 1) (also see data sources listed in CRWMS M&O 2000c, Attachment I, Table I-4). Additional features have been mapped, including the observations of an intensely

fractured zone in the southern part of the Exploratory Studies Facility main drift (Buesch and Spengler 1998, p. 19) and several recently discovered faults that show no surface expression in the western part of the ECRB Cross-Drift (see data sources listed in CRWMS M&O 2000c, Attachment I, Table I-4). The fracture density distributions from geologic mapping and geophysical imaging are illustrated in Figure 4-10. Nonwelded tuffs typically have few fractures (less than 1 per meter), while the densely welded tuffs generally have abundant fractures (approximately 1 to 4 per meter) (CRWMS M&O 2000bt, Section 6.1.2.3). Each lithostratigraphic unit generally has its own fracture network characteristics (fracture spacing, intensity, and connectivity) that are controlled by variations in lithology and degree of welding (Rousseau, Kwicklis et al. 1999, p. 23). Fracture characteristic data are used to estimate the potential for, and distribution and amount of, fracture flow within the welded and nonwelded layers in the unsaturated zone. It is important to reiterate that the exploratory tunnels do not penetrate units below the TSw; therefore, fracture characteristics below the TSw are available only from deep boreholes. There are limited fracture data from units below the TSw. For the CHn, vitric and zeolitic fracture frequencies are available from two boreholes (USW SD-12 and USW NRG-7a). Fracture frequencies and properties have not been determined for the CFu unit, which underlies the CHn and is present in the unsaturated zone only along the western margin and in the southwestern part of the repository area (CRWMS M&O 2000c, Section 3.2.2.5, Figure 3.2-3).

Some fracture property data were considered but not used in unsaturated zone flow modeling (CRWMS M&O 2000c, Section 3.6.3.2). In particular, fracture frequency data from the surface of the mountain, measured on outcrops and at the Large Block Test area, are not considered representative of fracture frequencies in the deep subsurface because unloading, or the absence of overburden at the surface, is likely to produce enhanced fracturing. Permeability data from air-injection testing in four Exploratory Studies Facility niches were not used because the scale on which the measurements were made was 0.3 m (1 ft); thus, the data may not be representative of the fracture perme-

ability at the scale of interest. The scale of the air-injection test data that are used for flow modeling is from 1 to 12 m (3 to 40 ft) (CRWMS M&O 2000bt, Section 6.1.1.1).

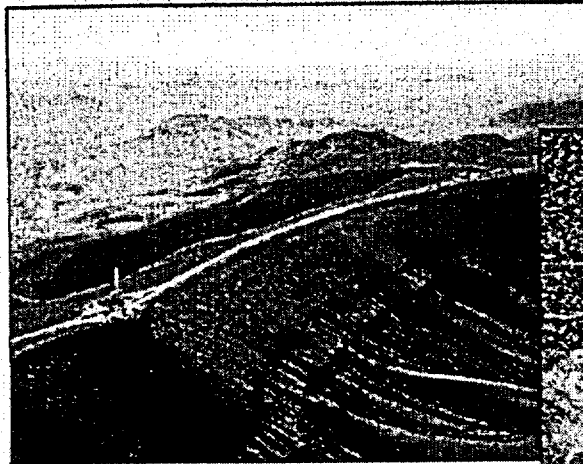
#### 4.2.1.2.6 Fault Properties

Fault permeability measurements are described by LeCain (1998, pp. 19 to 22). Direct measurements of fault-specific properties have been conducted using air-injection tests in Exploratory Studies Facility Alcoves 2 and 6 (the Bow Ridge Fault Alcove and the North Ghost Dance Fault Access Drift, respectively). Analyses of cross-hole tests run in the Bow Ridge Fault Alcove (LeCain 1998, p. 21) and the North Ghost Dance Fault Access Drift (LeCain et al. 2000, Table 8) give estimates of fracture permeability in the TCw and TSw fault layers, respectively. These data indicate that, within the welded units, the fractures in the faults are more permeable and porous than the fractures in the formation (or nonfaulted rock).

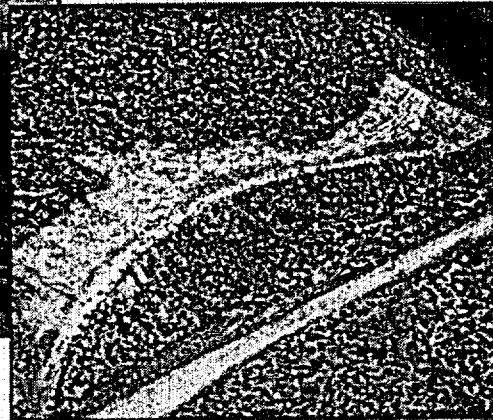
#### 4.2.1.2.7 Evidence for Fracture Flow

Currently, the estimates of percolation flux at Yucca Mountain range from 1 to 10 mm/yr (0.04 to 0.4 in./yr). Given the low matrix permeabilities of the welded tuffs (i.e., TCw and TSw), a large fraction of the percolation flux in the welded units must travel through fracture networks. This conceptual model is supported by the presence of relatively high fractional abundances of chlorine-36 measured in TCw samples from boreholes (CRWMS M&O 2000bv, Section 6.6.3). The source of the elevated (bomb-pulse) chlorine-36 has been attributed primarily to nuclear testing in the Pacific Ocean conducted in the 1950s, and its occurrence in the TCw indicates the presence of fast pathways for water flow within the unit (CRWMS M&O 2000bq, Section 6.1.2).

Episodic infiltration pulses are expected to move rapidly through the fracture system of the TCw unit with little attenuation by the rock matrix. This conceptual model of minimal flow attenuation by the densely welded matrix is partially supported by pneumatic data for the TCw unit (CRWMS M&O 2000bq, Section 6.1.2), which show little attenuation of the barometric signal in monitoring



(a) Drilling of Borehole SD-8 on the Crest of Yucca Mountain



(b) Pavement Cleared for Ghost Dance Fault Mapping

**Objectives:**

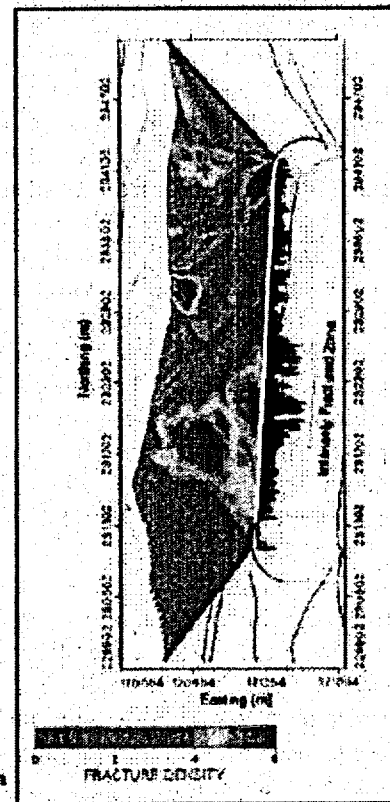
- Determine lithology and structural features of tuff units.
- Evaluate distribution of fractures and faults.

**Approaches:**

- Map features on bedrock, in trenches, and along Exploratory Studies Facility drifts.
- Conduct geophysical logging along boreholes.
- Deploy geophysical tomographic imaging techniques on the surface and in underground drifts.

**Results:**

- Refined geological maps of bedrock, washes, and faults.
- Improved geological framework of tuff layers and fault offsets.
- Detailed line surveys and full peripheral maps along drifts.
- Interpreted fracture density distributions between surface and underground drifts.



(c) Fracture Density Distributions by Detailed Line Survey and Seismic Tomograph

000530C\_ATF\_Z1542\_Fig-124b.ai

Figure 4-10. Geological and Geophysical Studies on the Surface and along the Exploratory Studies Facility  
Source: CRWMS M&O 2000c, Figure 2.2-1.

boreholes relative to the barometric signal observed at the land surface (Rousseau, Kwicklis et al. 1999, p. 89).

Other evidence for fracture flow comes from calcite-coating data, which are signatures of water flow history and indicate that most of the deposition is found within the fractures in the welded units (Paces, Neymark, Marshall et al. 1998, p. 37). As discussed in *Conceptual and Numerical Models for UZ Flow and Transport* (CRWMS M&O 2000bq, Section 6.1.2), carbon-14 ages of the perched water bodies below the TSw unit also suggest fracture-dominant flow within the TSw. These ages range from approximately 3,500 to 11,000 years (Yang, Rattray et al. 1996, p. 34), which is much younger than if the major path for water flow within the TSw was through the matrix (CRWMS M&O 2000bq, Section 6.1.2).

Field testing within Exploratory Studies Facility alcoves and niches also supports prevailing fracture flow within welded units. Figure 4-11, for example, summarizes the results of liquid release testing in Alcove 6, located within the fractured, densely welded, middle nonlithophysal unit of the TSw.

#### 4.2.1.2.8 Evidence for Flow Attenuation in the Matrix

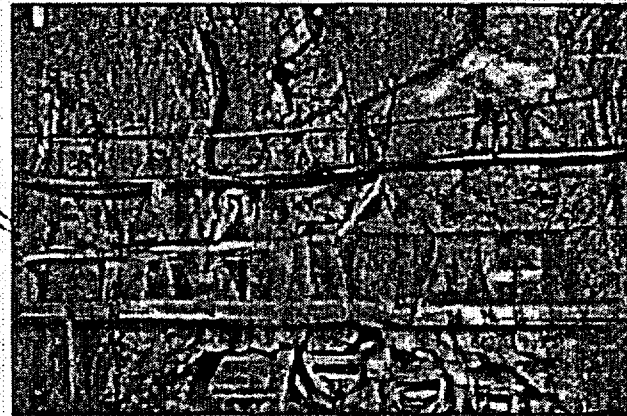
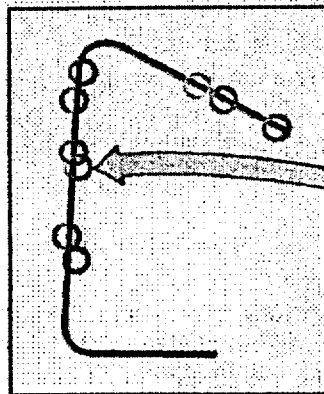
Liquid release tests conducted in Alcove 4 of the Exploratory Studies Facility, situated in nonwelded tuffs of the lower PTn, support the matrix flow-damping conceptual model of the PTn (CRWMS M&O 2000bu, Section 6.7). The Alcove 4 test bed includes a small fault within which tracer-tagged water was released, as illustrated in Figure 4-12. A mass-balance approach involving recovery of outflow in a slot was adopted. The matrix of the PTn effectively damped flow pulses along the fault. The data in Figure 4-12 show a slow decline in water intake rates with time. One explanation for the slow decline is the possible swelling of clays in the PTn layers and subsequent reduction of fault permeability. Another observation made during liquid release testing was that, with sequential wetting, detection of downgradient increases in saturation occurred faster (i.e., the wetting front moved faster with each liquid release test).

Geochemical data from the Exploratory Studies Facility also support the conceptual model of predominantly matrix flow through the PTn by showing a lack of widespread, elevated (bomb-pulse) chlorine-36 signatures at the base of the PTn (Fabryka-Martin, Wolfsberg, Levy et al. 1998).

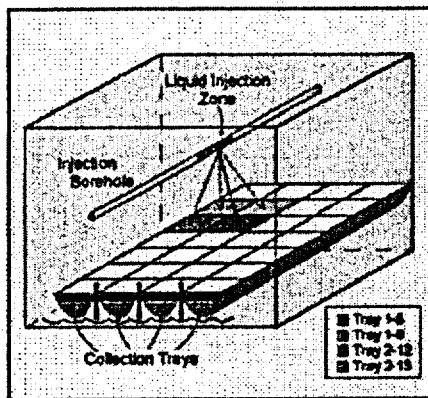
#### 4.2.1.2.9 Fracture-Matrix Interaction

Field observations show limited fracture-matrix interaction within welded units at Yucca Mountain. The chloride concentration data indicate that perched water is recharged mainly from fracture water, with a small degree of interaction with matrix water (CRWMS M&O 2000bq, Section 6.1.3). The small degree of interaction between fractures and the matrix at locations associated with geologic features is also suggested by the presence of bomb-pulse chlorine-36 (CRWMS M&O 2000bv, Section 6.6.3) at the potential repository level in the Exploratory Studies Facility. Studies by Ho (1997b, pp. 407 and 409) show that the match between simulations and observed matrix saturation data is improved by reducing the fracture-matrix interaction significantly.

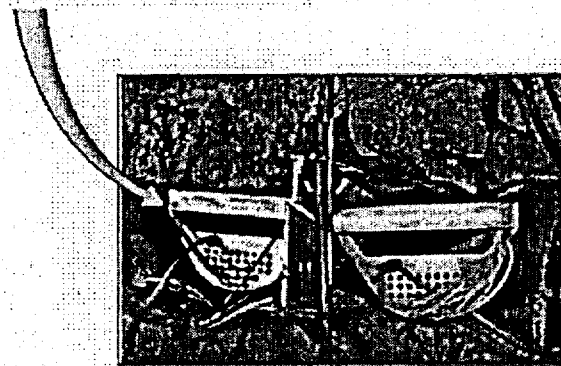
The concept of limited fracture-matrix interaction in welded tuff at the Yucca Mountain site is also supported by many other independent laboratory tests, as well as theoretical and numerical studies (CRWMS M&O 2000bq, Section 6.1.3). In a number of laboratory experiments without considering matrix imbibition, Glass et al. (1996, pp. 6 and 7) and Nicholl et al. (1994) demonstrated that gravity-driven fingering flow is a common flow mechanism in individual fractures. This can reduce the wetted area in a single fracture to fractions as low as 0.01 to 0.001 of the total fracture area (Glass et al. 1996, pp. 6 and 7), although the matrix imbibition can increase wetted areas of fingering flow patterns in individual fractures (Abdel-Salam and Chrysikopoulos 1996, pp. 1537 to 1538). A theoretical study by Wang and Narasimhan (1993, pp. 329 to 335) indicated that the wetted area in a fracture under unsaturated flow conditions is generally smaller than the geometric interface area between fractures and the matrix, even in the absence of fingering flow. This results from the consideration that liquid water in an unsaturated fracture occurs as saturated segments that cover



(a) Photograph of Alcove 6 Test Bed



(c) Schematic of Liquid Release Test



(b) Closeup of Trays on the Slot

**Objectives:**

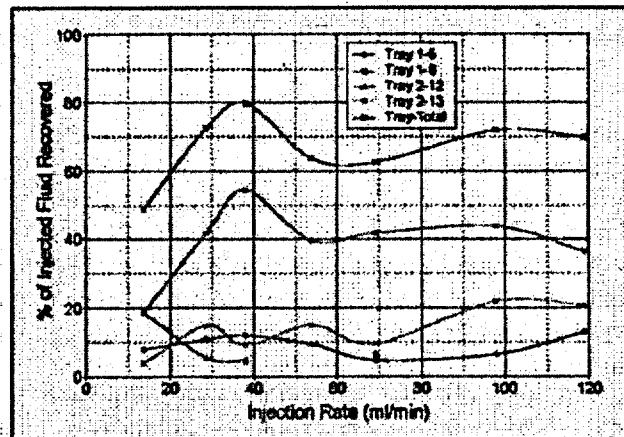
- Quantify fracture-matrix interaction and the fraction of fracture flow.

**Approaches:**

- Use a slot below boreholes to capture fracture flows.
- Estimate the fracture-matrix flow partitioning by mass balance.
- Use borehole sensors to detect wetting front arrivals.

**Results:**

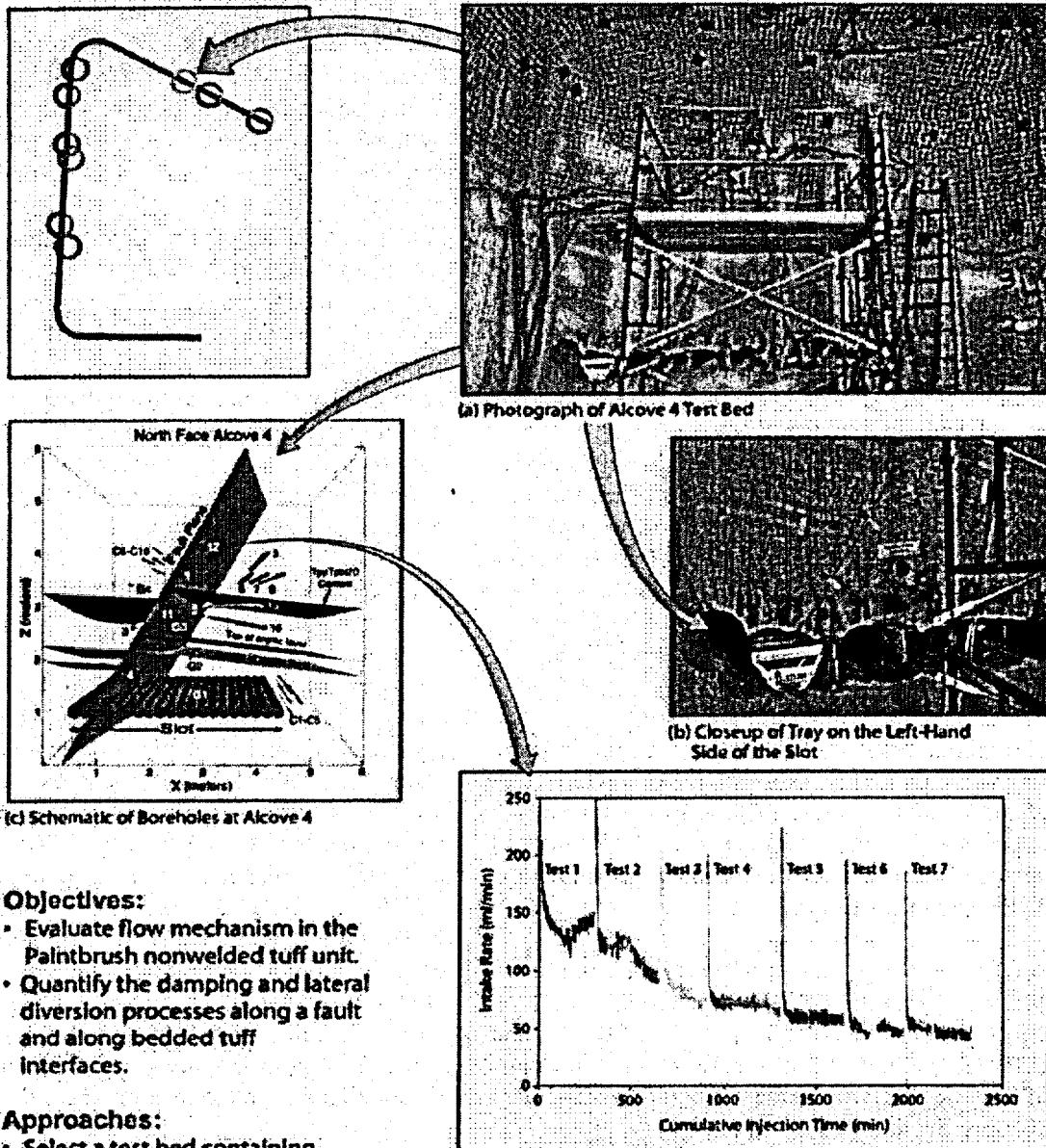
- A maximum of 80% of injected water was recovered for high-rate injection tests (i.e., 80% fracture flow).
- Out flows occurred in step increments which could be related to water stored in fracture flow paths.



(d) Water Collected in the Slot

000500C\_ATP\_21542\_Fig.128.a1

Figure 4-11. Fracture-Matrix Interaction Test at Alcove 6  
Sources: CRWMS M&O 2000c, Figure 2.2-6; CRWMS M&O 2000bu, Section 6.6.



**Objectives:**

- Evaluate flow mechanism in the Paintbrush nonwelded tuff unit.
- Quantify the damping and lateral diversion processes along a fault and along bedded tuff interfaces.

**Approaches:**

- Select a test bed containing bedded tuff layers (including an argillic layer), a fault, and a fracture.
- Release water under constant-head conditions to determine the intake rates.
- Monitor wetting front arrivals and measure potential changes in boreholes.

**(d) Water Intake Rate at PTn Fault**

**Results:**

- Water intake rate in the fault decreased as more water was introduced into the release zone.
- Clay swelling is one mechanism proposed to interpret the field data.
- Detection of downgradient increases in saturation occurred over shorter time intervals with each liquid release test.

000500C\_ATP\_21S42\_126a.ai

Figure 4-12. Paintbrush Fault and Porous Matrix Test at Alcove 4  
Sources: CRWMS M&O 2000c, Figure 2.2-7; CRWMS M&O 2000bu, Section 6.7.

only a portion of the fracture-matrix interface area. Liu et al. (1998, p. 2645) suggested that in unsaturated, fractured rocks, fingering flow occurs at both a single fracture scale and a connected fracture-network scale, which is supported by the field observations from the Rainier Mesa site (see Section 4.2.1.2.13) and by a numerical study of Kwicklis and Healy (1993). They found that a large portion of the connected fracture network played no role in conducting the flow. Studies have also shown that fracture coatings can either reduce or increase the extent of fracture-matrix interaction. Thoma et al. (1992) performed experiments on coated and uncoated tuff fractures and observed that the low-permeability coatings inhibited matrix imbibition considerably. In contrast, fracture coatings may in some cases increase the fracture-matrix interaction when microfractures develop in the coatings (Sharp et al. 1996, p. 1331).

#### 4.2.1.2.10 Mineralogic and Perched Water Data

The spatial distributions of vitric and zeolitic material within the CHn, along with the characterization of the basal vitrophyre (Ttpv3) of the TSw, are important for understanding the distribution of perched water and for determining potential flow paths for radionuclides.

Perched water has been encountered in a number of boreholes (e.g., USW UZ-14, USW NRG-7a, USW SD-7, USW SD-9, USW SD-12, and USW G-2) at the base of the TSw and above units of zeolitic tuff within the CHn (CRWMS M&O 2000bw, Sections 6.2.1 and 6.2.2).

The spatial distribution of low-permeability zeolites has been modeled using mineralogic and petrologic data from several boreholes and is presented in the Integrated Site Model (ISM3.1) of Yucca Mountain (CRWMS M&O 2000i, Section 3.4). Figure 4-13 shows the modeled distribution of zeolites for layers within the lower TSw (Ttpv3 and Ttpv2) and the upper CHn (Ttpv1 through Tcpu). Areas with less than or equal to 3 percent zeolite by weight are considered vitric, or unaltered. The figure shows that zeolites within the CHn are prevalent in the northern and eastern portion of the model domain. The areal extent of

the vitric region diminishes with depth and is considered to be largely confined to the fault block bounded in the north and east by the Sundance and Ghost Dance faults, respectively, and in the west by the Solitario Canyon fault. The northern half of the potential repository area is underlain by predominantly zeolitic CHn, while the southern half is underlain by the predominantly vitric upper portion of the CHn. However, below the vitric CHn (yet occurring above the water table) are nonwelded portions of the Prow Pass, Bullfrog, and Tram tuffs that are pervasively altered to zeolites. Thus, there is no evidence to support a model that includes a direct vertical pathway from the potential repository horizon to the water table that does not intersect zeolitic units, except, perhaps, within fault zones.

#### 4.2.1.2.11 Geochemical and Isotopic Field Measurements

Samples have been collected in boreholes and along the Exploratory Studies Facility for geochemical and isotopic measurements. Pore water is obtained by physical extraction from samples of tuff and used for chemical analyses and age dating. Measurements of total dissolved solids and chloride concentration in pore waters are mainly available for nonwelded tuff samples, which generally yield sufficient amounts of water by compression for chemical analyses (Yang, Yu et al. 1998, pp. 6 to 7). These pore waters tend to be more concentrated in dissolved solids than water flowing in fractures, which indicate that the percolation flux in the rock matrix is limited.

Chemical composition, including the total dissolved carbon dioxide concentration, is measured in pore water samples to determine the origin of calcite and amorphous silica solids found in the unsaturated zone and to characterize the evolution of carbonate as waters percolated downward. Ion-exchange reactions along flow paths generally increase the abundance of cations like calcium and strontium with depth in the tuff units. Deviation from the general trend of geochemical evolution with depth provides information about the effects of faults and other structural features. Strontium participates in ion-exchange with zeolites, and concentrations can be significantly

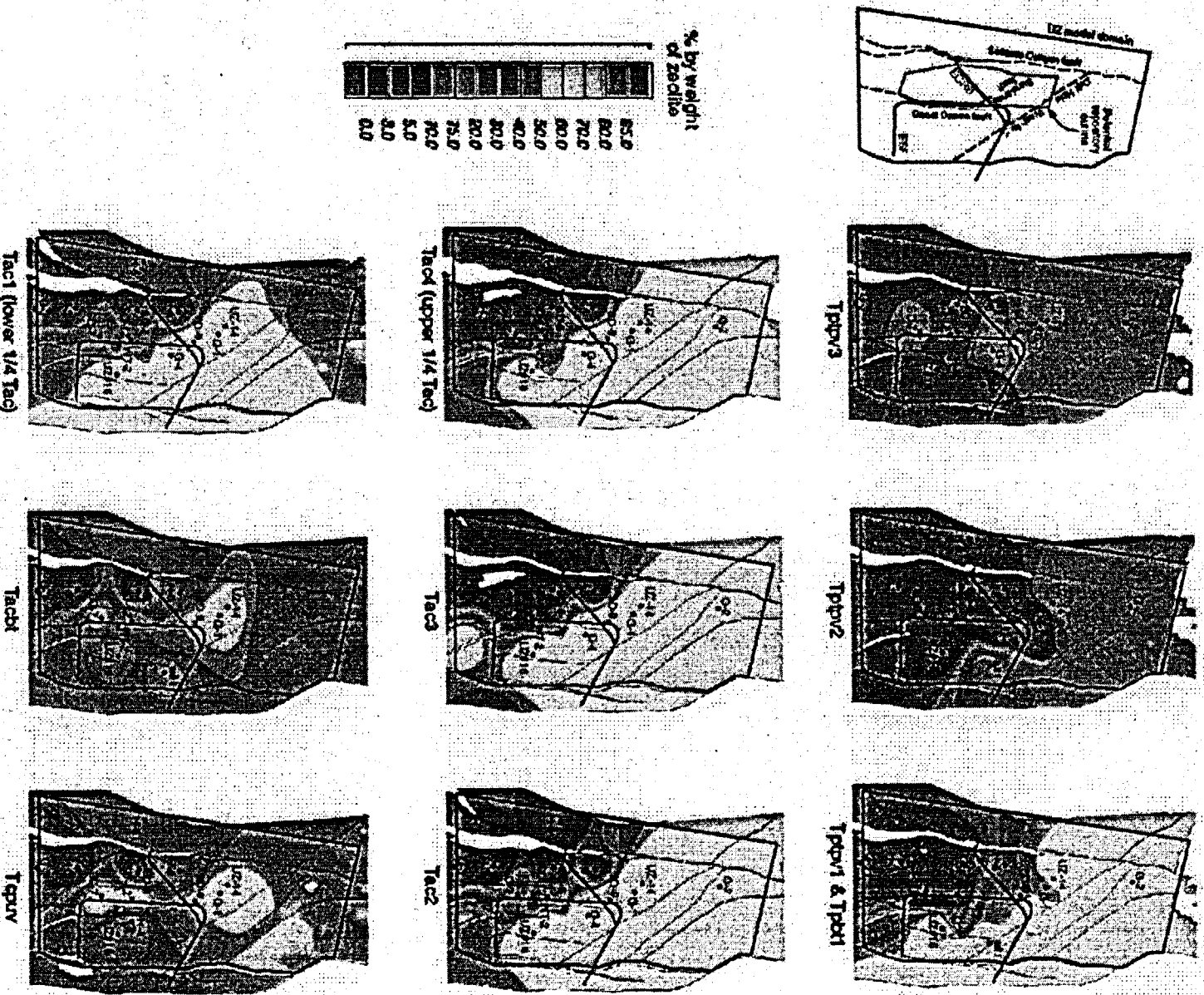


Figure 4-13. Distribution of Zeolites in Certain Layers below the Potential Repository Horizon  
 Areas of less than or equal to 3 percent zeolite are considered vlnrc, or unaltered. Source: CRWMS M&O 2000c,  
 Figure 3.2-7.

depleted in the zeolitically altered CHn unit, signifying effectiveness of hydrogeochemical processes (Sonnenthal and Bodvarsson 1999, pp. 143 to 147). The calcite and opal deposits found on fracture surfaces (Paces, Neymark, Marshall et al. 1998) and within lithophysal cavities (CRWMS M&O 2000bv, Section 6.10.1.1; CRWMS M&O 2000c, Section 3.9.7.1) are analyzed to evaluate flow in fractures and seepage into cavities over millions of years. Figure 4-14 shows examples of geochemical studies of tuff samples.

Environmental isotope data are used to infer the presence of fast flows from the ground surface through the unsaturated zone. Elevated chlorine-36 isotopic ratios well above background levels are related to global fallout from thermonuclear tests conducted in the Pacific Ocean within the last 50 years. The presence of such elevated concentrations (referred to as "bomb-pulse") of chlorine-36 in the unsaturated zone therefore suggests transport from the ground surface in 50 years or less. The bomb-pulse chlorine-36 signals, first observed in surface-based boreholes and later in the Exploratory Studies Facility at faults and other features, have received much attention and continue to be analyzed (Fabryka-Martin, Wightman et al. 1993; Fabryka-Martin, Wolfsberg, Dixon et al. 1996, Section 5.3; CRWMS M&O 2000bv, Section 6.6.3).

Other environmental isotopes have also been analyzed (CRWMS M&O 2000c, Section 3.8.1). Bomb-pulse tritium concentrations are present at depth in several locations and are associated with pathways for liquid and gas flow. The carbon-14 apparent age of the gas phase in the unsaturated zone increases with depth in borehole USW UZ-1, with less obvious trends in other boreholes. Deuterium and oxygen-18 data reflect climatic conditions at the time of groundwater recharge. Based on the analysis of these two isotopes, pore water in the CHn unit is inferred to have originated either during winter precipitation or during a time of colder climate. Perched water appears to be up to 11,000 years old, based on apparent carbon-14 and chlorine-36 ages. The perched water does not appear to have equilibrated with matrix water, based on major constituent concentrations and uranium isotope data (Paces, Ludwig et al. 1998;

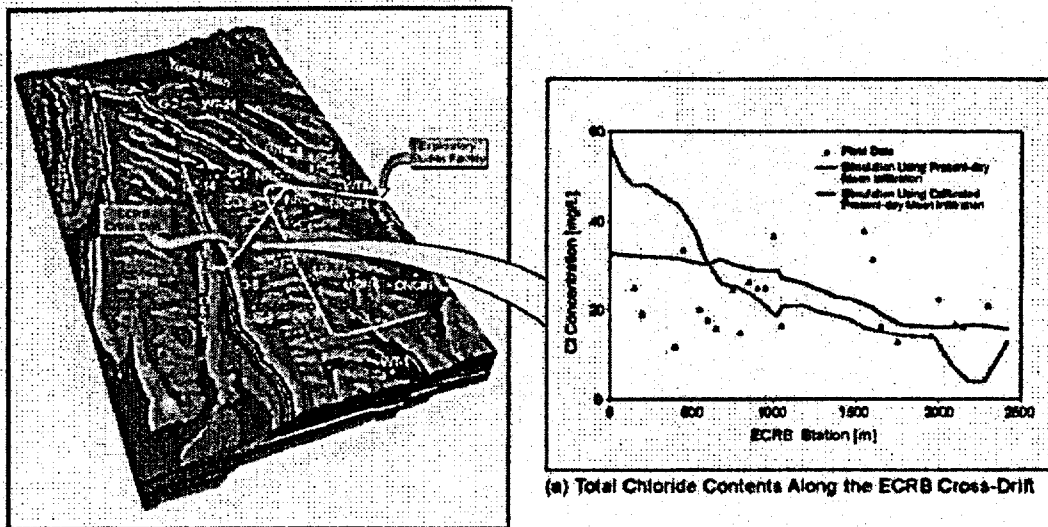
CRWMS M&O 2000bv, Section 6.6). Figure 4-15 illustrates examples of isotopic studies of tuff samples.

#### 4.2.1.2.12 Seepage Data

Diversion of flow around underground openings in the potential repository host rock units at Yucca Mountain has been investigated through a series of tests conducted in "niche" openings constructed off the exploratory tunnels. More detailed descriptions of these tests and the associated modeling are provided in supporting documentation (Wang, Trautz et al. 1999; CRWMS M&O 2000bu, Section 6.2; CRWMS M&O 2000c, Sections 2.2.2 and 3.9).

Four niches were excavated along the Exploratory Studies Facility main drift to test drift seepage processes. The seepage tests were motivated by the observed absence of continuous seepage in the Exploratory Studies Facility drifts following their excavation. For each niche test, pretest characterization of the rock was performed and the openings were excavated using a boom-cutter excavating machine (Figure 4-16). The use of water during excavation was controlled so that it did not spread into the rock above the openings. Seepage into the niche openings was monitored while pulses of water were infused at very low injection pressure into the rock above. Staining dyes were used to monitor the presence of seepage and the extent of seepage water movement within fractures and openings.

**Pre- and Post-Excavation Permeability Distribution**—Air-injection tests were performed in horizontal boreholes drilled at niches, and air-permeability values were determined before and after excavations (CRWMS M&O 2000bu, Section 6.1). The average excavation-induced increases in permeability are in the range of one to two orders of magnitude (i.e., increases by factors of ten to a hundred). The permeability enhancements could be interpreted as the opening of preexisting fractures induced by stress releases associated with niche excavation (Wang and Elsworth 1999; Bidaux and Tsang 1991). A geostatistical analysis of these postexcavation air permeabilities provided a measure of statistical variability and spatial corre-



(a) Total Chloride Contents Along the ECRB Cross-Drift

**Objectives:**

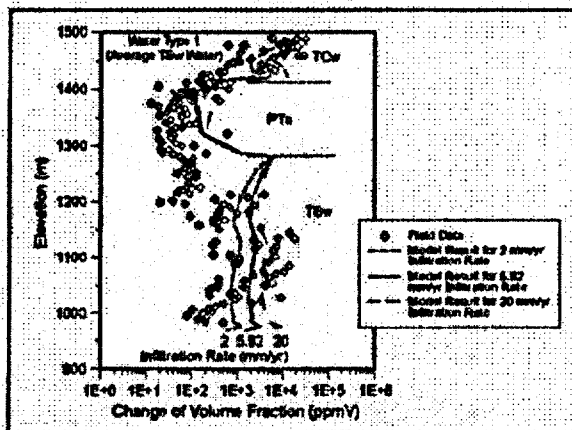
- Provide data to define geochemical evolution of water in the unsaturated zone.
- Provide data to estimate percolation flux at depth.

**Approaches:**

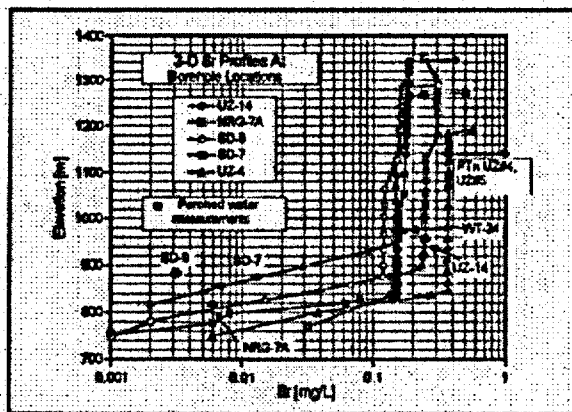
- Collect gas and perched water samples by pumping.
- Extract pore water by compression, ultracentrifuge, or vacuum distillation.
- Determine major ion concentrations by chemical analyses.

**Results:**

- Total dissolved solid and chloride are used to estimate infiltration rates and percolation fluxes.
- Pore waters are related to soil-zone processes: evapotranspiration, dissolution, and precipitation of pedogenic calcite and amorphous silica.
- Deep pore waters are used to evaluate restricted water-rock interactions and significant lateral movement within Calico Hills unit.



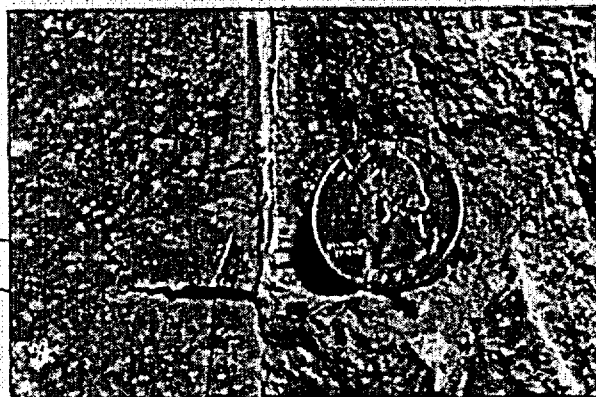
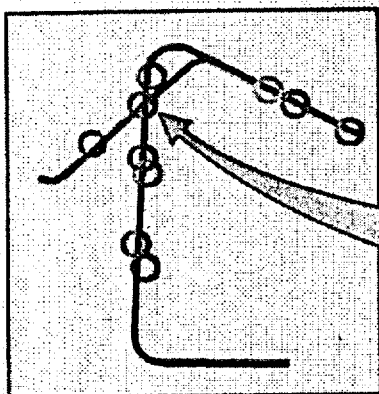
(b) Calcite Distributions Used for Infiltration and Percolation Evaluations



(c) Strontium Profiles Used for Zeolite Quantification

000600C\_ATP\_21842\_140a.N

Figure 4-14. Geochemical Studies of Tuff Samples  
Sources: CRWMS M&O 2000c, Figure 2.2-10; CRWMS M&O 2000bw, Section 6.5; Sonnenthal and Bodvarsson 1999, p. 145.



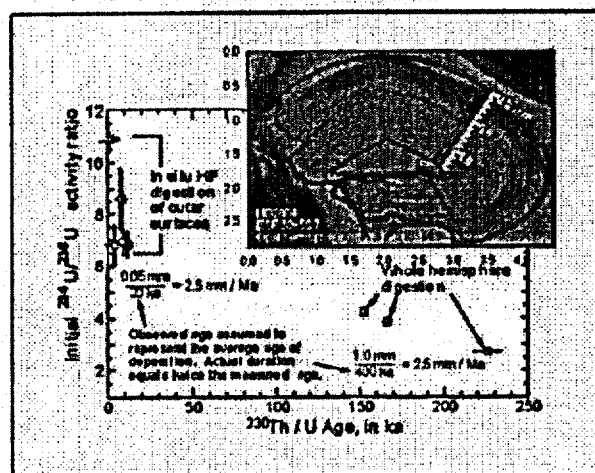
(a) Photograph of a Fracture with Calcite Infill

**Objectives:**

- Provide isotopic data to define age evolution of water in the unsaturated zone.
- Provide data to delineate flow paths over geological time scales.

**Approaches:**

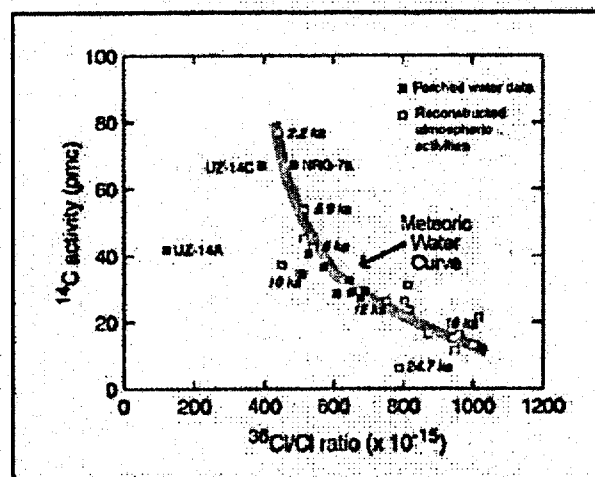
- Leach salts from unsaturated zone cores or cutting for  $^{36}\text{Cl}$  and Sr isotopic analyses.
- Extract water for tritium, hydrogen and oxygen stable isotopes, and carbon isotopic analyses.
- Digest mineral samples for analyses of Sr isotope ratios and of U series nuclides.



(b) Ages of Opal Indicate Long Term Flow in Fractures

**Results:**

- Bomb-pulse  $^{36}\text{Cl}/\text{Cl}$  signals are present in the vicinity of some fault zones in the Exploratory Studies Facility
- Detectable levels of tritium are present in ~6% of pore water samples.
- Bomb-pulse  $^{36}\text{Cl}/\text{Cl}$  and tritium signals are not present in perched waters.
- Age of perched waters, mixing between fast and slow flows, climate of recharge are estimated by carbon and stable isotope analyses.
- $^{234}\text{U}/^{238}\text{U}$  activity ratios indicate recharge through fractures and minimal exchange between pore water and fracture water.

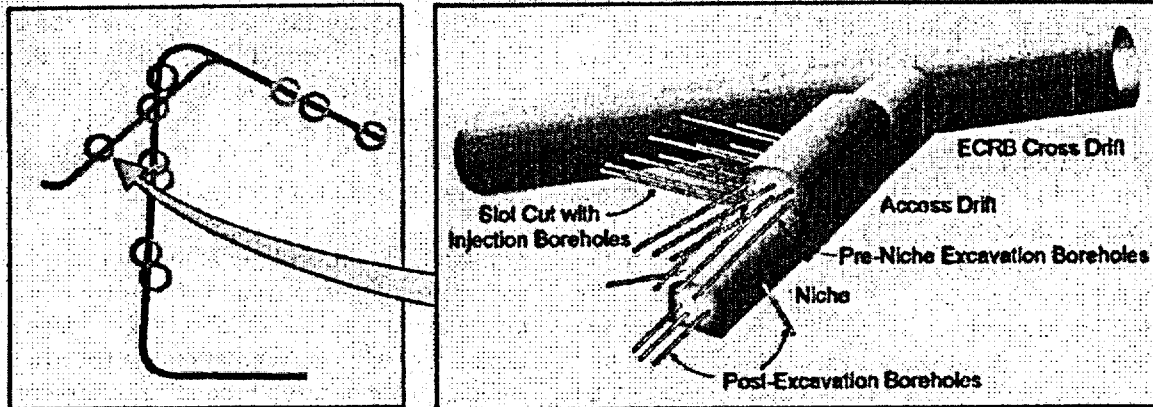


(c) Perched Water Ages Determined by  $^{14}\text{C}$  and  $^{36}\text{Cl}/\text{Cl}$  Data

000500C\_ATP\_Z1642\_141b.d

Figure 4-15. Isotopic Studies of Tuff Samples

pmc = percent modern carbon. Sources: CRWMS M&O 2000c, Figure 2.2-11; CRWMS M&O 2000bv, Section 6.6.



(a) Schematic of Niche 3

**Objectives:**

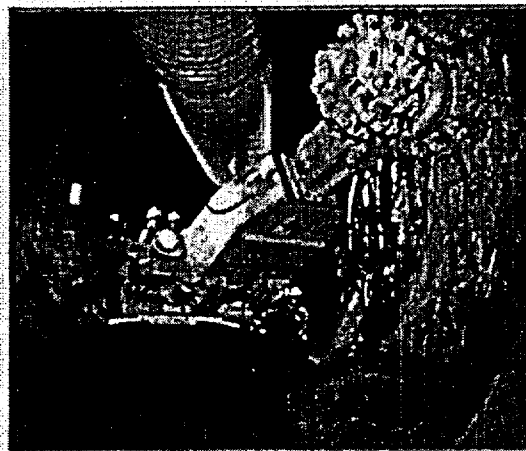
- Quantify seepage into drift in the lower lithophysal unit at a cavity-rich zone.
- Characterize the pneumatic and liquid flows in the presence of lithophysal cavities and porous tuff.
- Determine the differences between lower lithophysal unit and middle nonlithophysal unit of the potential repository rock.
- Quantify fracture-matrix interaction at lower lithophysal unit.

**Approaches:**

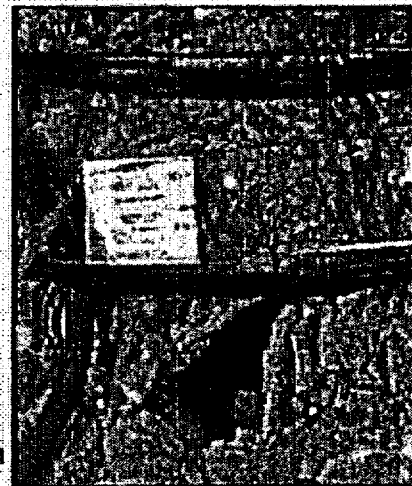
- Observe flow paths during dry excavation, use air-injection tests to characterize liquid release intervals, and conduct drift seepage tests with liquid releases at different rates.
- Adopt, improve, and extend the methodologies used in tests conducted in the middle nonlithophysal niches and test beds.

**Results:**

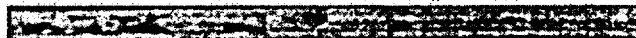
- Pre-excavation air-injection test results suggest that lower lithophysal unit has higher permeability than middle nonlithophysal unit.
- Access drift has been excavated with an Alpine Miner.
- Seepage tests are prepared to be conducted after niche excavations.



(b) Alpine Miner Excavating the Access Drift



(c) Example of a Cavity in the Lower Lithophysal Tuff Unit



(d) Scanner Image along Borehole AK-1 at Niche 5

000500C\_ATP\_Z1842\_181a.ai

Figure 4-15. Lower Lithophysal Seepage Test at Cross-Drift Niche 5  
Source: Adapted from CRWMS M&O 2000c, Figure 2.2-5.

lation. The air-permeability field at Niche 2 (located at Station 36+50) was found to be largely random, with fairly weak spatial correlation.

**Seepage Threshold Tests**—A series of short-duration liquid release tests was performed at Niche 2 (Wang, Trautz et al. 1999; CRWMS M&O 2000bu, Section 6.2). Any water that migrated from the injection boreholes and dripped into the niche opening was captured and weighed. The seepage percentage, defined as the mass of water that dripped into the capture system divided by the total mass of water injected, was used to quantify seepage into the drift from a localized water source of known duration and flow rate. The seepage threshold was estimated for each location from a series of injection tests with decreasing flow rates, continuing until no seepage occurred.

Dye tracers were injected as pulses designed to represent repeated, episodic percolation events, as illustrated in Figure 4-17, for the seepage tests at Niche 2. Seepage flow paths indicated by dye tracers were used to observe wetting-front movement through the fractures. Seepage threshold data and wetting-front movement data were used to estimate the unsaturated hydrologic properties for the fractures (Wang, Trautz et al. 1999; CRWMS M&O 2000bu, Section 6.2).

Drift seepage tests were also conducted at Niche 3 (located at Station 31+07), near the crossover point between the Exploratory Studies Facility Main Drift and the ECRB Cross-Drift, and at Niche 4 (located at Station 47+88), which is in an intensely fractured zone. All the niche studies were conducted behind bulkheads to isolate them from ventilation, so that high-humidity conditions were maintained.

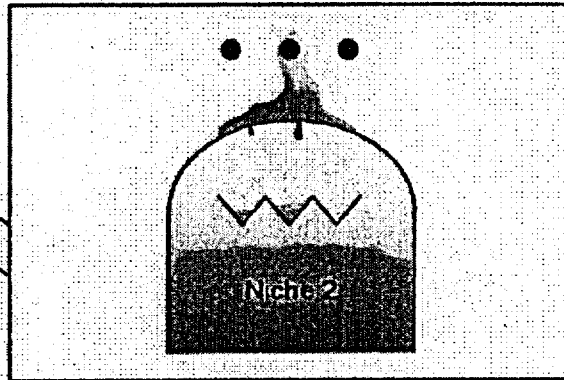
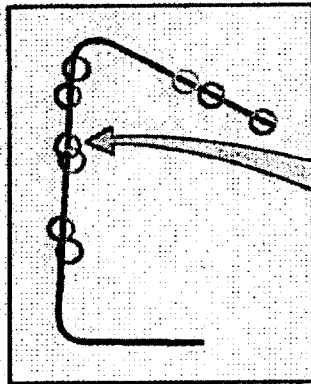
**Flow Path Associated with Fault**—In the excavation of Niche 1 (located at Station 35+66) in the vicinity of the Sundance fault (Figure 4-18a), a damp feature was observed, as illustrated in Figure 4-18b (Wang, Trautz et al. 1999, pp. 331 to 332). The feature was nearly vertical and approximately 0.3 m (1 ft) wide by over 3 m (10 ft) long. It dried out before the bulkhead could be installed to prevent contact by ventilation air. Full rewetting of this feature was not observed after more than

2 years of observation with the bulkhead closed. Figure 4-18c shows that the Sundance fault is one of several faults and features with bomb-pulse signals detected from chlorine-36 isotopic measurements along the Exploratory Studies Facility, as discussed previously.

**Moisture Monitoring**—Ventilation needed for underground operations and construction activities may explain the lack of observed seepage in the exploratory tunnels. Ventilation can remove a large amount of moisture, producing a dryout zone around the openings, thereby suppressing seepage. Ventilation would be used during repository operations to remove heat during thermal periods (CRWMS M&O 2000c, Section 2.2.2.1). To further investigate seepage processes without the influence of ventilation, two additional bulkhead sealing studies are ongoing. The first is at Alcove 7 in an over 100-m (330-ft) long drift segment that intersects the Ghost Dance fault. The second is at the furthest extent of the ECRB Cross-Drift, in an over 1,000-m (3,300-ft) long drift segment that intersects the Solitario Canyon fault. Both studies use double bulkheads for isolation from ventilation effects. To date, no continuous seeps have been observed in either of these two drift segments (CRWMS M&O 2000c, Section 2.2.2). Results will be documented following the completion of the tests. There have, however, been as yet undocumented reports of observations of the effects of liquid water, including organic growths, in the closed section. The closed sections were selected based on inferences from the unsaturated zone models of areas most likely to show seepage under ambient conditions. The lack of observable seepage could be due to incomplete rewetting of the rock following the period of ventilation. The observed effects of liquid water could be due to processes other than seepage. Condensation related to the effects of heat sources or leakage of moist air through fractured rock around the bulkheads could also lead to these effects. Studies to address this issue are continuing, and results will be documented following the completion of these studies.

#### 4.2.1.2.13 Natural Analogues

Natural and man-made analogues with geological or archaeological records can be used to support



(a) Schematic of Niche 2 in the Exploratory Studies Facility

**Objectives:**

- Quantify seepage threshold below which no seepage occurs.
- Evaluate capillary barrier mechanism and measure drift-scale parameters.

**Approaches:**

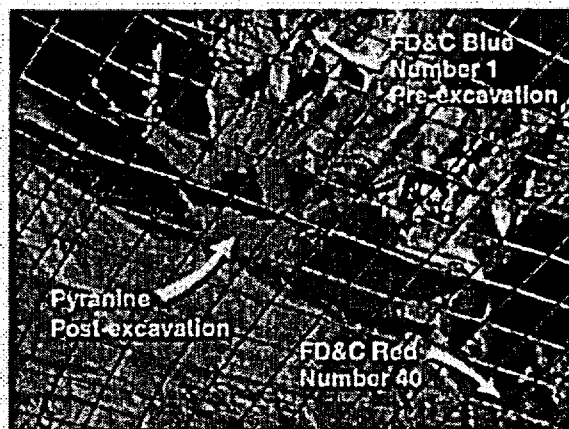
- Use air injection tests to characterize the niche site with resolution of 0.3-m scale (one tenth of drift dimensions).
- Use pulse releases to represent episodic percolation events.
- Determine seepage thresholds by sequences of liquid releases with reducing rates.
- Derive in situ fracture characteristic curves with wetting front arrival analyses.



(b) Water Collection During a Drift Seepage Test

**Results:**

- Measured seepage threshold ranges from 200 mm/yr to 136,000 mm/yr at localized release intervals.
- Six out of sixteen tested intervals did not seep.
- Observed both flow along high-angle fractures and flow through fracture network.
- Derived fracture capillary parameters and characteristic curves, with equivalent fracture porosity as high as 2.4%.

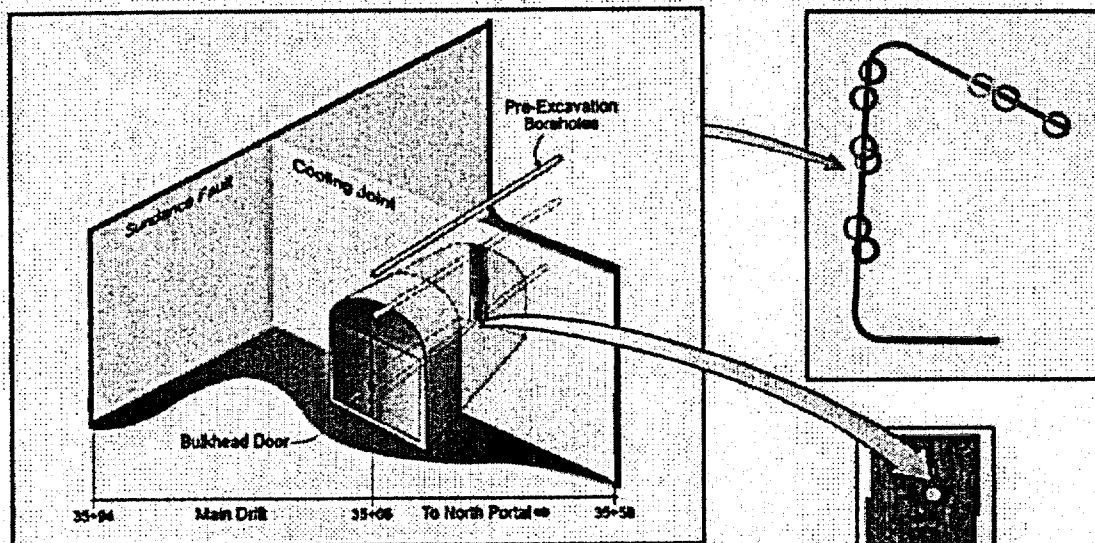


(c) Flow Paths Indicated by Dye Tracers on Niche Ceiling

000600C\_ATP\_21842\_148b.e

Figure 4-17. Drift Seepage Test at Niche 2

Sources: CRWMS M&O 2000c, Figure 2.2-3; CRWMS M&O 2000bu, Section 6.2.



(a) Schematic of Sealed Niche 1 in the Exploratory Studies Facility

**Objectives:**

- Characterize the hydrologic setting of a site with bomb-pulse  $^{36}\text{Cl}$  signals, the Sundance fault and its first cooling joint.
- Quantify seepage processes.

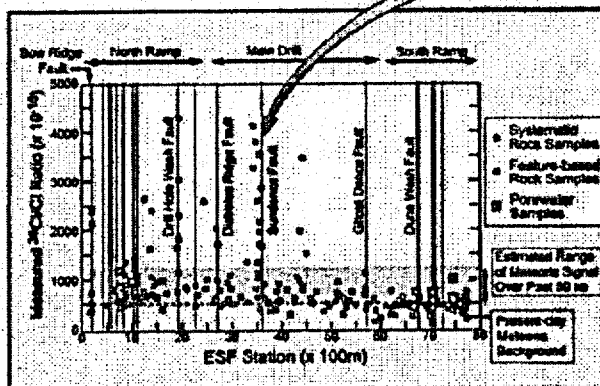
**Approaches:**

- Mine the niche without spreading water to the ceiling during excavation.
- Close the bulkhead to prevent moisture removal by ventilation.
- Monitor the rock and drift over long time periods.

**Results:**

- One damp feature observed after dry excavation at end of the niche. It dried up before bulkhead installation and did not rewet after long-term monitoring over two years.

(b) Photograph of a Damp Feature in the Brecciated Zone at the Back of Niche 1



(c) Distribution of  $^{36}\text{Cl}$  in the Exploratory Studies Facility

000300C\_ATP\_Z1542\_149a.ai

Figure 4-18. Damp Feature Observed during Dry Excavation of Niche 1 and Bomb-Pulse Chlorine-36 Isotopic Signals along the Exploratory Studies Facility

ESF = Exploratory Studies Facility. Sources: CRWMS M&O 2000c, Figure 2.2-4; Wang, Trautz et al. 1999, pp. 331 to 332; CRWMS M&O 2000bv, Section 8.6.

long-term predictions of future performance of a repository at Yucca Mountain. Short-term field experiments cannot predict long-term performance, but many examples from the geologic record can be used qualitatively to evaluate aspects of repository performance for tens of thousands of years or more. The Yucca Mountain Site Characterization Project has used analogue studies for testing conceptual models and evaluating coupled processes as both quantitative and qualitative tools. An analogue relates a process or set of properties to a similar process or set of properties, either in another place or another time. Natural and man-made analogues offer direct comparisons for some of the actual long-term processes and functions of a repository. The confidence in the safe emplacement of nuclear wastes in the unsaturated zone may be greatly enhanced with natural analogue studies to supplement field testing and modeling (CRWMS M&O 2000bp; CRWMS M&O 2000b, Section 13; Stuckless 2000). Figure 4-19 illustrates examples of analogue sites for unsaturated flow, transport, and seepage process evaluations.

**Climate and Infiltration**—A set of natural analogues related to climate and infiltration is listed in Table 4-5. The current climate and paleoclimate records of several sites in the southwestern and western United States were used to derive the climate and infiltration fluxes for future periods. Infiltration at Yucca Mountain under wetter conditions cannot be measured directly, but infiltration under wetter conditions at a geologically similar location can be measured, and the results can be used quantitatively. Monsoonal climates have been studied at Nogales, Arizona, and Hobbs, New Mexico. Beowawe, Nevada currently has a climate

similar to that expected at Yucca Mountain during a glacial-transition period (USGS 2000a, Section 6.6.2).

Future climates can be modeled based on determinations of past climates because climates worldwide have been cyclical for the past 2 million years and are expected to remain cyclical in response to astronomical cycles. There is a calcite deposit at Devils Hole, Nevada, that has been precipitated continuously for the last 500,000 years (Winograd et al. 1992). Minute changes in the composition of this calcite provide an accurate record of the climate in southern Nevada for that time. In a similar fashion, sedimentary deposits at Owens Lake, California (Forester et al. 1999) provide a nearly 425,000-year record of past climates in the region (USGS 2000a, Section 6.5.1). These two records can be used to model likely future climates at Yucca Mountain.

**Unsaturated Flow and Fracture-Matrix Interaction**—The series of natural analogues for unsaturated flow and seepage processes is listed in Table 4-6. The conceptual and numerical modeling methodologies for the unsaturated zone at Yucca Mountain are applicable to other sites, including Rainier Mesa, Apache Leap, Box Canyon, and other arid and semiarid sites where there is fractured rock. The Peña Blanca site evaluation of uranium migration and the Box Canyon, Idaho, infiltration test modeling are two examples of analogue studies presented in *Natural Analogs for the Unsaturated Zone* (CRWMS M&O 2000bp). Field sampling of borehole cores, evaluation of migration from veins, and assessment of seepage into mine adits was conducted at the Nopal I mine

**Table 4-5. Natural Analogues for Climate and Infiltration Process Evaluation**

| Analogue                                   | Data and/or Process   |
|--|---|
| Devils Hole, Nevada                        | Paleoclimate, calcite deposit (Winograd et al. 1992)                |
| Beowawe, Nevada                            | Climate-glacial-transition period lower bound analogue (USGS 2000a) |
| Spokane, Rosalia, and St. John, Washington | Climate-glacial-transition period upper bound analogue (USGS 2000a) |
| Nogales, Arizona                           | Climate-monsoon period upper bound analogue (USGS 2000a)            |
| Owens Lake, California                     | Paleoclimate (Forester et al. 1999)                                 |
| Hobbs, New Mexico                          | Climate-monsoon period upper bound analogue (USGS 2000a)            |

Source: Adapted from CRWMS M&O 2000c, Table 2.3-1.

**Objectives:**

- Enhance understanding of unsaturated zone flow and transport processes.
- Demonstrate the feasibility of long-term waste isolation in underground drifts.

**Approaches:**

- Evaluate analogue site information and review available data.
- Apply methodologies used at Yucca Mountain to selected analogue sites for comparison.

**Examples:**



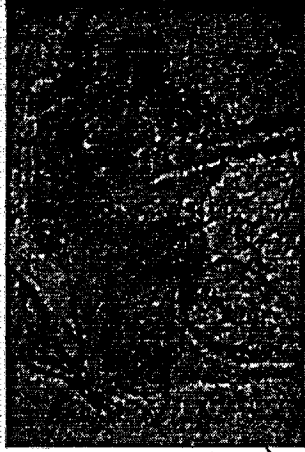
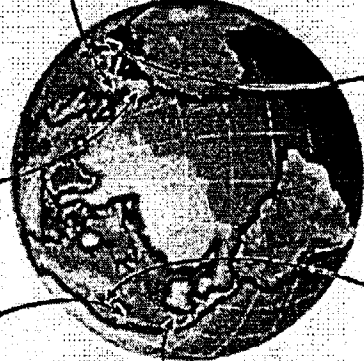
(a) Rainier Mesa, Nevada Test Site

- Nuclear testing tunnel complex within similar tuff units in semiarid climate.
- No seepage in dry drifts in nonwelded Paintbrush tuff and heterogeneous seeps along drifts in and below perched water bodies.



(b) Peña Blanca, Mexico

- Uranium deposits and mine galleries in arid climate.
- Radionuclide migration over only a few meters and along a few major fractures under oxidizing conditions.



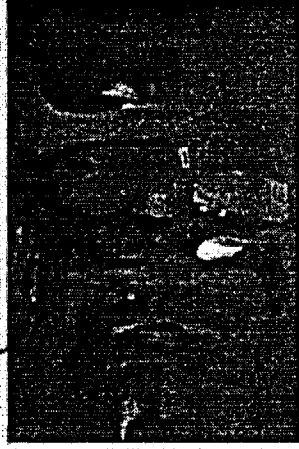
(d) Altamira, Spain

- 14,000-year-old iron oxide and charcoal painting on the ceiling with no apparent water damage.
- ~1% of 400 mm<sup>2</sup>yr infiltration seeps into a limestone/mudstone cave 7 m below surface.



(e) Chauvet Cave, France

- Over 32,000-year-old charcoal painting in large caves (1-5 m wide) in subhumid region.
- Evidence of the process of water flow down the wall over otherwise well-preserved painting.



(f) Underground City of Kaymakli, Turkey

- Eight levels of ancient (second to eleventh centuries A.D.) habitation in partially welded, rhyolite ash-flow tuff.
- No evidence yet observed of active seeps and minerals deposited by seeps.



(c) Box Canyon, Idaho

- Fractured basalt with heterogeneous flow structures exposed on canyon wall.
- Infiltration tests analyzed with the same modeling approach used at Yucca Mountain.

000000C\_A1P\_21502\_172a.zf

**Figure 4-19. Analogue Studies for Unsaturated Zone Flow, Transport, and Seepage**

Table 4-6. Natural Analogues for Unsaturated Flow and Seepage Process Evaluation

| Analogue  | Data and/or Process  |
|---|--|
| Rainier Mesa, Nevada Test Site, Nevada  | Seepage into drifts, discrete fractures, percolation, perched water (Thordarson 1965; Russell et al. 1987; Wang, Cook et al. 1993) |
| Caves and rock shelters, Nevada Test Site and vicinity  | Packrat midden preservation (Spaulding 1985)   |
| Archaeological finds: preservation of cave arts in France and Germany; preserved seeds and Dead Sea scrolls in Israel; wood, textiles, and plants in Peruvian cave; mummies in Chilean pits; manuscripts in Gobi desert; Chinese cave temples, etc. | Demonstrating the efficacy of an unsaturated environment in isolating nuclear wastes (Winograd 1986)                               |
| Caves, western North America  | Biotic remains preservation (Davis 1990)   |
| Apache Leap, Arizona  | Seepage into drifts, discrete fractures, transient flow (Bassett et al. 1997)  |
| Mitchell Caverns, California  | Infiltration, dripping water deposits (CRWMS M&O 2000b, Section 13.4.2.2.3)  |
| Idaho National Engineering and Environmental Laboratory, Box Canyon, Idaho  | Seepage, discrete fractures, transient flow, colloid-facilitated transport (Faybishenko et al. 1998; CRWMS M&O 2000bp)             |
| Negev Desert, Israel  | Infiltration (Nativ et al. 1995)   |
| Cappadocia, Turkey  | Drift stability and insulation (Aydan et al. 1999)   |
| Altamira, Spain   | Cave seepage (Villar et al. 1985)  |
| Chauvet, Cosquer, and Lascaux, France   | Cave painting preservation (Stuckless 2000)  |
| Angola  | Rock shelter painting preservation (Stuckless 2000)  |

Source: Adapted from CRWMS M&O 2000c, Table 2.3-1.

at Peña Blanca, Mexico (Figure 4-19b). For the Box Canyon site, the modeling approach used in the unsaturated zone model for Yucca Mountain is used to interpret ponded-infiltration results through fractured rock (Figure 4-19c).

The calculated rate and amount of radionuclides that could be transported away from a repository is, in part, dependent upon the interaction between fracture flow and pore water in the matrix. The amount of naturally occurring fracture water at Yucca Mountain has been too small to allow direct observations of these important processes. However, Rainier Mesa (Figure 4-19a), located about 40 km (25 mi) northeast of Yucca Mountain, is also composed of alternating welded and nonwelded tuffs, and both pore and fracture water can be collected due to the higher moisture content. With the matrix close to saturation at Rainier Mesa, there should be limited fracture-matrix interaction. Thordarson (1965, pp. 6, 7, and 75 to 80) noted that typically only portions of fractures carried water, and that the chemical composition of water obtained from fractures was substantially different from that of water samples extracted from the nearby rock matrix at that site, which supports the concept of limited fracture-matrix interaction

under conditions of near saturation. Further support for this concept can be found at a field site in the Negev Desert, Israel, where man-made tracers were observed to migrate with velocities of several meters per year across a 20- to 60-m (66- to 200-ft) thick unsaturated zone of fractured chalk (Nativ et al. 1995). Such high velocities could only occur for conditions of limited fracture-matrix interaction.

Seepage—Hydrologic models indicate that much of the water moving through the unsaturated zone will preferentially move around openings such as waste emplacement drifts. This modeling result is supported by the natural preservation of paintings, artifacts, and other remains in caves, man-made openings, and rock shelters (Stuckless 2000). Well known examples of this phenomenon include the Paleolithic caves of France and Spain, which contain paintings as old as 30,000 years in an environment 3 to 4 times wetter than that of Yucca Mountain. Figure 4-19e shows a painting made with charcoal from Chauvet cave in southern France that has been dated by the carbon-14 method to be approximately 32,000 years old (Stuckless 2000, p. 4). In addition to the remarkable preservation of these fragile paintings, the

figure shows a common phenomenon for seepage in underground openings: much of the seepage flows down the walls. Current models do not take credit for seepage that would be diverted around waste canisters by this mechanism, and the models are, therefore, conservative in their estimates of the effects of seepage.

Spirit Cave, about 75 miles east of Reno, Nevada, is another example of a natural analogue to a repository. In this cave, several small burial pits were discovered. In one of these pits was found an almost completely intact human body, mummified by the dryness of the climate. Subsequent analyses, including carbon-14 testing, have shown the body to be that of a 45- to 55-year-old male who died around 9,400 years ago. His scalp was complete with a small tuft of hair. He wore a breechcloth of fiber and was wrapped in mats woven of fibers from tule leaves, all highly preserved (Barker et al. 2000).

Spirit Cave Man is not alone in being preserved by the dry air that circulates in the caves and rock shelters of the desert Southwest. Among other preserved biologic remains are numerous packrat middens. These middens consist of twigs, fecal droppings, and other debris cemented together by dried urine. Some of the packrat middens analyzed have been preserved for over 50,000 years (Stuckless 2000, pp. 2 to 4).

Elsewhere, in the western United States, caves and rock shelters have preserved fragile biologic remains for tens of thousands of years (Spaulding 1985; Davis 1990). These examples of natural preservation, plus archaeological artifact preservation (Winograd 1986; Stuckless 2000), support the results of mathematical models that predict waste isolation at Yucca Mountain over similar time periods. In addition to flow and transport data and geological records from analogue sites, archaeological records can be more comprehensible to the public than hydrologic-geochemical data and mathematical-numerical models. Paintings and tools preserved in caves, man-made openings and rock shelters (partial openings), structure integrity of underground dwellings (Figure 4-19f), and artifacts found in underground chambers can be used to demonstrate the possibility of preserving man-

made materials surrounded by dry air over geological time scales.

Man-made structures include the subterranean tombs of Egypt that are 3 to 4 thousand years old and contain perfectly preserved wood, fabric, and murals. Although this example is from a drier climate than that of Southern Nevada, similar preservations of murals carved into volcanic rock as much as 2,200 years ago can be found in Buddhist temples carved into volcanic rock in India. In this area of India, the climate is monsoonal, with over four times as much precipitation in just four months as occurs annually in the Yucca Mountain region (Stuckless 2000, p. 19).

A particularly well-studied analogue is the paleolithic cave near Altamira, Spain, which is located in the unsaturated zone of a fractured limestone formation that contains clay-rich layers (Villar et al. 1985). Annual precipitation at this site is approximately six times greater than at Yucca Mountain. Nevertheless, seepage rates into the caves are observed to be a small fraction—about 1 percent—of the calculated percolation flux (Stuckless 2000, p. 6). Also, there is virtually no fluctuation in the observed seepage rate despite monthly changes in the amount of precipitation, even though the unsaturated zone is only about 7 m (23 ft) thick (CRWMS M&O 2000c, Section 3.9.7.3), which supports the hydrologic modeling prediction of the buffering effect of the unsaturated zone.

Seepage was also measured in the tunnels at Rainier Mesa. Most of the tunnels excavated for nuclear testing are in a sequence of zeolitized and fractured tunnel bed units within or below perched water zones. When intersected by tunnels or boreholes, a fraction of fractures and faults yielded significant amounts of water, with the total discharge from one tunnel complex equal to 8 percent of the measured precipitation (320 mm or 12.6 in. per year) (Russell et al. 1987; Wang, Cook et al. 1993). In a tunnel excavated above the perched water bodies in the Paintbrush nonwelded unit, no measurable seepage was observed. While this analogue is not ideal because of the near-saturation of the tuffs and because most of the tunnel penetrations are through the lower nonwelded

zeolitic tuff with perched water bodies, it provides a conservative example because of the high precipitation relative to that at Yucca Mountain. The potential waste emplacement drifts would be located in welded tuff above the perched water bodies.

#### 4.2.1.3 Process Model Development and Integration

##### 4.2.1.3.1 Unsaturated Zone Flow Model

The unsaturated zone flow model simulates present and future hydrologic conditions between the ground surface and the water table (CRWMS M&O 2000c, Section 3.7). The flow model integrates site characterization data into a single, calibrated three-dimensional model. It captures infiltration at the ground surface and estimates the distribution of percolating water in the unsaturated zone. It quantifies the movement of water through fractures and through the porous tuff matrix at the site. The model includes the occurrence of perched water, which has implications for lateral diversion of flow along interfaces between rock layers. The flow model incorporates the damping of infiltration pulses from the surface as water percolates downward through the rock layers and also includes the effects of faults on water movement.

The unsaturated zone flow model is a tool used to (1) quantify the movement of moisture as liquid and vapor through the unsaturated zone for present-day and future climate scenarios; (2) develop hydrologic properties and other model inputs for predicting seepage into drifts and radionuclide transport; and (3) provide the scientific basis for representing unsaturated zone flow processes in TSPA. Output from the unsaturated zone flow model that is used by other models consists primarily of infiltration and percolation flux distributions and hydrologic properties for hydrogeologic units and fault zones. The flow model supports these outputs with extensive analysis and interpretation of the flow regime, perched-water occurrence, and chemical and isotopic data from the site.

Input to the flow model includes Yucca Mountain geologic and rock properties data in addition to site

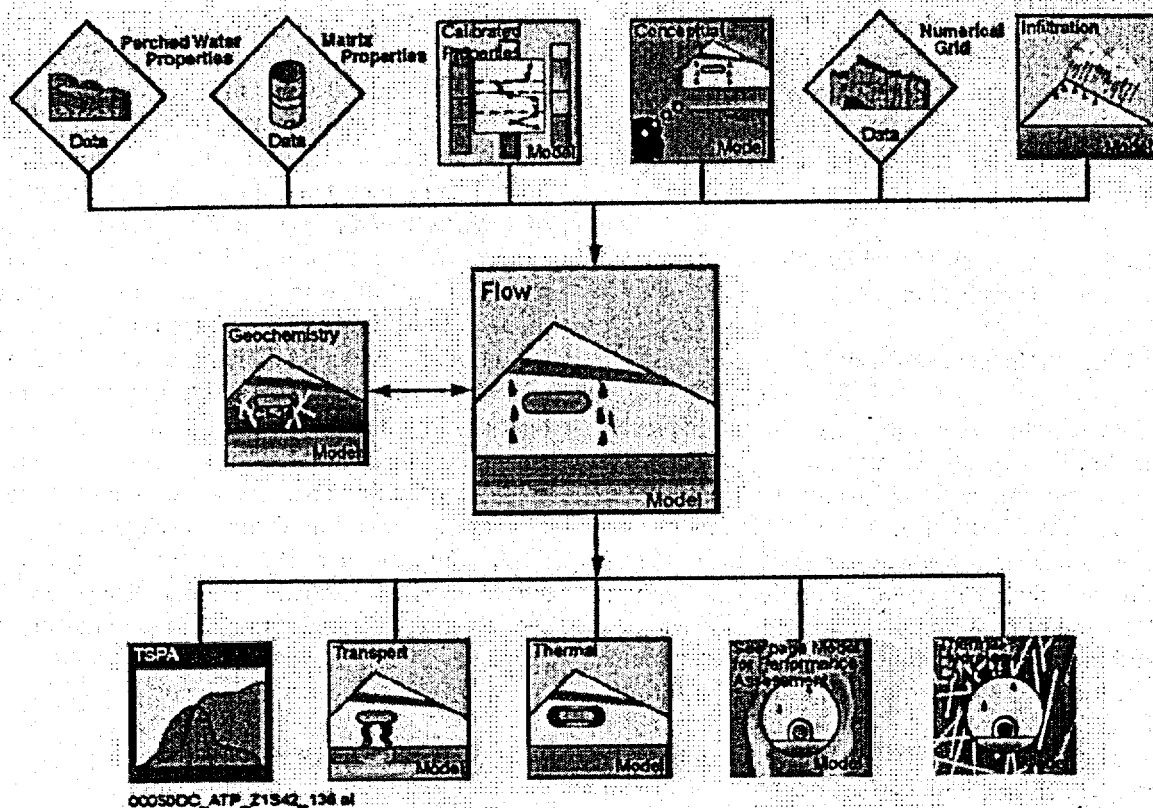
characterization data from surface hydrology investigations, borehole testing, field tests performed underground in exploratory tunnels, geochemical sampling, and isotopic sampling of the unsaturated zone. These inputs are among the input data represented in Figure 4-20. Section 3.7.2 of *Unsaturated Zone Flow and Transport Model Process Model Report* (CRWMS M&O 2000c) describes the development of the component models shown in the figure based on site characterization data. Modeling changes associated with such issues as ventilation and transportation in the drift shadow, thermally coupled processes, with a change of the proposed repository footprint for analysis of a lower-temperature operating mode case are discussed in Volume 1, Section 11.3.4 of *FY01 Supplemental Science and Performance Analyses* (BSC 2001a). Output from the flow model directly feeds the assessments of drift seepage, thermal-hydrology, and radionuclide transport, which ultimately support the TSPA.

##### 4.2.1.3.1.1 Modeling Assumptions

Numerous methods exist for mathematically representing the unsaturated flow processes occurring at Yucca Mountain. These representations range from the relatively simple to the extremely complex. The existing site characterization data for Yucca Mountain suggest that flow between the land surface and the water table is complex. Even though large amounts of site characterization data exist for certain areas of the mountain, for other areas information is based on natural analogues and other sources. Therefore, any mathematical representation of the unsaturated zone at Yucca Mountain must avoid any unjustified complexity, as well as oversimplifications of the flow behavior beneath the mountain.

Mathematical representations of complex, actual phenomena will always require some simplification. Assumptions are made, with justification provided to lend confidence to the model. Some of the important assumptions made in the development of the unsaturated zone flow model of Yucca Mountain are summarized below.

**Selection of Continuum Models**—Estimates of the number of potentially water-conducting frac-



000500C\_ATF\_Z1342\_134 al

Figure 4-20. Schematic of the Major Input Data to the Unsaturated Zone Flow Model and Models that Use Its Output  
Source: CRVMS M&O 2000c, Figure 3.7-5.

tures at Yucca Mountain are on the order of one billion (Doughty 1999, p. 77). It is not feasible to model discrete fractures at this scale, so a continuum modeling approach is used. This is justified by considering two important aspects of flow and transport behavior that are expected to occur in the unsaturated zone. The first, as further discussed in this section, is that where fast flow occurs, it will do so along a few flow pathways that carry relatively small amounts of water. There are numerous slower flow paths dispersed throughout the unsaturated zone, so the continuum model is a reasonable choice for simulating flow and transport. The second aspect is the coexistence of matrix-dominated flow in nonwelded units and fracture-dominated flow in welded units. This is readily accommodated by continuum models but not by other approaches, such as fracture-network modeling. Because continuum models are relatively simple and straightforward to implement,

they are preferred for most practical applications (National Research Council 1996b, p. 331).

**Dual-Permeability Models**—Flow processes in fractured rock have been studied intensively. In order to make continuum models represent observed flow behavior more accurately, dual-permeability models have been developed that represent the rock matrix and the fracture network by different continua. The two continua are coupled together to represent flow interaction between the fractures and the rock matrix (National Research Council 1996b, p. 380). Darcy's law is used to represent flow in each continuum. The van Genuchten model (van Genuchten 1980), which is widely used to relate capillary pressure and saturation in porous media, is employed for both the fracture and matrix continua. Fracture flow in unsaturated media is believed to occur only in a subset of all fractures (called active fractures),

depending on the flux of water moving through the fracture network. For such media, the active fracture model describes the relationship between fracture saturation and the flow interaction between the fracture and matrix continua (Liu et al. 1998; CRWMS M&O 2000bq, Section 6.4.5).

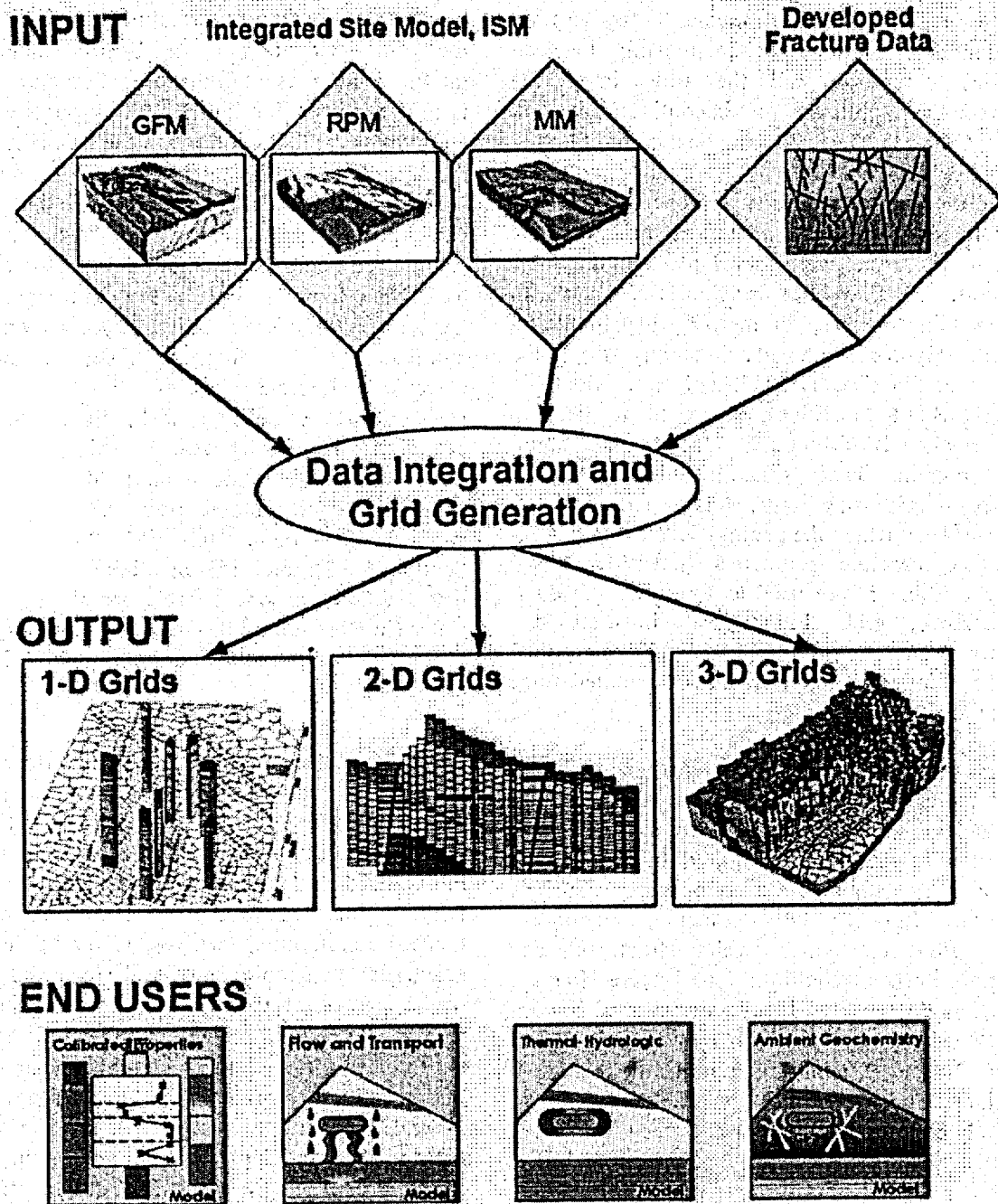
Using the dual-permeability approach, one-, two-, and three-dimensional numerical grids of the unsaturated zone were developed. Figure 4-21 illustrates the flow of information associated with the gridding process, summarizing key input and output. Hydrogeologic data, mainly from the Integrated Site Model (ISM3.1) of Yucca Mountain (CRWMS M&O 2000i), are used to develop numerical grids of the unsaturated zone mountain-scale domain. These grids include layering of hydrogeologic rock units, faults, and different types of rock where the geology is laterally heterogeneous. Fracture properties (CRWMS M&O 2000br, Table 5) are used to formulate the dual-permeability grids. Figure 4-22 illustrates the structural and stratigraphic framework established in the numerical grids of the unsaturated zone domain.

**Fracture-Matrix Interaction**—An active fracture model was developed by Liu et al. (1998) to account for the portion of fracture surfaces interacting with the matrix. Limited fracture-matrix interaction occurs for a variety of reasons, such as fingering flow (gravity-dominated, nonequilibrium, flow channeling within fractures) and fracture surface coatings. The active fracture model is documented in *Conceptual and Numerical Models for UZ Flow and Transport* (CRWMS M&O 2000bq, Section 6.4.5). In the model, only a portion of connected fractures are considered to actively conduct liquid water at a fracture network scale.

**Transient Versus Steady-State Flow**—Temporal variation in the infiltration rate drives the time-dependent or transient nature of flow in the unsaturated zone. The temporal variation of infiltration may be short-term due to weather fluctuations that drive episodic flow or occur over much longer time periods corresponding to climate change. As discussed previously, the PTn is believed to greatly attenuate episodic infiltration pulses such that

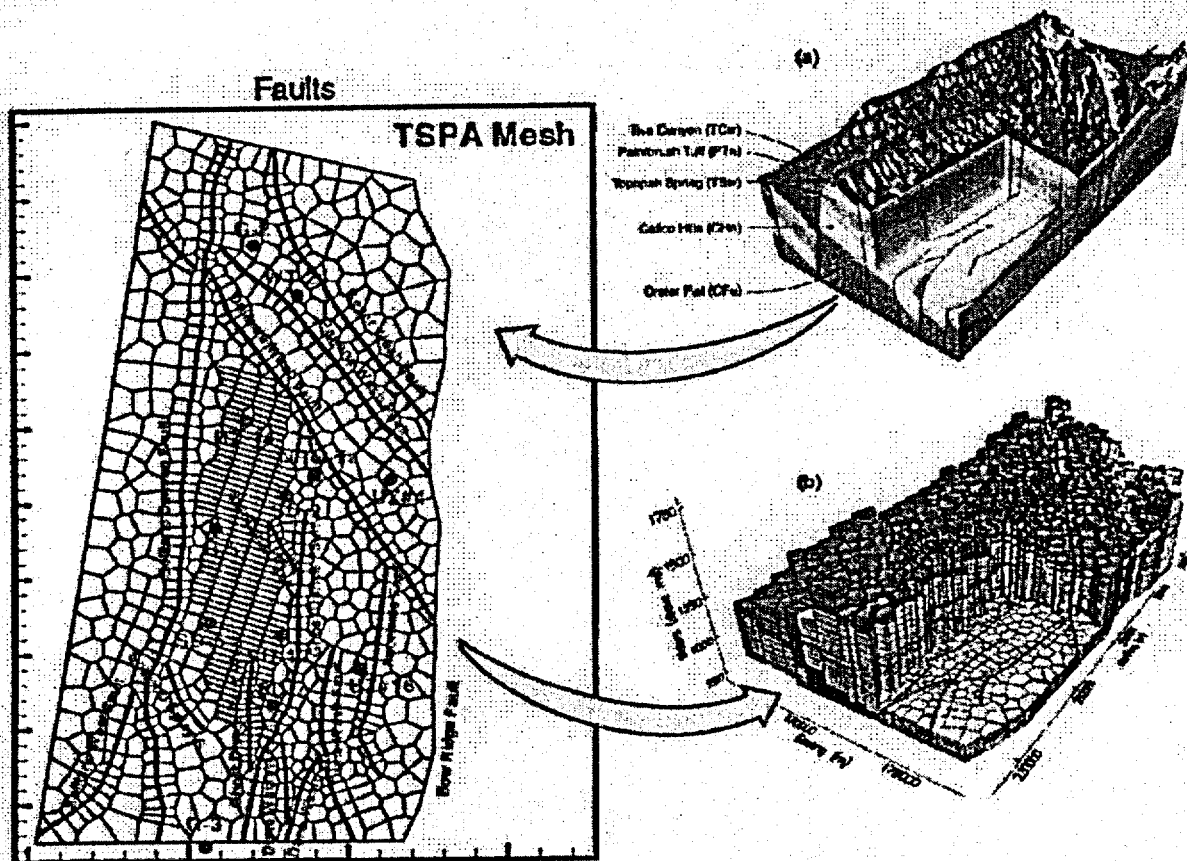
water flow below the PTn is approximately steady. However, water flow in a relatively small area near the Solitario Canyon fault may be transient because the PTn is not present in that area. Some transience is also expected for liquid flow through isolated fast flow paths that cut through the PTn because of the lack of a significant attenuation mechanism. However, these isolated flow paths are believed to carry only a small amount of water because (1) inferred bomb-pulse chlorine-36 isotopic ratios have been found in only a few locations in the Exploratory Studies Facility; (2) no significant correlation between high matrix saturation and elevated chlorine-36 isotopic ratios has been reported; (3) these discrete fast paths are not associated with large catchment areas involving large volumes of infiltrating water; (4) bomb-pulse signatures of chlorine-36 were not found in the perched water bodies (CRWMS M&O 2000bv, Section 6.6.3); and (5) post-bomb tritium was detected only in one sample from the perched water (in Borehole NRG-7a) but not in any of the other samples (CRWMS M&O 2000bv, Section 6.6.2).

The PTn is expected to damp episodic flow in the unsaturated zone resulting from the temporally occasional nature of storms in the site area and the local nature and wide scattering of storm tracks. Individual locations may receive significant rainfall only once in several years, even in the case of focused runoff along arroyos. Geomorphic character, such as conditions of soil cover and slope, further contribute to the variability of infiltration from storms. Larger-scale variation in infiltration is the result of altitude, which controls seasonal rainfall quantity by influencing storm frequency. In general, the northernmost part of the site area is highest, the central part is intermediate in elevation, and the southern part is lowest. The site-scale pattern of infiltration magnitude as well as that of percolation flux at the proposed repository level reflects the site altitude (Figure 4-23). The percolation flux patterns in the unsaturated zone below the PTn (Figure 4-24) do not reflect differences in infiltration magnitude resulting from local storm tracks or surface conditions in regions of the site that are about at equal altitude because of the damping influence of the PTn.



000500G\_ATP\_21542\_Fig.129.d

Figure 4-21. Flow Diagram Showing Key Input Data Used in Numerical Grid Development, the Types of Grids Generated, and the End Users  
 GFM = geologic framework model; RPM = rock properties model; MM = mineralogic model. Source: CRWMS M&O 2000c, Figure 3.4-2.



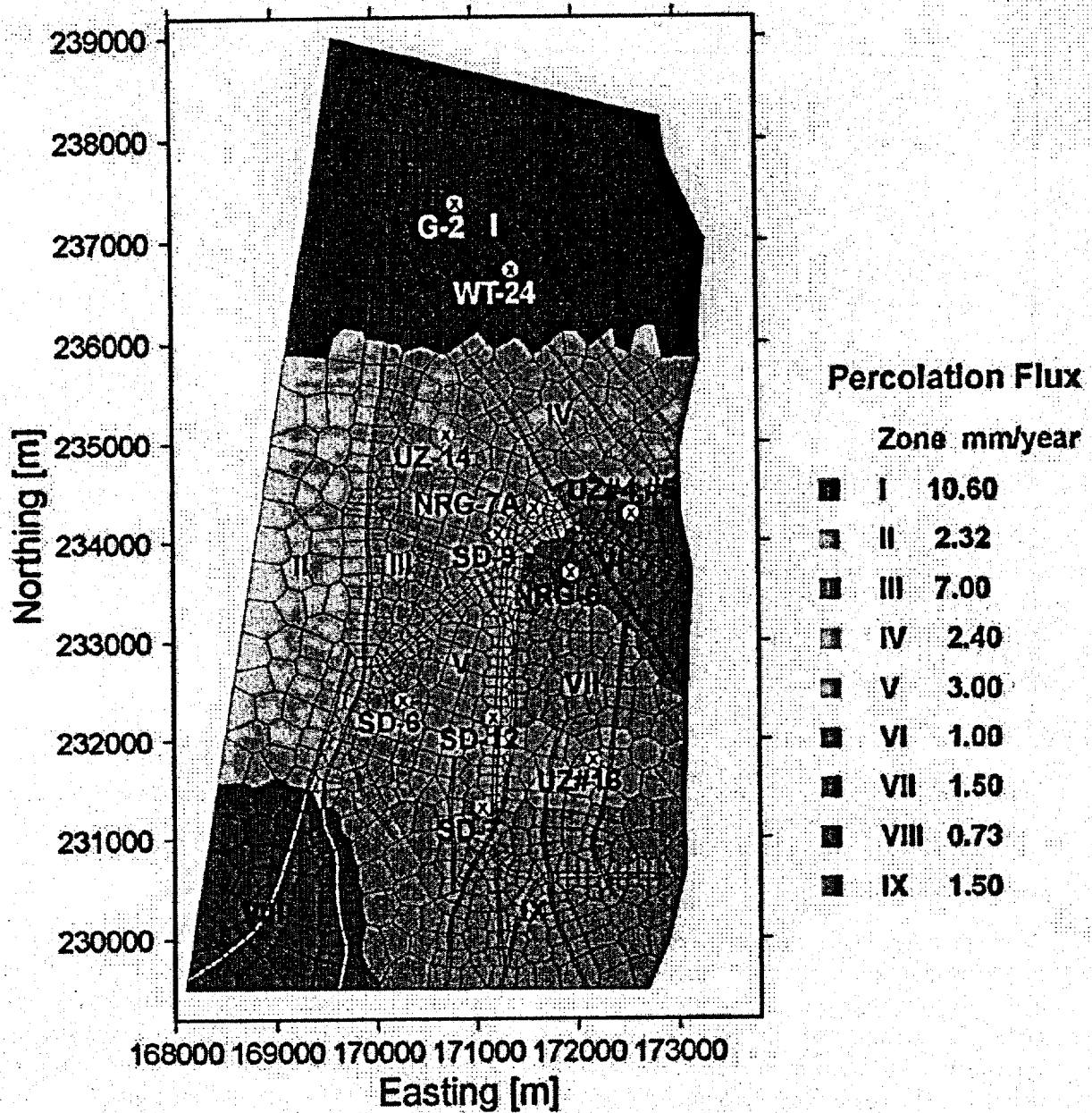
000500C\_ATP\_21542\_130.H

Figure 4-22. Perspective View of the Unsaturated Zone Model Domain of Yucca Mountain, Showing Hydrogeologic Units, Layers, and Major Faults

(a) Geologic model. (b) Numerical grid. Source: CRWMS M&O 2000c, Figure 3.7-2.

Percolation flux in the unsaturated zone is expected to be episodic on the scale of seconds, minutes, hours, or days. Percolation is periodic flow especially in unsaturated, interconnected fracture systems because water must accumulate to gravitationally overcome capillary and frictional resistance to flow at tight asperities. The rate of episodic pulses of water movement in such a system is regulated by the overall flux rate, by evaporation, and by imbibition of water flowing in the fractures by the matrix, which together limit the storage necessary to push flow episodes. The volume and period of episodic flow events, therefore, is limited by ambient conditions. No large, long-period episodic flow surge has been observed at Yucca Mountain (BSC 2001a, Section 4.3.5.6.2). Geologic evidence at Yucca Mountain (Whelan,

Roedder, and Paces 2001), based on the distribution of secondary minerals deposited in the unsaturated zone, clearly supports a flow regime in which most flow is film flow and void spaces along fracture networks are never filled. Such a flow environment is not conducive to larger-scale, long-period episodic flow. Episodic flow severe enough to impact seepage fractions into drifts and transport rates from the repository to the saturated zone has been proposed as a tentative alternative conceptual model based only on numerical simulation of thermally influenced flux (BSC 2001a, Section 4.2.2). The existence of episodic flow of sufficient magnitude to cause such impact in the nonthermal ambient environment in the unsaturated zone remains very improbable (BSC 2001a, Section 4.3.5.6.2).



000500C\_ATP\_Z1S42\_142 at

Figure 4-23. Percolation Flux Map for Three-Dimensional Calibration Grid  
 Sources: Adapted from CRWMS M&O 2000bw, Figure 6-24; CRWMS M&O 2000c, Figure 3.8-4.

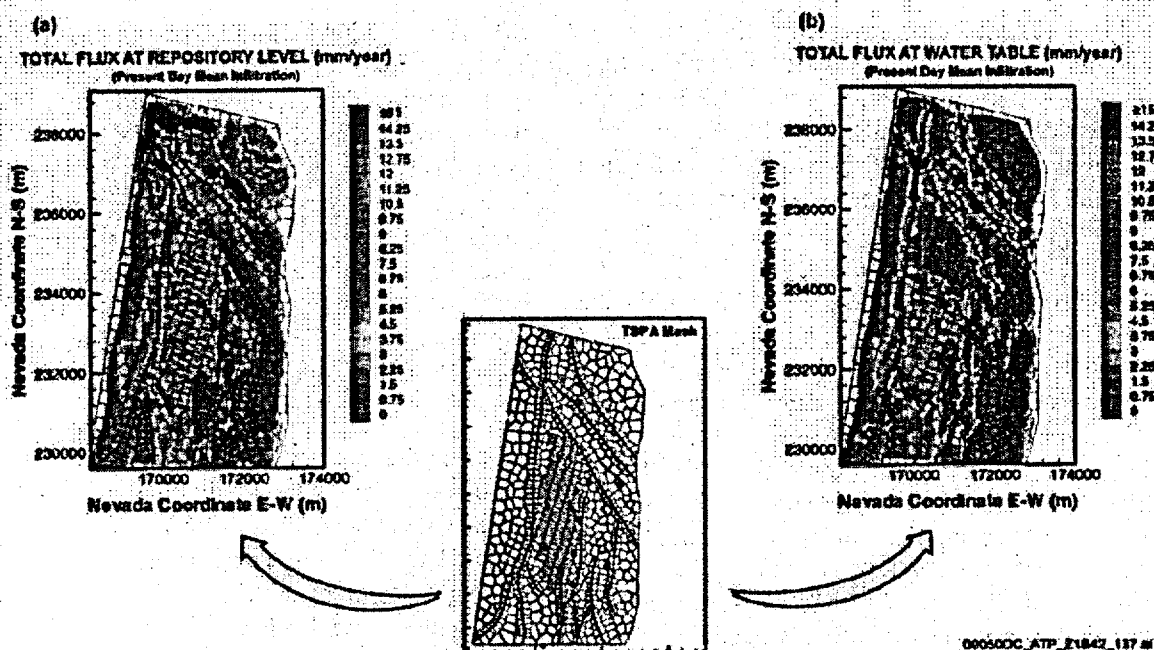


Figure 4-24. Comparison between Simulated Percolation Flux (mm/yr) Contours at the Potential Repository Horizon and at the Water Table Under the Present-Day Mean Infiltration Rate  
(a) Total flux at the potential repository horizon. (b) Total flux at the water table. For labeled details of the TSPA mesh, see Figure 4-23. Sources: Adapted from CRWMS M&O 2000c, Figure 3.7-10; data from CRWMS M&O 2000bw, Section 6.6.3.

Inferred occurrences of bomb-pulse chlorine-36 may exist in the deep unsaturated zone only in association with small volumes of water that flowed rapidly down permeable fault zones. The representation of ambient percolation flux in the unfaulted regions of the deep unsaturated zone in the unsaturated zone flow model and the seepage model as steady flow is appropriate.

The principal variable contributing to the regulation of episodic fracture flow volume and period resulting from capillary resistance is the overall flux rate. Condensation resulting from evaporation due to waste heat may locally cause accelerated percolation flux above the potential emplacement drifts. This local acceleration of percolation flux has the potential to impact seepage flux by generating enhanced episodic flow pulses near the potential emplacement drifts (BSC 2001a, Section 4.3.5). In the cases of higher-temperature operating modes, the boiling front may provide some protection of the emplacement drifts from episodic flow

surges. In both the higher- and lower-temperature operating modes, the enhanced episodic flow may impact the seepage fraction in the emplacement drifts during the heating and cooldown periods (BSC 2001a, Section 4.3.5). No impact is expected after cooldown is complete. Sensitivity studies indicate that variability in seepage flow rates has only minimal impact on performance.

Based on these considerations, flow and transport in the unsaturated zone from episodic infiltration is believed to have low consequence; therefore, transient flow behavior is not considered in the unsaturated zone process model.

#### 4.2.1.3.1.2 Unsaturated Zone Flow Submodels

A number of applications of the flow model have been developed for detailed study of the effects of specific hydrogeologic features on flow in the unsaturated zone. These include (1) flow through the PTn unit (CRWMS M&O 2000c, Section

3.7.3.1); (2) the occurrence of perched water and the effect of alteration within the CHn unit on flow (CRWMS M&O 2000c, Section 3.7.3.3); and (3) the role of major faults as potential conduits or as barriers to flow (CRWMS M&O 2000c, Section 3.7.3.2). Each of these topics is summarized below.

**Flow through the PTn and at the Potential Repository Horizon**—Flow behavior within the predominantly nonwelded PTn unit was evaluated using the mountain-scale flow model with the three climate states (i.e., present day, monsoonal, and glacial-transition). Table 4-7 compares the proportions of vertical fracture flow and matrix flow at the middle of the PTn unit and at the potential repository horizon. The model results support the hypothesis that matrix flow is dominant in the PTn, taking nearly 90 percent of the total flow, with little variation among the three climate scenarios. This is consistent with observed pneumatic responses to barometric pressure fluctuations, which showed attenuated response within the PTn unit (Ahlers et al. 1999). As indicated in Table 4-7, the conditions change to fracture-dominated flow at the interface between the PTn and the underlying TSw unit (potential repository host rock).

Table 4-7. Comparison of the Water Flux through Matrix and Fractures as a Percentage of the Total Flux at the Middle PTn and at the Potential Repository Horizon

| Climate            | Flux at middle PTn (%) |        | Flux at Potential Repository (%) |        |
|--------------------|------------------------|--------|----------------------------------|--------|
|                    | Fracture               | Matrix | Fracture                         | Matrix |
| Present-Day        | 11.6                   | 88.4   | 88.3                             | 11.3   |
| Monsoonal          | 12.1                   | 87.9   | 89.5                             | 10.5   |
| Glacial-Transition | 11.8                   | 88.2   | 91.4                             | 8.6    |

Sources: CRWMS M&O 2000bw, Section 6.6.3; CRWMS M&O 2000c, Table 3.7-2.

More recent studies with new geochemical field data (BSC 2001a, Section 3.3.3) showed that the PTn acted as a buffer, damping out variations in the transient net infiltration, so that flow beneath the PTn was essentially steady-state. Lateral flow diverted net infiltration above the potential repository area eastward to the Ghost Dance and Drill Hole Wash faults. Flow thus diverted bypassed the potential repository block.

**Effects of Major Faults**—The effect of faults is important for site characterization because faults could provide direct flow pathways from the potential repository to the water table, which could bypass sorptive layers within the CHn unit that have the capacity to retard migration of radionuclides. Consequently, radionuclides could enter the saturated zone where such faults intersect the water table. Alternatively, faults could benefit potential repository performance if they cause water to be diverted away from emplacement drifts.

Based on the representation of faults in the unsaturated zone flow model, the model simulations indicate that the fraction of flow occurring through the modeled faults, as a percentage of the total flow (through fractures, matrix, and faults), increases with depth. Table 4-8 lists these predicted percentages at four different depth horizons for the three climate scenarios and for the northern and southern parts of the model domain. A recent analysis with a refined model indicates that flow through faults at the PTn-TSw interface may be slightly higher than shown here (BSC 2001a, Section 3.3.3.4.2). The table shows that flow percentages through faults at the water table would be very different in the southern part (where the CHn unit is thinner and highly porous) than in the northern part (where the CHn unit is thicker and altered to zeolites). This indicates that more lateral flow diversion on or within the CHn unit would occur in the northern part of the site area.

The simulations predict that percolation flow in the unsaturated zone will converge into the faults as water flows downward through the geologic units, and that lateral diversion of water into faults occurs mainly in the CHn unit below the potential repository horizon. Some lateral diversion into faults is also predicted to occur in the PTn unit above the potential repository horizon, as indicated in Table 4-8. In addition, although the percentage of fault flow at the water table below the potential repository is predicted to increase as the average infiltration increases, the percentage of fault flow above and at the level of the potential repository horizon is predicted to decrease as infiltration increases.

Table 4-8. Comparison of Water Flux through Faults as a Percentage of the Total Flux at Four Different Horizons for the Three Mean Infiltration Scenarios

| Climate Scenarios         | Fraction of Total Flow through Faults (%) |       |       |                   |       |       |                            |       |       |             |       |       |
|---------------------------|---|-------|-------|-------------------|-------|-------|----------------------------|-------|-------|-------------|-------|-------|
|                           | Ground Surface                            |       |       | PTn-TSw Interface |       |       | Potential Repository Level |       |       | Water Table |       |       |
|                           | Total                                     | South | North | Total             | South | North | Total                      | South | North | Total       | South | North |
| Present-Day (4.6)         | 3.8                                       | 3.6   | 3.9   | 14.3              | 18.9  | 12.7  | 14.6                       | 19.8  | 12.7  | 34.9        | 15.9  | 42.0  |
| Monsoonal (12.2)          | 4.1                                       | 3.8   | 4.2   | 10.5              | 13.0  | 9.6   | 10.5                       | 13.3  | 9.5   | 42.4        | 21.9  | 51.3  |
| Glacial-Transition (17.8) | 4.0                                       | 3.7   | 4.1   | 9.1               | 10.8  | 8.4   | 9.1                        | 11.0  | 8.2   | 44.4        | 24.3  | 54.2  |

NOTES: "Total" denotes flow over the entire model domain, "South" denotes flow over the southern part/half of the model domain, and "North" denotes flow over the northern part/half of the model domain. Sources: CRWMS M&O 2000c, Tables 3.7-3 and 3.5-4; data from CRWMS M&O 2000bw, Section 6.6.3.

**Studies of the CHn and Perched Water Occurrence**—The CHn unit lies between the potential repository horizon and the saturated zone; thus, for groundwater flow and radionuclide transport from the potential repository, the CHn unit has an important role in site performance. Prolonged rock-water interaction in the geologic past has produced low-permeability clays and zeolites within the CHn, particularly in the northern part of the site area. This alteration has important implications for occurrence of perched water, for groundwater flow paths, and for radionuclide transport.

Model simulations have been performed using the three climate states (i.e., modern, monsoonal, and glacial transition) (CRWMS M&O 2000c, Section 3.7). The results generally match the observed perched water table elevations from Yucca Mountain boreholes, provided that percolation flux greater than 1 mm/yr (0.04 in./yr) exists at the site. All modeling results indicate significant lateral flow diversion (40 to 50 percent of the total flow) just above or within the CHn where low-permeability zeolites occur.

The effect of perched water zones on flow through the CHn is best explained by comparing percolation fluxes simulated at the repository level and the water table. Figure 4-24 presents map views of the simulated vertical percolation flux distributions at the potential repository horizon and at the water

table. Comparison of these views shows large differences in the percolation flux distributions at the potential repository horizon and at the water table, a result that is consistent with the expectation of significant lateral flow diversion occurring just above or within the CHn unit. Simulated results for the northern part of the site area show that percolation flux at the water table tends to be focused along faults. Simulated results for the southern part of the site area show that percolation tends to flow vertically through the CHn unit as matrix-dominated flow in relatively high-permeability vitric zones. Below these vitric zones, however, are zeolitic layers (above the water table) that laterally divert some of the flow eastward, where it is intercepted by faults (Figure 4-24).

#### 4.2.1.3.1.3 Percolation Flux at the Potential Repository Horizon

Percolation flux through the unsaturated zone is important to performance of the potential repository because it directly controls drift seepage and radionuclide transport and also influences the evolution of temperature and humidity in the emplacement drifts (CRWMS M&O 2000c, Section 3.7.4.1). Because the low percolation flux through the unsaturated zone at Yucca Mountain cannot be readily measured, results from the unsaturated zone flow model are used to estimate the flux.

At the mountain scale, percolation flux at the potential repository horizon is mainly a reflection of the infiltration distribution at the ground surface. Areas with greater infiltration (i.e., the northern part of the site area and the crest of Yucca Mountain) have greater percolation flux, while areas with less infiltration have correspondingly less percolation flux. Percolation throughout the unsaturated zone reflects the redistribution of infiltration below the ground surface because of lateral flow, fracture-matrix flow partitioning, flow into faults, and other flow processes. Over an infinite area, the average infiltration flux would be equal to the average percolation flux. Over a limited area, such as within the repository footprint, percolation flux

may be either greater or less than infiltration because of flow redistribution over a larger area.

Figure 4-25 shows the simulated distribution of vertical percolation flux at the repository level for the three climate states (i.e., present-day, monsoonal, and glacial-transition). Areas of higher percolation (shown in blue) are located principally in the northern part of the site area and along the Solitario Canyon fault. The distribution of percolation flux at the potential repository horizon closely matches the distribution of the infiltration at the ground surface (Figure 4-26) because of the limited lateral flow diversion between the surface and the potential repository level, as discussed previously.

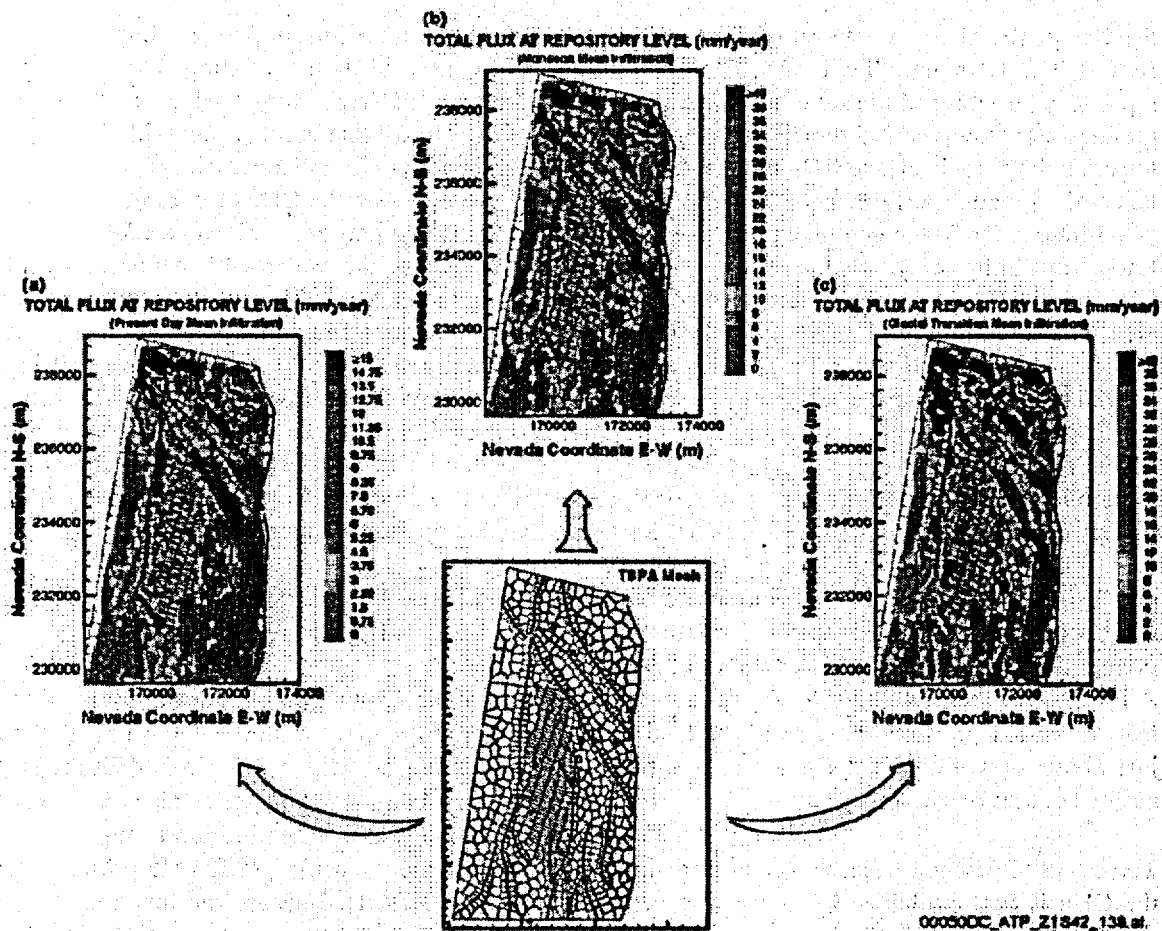


Figure 4-25. Simulated Percolation Fluxes at the Potential Repository Horizon Under the Mean Infiltration Scenarios

(a) Present-day infiltration scenario. (b) Monsoon scenario. (c) Glacial-transition scenario. For labeled details of the TSPA mesh, see Figure 4-23. Source: Adapted from CRWMS M&O 2000c, Figure 3.7-11.

Table 4-9 lists summary statistics for the averaged percolation fluxes within the potential repository footprint. The table indicates that the average percolation within the potential repository horizon is similar to the average infiltration over the entire model domain.

#### 4.2.1.3.1.4 Fracture and Matrix Flow Components

Fracture flow has important implications for seepage flow into emplacement drifts and radionuclide transport and will directly influence the performance of a repository (CRWMS M&O 2000c, Section 3.7.4.3). The partitioning of flow between fractures and matrix is inferred from model results. Figure 4-27 shows the simulated

steady-state distribution of the total percolation flux through both the matrix and fractures at the potential repository horizon for the present-day climate state. In the potential repository host rock, fracture flow controls percolation wherever the total flux exceeds the hydraulic conductivity of the matrix.

Table 4-10 lists the proportion of fracture flux at the potential repository horizon and at the water table as a percentage of the total flux. Calculated results are shown for nine scenarios (i.e., present-day, monsoonal, and glacial-transition climate states, each with upper bound, mean, and lower bound infiltration). Fracture flow dominates both at the potential repository horizon and at the water table. As expected, the percentage of fracture flow

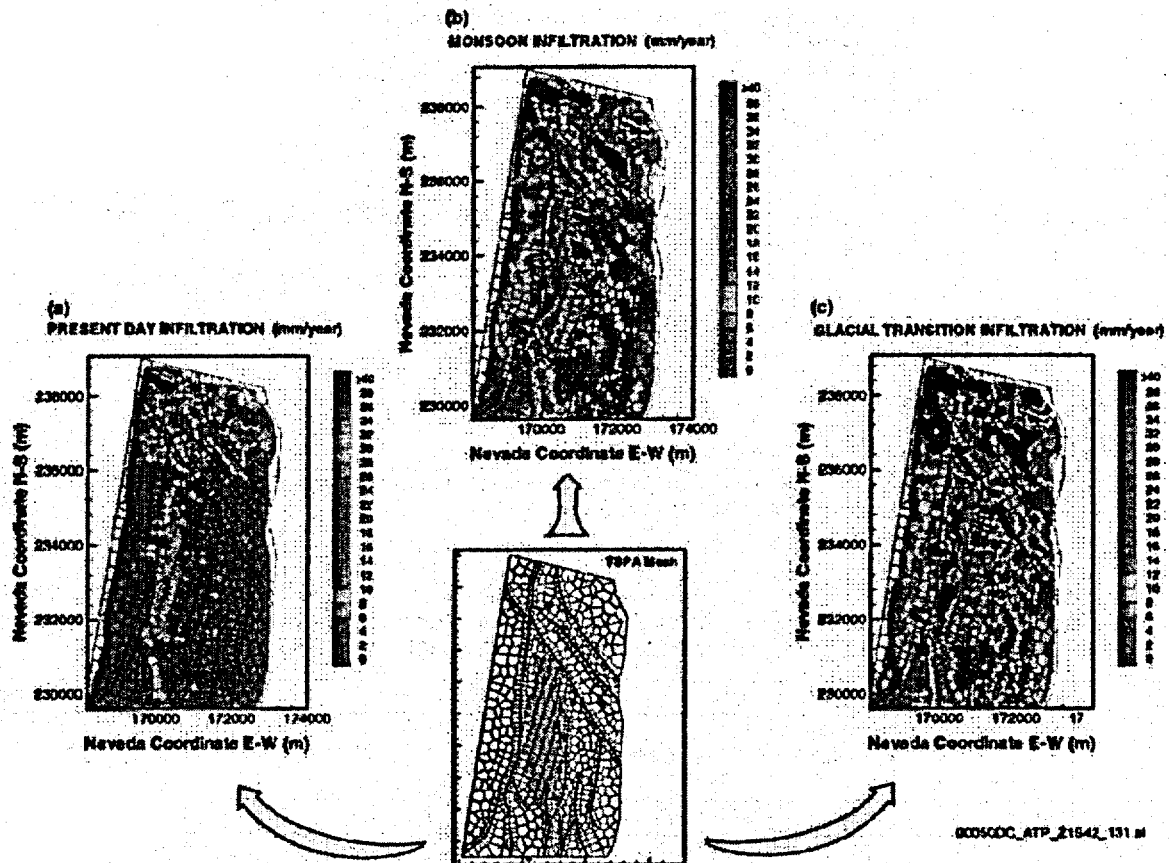


Figure 4-26. Infiltration Distribution over the Flow Model Domain for the Mean Infiltration Scenarios (a) Present-day climate scenario. (b) Monsoon climate scenario. (c) Glacial-transition climate scenario. For labeled details of the TSPA mesh, see Figure 4-23. Source: Adapted from CRWMS M&O 2000c, Figure 3.7-4.

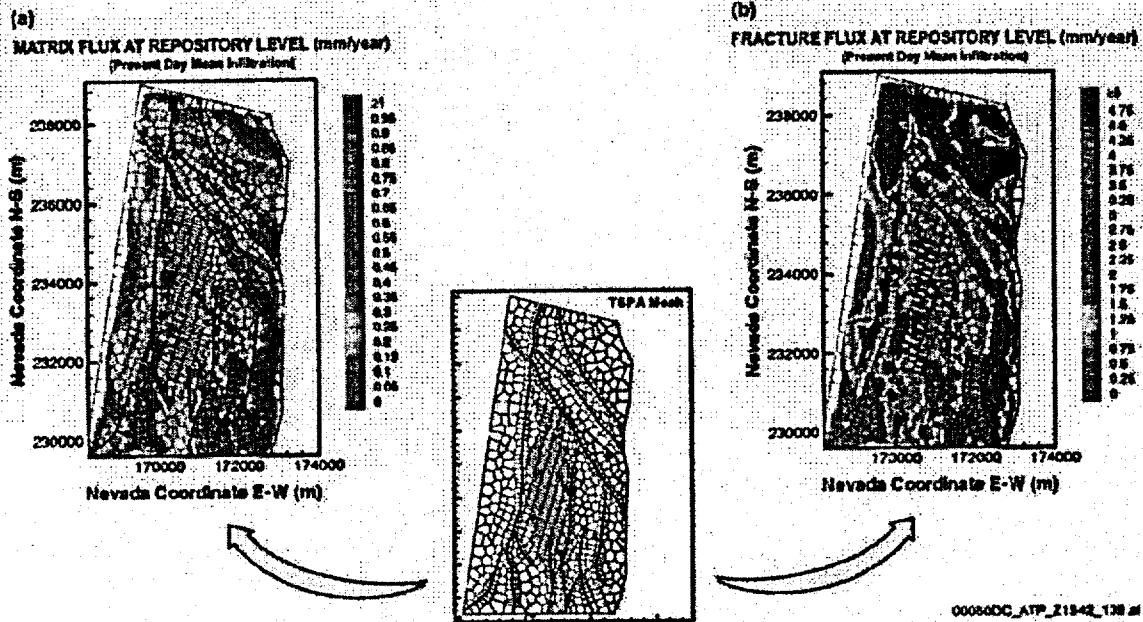


Figure 4-27. Simulated Percolation Flux in the Matrix and In Fractures at the Potential Repository Horizon, Using Present-Day Mean Infiltration Rate  
(a) Matrix percolation flux. (b) Fracture percolation flux. For labeled details of the TSPA mesh, see Figure 4-23.  
Source: CRWMS M&O 2000c, Figure 3.7-13.

Table 4-9. Average Percolation Fluxes Simulated within the Potential Repository Footprint for the Three Mean Infiltration Scenarios

| Climate Scenario   | Average Infiltration over Model Domain<br>mm/yr (in./yr) | Average Percolation Flux within Potential Repository<br>mm/yr (in./yr) |            |             |
|--------------------|--|--|------------|-------------|
|                    |  | Fracture   | Matrix     | Total       |
| Present-Day        | 4.8 (0.18)   | 4.0 (0.16)   | 0.5 (0.02) | 4.5 (0.18)  |
| Monsoonal          | 12.4 (0.49)  | 12.1 (0.48)  | 0.8 (0.03) | 12.9 (0.51) |
| Glacial-Transition | 18.0 (0.71)  | 19.5 (0.77)  | 0.9 (0.04) | 20.5 (0.81) |

NOTES: The average percolation flux values in mm/yr have been rounded to one decimal place. Sources: CRWMS M&O 2000c, Table 3.7-4; data from CRWMS M&O 2000bw, Section 8.6.3.

Table 4-10. Comparison of Water Flux through Fractures as a Percentage of the Total Flux at the Potential Repository and at the Water Table, Using the Nine Infiltration Scenarios

| Climate     | Present-Day              |                 | Monsoonal                |                 | Glacial-Transition       |                 |
|-------------|--------------------------|-----------------|--------------------------|-----------------|--------------------------|-----------------|
|             | Potential Repository (%) | Water Table (%) | Potential Repository (%) | Water Table (%) | Potential Repository (%) | Water Table (%) |
| Lower Bound | 88.6                     | 84.7            | 90.0                     | 90.1            | 86.9                     | 87.2            |
| Mean        | 83.7                     | 86.7            | 89.5                     | 90.2            | 91.4                     | 90.5            |
| Upper Bound | 94.5                     | 95.4            | 95.8                     | 98.5            | 96.5                     | 98.9            |

Sources: CRWMS M&O 2000c, Table 3.7-5; data from CRWMS M&O 2000bw, Section 8.6.3.

is somewhat higher for the future climate scenarios compared to the present-day climate scenario because the total flux is greater. The results from fracture-matrix interaction tests at Alcove 6 in the Exploratory Studies Facility (shown in Figure 4-11) illustrate the dominance of fracture flow for high fluxes.

#### 4.2.1.3.1.5 Supporting Geochemical Analysis

Geochemical processes are useful for estimating and bounding infiltration rates and percolation flux in the potential repository host rock (CRWMS M&O 2000bv, Section 6.9). Upper-bound limits on infiltration rates and percolation flux at the potential repository horizon have been estimated from geochemical data, using several analyses and models (CRWMS M&O 2000c, Section 3.8). Collectively, these conceptual models and analyses are referred to in supporting documentation as the ambient geochemistry model. The primary data used for calibration and validation in this overview are pore water chloride concentrations, relative abundance of chlorine-36 in pore water (or extracted salts), and calcite abundance.

**Calcite Deposition Analysis**—Calcite and carbon-14 ages in the unsaturated zone have been used as a tool for estimating percolation fluxes (CRWMS M&O 2000bv, Sections 6.6.4.3, 6.7.2.2, 6.10.1.1, and 6.10.3.9). Modeling studies incorporating reactive transport in unsaturated zone flow simulations were used to investigate the relationship of calcite deposition to infiltration rate, water and gas compositions, and reactive surface area (CRWMS M&O 2000bw, Section 6.5). Model results for borehole USW WT-24 indicated that the infiltration rate ranges from about 2 mm/yr to 20 mm/yr (0.08 to 0.8 in./yr), which bounds the observed range of calcite abundance. An infiltration rate of approximately 6 mm/yr (0.2 in./yr) can account for the average abundance of calcite in the TSw unit (Figure 4-14b).

**Chloride Mass Balance**—Small concentrations of chloride occur in rainfall at Yucca Mountain, averaging approximately 1 mg/L (CRWMS M&O 2000bv, Section 6.3.2). The chloride becomes more concentrated as evaporation occurs. The water that does not run off or evaporate infiltrates

into the unsaturated zone, carrying the dissolved chloride. The resulting concentration of chloride in unsaturated zone pore waters indicates the extent of evaporative concentration relative to rainwater, and the infiltration flux is inferred using the average annual precipitation and runoff.

Chloride concentrations in unsaturated zone pore waters can be used to evaluate the unsaturated zone flow model. The comparison of concentrations for the present-day climate state and mean infiltration (CRWMS M&O 2000c, Section 3.8) are shown in Figure 4-14. The modeled concentrations were higher than measured concentrations toward the northeast end (left side of Figure 4-14a) and lower at the southwest end of the Exploratory Studies Facility (right side). The northeast end of the drift corresponds to an area of very low infiltration rates, whereas the southwest end is beneath the crest of Yucca Mountain, where infiltration is greater. Measured chloride concentrations exhibit a smaller range of variation than is predicted using the present-day, steady-state infiltration rates. The general agreement among these results indicates that the average of present-day infiltration over the model domain for the mean infiltration distribution, 4.6 mm/yr (0.18 in./yr), is accurate.

As an alternative interpretation of the observed chloride data, infiltration rates were adjusted in the UZ flow and transport models to match with the measured pore water chloride concentration data. The match can be achieved by adjusting infiltration rates in those areas where the match can be improved, while maintaining the average infiltration the same as the current model (USGS 2000b, Section 6.11; CRWMS M&O 2000bw, Section 6.4.3.1). The modified percolation flux map is shown in Figure 4-23. The domain was divided into 9 regions, and for those regions where pore water chloride data were unavailable (Regions I, II, and VIII), the map was filled in using average infiltration values from the unsaturated zone flow model.

The modified model has a more uniform spatial distribution of infiltration rates. However, it is possible to have an alternative interpretation if the PTn, between the shallow infiltration zone in TCw and the potential repository unit in TSw, has strong

damping capacity and the large lateral diversion of flow occurs in the PTn. The spatial variation of infiltration can remain the same as the current model while flow redistribution occurs in the PTn. Significant damping and lateral diversion of flow by the PTn is strongly supported by the recent analyses (Section 4.2.1.1.2). It is therefore demonstrated that alternative models can be formulated to maintain both the heterogeneous distribution of infiltration near the surface and more uniform distribution of chloride content along the underground drifts in the potential repository unit.

Applying the chloride mass balance approach to estimating percolation (using measured pore water chloride concentration data), a modified percolation flux map was developed (Figure 4-23). The domain was divided into 9 regions, and for those regions where pore water chloride data were unavailable (Regions I, II, and VIII), the map was filled in using average infiltration values from the unsaturated zone flow model. The percolation flux values estimated in this manner were then evaluated as estimates of the infiltration rates (USGS 2000b, Section 6.11). The infiltration rates estimated by chloride mass balance are similar to the mean infiltration rates obtained by averaging the rates over the same area (CRWMS M&O 2000bw, Section 6.4.3.1). This provides confirmation that the infiltration data used in the unsaturated zone flow model represent the present-day climate state.

As an alternative interpretation of these data, chloride concentrations modeled from the mean infiltration rates were compared to the measured chloride concentrations (Figure 4-14). The modeled concentrations were higher toward the northeast end (left side of Figure 4-14a) and lower at the southwest end of the exploratory drift (right side). The northeast end of the drift corresponds to an area of very low infiltration rates, whereas the southwest end is beneath the crest of Yucca Mountain, where infiltration is greater. Measured chloride concentrations exhibit a smaller range of variation than is predicted using the present-day, steady-state infiltration rates. However, the general agreement among these results indicates that the average of present-day infiltration over the model domain for the mean infiltration distribution, 4.6 mm/yr (0.18 in./yr), is accurate.

**Chlorine-36 Isotopic Analysis**—Measured background chlorine-36 isotopic ratios in extracted pore waters, while highly variable, are uniformly lower over much of the south ramp compared to the north ramp of the Exploratory Studies Facility. Modeled results indicate that chlorine-36 isotopic ratios in the south ramp should be much lower than in the north ramp, even though the PTn unit is thinner, because the infiltration flux is less. The greater background chlorine-36 isotopic ratios in the north ramp could also be the result of mixing of bomb-pulse water with older matrix pore water. Bomb-pulse chlorine-36 isotopic ratios, indicating fast flow paths, are found in several locations in the vicinity of some fault zones in the exploratory tunnels. Elevated chlorine-36 signatures are confined to the immediate vicinity of faults and other structural features, fast flow zones are localized, and large areas of the potential repository appear to be unaffected by fast-path flow (CRWMS M&O 2000bv, Section 6.6). With regard to perched water, the lack of bomb-pulse chlorine-36 is difficult to interpret because of potential mixing with older water. However, low tritium signatures in perched waters below the potential repository horizon are consistent with the interpretation of limited fast flow at this depth.

Because of the important implications of the occurrence of bomb-pulse chlorine-36 to the site-scale unsaturated zone flow and transport model, the project has undertaken a study to confirm the occurrence of bomb-pulse chlorine-36 at two locations in the Exploratory Studies Facility (the Drill Hole Wash fault zone and the Sundance fault zone). Preliminary results from this ongoing study have not confirmed the presence of chlorine-36, and the analyses of the validation samples at two different laboratories are not consistent. The project has defined a path forward to understand the reasons for the differences: a common set of protocols will be developed, and analyses of the validation samples will continue. However, the unsaturated zone flow and transport model and the TSPA are based on the original data set used in the conceptualization of unsaturated zone behavior. Hence, the project approach conservatively bases the model on the presence of bomb-pulse chlorine-36.

**4.2.1.3.1.6 Summary and Conclusions from Unsaturated Zone Mountain-Scale Modeling**

Results from the unsaturated zone flow model and from analysis of supporting geochemical data are summarized in Figures 4-28 and 4-29, respectively. In summary, available site data have been used to construct an unsaturated zone flow model that has provided infiltration and percolation flux distributions and hydrologic properties, as intended. The model accounts for the occurrence of perched water and enhances the understanding of the effects of the PTn unit and fault zones on flow in the unsaturated zone at the site. The flow model has been interpreted for comparison with chemical and isotopic data, confirming the flow model results in an average sense.

Upper-bound limits on infiltration rates and percolation fluxes at Yucca Mountain are estimated based on multiple approaches (CRWMS M&O 2000bw, Sections 6.2, 6.4, 6.5, and 6.6). These include analyses of chloride and chlorine-36 isotopic ratios, calcite deposition, and the occurrence of perched water. The analysis of chloride data indicates that the average percolation rate over the model domain at Yucca Mountain is about 4.6 mm/yr (0.18 in./yr). Analysis of calcite deposition gives infiltration estimates of 2 to 20 mm/yr (0.08 to 0.8 in./yr) in the vicinity of borehole USW WT-24. To match perched water occurrences, three-dimensional model calibrations require that the present-day average infiltration rate be greater than 1 mm/yr (0.04 in./yr), with an upper limit of about 15 mm/yr (0.6 in./yr).

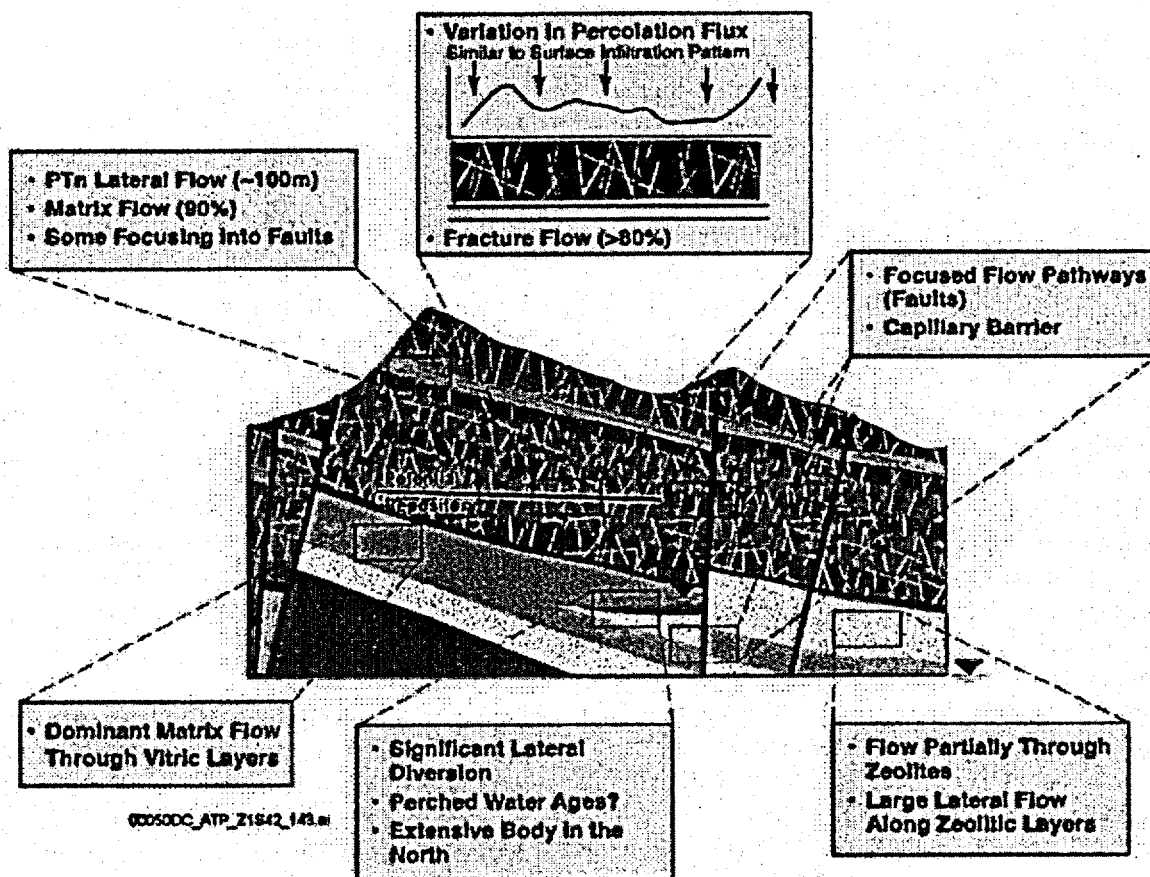


Figure 4-28. Summary of the Unsaturated Zone Flow Model Results  
Source: CRWMS M&O 2000c, Figure 3.7-19.

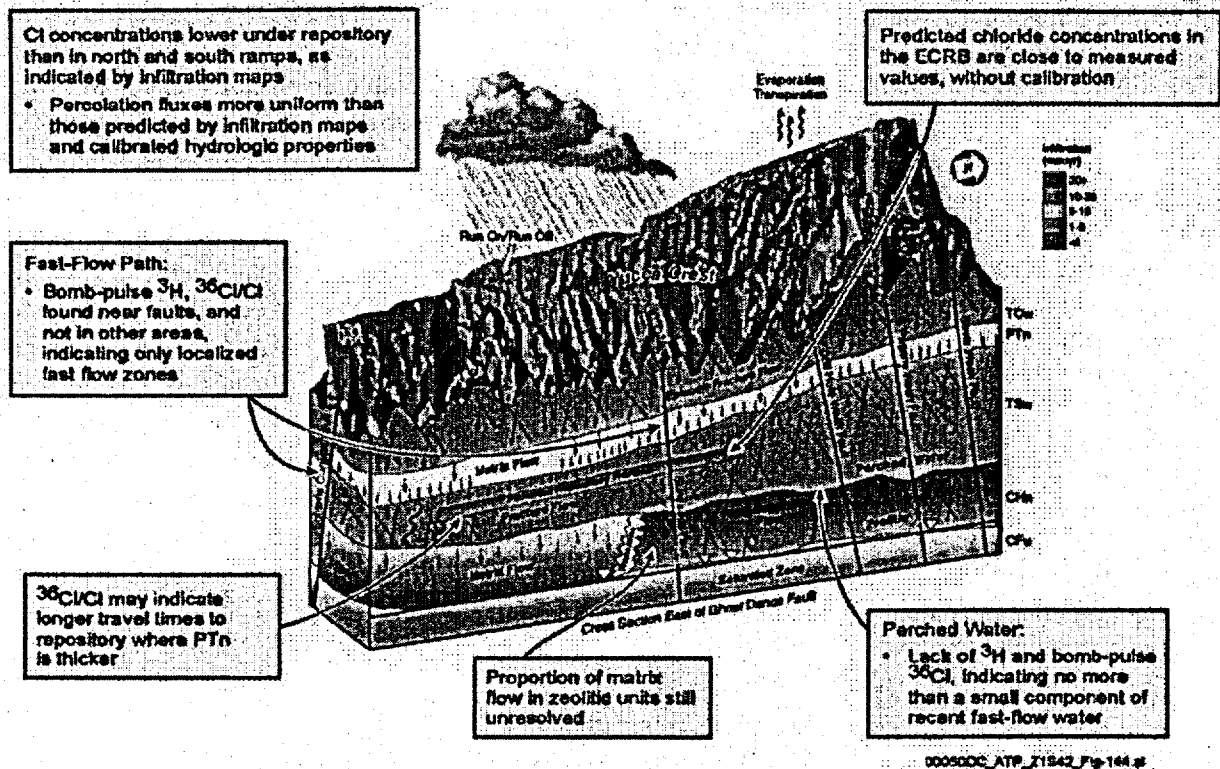


Figure 4-29. Conceptual Model of Unsaturated Zone Flow and Transport at Yucca Mountain Showing Results from Analysis of Geochemical Data  
Source: CRWMS M&O 2000c, Figure 3.8-8.

#### 4.2.1.3.2 Drift Seepage Model

A qualitative description of drift seepage processes was provided in Section 4.2.1.1.5. The characterization and modeling approach presented here for the seepage calibration model focuses on obtaining effective hydrologic properties based on relevant seepage test data (CRWMS M&O 2000c, Section 3.9.1). Figure 4-30 schematically shows the relationships between the different seepage models, as well as data input and the exchange of information. Seepage test data, such as those from the niche studies, are used for developing the seepage calibration model. The modeling approach and parameters are then used in the seepage model for performance assessment. This model supports the abstraction of drift seepage for use directly in TSPA calculations.

The seepage calibration model is a porous-medium model of the fracture continuum that has spatially variable permeability based on air-permeability

data (CRWMS M&O 2000c, Section 3.9.4.4) and is calibrated to the test data from Niche 2 in the Exploratory Studies Facility (CRWMS M&O 2000c, Section 3.9.4.5). Model calibration was used to determine effective hydrologic properties that represent the potential effects of individual fractures and microfractures on drift seepage. Simulations with multiple realizations of the heterogeneous property field were performed to account for the random nature of the fracture network (CRWMS M&O 2000bx, Section 6.3). The steps involved in development of the seepage calibration model are shown schematically in Figure 4-31.

**Model Assumptions**—All seepage models presented in this section are single-continuum models, explicitly representing only the fracture network (not the rock matrix). The justification for this approach is based on the conceptual framework that the fracture network is extensive and well connected, and that flow conditions are steady-state or very slowly varying throughout

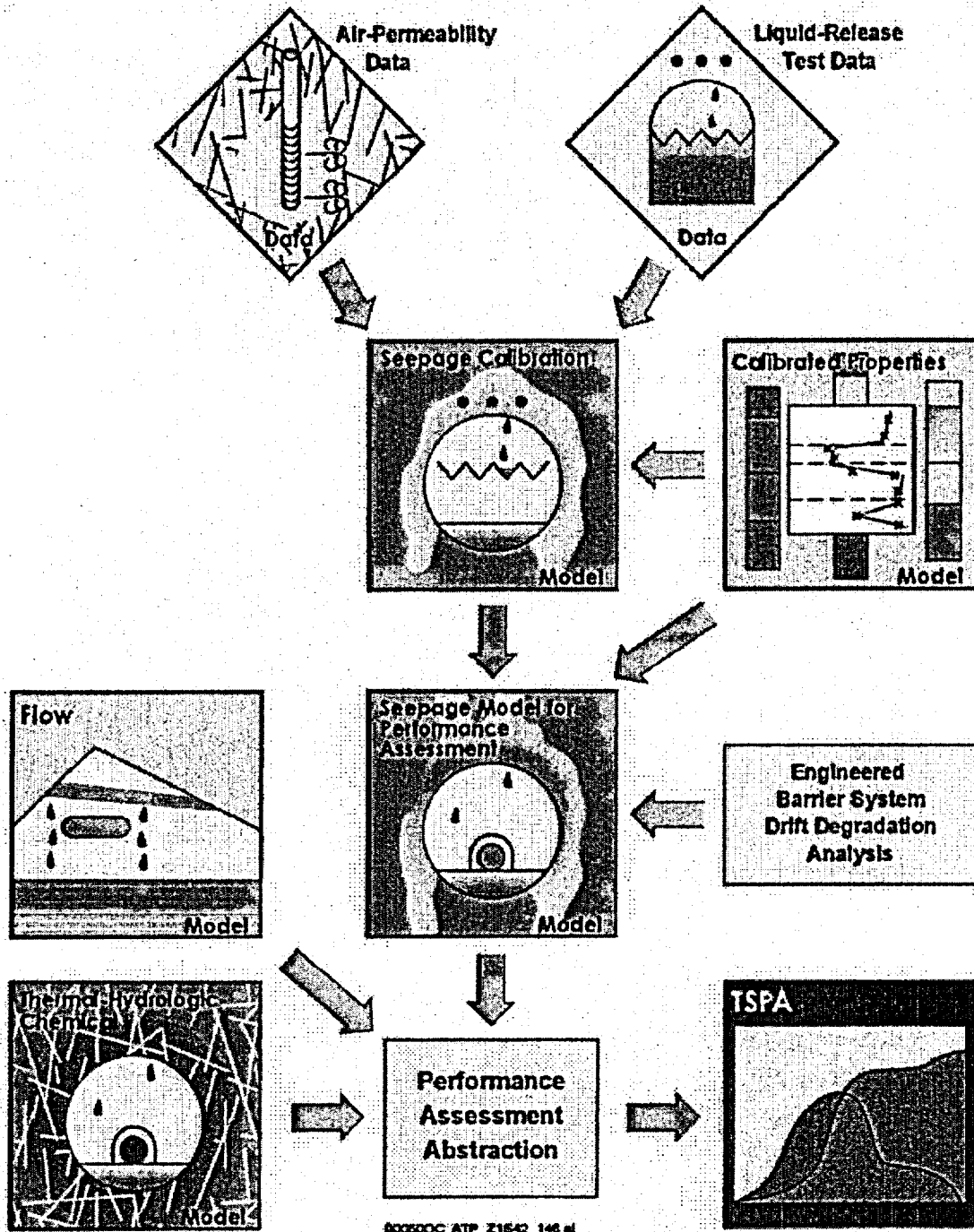


Figure 4-30. Schematic Showing Data Flow and Series of Models Supporting Evaluation of Drift Seepage  
Source: CRWMS M&O 2000c, Figure 3.9-2.

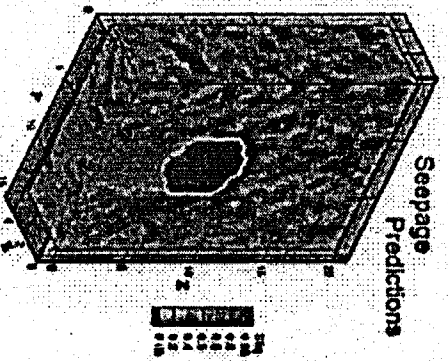
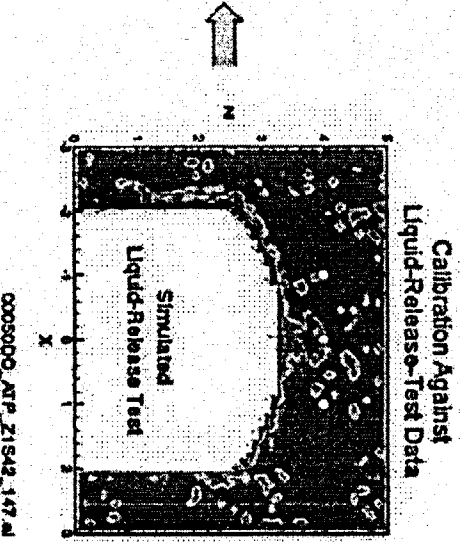
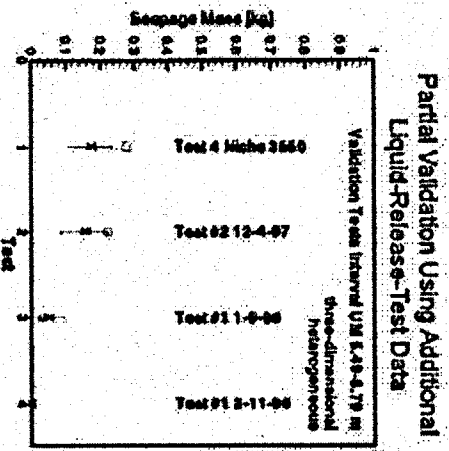
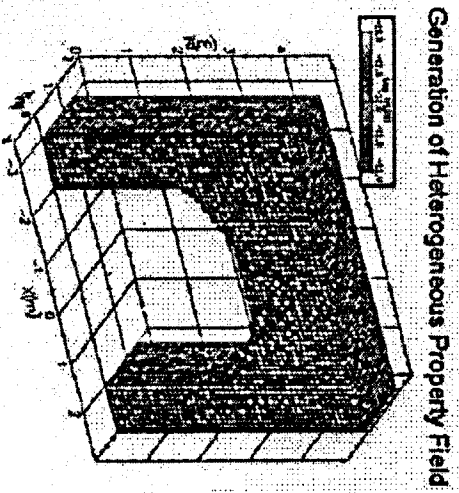
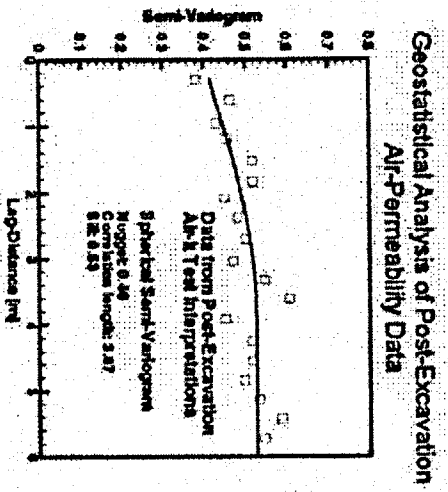


Figure 4-31. Schematic Showing General Approach for the Development of the Seepage Calibration Model  
 Source: Adapted from CRMMS M&O 2000c, Figure 3.9.4.

much of the potential repository host rock because of the moderating influence of the overlying PTn unit. Under steady flow conditions, the flow interaction between the fractures and the matrix in the vicinity of the emplacement drifts will be negligible because of the low permeability of the rock matrix relative to that of the fractures (CRWMS M&O 2000c, Sections 3.3.13 and 3.6.3.2).

The continuum approach is valid for simulating drift seepage, as well as percolation flux, based on the observation that the fracture network in the middle nonlithophysal unit of the Topopah Spring Tuff is well connected (CRWMS M&O 2000bx, Section 6.7). The appropriateness of using the continuum approach to simulate flow through fractured rock was also studied by Jackson et al. (2000) using synthetic and actual field data. They concluded that heterogeneous continuum representations of fractured media are self-consistent (i.e., appropriately estimated effective-continuum parameters can represent the underlying fracture network characteristics).

Adopting the continuum approach, unsaturated flow of liquid water is governed by Richards' equation, the governing equation of water content or capillary pressure based on mass conservation law (Richards 1931). Relative permeability and capillary pressure are described according to the van Genuchten-Mualem model (Luckner et al. 1989, pp. 2191 to 2192). Within the heterogeneous property distribution, capillarity of the effective medium is correlated to absolute permeability according to the Leverett scaling rule, with capillary strength inversely proportional to the square root of permeability (Leverett 1941, p. 159).

Since percolation flux cannot be directly measured in the field, the average percolation flux in the host rock is estimated by the unsaturated zone flow model and multiplied by flow-focusing factors derived using the active-fracture concept (CRWMS M&O 2000by, Section 6.3.3).

In-drift evaporation and ventilation effects are not included in the current seepage model, but neglecting them is conservative because it produces greater estimates of predicted seepage. The evaporation reduces drop formation and drip-

ping (Ho 1997a) and enhances the vapor diffusion into the drift. Neglecting evaporation effects increases predicted seepage of liquid water (CRWMS M&O 2000c, Section 3.9.3.3).

**Seepage Threshold Prediction**—Steady-state seepage simulations were performed with the seepage calibration model (CRWMS M&O 2000bz, Section 6.6). In this application, percolation flux was applied at the top of the model, instead of from a borehole as in the niche tests. The ambient percolation flux was varied over a wide range, starting from a small value yielding zero seepage, increasing stepwise until seepage was predicted to occur, and increasing further to estimate seepage percentage. Using this procedure, a seepage threshold of approximately 200 mm/yr (7.8 in./yr) was obtained for the middle nonlithophysal unit of the Topopah Spring Tuff. The seepage-threshold prediction obtained for Niche 2 suggests that diversion of flow around the emplacement drift openings is an effective barrier to water that could otherwise contact waste packages (BSC 2001a, Sections 4.2.2 and 11.3.1.1.1).

#### 4.2.1.3.3 Model Calibration and Validation

An important objective for the unsaturated zone flow model is to produce a model consistent with the available site characterization data. This is accomplished through an iterative process of model calibration to the data, adjusting the hydrologic properties that represent the rock units (CRWMS M&O 2000c, Section 3.9.4.5). A combination of one-, two-, and three-dimensional numerical models is used to represent the lateral variation of hydrologic conditions in the unsaturated zone, for example, from the northern to the southern ends of the potential repository layout area. The data that constrain the calibration process include borehole-measured matrix saturation, water potential, temperature, the presence of perched water, pneumatic-pressure measurements, and geochemical data. The model calibrations require specification of the water infiltration at the ground surface and its variation throughout the site area (USGS 2000b, Section 6.11). To represent uncertainty in the infiltration estimates, separate infiltration distributions are used, representing upper-bound, mean, and lower-bound conditions.

Separate model calibrations (i.e., hydrologic property sets) are developed for the three infiltration distributions. The distributions of infiltration for future monsoonal and glacial-transition climate conditions were developed using the infiltration model (CRWMS M&O 2000c, Section 3.5.2), which was calibrated using data for present-day infiltration rates. Table 4-11 summarizes average precipitation and infiltration rates. Figure 4-25 shows mean infiltration distributions over the model domain for each climate state.

Model calibrations were performed using one-dimensional numerical grids to estimate mountain-scale hydrologic properties for the hydrogeologic units. The one-dimensional calibration model consists of 11 vertical columns, shown schematically in Figure 4-32, representing the hydrostratigraphy at 11 boreholes for which suitable site characterization data are available. The use of a one-dimensional vertical model implicitly assumes that flow is adequately approximated as one-dimensional and vertical (i.e., that lateral flow is not important). In the TCw, PTn, and TSw rock units, this assumption is supported by the absence of perched water (CRWMS M&O 2000c, Sections 3.6.4.1). At the bottom of the TSw unit and below, perched water does exist in some areas, especially to the north. Perched water is investigated using the three-dimensional model (CRWMS M&O 2000c, Section 3.7.3.3).

The one-dimensional calibrated mountain-scale formation properties are then used as input to a

two-dimensional model, which is used to calibrate the fault properties. The two-dimensional model consists of an east-west cross section, shown schematically in Figure 4-33. This cross section is located where there are borehole data available for the ambient hydrologic conditions in a fault at Yucca Mountain. Use of a two-dimensional model implies that flow constrained to the vertical and east-west directions adequately represents ambient conditions. The dip of the bedding and the strike of the fault are approximately parallel to the cross section; therefore, the assumption is reasonable. The same types of properties calibrated for the mountain-scale formation properties are calibrated for the faults. Figure 4-33 also shows the match between the calibrated simulation and the saturation, water potential, and pneumatic data for present-day ambient conditions (mean infiltration).

The resulting calibrated hydrologic properties (including fracture and matrix permeability, fracture and matrix van Genuchten parameters, and active-fracture parameters) are then used as input to mountain-scale and drift-scale hydrologic models. Calibration activities in three dimensions (involving hydrologic measurements, perched water, temperature, and ambient geochemical data) are carried out for additional refinement of mountain-scale properties. Figure 4-34 shows an example of the results from the three-dimensional calibration. This figure compares the observed and simulated matrix saturation and perched water

**Table 4-11. Average Precipitation and Average Infiltration Rates over the Unsaturated Zone Flow Model and Transport Model Domain**

|   | Present-Day Climate<br>(to 600 years) |                 |                 | Monsoon Climate<br>(600 to 2,000 years) |                  |                 | Glacial-Transition Climate<br>(beyond 2,000 years) |                  |                 |
|---|---------------------------------------|-----------------|-----------------|---|------------------|-----------------|--|------------------|-----------------|
|   | Upper bound                           | Mean            | Lower bound     | Upper bound                             | Mean             | Lower bound     | Upper bound  | Mean             | Lower bound     |
| Average Precipitation Rate, <sup>a</sup> mm/yr (in./yr) | 268.6<br>(10.58)                      | 190.6<br>(7.50) | 188.8<br>(7.35) | 414.8<br>(16.33)                        | 302.7<br>(11.92) | 190.6<br>(7.50) | 433.5<br>(17.07)                                   | 317.8<br>(12.51) | 202.2<br>(7.96) |
| Average Infiltration Rate, <sup>b</sup> mm/yr (in./yr)  | 11.1<br>(0.44)                        | 4.6<br>(0.18)   | 1.3<br>(0.05)   | 19.8<br>(0.78)                          | 12.2<br>(0.48)   | 4.6<br>(0.18)   | 33.0<br>(1.30)                                     | 17.8<br>(0.70)   | 2.5<br>(0.10)   |

Source: <sup>a</sup>CRWMS M&O 2000c, Table 3.5-2.  
<sup>b</sup>CRWMS M&O 2000c, Table 3.5-4.

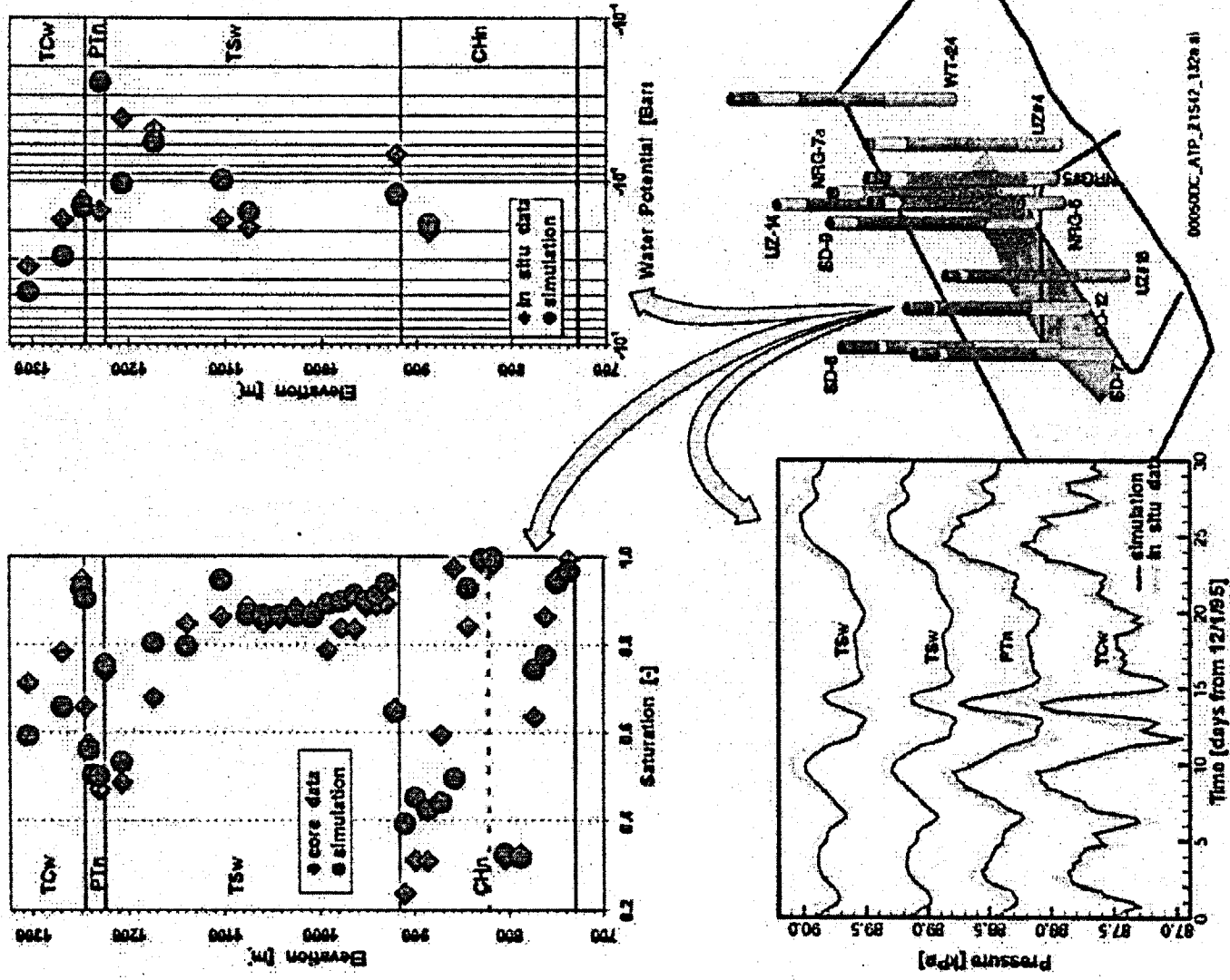


Figure 4-32. Calibrated One-Dimensional Simulation Match to Saturation, Water Potential, and Pneumatic Data from Borehole USW SD-12 and simulation results for the present-day mean infiltration rate. Source: CRWMS M&O 2000c, Figure 3.6-4.

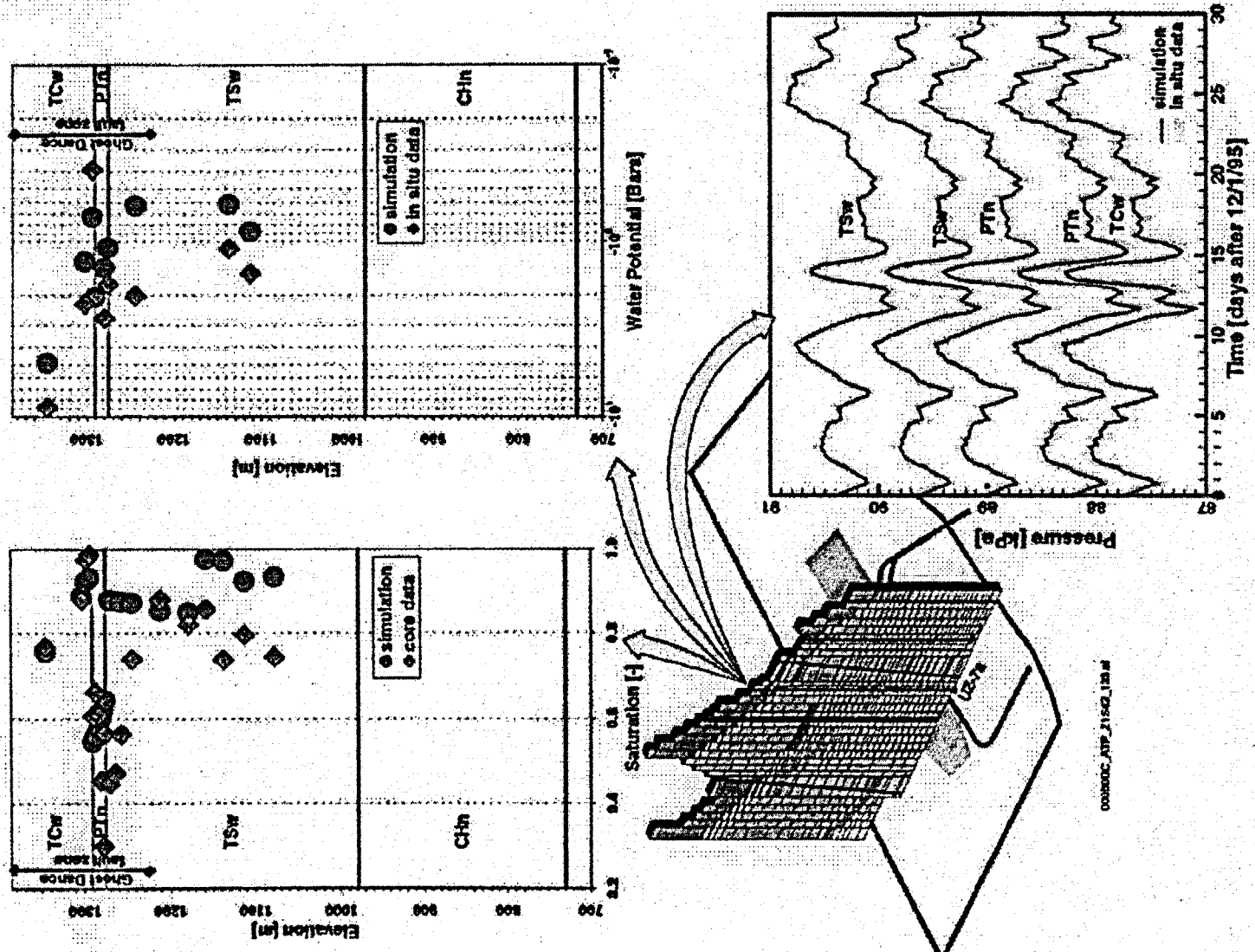
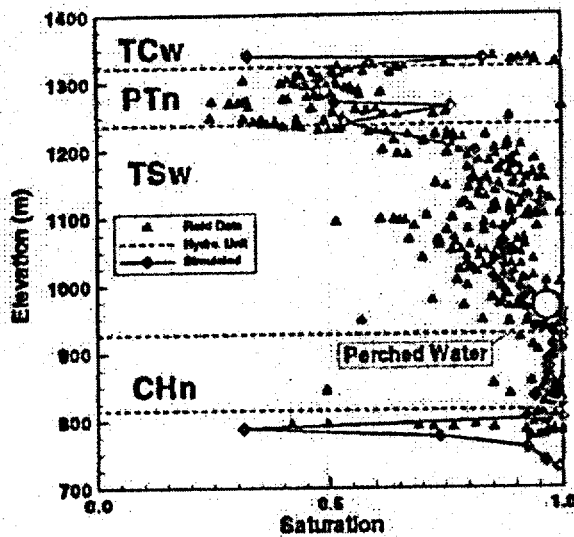


Figure 4-33. Calibrated Two-Dimensional Simulation Match to Saturation, Water Potential, and Pneumatic Data from Borehole USW UZ-7a and simulation results for the present-day mean infiltration rate. Source: CRWMS M&O 2000c, Figure 3.6-5.



000500C\_ATP\_Z1842\_134.ai

Figure 4-34. Comparison of Simulated and Observed Matrix Liquid Saturations, Showing Perched Water Elevations Data from Borehole USW UZ-14 and simulation results for the present-day mean infiltration rate. Source: Data from CRWMS M&O 2000bw, Section 6.6.3; Figure 6-41; figure adapted from CRWMS M&O 2000c, Figure 3.7-14.

elevation at borehole USW UZ-14, using the present-day-ambient conditions (mean infiltration). Overall, the simulation results for this borehole (and others used in the calibration activity) are generally consistent with the observed saturation and perched water data.

**Model Validation and Confidence Building—**Validation of the calibrated hydrologic property sets constituting the calibrated properties model was performed using the three-dimensional model (CRWMS M&O 2000bw, Section 6.8). In situ water potential data measured from the ECRB Cross-Drift compare well with predicted water potentials, as shown in Figure 4-35. Although the predicted water potentials are generally lower, the difference is only a few tenths of a bar (1 bar =  $10^5$  Pa). Pneumatic pressure data also compare well to the predicted pneumatic pressures shown in Figure 4-35. These and other results presented in *Unsaturated Zone Flow and Transport Model Process Model Report* (CRWMS M&O 2000c, Section 3.6.5.3) show that the calibrated properties are

valid for predicting ambient conditions, and that the assumptions of one-dimensional and two-dimensional flow are suitable for use in the calibration process.

Pore water chemical composition data have been used to validate the unsaturated zone flow model to bound the infiltration flux, flow pathways, and transport time through the unsaturated zone. Infiltration rate calibrations are performed using the pore water chloride concentration data. Agreement between the predicted chloride distributions and observed data are improved when the calibrated infiltration rates are used. Similar analyses have been performed using calcite deposition to further constrain hydrologic parameters, such as infiltration flux. These geochemical studies provide additional support for validation of flow and transport models (CRWMS M&O 2000bw, Sections 6.4 and 6.5; CRWMS M&O 2000c, Sections 3.7 and 3.8).

**Seepage Model Calibration—**Data from five tests (CRWMS M&O 2000bz, Table 6) were selected for calibration of the seepage model. The five tests were conducted in a 0.3-m (1-ft) long borehole interval at various injection rates to sample the dependence of seepage on flux. Approximately 1 liter of water was injected in each test. Seepage percentages from the test series demonstrate storage effects and seepage rates above and below a seepage threshold. Analysis of all five tests provided a match between model results and observed seepage. As shown in Figure 4-36, the heterogeneous three-dimensional seepage calibration model matches the observed seepage data better than the two-dimensional or homogeneous alternatives.

**Seepage Model Validation—**The seepage calibration model was used to make predictions of observed seepage percentages from liquid injection tests that were performed in a different borehole interval using different injection rates and varying other test conditions. The uncertainty of the model predictions was evaluated using linear error propagation analysis and Monte Carlo simulation. (This approach reflects the intended use of the resulting seepage models, in which seepage is treated statistically.) Observed seepage percentages lay within

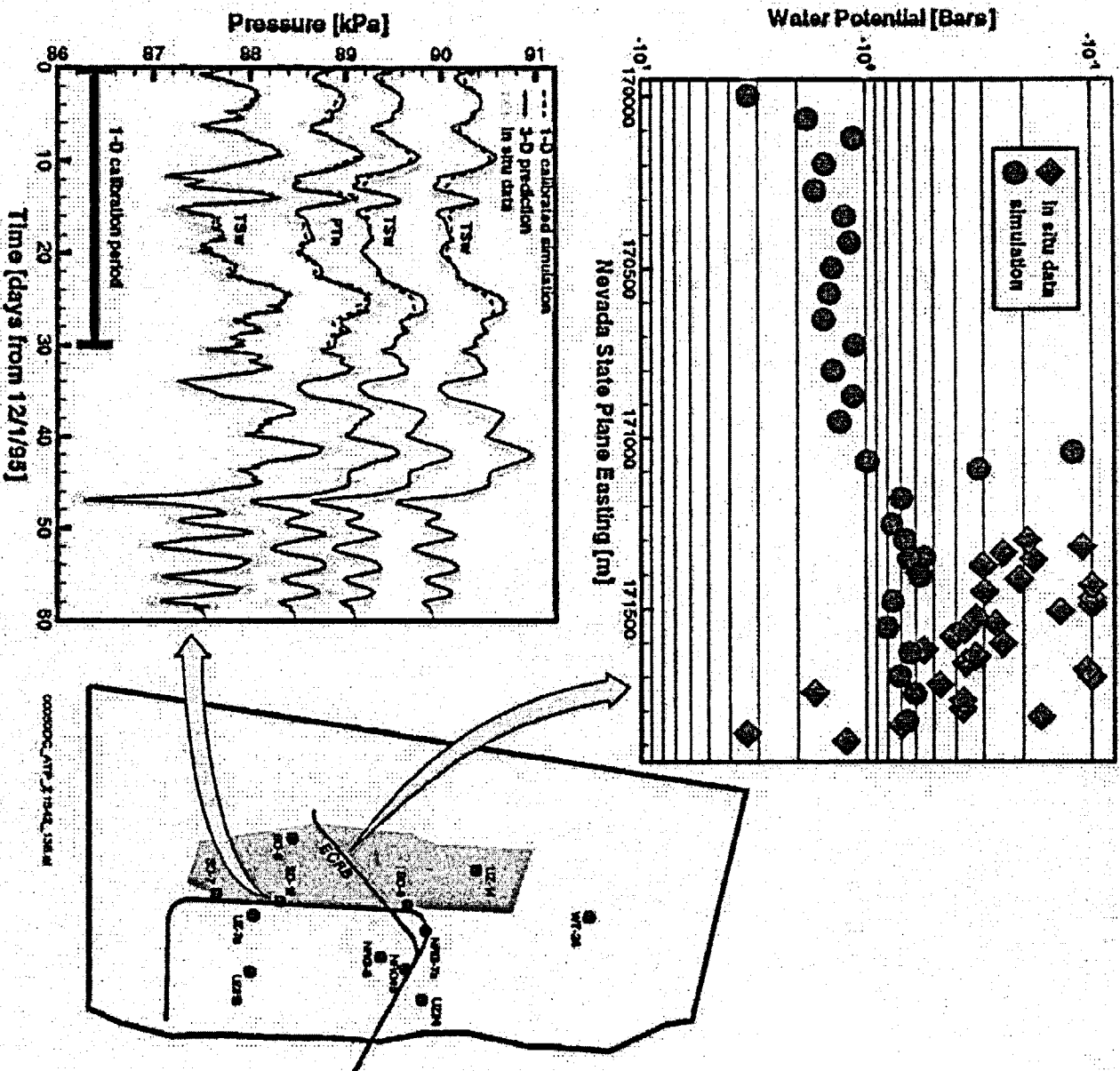


**Figure 4-35. Comparison of Predictions from the Three-Dimensional Model with In Situ Water Potential and Pneumatic Pressure Data**  
 Water potential data from the ECRB Cross-Drift and pneumatic pressure data from Borehole USW SD-12. Source: CRWMS M&O 2000c, Figure 3.6-8.

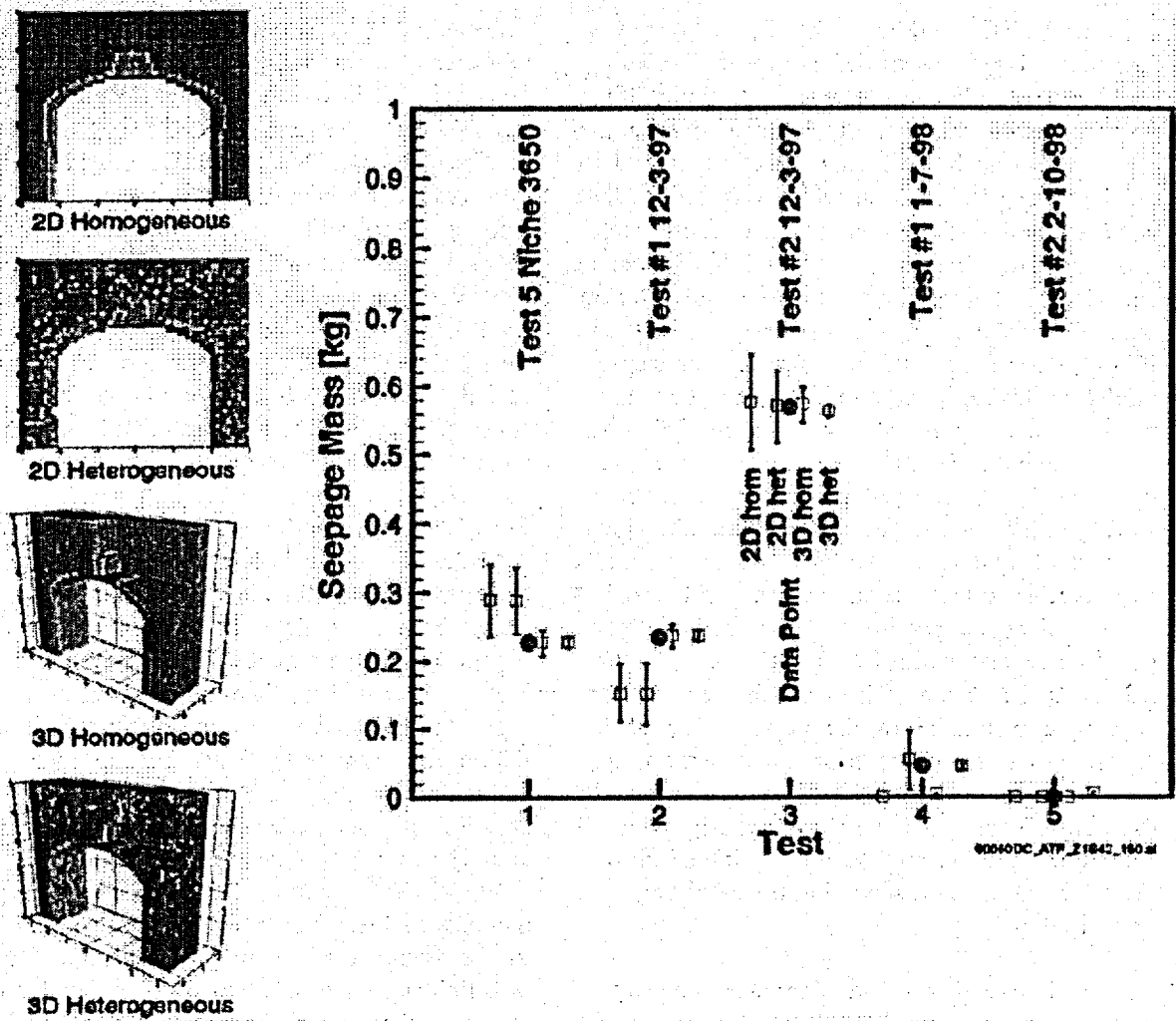


Figure 4-36. Comparison between the Measured Seepage Mass and Seepage Mass Calculated with Two-Dimensional and Three-Dimensional Homogeneous and Heterogeneous Models  
Measured seepage mass is plotted with black dots. The model predictions are plotted with squares. The four models are visualized on the left and labeled by color, as indicated inside the plot. The uncertainty of the model predictions is shown as error bars on the 95 percent confidence level. The three-dimensional heterogeneous seepage calibration model matches the data best. Source: CRWMS M&O 2000c, Figure 3.9-6.

the uncertainty range of the model predictions. This favorable result provides confidence in the validity of the seepage model. More details about the seepage calibration model can be found in *Seepage Calibration Model and Seepage Testing Data* (CRWMS M&O 2000bz).

#### 4.2.1.3.4 Alternative Conceptual Processes

In developing models of water movement through the unsaturated zone at Yucca Mountain, alterna-

tive conceptual processes were identified and considered (CRWMS M&O 2000c, Section 1.2.4). This section summarizes some key alternative concepts for processes governing water movement through the unsaturated zone.

**PTn Lateral Flow**—In an early conceptual model of Yucca Mountain, Montazer and Wilson (1984, pp. 45 to 47) hypothesized that significant lateral flow occurs within and above the PTn unit because of the contrast in hydraulic properties at the contact

between the TCw and PTn units. They also showed that vertical heterogeneities within the PTn may result in a much larger effective permeability of the unit in the direction of dip, compared with the effective permeability in the direction normal to the bedding plane. Montazer and Wilson (1984, p. 47) argued that the combination of this factor and capillary barrier effects might introduce considerable lateral flow within the unit. Recent modeling of the potential for diversion on or in the PTn supports the Montazer and Wilson conceptual model of lateral flow and diversion. Pneumatic measurement of permeability on, in, and below the PTn, geochemical data, and saturation and water potential data were used to calibrate unsaturated zone parameters and to differentiate alternative conceptual models. Modeling based on the capillary barrier effect using a fine grid spacing supports the concept of diversion of flow above the potential repository horizon (BSC 2001a, Section 3.3.3.4.2). Diversion of flow above the repository would be beneficial to the performance of the repository. It is not necessary for diversion large enough to result in diversion to faults to occur for the PTn to damp episodic flow in the unsaturated zone, but diversion might be an additional mechanism for uniformly distributing the areal variation of infiltration.

**PTn Fracture Flow**—An alternative conceptual model for water flow through the PTn is one that assumes pervasive fracture flow through this unit (CRWMS M&O 2000c, Section 3.3.3). However, the available data, which show high matrix porosity and storage capacity combined with relatively high matrix permeability and limited fracturing (see to Sections 4.2.1.2.3 through 4.2.1.2.5)—in addition to geochemical data that indicate a lack of widespread bomb-pulse chlorine-36 signatures in the PTn (see Section 4.2.1.2.8)—support the preferred conceptual model of predominantly matrix flow through the PTn.

**Episodic Flow Within the TSw**—In the prevailing conceptual model, episodic flow into the TSw unit is considered to be damped by the PTn to the extent that flow can be regarded as steady-state when it enters the TSw. The exception is that at or near major faults, episodic flow may still persist through the PTn, though these isolated fast flow

paths are considered to carry only a small amount of water. An alternative view to this conceptual process is one in which episodic flow is pervasive through the TSw unit (CRWMS M&O 2000c, Section 3.7.3.1). This alternative may be a more conservative conceptualization because a greater amount of episodic flow could lead to greater seepage into potential waste emplacement drifts. However, for the reasons presented in Section 4.2.1.3.1.1 (in the discussion of transient versus steady-state flow), flow and transport in the unsaturated zone has been found to have low consequence; thus, the approach that is regarded as more plausible has been taken.

**Flow Through Faults**—As discussed in Section 4.2.1.2.6, limited fault permeability measurements are only available for the welded units, TCw and TSw. From these data, it is inferred that faults within the PTn and CHn/CFu units have relatively higher permeabilities than the adjacent nonfaulted rock. An alternative view is one in which faults within the PTn and CHn/CFu units have low permeabilities and retard the movement of water because of the occurrence of low-permeability alteration minerals within the fault zones (CRWMS M&O 2000c, Section 3.3.5). This conceptual model would result in slow transport from the TSw to the water table. Available measured data are insufficient to confirm either conceptual model. However, the conceptualization of faults as higher-permeability structures in the PTn and CHn/CFu units is adopted because it is the conservative approach, providing fast flow pathways to the water table and allowing discharge from perched water bodies.

**Discrete Fracture Network Model for Seepage**—A discrete fracture network model is an alternative conceptual model to the heterogeneous fracture continuum model (CRWMS M&O 2000bz, Section 6.7). A high-resolution discrete fracture network model, in principle, should be capable of simulating channelized flow and discrete seepage events. However, the development of a defensible discrete fracture network model for the unsaturated zone at Yucca Mountain would require the collection of geometric and hydrologic property data on billions of fractures. While some of the required geometric information could be

obtained from fracture mappings, the detailed description of the fracture network would be incomplete and highly uncertain. Moreover, measurement of unsaturated hydrologic parameters on the scale of individual fractures would be required, which would be largely impractical. The development of a discrete fracture network model at the mountain scale is therefore impractical (CRWMS M&O 2000bz, Section 6.7), so an equivalent fracture continuum model is used to represent the fracture system for the prediction of effective seepage quantities. The appropriateness of this model is demonstrated by Finsterle (2000).

#### 4.2.1.3.5 Limitations and Uncertainties

The assessment of the current understanding of flow through the unsaturated zone needs to take into account the limitations and uncertainties in the unsaturated zone flow model. The model is limited mainly by the current characterization of the unsaturated zone flow system within Yucca Mountain, including geologic and conceptual models; by the applicability of the volume-averaging modeling approach; by the assumption of steady-state moisture flow; and by the available field and laboratory data (CRWMS M&O 2000c, Section 3.7.4.5). Remaining uncertainties in the model parameters include (1) accuracy in the estimated present-day, past, and future net infiltration rates over the mountain; (2) quantitative descriptions of heterogeneity within the welded and nonwelded tuff units, the flow properties associated with these units, and the detailed spatial distribution of these units within the mountain, especially below the potential repository horizon; (3) sufficiency of field studies and data, especially for characterizing hydrologic properties of faults and fractures within the zeolitic units; (4) alternative conceptual models quantifying the fluid transmissive properties of faults; and (5) evidence for lateral diversion above or within the zeolitic portions of the Calico Hills nonwelded hydrogeologic unit beneath the potential repository horizon (CRWMS M&O 2000c, Section 3.7.4.5).

As noted in Section 4.1.1.2, the DOE has initiated several activities to improve the treatment of uncertainty in current models (BSC 2001a, Section 2.1). Some of the unsaturated zone models will be

updated as a result of those activities. Those updates will be documented in future reports.

The identification and propagation of uncertainties is important for the appropriate treatment of the models used in TSPA-SR calculations. Uncertainties associated with the major unsaturated zone model components are described in detail in the *Unsaturated Zone Flow and Transport Model Process Model Report* (CRWMS M&O 2000c, Section 3.13).

The uncertainty and variability in the model parameters are due, in part, to the natural, variability and heterogeneity in the geological, hydrologic, chemical, and mechanical systems that are difficult to characterize in situ, such as the precise fracture network in the unsaturated zone. Uncertainties in models may also be due to conditions that are difficult to predict, such as future climate states.

**Uncertainties Associated with Climate**—As described in *Future Climate Analysis* (USGS 2000a, Section 6.5), future climates cannot be predicted in any precise way. Uncertainty arises because of the complexity of global climate systems and because climate changes can be triggered by unforeseen circumstances, such as major tectonic events (e.g., volcanic eruptions) or human activity. However, studies of past climates (paleoclimate studies) demonstrate that changes can be correlated with cyclical variations in the earth's orbit and the tilt of the earth's axis of rotation, both of which affect the amount of solar radiation the atmosphere receives. The earth's orbit changes in a regular and predictable manner over a cycle of about 400,000 years. Paleoclimate studies, which include geochemical analyses of sediments deposited in lakes, minerals deposited in springs, fossils of microorganisms that lived in both lakes and springs, and plant and animal remains preserved in caves, suggest that the sequence of climate changes in the 400,000-year cycle is not random, and that future climate conditions will evolve systematically. The variability of the glacial-transition period has large impacts to the model predictions as the results of long duration and high precipitation values. In the TSPA-SR, a conservative approach is adopted, with the glacial-transition

climate extending beyond 10,000 years and the shorter and drier interim periods not taken into account (CRWMS M&O 2000a, Section 3.2.1.2).

Although future climate conditions cannot be precisely predicted and climate varies considerably even within glacial and interglacial periods, studies provide a reasonable basis for forecasting the range of climates Yucca Mountain will probably experience in the future (USGS 2000a). This forecast, which incorporates the variability observed in studies of the past climate, has been used as input to models that assess the future performance of a repository at Yucca Mountain. The present warm, dry interglacial period will probably end in the next 400 to 600 years, and may be followed by a transition to a warm, wet monsoon climate for approximately 900 to 1,400 years. The climate would then shift to a glacial-transition period. The variability of the climate conditions is quantified by upper bounds for wetter climates and lower bounds for drier climates, as presented in Section 4.2.1.3.1.

**Uncertainties Associated with Lower Tuff Units**—The relatively high density of data in the potential repository area, particularly within and above the TSw, helps to reduce uncertainty in the understanding of flow behavior between the land surface and potential repository horizon. Greater uncertainty exists, however, below the TSw (i.e., within the CHn and CFu) because rock hydrologic properties are highly variable and few data are available to capture the spatial variability. Modeling uncertainties also increase rapidly with lateral distance away from the potential repository area as the density of data points is greatly reduced.

As a result, many of the hydrologic properties used in unsaturated zone modeling studies of Yucca Mountain for layers within the CHn and CFu have been estimated using analogue data from the PTn, the TSw, and portions of the CHn for which data are available. Despite similar welding characteristics, the PTn data (specifically, fracture permeability) used as an analogue to the CHn tend to be conservative because of many inherent differences in the depositional and postdepositional history of these tuffs. Fault properties were esti-

mated for the CHn/CFu, derived from in situ fault testing in the TSw; however, there are different welding textures associated with each major unit. For example, faults may be more permeable within the TSw because the brittle nature of the densely welded tuffs can lead to the development of well-connected fracture networks. Within the CHn, however, the predominantly nonwelded tuffs are likely to exhibit more plastic deformation (producing fewer well-connected fractures) and are much more susceptible to alteration (producing low-permeability clays and zeolites that hinder vertical flow) when exposed to percolating water.

**Uncertainties Associated with Calibrated Property Values**—Calibrated rock hydrologic property values derived from core-sample measurements, fracture mapping, and in situ field data provide important input to the unsaturated zone model in that they define the hydrologic characteristics of each cell within the numerical grid. Uncertainties related to calibrated hydrologic properties include (1) variability in measured properties of rock core samples and uncertainty in cross-correlations between measured properties; (2) spatial variability in rock properties; (3) uncertainty in the initial estimates of rock properties and in upscaling of measured data to model grid blocks; and (4) nonuniqueness of results generated by the estimation procedure (CRWMS M&O 2000c, Table 3.13-1). With a total of 194 calibrated properties (all the calibrated hydrogeologic unit and fault properties), the quantitative estimation of uncertainty is complex. Cross correlations between some of the properties tend to compound the uncertainties assigned to individual properties. Furthermore, the statistical assumptions that underlie the uncertainty analysis implemented in the estimation procedure are not justified if the estimation uncertainties become very large because of cross correlations. However, the calibrated property values generally do not vary much from the initial values input to the estimation procedure, and the initial values are chosen to be plausible. Because the initial and calibrated properties are generally similar, the uncertainties of the initial property estimates can be used as surrogates for the uncertainties of the calibrated property values (CRWMS M&O 2000c, Section 3.6.5.2).

Where the calibrated properties change significantly with respect to the initial values, the numerical model produces results that differ from the initial interpretation. For example, the transitions between matrix-dominated and fracture-dominated flow, at interfaces between nonwelded and welded tuff, depend on processes that occur at scales smaller than the numerical grid spacing. Consequently, the calibrated property values at these interfaces reflect the response of the numerical model, which uses coarser spacing.

**Uncertainties Associated with the Numerical Approach**—An additional uncertainty in unsaturated zone modeling is the mathematical representation of complex flow phenomena. The volume-averaging approach used, and the model assumption of steady-state moisture flow (used in interpreting ambient conditions), simplify the representation of water flow through the site, adding uncertainty to the model results.

**Uncertainties Associated with Geochemical Analyses**—The amount of calcite precipitated over time is sensitive to the water and gas composition, the reactive surface area, and the thermodynamic and kinetic parameters used in the model (CRWMS M&O 2000bw, Section 6.5). Because calcite abundances are highly variable at the different locations sampled (CRWMS M&O 2000bv, Section 6.10.1.1; see also Figure 4-14 in Section 4.2.1.2.12), the calcite analysis approach is suitable for estimating a range of percolation fluxes, as discussed in Section 4.2.1.3.

The use of chloride to estimate percolation fluxes or infiltration rates is directly related to the initial estimate of the effective chloride concentration in precipitation, the spatial variation, and changes over time (Ginn and Murphy 1997, pp. 2065 to 2066). The long-term projection of spatial and temporal patterns of precipitation is uncertain because the patterns have been measured for less than 100 years, which is short compared to the time period over which the chloride concentrations have developed in the unsaturated zone (tens of thousands of years) (Sonnenthal and Bodvarsson 1999, pp. 107 to 111). Given these uncertainties, the chloride mass balance approach is used to estimate ranges in the infiltration rate for comparison to the

flow model. The distribution of chloride in the unsaturated zone is also influenced by lateral flow diversion, as well as diffusion and dispersion processes, and thus may not accurately represent local infiltration conditions. However, the average chloride concentration for pore water in the unsaturated zone is a better indicator of the average infiltration flux.

Bomb-pulse chlorine-36 signatures can be clearly identified in isotopic data. However, the chlorine-36 background analysis is more uncertain because of the possibility for contamination of older chlorine by bomb-pulse chlorine-36. Accordingly, the chlorine-36 method is used to detect clear indications of modern fast pathways and to identify regions of the unsaturated zone with faster transport to the repository horizon (which may also be associated with fast pathways). Bomb-pulse tritium signatures can be attributed to liquid or vapor movement, both of which are prevalent in the unsaturated zone. The presence of bomb-pulse tritium can indicate fast liquid flow from the surface or redistribution of modern infiltration by evaporation and gas-phase movement of water vapor.

**Uncertainties Associated with Seepage**—Seepage threshold predictions are expected to vary with location. The seepage threshold value of 200 mm/yr (7.8 in./yr) applies to Niche 2 (CRWMS M&O 2000c, Section 3.9.4.7). Further abstraction analysis is used to extend the seepage calibration model to the repository area (CRWMS M&O 2000c, Section 3.9.6.4). Much of the potential repository area is located in the lower lithophysal zone of the Topopah Spring Tuff, which is more permeable than the middle nonlithophysal zone, with shorter fractures and pervasive lithophysal cavities. Some of the frames of Figure 4-18 for Niche 5 in the ECRB Cross-Drift show an example of a large lithophysal cavity and a borehole image of lithophysal cavities.

The greater permeability of the lower lithophysal unit of the Topopah Spring Tuff may enhance the capillary barrier effect (i.e., reduce seepage), either by the presence of more permeable fractures or by higher porosity and permeability in the rock matrix that can absorb more water. Geologic mapping

along the ECRB Cross-Drift indicates that the lower lithophysal zone is very heterogeneous; investigations of the hydrologic properties of this rock unit are ongoing.

#### 4.2.1.3.6 Summary of the Current Understanding of Unsaturated Zone Flow and Seepage into Drifts

Current understanding of unsaturated flow at Yucca Mountain has been gained through collection of site data and modeling of the relevant processes. Table 4-12 summarizes the current understanding of flow parameters and processes. The table identifies features, events, and processes that are important to unsaturated zone flow processes and could affect the waste isolation performance of a repository. The statements listed under the "Current Understanding" column are a mixture of observations, hypotheses, and insights that constitute only abridged, summary information. Additional detail is provided in the *Unsaturated Zone Flow and Transport Model Process Model Report* (CRWMS M&O 2000c). Note that Table 4-12 summarizes current understanding only for flow processes occurring in the unsaturated zone hydrogeologic units and for seepage. A discussion of issues related to flow and transport processes occurring below the potential repository is presented in Section 4.2.8.

#### 4.2.1.4 Total System Performance Assessment Abstraction

##### 4.2.1.4.1 Unsaturated Zone Flow Abstractions for Total System Performance Assessment

A total of nine flow fields are used in the TSPA base case calculations. These consist of three infiltration cases (lower, mean, and upper) within each of the three climate states (present-day, monsoon, and glacial-transition).

**Abstraction of Water Table Rise**—The two future climate states (monsoon and glacial-transition) are expected to be wetter than the present-day climate, and, as a result, the water table is expected to rise. However, uncertainty exists regarding the amount of water table rise for each climate state.

Therefore, as discussed in Section 4.3.3.1 and in *Abstraction of Flow Fields for RIP (ID: U0125)* (CRWMS M&O 2000ca, Section 6.2), a conservative water table rise of 120 m (390 ft) is used for all flow fields using future climate states. Recent analyses described in Section 4.3.3.1.3 indicate that the maximum rise in the last 2 million years has been about 17 to 30 m (56 to 98 ft).

The impact of the water table rise on transport beneath the potential repository was evaluated in *Analysis of Base-Case Particle Tracking Results of the Base-Case Flow Fields (ID: U0160)* (CRWMS M&O 2000cb, Section 6.2.4). Results showed that the elevated water table reduces transport times beneath the repository (the median breakthrough for a sorbing tracer, neptunium, decreased by nearly a thousand years for the mean infiltration case).

**Abstraction of Groundwater Breakthrough**—The breakthrough time to the water table of a nonsorbing tracer (technetium) released uniformly in the repository region is simulated for TSPA to gain insight into the range of possible radionuclide transport times that can result based on the different possible infiltration cases for the present-day climate. Breakthrough for future climates is presented in *Analysis of Base-Case Particle Tracking Results of the Base-Case Flow Fields (ID: U0160)* (CRWMS M&O 2000cb, Section 6.2.6).

Breakthrough curves for technetium using the present-day climate and three infiltration cases show that median breakthrough times are approximately 400 years, 2,000 years, and 600,000 years for the upper, mean, and lower infiltration cases, respectively. As expected, the higher infiltration rates yield shorter breakthrough times relative to lower infiltration rates.

More recent modeling of unsaturated zone transport is presented in Volume 1, Section 11 of *FY01 Supplemental Science and Performance Analyses (BSC 2001a)*. Influence of model refinements of five issues in the travel of radionuclides between the potential repository horizon and the saturated zone is treated (BSC 2001a, Table 11-1). These issues are the degree of advection-diffusion split-

**Table 4-12. Summary of Current Understanding Used to Develop Conceptual and Numerical Models for Unsaturated Zone Flow and Seepage Into Drifts**

| Feature, Event, or Process | Current Understanding  | Sections of UZ PMR Where Addressed               |
|----------------------------|--|--|
| Climate/infiltration       | Rainfall for the modern mean climate is about 190 mm/yr (7.5 in./yr) resulting in average steady-state net infiltration of 4.6 mm/yr (0.2 in./yr).   | 3.5.1.8; 3.5.2.10                                |
|                            | After 600 years, the average rainfall is forecast to increase to about 300 mm/yr (11.8 in./yr) for a monsoon climate; in response, the average net infiltration is predicted to increase to 12.2 mm/yr (0.5 in./yr).   | 3.5.1.8; 3.5.2.10                                |
|                            | After 2,000 years, the average rainfall is predicted to increase to about 320 mm/yr (12.6 in./yr) for a glacial-transition climate; in response the average net infiltration is predicted to increase to 17.8 mm/yr (0.7 in./yr).  | 3.5.1.8; 3.5.2.10                                |
| Infiltration               | The net infiltration is episodic, with a significant amount infiltrating only every few years.   | 3.3.2  |
|                            | There is large spatial variability of infiltration, with most water infiltrating on ridgetops and in the upper reaches of washes where there is little alluvial cover.   | 3.3.2; 3.5.2.5; Figures 3.5-4c, 3.5-5a and b     |
| Flow through TCw           | Flow through the Tiva Canyon welded hydrogeologic unit (TCw) is episodic as controlled by infiltration.  | 3.3.3.1; 3.7.3.1                                 |
|                            | Fracture flow dominates in the TCw, transmitting water rapidly through the TCw.  | 3.3.3.1; 3.7.3.1                                 |
| Flow through PTn           | Flow through the Paintbrush tuff nonwelded hydrogeologic unit (PTn) is primarily matrix flow.  | 3.3.3.2; 3.7.3.1                                 |
|                            | The PTn consists of up to nine stratigraphic units with different degrees of welding and alteration and different hydrologic properties.   | 3.2.2.2  |
|                            | Lateral flow occurs in the PTn.  | 3.3.3.2; 3.7.3.1; 3.7.3.2                        |
|                            | Most of the fast flow through the PTn occurs via faults, though this represents only a very small fraction of the total flow.  | 3.3.7; 3.11.8                                    |
| Flow through TSw           | Episodic flow into the Topopah Spring welded hydrogeologic unit (TSw) is damped by the PTn to the extent that flow can be considered steady-state when it enters the TSw. The exception is that at or near major faults episodic flow may still persist through the PTn.   | 3.3.3.2; 3.3.3.3; 3.3.5; 3.3.6; 3.7.3.1; 3.7.3.2 |
|                            | Fracture flow dominates in the TSw because this unit is densely welded and highly fractured; additionally, within some subunits of the TSw, the low-permeability matrix is incapable of transmitting the percolation flux estimated to be moving through the unit.   | 3.3.3.3; 3.7.4.3                                 |
|                            | Fracture flow in the potential repository horizon, which intersects the Topopah Spring middle nonlithophysal, lower lithophysal, and lower nonlithophysal stratigraphic units, is estimated to range from 84 to 94 percent of the total water flow for the three present-day climate scenarios.                              | 3.7.4.2; 3.7.4.3                                 |
|                            | Water drainage in the potential repository units, Topopah Spring middle nonlithophysal, lower lithophysal, and lower nonlithophysal stratigraphic units, is expected to be good due to the generally high fracture permeability ( $\sim 10^{-11}$ to $10^{-10}$ m <sup>2</sup> [ $10^{-10}$ to $10^{-9}$ ft <sup>2</sup> ]). | 3.6.5.1, Figure 3.6-6                            |
|                            | Current average percolation flux in the potential repository horizon is estimated to be about 5 mm/yr (0.2 in./yr), with spatial variability between 0 and 60 mm/yr (0 and 2.4 in./yr).  | 3.7.4.1; 3.7.4.2; 3.7.4.5                        |
|                            | Long-term average percolation flux at the potential repository horizon, averaged over the last 1,000 to 10,000 years, is estimated to be about 6 mm/yr (0.2 in./yr) based on calcite abundances, with a range of 2 to 20 mm/yr (0.1 to 0.8 in./yr).  | 3.8.4.2  |
|                            | Evidence for fast/preferential flow is seen at the potential repository horizon, primarily near major faults. It is estimated that the fast component of flow is less than a few percent of the total flow.  | 2.2.3.3; 3.3.7; 3.8.3; 3.11.8                    |

Table 4-12. Summary of Current Understanding Used to Develop Conceptual and Numerical Models for Unsaturated Zone Flow and Seepage into Drifts (Continued)

| Feature, Event, or Process | Current Understanding  | Sections of UZ PMR Where Addressed   |
|----------------------------|--|--------------------------------------|
| Seepage                    | Open emplacement drifts act as capillary barriers, impeding water from seeping into the drifts and diverting some fraction of the prevailing percolation flux around the drifts.   | 3.3.9; 3.9.1; 3.9.9;<br>3.9.3.5      |
|                            | A critical percolation flux (seepage threshold) exists below which no seepage occurs. The distribution of seepage thresholds depends on the hydrologic characteristics and variability of the unit, especially the fracture permeability and the van Genuchten alpha values.   | 3.9.3.5                              |
|                            | Seepage flux is always smaller than the percolation flux as a result of partial flow diversion around the drift.   | 3.9.1; 3.9.6.1                       |
|                            | Ventilation reduces seepage of liquid water. Neglecting ventilation effects in seepage models is conservative.   | 3.9.3.3                              |
|                            | Seepage percentages are expected to be similar for all potential repository units because permeability and capillary strength are inversely related, canceling their respective effects on seepage.  | 3.9.6.2                              |
| Perched water              | Several perched water bodies have been found below the potential repository horizon, with the perching layer generally being the basal vitrophyre of the TSw or the zeolitic part of the Calico Hills nonwelded hydrogeologic unit (CHn).  | 3.3.3.4; 3.3.8; 3.7.3.3              |
|                            | The largest perched water body is found in the vicinity of Borehole UZ-14, north of the potential repository region; this perched water body may be connected to those found in Boreholes WT-24, SD-9 and SD-12.   | 3.7.3.3                              |
|                            | A very small perched water body is found in the southern part of the potential repository region at Borehole SD-7. This perched water body is expected to have little impact on the performance of the potential repository.   | 3.7.3.3                              |
|                            | The perched water bodies contain a mixture of Pleistocene and Holocene water, with average ages ranging from 3,500 to 11,000 years old.  | 2.2.3.3; 3.3.3.3; 3.8.3;<br>3.10.3.4 |
|                            | Infiltration rates needed to form perched water bodies are higher than present-day values.   | 3.8.2; 3.8.3                         |
|                            | The minute fractions of bomb-pulse <sup>36</sup> Cl and tritium in perched water suggest that the fast flow fraction over the past 50 years is very small.   | 3.8.3                                |
| Flow through CHn           | Perched water is formed because the ambient percolation flux exceeds the capacity of the geologic media to transmit the flux vertically through the underlying low-permeability units. Water may flow either through the units or laterally to major faults or other vertical conduits for flow.                           | 3.7.3.2; 3.7.3.3                     |
|                            | The CHn consists of unaltered vitric zones, primarily in the south, and altered zeolitic zones, primarily in the north. Water flow through the zeolitic units is primarily in the fractures, while flow through the vitric units is mostly or all in the matrix.   | 3.7.3.3; 3.3.3.4                     |
|                            | Lateral flow in perched water bodies toward faults and other major permeable features causes partial bypassing of the low permeability zeolitic units of the CHn.  | 3.7.3.2; 3.7.3.3                     |
| Flow through faults        | Water entering the CHn vitric unit from the TSw transitions from discrete fracture flow to heterogeneous matrix flow.  | 3.11.4                               |
|                            | Fault properties are variable and generally controlled by rock type and stratigraphic displacement.  | 3.2.3; 3.3.5                         |
|                            | Faulting enhances fracturing in the fault zones, contributing to increased permeability. Permeability in the TCw and TSw fault zone is $6$ to $9 \times 10^{-11} \text{ m}^2$ ( $9 \times 10^{-10} \text{ ft}^2$ ). In the PTn fault zone it is $\sim 2 \times 10^{-11} \text{ m}^2$ ( $2 \times 10^{-10} \text{ ft}^2$ ). | 3.7.3.2; 3.6.5.1                     |
|                            | Faults are high permeability features through the CHn and Crater Flat undifferentiated hydrogeologic unit (CFu), provide a fast flow path from the TSw to the water table, and allow discharge from perched water bodies.  | 3.3.5                                |

NOTES: UZ PMR = *Unsaturated Zone Flow and Transport Model Process Model Report* (CRWMS M&O 2000c). Source: Adapted from CRWMS M&O 2000c, Table 1.2-3.

ting in the drift shadow zone; the effects of the drift shadow concentration boundary on engineered barrier system release rates; the effect of matrix diffusion; the significance of three-dimensional transport modeling; and the effects of coupling of thermal-hydrologic, thermal-hydrologic-chemical and thermal-hydrologic-mechanical processes on transport. Results of model refinement of breakthrough time are presented in Volume 1, Section 11 of *FY01 Supplemental Science and Performance Analyses* (BSC 2001a, Figures 11.3.1-7, 11.3.1-8, and 11.3.2-8).

#### 4.2.1.4.2 Seepage Model for Performance Assessment

Abstraction of seepage models for the TSPA, as documented in *Abstraction of Drift Seepage* (CRWMS M&O 2000by), focuses on providing conservative seepage estimates for a wide range of hydrologic conditions.

**Selection of Parameter Ranges and Case Studies**—Table 4-13 shows four parameters identified for prediction of seepage into the potential repository drifts. Ranges of values are shown for each parameter, which were used as the basis for an extensive sensitivity analysis. The maximum and minimum values for each parameter were selected based on field data and modeling studies. For example, seepage is evaluated for percolation flux as small as 5 mm/yr (0.2 in./yr) and as great as 500 mm/yr (20 in./yr) (CRWMS M&O 2000bx, Section 6.3.6). The higher value accounts for a hypothetical future climate scenario with spatial and temporal focusing effects (CRWMS M&O

2000c, Sections 3.9.3.1, 3.9.3.2, and 3.9.6.4). The rationale for selecting the parameter ranges shown in Table 4-13 is further discussed in supporting documentation (CRWMS M&O 2000bx, Section 6.3). The results of this sensitivity analysis are used in seepage abstraction for the TSPA (CRWMS M&O 2000c, Section 3.9.6) to account for uncertainty in the seepage calibration model.

**Results from Modeling of Seepage for Performance Assessment**—The seepage percentage is defined as the seepage flux into a drift opening divided by the average percolation flux over the drift footprint (CRWMS M&O 2000c, Section 3.9.1). The seepage model was implemented to evaluate seepage percentage for multiple statistical realizations of the hydrologic property field representing fractured host rock and for many combinations of parameters in Table 4-13 (CRWMS M&O 2000c, Section 3.9.5.3). The results confirm the seepage behavior observed in testing: seepage increases with decreasing permeability, decreasing capillarity, and increasing percolation flux. For most of the realizations examined, the capillary barrier effect resulted in seepage flux that was substantially less than the percolation flux (i.e., seepage percentage much less than 100 percent). Zero seepage was obtained for a significant portion of the realizations calculated.

**Abstraction of the Seepage Model for Performance Assessment**—The seepage model for performance assessment was used to simulate seepage for a large number of realizations (CRWMS M&O 2000c, Section 3.9.5). Examination of the results revealed that seepage percentage

Table 4-13. Parameter Ranges for Which Seepage is Evaluated Using the Seepage Model for Performance Assessment

| Parameter                                  | Minimum  | Maximum  | Parameter Description                        |
|--|--|--|--|
| $k$ , m <sup>2</sup><br>(ft <sup>2</sup> ) | $0.9 \times 10^{-14}$<br>( $0.9 \times 10^{-13}$ ) | $0.9 \times 10^{-11}$<br>( $0.9 \times 10^{-10}$ ) | Mean permeability of fracture-continuum      |
| $1/\alpha$ , Pa<br>(psi)                   | 30<br>( $4.4 \times 10^{-3}$ )                     | 1,000<br>(0.15)                                    | van Genuchten's capillary-strength parameter |
| $\sigma \ln(k)$                            | 1.66   | 2.50   | Standard deviation of log-permeability field |
| $Q_p$ , mm/yr<br>(in./yr)                  | 5<br>(0.2)   | 500<br>(20)  | Percolation flux                             |

Source: CRWMS M&O 2000c, Table 3.9-1.

is most sensitive to a combination of parameters ( $k/\alpha$ ): the product of fracture permeability,  $k$ , and the capillary strength parameter,  $1/\alpha$ . With this simplification, seepage can be treated as a function of just two variables (i.e., percolation flux and  $k/\alpha$ ).

The abstraction for TSPA focuses on two quantities: (1) the seepage fraction, which is the fraction of waste package locations (i.e., model realizations) for which seepage is predicted and (2) the seepage flow rate, which is the volumetric flow rate of seepage in a drift segment of specified length. Details of the abstraction procedure are provided in supporting documentation (CRWMS M&O 2000by, Sections 6.2.2 and 6.4). Table 4-14 summarizes the abstracted seepage distributions as they vary with percolation flux for ambient conditions (not the nearly dry conditions expected during repository heating). Seepage threshold values of approximately 200 mm/yr (7.8 in./yr), 15 mm/yr (0.6 in./yr), and 5 mm/yr (0.2 in./yr) are estimated for the minimum, expected (i.e., most likely), and maximum seepage conditions, respectively. Note that these values are different from the previously discussed seepage threshold of 200 mm/yr (7.8 in./yr) (CRWMS M&O 2000c, Section 3.9.4.7) for a single location in Niche 2 in the middle nonlithophysal zone.

**Summary and Conclusions for the Drift Seepage Model**—Seepage into waste emplacement drifts is important to the performance of a repository at Yucca Mountain. Numerical modeling, field testing, and observations at analogue sites suggest that seepage into repository emplacement drift openings would be substantially less than the local percolation flux. This performance results mainly from capillarity retaining the water in the rock and diverting the flow around the openings. The effectiveness of this capillary barrier principle depends on the percolation flux magnitude, the hydrologic properties of the rock, and the drift opening geometry.

A sequence of models was developed to predict the seepage percentage, seepage threshold, and seepage flow rate for waste emplacement drifts. The seepage model was calibrated against relevant data from liquid injection tests in the Exploratory Studies Facility. Seepage percentages and flow rates were then calculated for a wide range of parameter values representing uncertainty in the model and summarized in a probabilistic abstraction model for TSPA. The results indicate that only 13 percent of waste packages are likely to be

Table 4-14. Uncertainty in Seepage Parameters as a Function of Percolation

| $q$ , mm/yr<br>(in./yr) | Minimum Value of $k/\alpha$ |   |  | Peak Value of $k/\alpha$ |   |  | Maximum Value of $k/\alpha$ |   |  |
|-------------------------|-----------------------------|---|--|--------------------------|---|--|-----------------------------|---|--|
|                         | $f_s$                       | Mean $Q_p$ ,<br>$m^3/yr$<br>( $ft^3/yr$ ) | Std. Dev. $Q_p$ ,<br>$m^3/yr$<br>( $ft^3/yr$ ) | $f_s$                    | Mean $Q_p$ ,<br>$m^3/yr$<br>( $ft^3/yr$ ) | Std. Dev. $Q_p$ ,<br>$m^3/yr$<br>( $ft^3/yr$ ) | $f_s$                       | Mean $Q_p$ ,<br>$m^3/yr$<br>( $ft^3/yr$ ) | Std. Dev. $Q_p$ ,<br>$m^3/yr$<br>( $ft^3/yr$ ) |
| 5<br>(0.2)              | 0                           | 0   | 0  | 0                        | 0   | 0  | $1.97 \times 10^{-3}$       | $3.21 \times 10^{-3}$<br>(0.113)          | $3.16 \times 10^{-3}$<br>(0.112)               |
| 14.8<br>(0.8)           | 0                           | 0   | 0  | $2.45 \times 10^{-3}$    | $7.95 \times 10^{-3}$<br>(0.28)           | $7.09 \times 10^{-3}$<br>(0.25)                | $5.75 \times 10^{-2}$       | $2.28 \times 10^{-2}$<br>(0.799)          | $2.45 \times 10^{-2}$<br>(0.865)               |
| 73.2<br>(2.9)           | 0                           | 0   | 0  | 0.250                    | 0.108<br>(3.74)                           | 0.198<br>(8.99)                                | 0.744                       | 0.404<br>(14.3)                           | 0.409<br>(14.4)                                |
| 213<br>(8.4)            | $4.91 \times 10^{-3}$       | 0.284<br>(10)                             | 0.188<br>(8.84)                                | 0.487                    | 1.51<br>(53.3)                            | 1.15<br>(40.8)                                 | 0.944                       | 3.31<br>(117)                             | 2.24<br>(79.1)                                 |
| 500<br>(20)             | $6.01 \times 10^{-2}$       | 0.992<br>(35)                             | 1.05<br>(37.1)                                 | 0.925                    | 5.50<br>(194)                             | 4.48<br>(158)                                  | 0.999                       | 13.0<br>(459)                             | 5.74<br>(203)                                  |

NOTES:  $q$  = percolation flux;  $f_s$  = seepage fraction;  $Q_p$  = seep flow rate. Source: Modified from CRWMS M&O 2000by, Table 11.

subject to seepage (CRWMS M&O 2000a, Section 4.1.2). Alternative conceptual models leading to as much as 48 percent of waste packages subject to seepage have been considered (BSC 2001b, Section 4.2.2), although such a high percentage of impacted waste packages is supported only by an inference from an uncalibrated model. The qualitative and quantitative results from seepage testing and modeling, as reflected in the abstraction model, are summarized in Figure 4-37 (CRWMS M&O 2000c, Section 3.9.3).

#### 4.2.2 Effects of Decay Heat on Water Movement

After permanent closure, the heat produced by radioactive decay of the nuclear waste will have an immediate effect on seepage into the repository drifts, water movement through the repository, and the patterns of natural water flow in the unsaturated rock layers. The nature and extent of these effects, however, will depend on thermal loading (or areal heat output), ventilation rates and durations, and attendant thermal operating conditions (i.e., above-

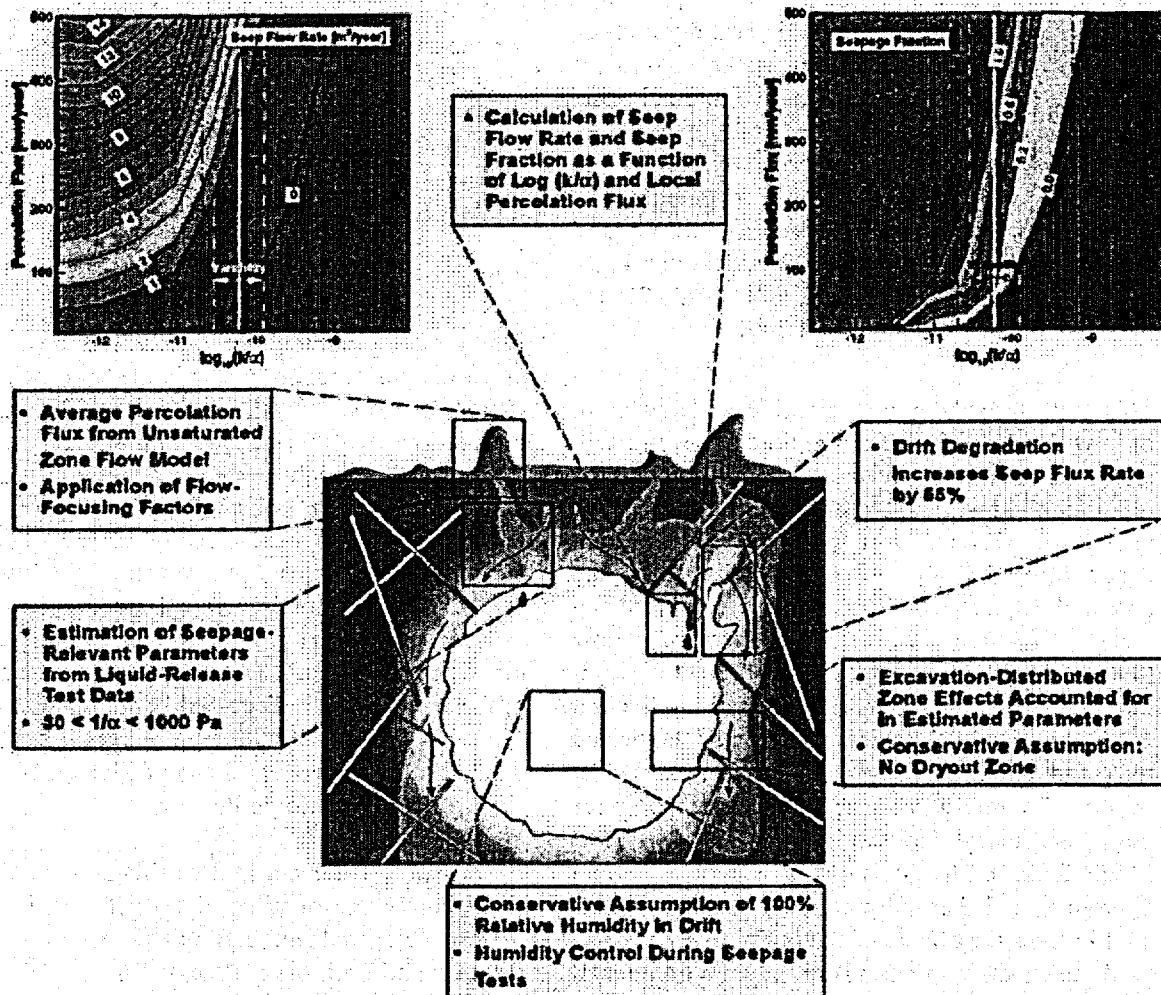


Figure 4-37. Summary of Qualitative and Quantitative Results from Seepage Testing and Modeling  
 $\alpha$  = van Genuchten "alpha" parameter defining capillary strength;  $k$  = fracture permeability. Source: CRWMS M&O 2000c, Figure 3.9-12.

boiling or below-boiling). The analytical and experimental studies conducted to date have examined these heat effects in detail but with emphasis on environmental conditions associated with the higher-temperature operating mode described in Section 2.1.2.3 of this report. The data and analytical results presented in this section mainly describe the effects of higher-temperature conditions on water movement and, specifically, the process models and abstractions employed in the TSPA-SR model, as reported in *Total System Performance Assessment for the Site Recommendation* (CRWMS M&O 2000a).

As noted in Section 4.1.4, the DOE is evaluating operating the repository at lower temperatures, which may reduce the magnitude and duration of the effects of decay heat on water movement described in this section. Alternative thermal operating modes and supplemental uncertainty evaluation results related to thermal hydrology and thermally coupled models are documented or summarized in *FY01 Supplemental Science and Performance Analyses* (BSC 2001a, Sections 4.3.5, 4.3.6., 4.3.7, 5.3, 5.4, and 6.3; BSC 2001b, Sections 3.2, 4.2.2, 4.2.3, and 4.2.4).

This section explains the scientific understanding of how the decay heat from radioactive waste will affect natural water movement into and through the repository and water flow in the surrounding unsaturated rock layers. During the period in which decay heat strongly influences fluid flow, the potential sources of water seeping into emplacement drifts are heat-driven condensate flow (thermal seepage), as opposed to ambient percolation and drift seepage, as discussed in Section 4.2.1. Because of the thermal inertia of the heated rock and the continuing (though declining) heat source, the return to near-ambient temperatures may take many thousands of years (CRWMS M&O 2000a). The goals of the near-field thermal hydrology and thermally coupled process models are to assess the effects of the initial thermal pulse (and longer thermal period) on key environmental conditions, such as temperature and relative humidity in the emplacement drifts. These conditions, in turn, may affect the performance of the engineered barriers and the transport of radionu-

clides (CRWMS M&O 2000a; CRWMS M&O 2000as).

The abstraction of thermal-hydrologic data for use in TSPA represents the potential variability and uncertainty in thermal-hydrologic conditions. It provides a quantitative description of thermal-hydrologic variability (i.e., from variability in the host rock unit, edge proximity, waste package type, infiltration rate, and climate state) and also incorporates uncertainty associated with the infiltration (i.e., lower, mean, and upper). Multiscale model results that are used directly in the TSPA include waste package temperature, relative humidity at the waste package surface, and the percolation flux in the host rock 5 m (16 ft) above the emplacement drift. Temperature and relative humidity are used for the corrosion model, and percolation flux is used for the seepage model. Time-histories of waste package temperature, percolation flux, evaporation rates, and maximum and minimum waste package surface temperatures are also provided (CRWMS M&O 2000cc, Section 6.3).

#### 4.2.2.1 Conceptual Basis

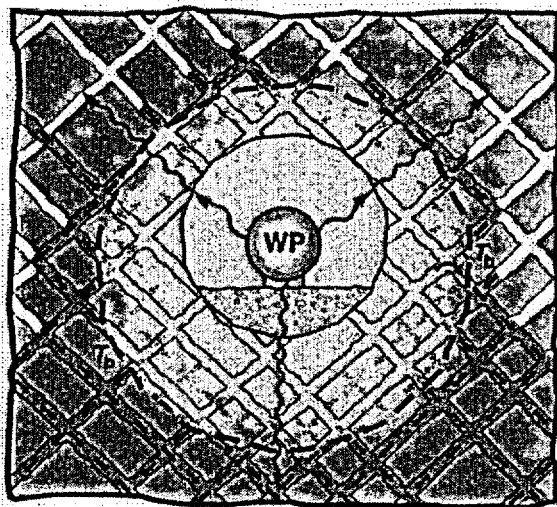
Decay heat generated by radioactive waste may affect the movement of water in the host rock units (CRWMS M&O 2000a, Section 1.1). The conceptual processes described in this section assume thermal loading high enough to result in conditions above the boiling point of water. Under these conditions, decay heat directly affects thermal-hydrologic processes (i.e., movement of water). Heat-driven thermal-chemical processes and thermal-mechanical processes may also affect the movement of water. The conceptual basis for each of these processes is discussed in this section.

##### 4.2.2.1.1 Conceptual Basis of Thermal-Hydrologic Process

Evaporation will occur in the drifts and in the rock immediately surrounding the drift openings. A region of elevated temperature and rock dryout will form around each drift (Pruess, Wang et al. 1990, p. 1241). Heating can change the flow properties of the rock, and the chemical composition of water and minerals in the affected region. These changes can also occur within the drifts in the engineered

barrier system. Figures 4-38 and 4-39 illustrate the conceptual processes of heat-driven water movement.

Calculations indicate that the heat generation rate from radioactive decay decreases rapidly with age relative to the initial output. Heat generation continues at decreased output for thousands of years. Both the initial heat output and its rate of decrease with time depend upon the type of nuclear waste. Calculations indicate that the repository would initially produce approximately 80 MW of thermal power (CRWMS M&O 2000cd, Attachment II). The thermal power output will decrease to approximately 25 percent in 100 years, 12 percent in 300 years, and 2 percent of its initial value in 10,000 years (CRWMS M&O 2000ce, Table I-1).



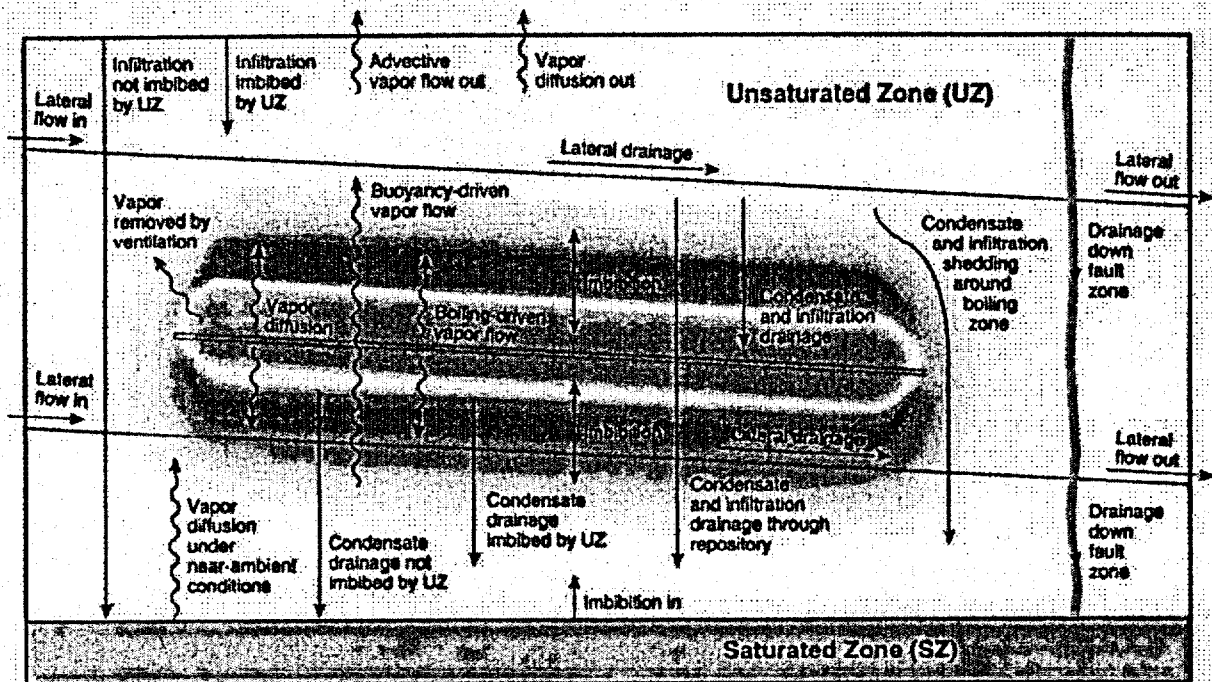
80080DC\_ATP\_X1842\_102.ai

Figure 4-38. Drift-Scale Schematic Illustration Showing Decay-Heat-Driven Thermal-Hydrologic Flow and Transport Processes

Fracture flow is shown with solid arrows (green features), water vapor flow is shown with dashed arrows (yellow features), and heat flow is indicated with oscillatory arrows. The ambient (preheating) state of the rock is shown with white fractures and a blue matrix. The boiling isotherm is labeled  $T_b$ , and the waste package is labeled WP. The fractures and in-drift features are stylized for the illustration. Source: Modified from CRWMS M&O 2000al, Figure 3-4.

Continuous forced ventilation of emplacement drifts during operations will remove 70 percent of the total decay heat generated during a period of 50 years after the first waste is emplaced. A conservative model, accounting only for heat removed as sensible heat in the ventilation air (and ignoring heat removed by evaporation of moisture), indicates that a ventilation air flow rate of up to 15 m<sup>3</sup>/s in each emplacement drift will provide this level of heat removal (CRWMS M&O 2000cd, Section 6.5). The remaining heat output during the preclosure period will be transferred to the host rock by radiation, conduction, and convection, increasing the host rock temperature. Some moisture, and the associated latent heat of evaporation, will be removed by ventilation during this period. At closure, ventilation will cease after drip shields have been placed over the waste packages. This would cause an abrupt increase of heat flux into the host rock.

The major effects of decay heat on water movement would occur after closure (CRWMS M&O 2000cf, Section 6.11.4). Initially, heat will be transported radially away from the drifts by heat conduction through the rock and movement of air through fractures. A portion of the heat will be transported by water that vaporizes near the heat sources and condenses in cooler rock farther away. If the heat flux is high enough, rock near the drifts will be heated to the boiling point of water (nominally 96°C [205°F] at the elevation of the repository) and then to higher temperatures after most of the water in this region has evaporated. The region within which substantially all the water has evaporated is called the dryout zone. Surrounding the dryout zone, a heat pipe zone would form, within which the temperature is essentially constant at the boiling point. The heat pipe zone in turn would be surrounded by a condensation zone of increased water saturation and temperature below the boiling point. After closure, these regions will first expand, then contract as the heat output diminishes over time. The timing of these events will depend on local thermal loading, percolation flux, and location in the potential repository layout (i.e., near the center or the edge). After sufficient time has passed, the temperature will return to preemplacement levels. For purposes of this section, "thermal pulse" is used to describe



00050DC\_ATP\_Z1842\_104.ai

Figure 4-39. Mountain-Scale Schematic Illustration Showing Decay-Heat-Driven Thermal-Hydrologic Flow and Transport Processes that Influence Moisture Redistribution and the Moisture Balance in the Unsaturated Zone

Source: CRWMS M&O 2000a, Figure 3-5.

the development of above-boiling conditions and the heat pipe zone, a process which may last on the order of a few hundreds of years (CRWMS M&O 2000cf, Figure 6-53). "Thermal period" is generally used to describe the time required for temperatures to return to ambient and may last on the order of tens of thousands of years (CRWMS M&O 2000a). Figures 4-38 and 4-39 provide, respectively, conceptual drift-scale and repository-scale illustrations of thermally driven features and processes during the thermal pulse (CRWMS M&O 2000a, Section 3.2.1).

In the investigation of thermal-hydrologic processes, it has been assumed that heating, cooling, and the resulting movement of water will occur in a system with fixed thermal and hydrologic properties (such as porosity, permeability, and thermal conductivity). Properties of the rock may vary with temperature and water saturation but are assumed to return to preemplacement

values after the temperature returns to ambient levels (CRWMS M&O 2000a, Sections 3.2.2 and 3.3.5). This concept is used to develop process models like those described in Section 4.2.2.3. Thermal-hydrologic processes in the near field will determine the environmental conditions in the drift, including temperature, relative humidity, and seepage at the drift wall.

#### 4.2.2.1.2 Conceptual Basis of Thermal-Hydrologic-Chemical Process

Thermal-hydrologic-chemical processes involve liquid and vapor flow, heat transport, and thermal effects resulting from boiling and condensation; transport of aqueous and gaseous chemical species; mineralogical characteristics and changes; and aqueous and gaseous chemical reactions. Figure 4-40 shows schematically the relationships between thermal-hydrologic and geochemical processes in the zones of boiling, condensation,

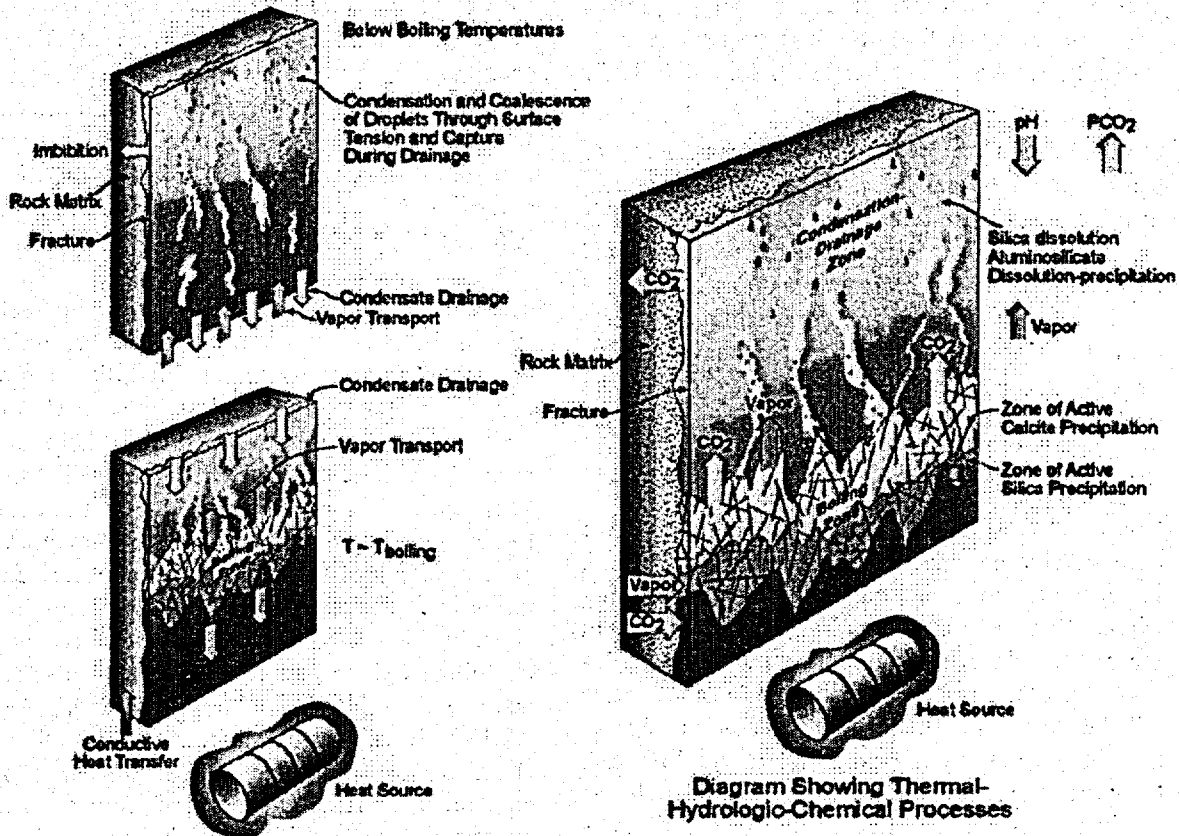


Diagram Showing Thermal-Hydrologic Processes

000500C\_ATP\_Z1842\_8p-34a

Figure 4-40. Schematic Diagram Showing Relation between Thermal-Hydrologic Processes and Geochemical Processes

Source: CRWMS M&O 2000c, Figure 3.10-2.

and water drainage in the rock surrounding a repository, particularly in the rock above emplacement drifts.

Heat transfer to the drift wall and surrounding rock will evaporate water in fractures first, then the rock matrix. Vapor will migrate out of the matrix blocks and into fractures, where it will move away from the emplacement drifts because of pressure effects and buoyant convection (CRWMS M&O 2000a, Sections 3.1.5 and 3.2.1). In cooler regions further away from the emplacement drifts, vapor will condense on fracture walls. The condensate will then drain through the fracture network; some of this water will drain back toward the heat source.

The resulting localized counter-flow of water vapor and liquid (thermal reflux) is called a heat pipe. A heat pipe zone will develop between the dryout zone and the condensation zone (Pruess, Wang et al. 1990), as discussed previously in Section 4.2.2.1.1.

Chemical evolution of waters, gases, and minerals is coupled to thermal-hydrologic processes. The distribution of condensate in the fracture system will determine where mineral dissolution and precipitation can occur in the fractures and where there can be direct interaction (via diffusion) between matrix pore waters and fracture waters. Investigation of the reactive-transport processes in

the potential repository host rock accounts for different rates of transport in the very permeable fractures, compared to the less permeable rock matrix (Steefel and Lichtner 1998, pp. 186 to 187).

One important aspect of the system is release of carbon dioxide from the liquid phase as temperature increases. The release of carbon dioxide and its transport out of the boiling zone will cause pH to increase in the boiling zone and decrease in the condensation zone. Because gases are more mobile than liquids, the region of gas-phase carbon dioxide transport could be much larger than the region affected by thermally driven water movement (CRWMS M&O 2000a, Section 3.3.1.2).

Conservative species (i.e., those that are unreactive and nonvolatile), such as chloride, will become increasingly concentrated in waters undergoing evaporation or boiling but will be more dilute in the condensate zone. The concentrations of chloride and other constituents in condensate waters will be determined mainly by interaction of fracture waters with matrix pore waters via diffusion. Concentrations of aqueous species, such as calcium, will also be affected by mineral dissolution or precipitation and by reactions involving zeolites, clays, and plagioclase feldspar. Calcite may precipitate in fractures over a broad zone of elevated temperature. Silica precipitation will be confined to a narrower zone where evaporative concentration from boiling causes the silica concentration to exceed solubility limits. Alteration of feldspars to clays and zeolites will be most rapid in the boiling zone. As waters drain away from the emplacement drifts, mineral dissolution and precipitation may occur in fractures or in the adjacent rock matrix (CRWMS M&O 2000a, Section 3.3.1.2).

The composition of the percolating waters above the potential repository (before mixing with condensate) may be similar to matrix pore water, or it may reflect more dilute water that has traveled through fractures (CRWMS M&O 2000a, Section 3.3.1.3). The chemical composition selected for input to the thermal-hydrologic-chemical model is described in Sections 4.2.2.1.3, 4.2.2.3.3, and 4.2.3.3.1 of this report.

Changes in the percolation flux can affect the extent of mineral deposition and dissolution because of changes in the fluxes of dissolved species. For example, with more calcium transported toward the emplacement drifts, more calcite would tend to be precipitated. Also, a greater percolation flux will tend to increase the dissolution of minerals that are undersaturated in the fluid (CRWMS M&O 2000a, Section 3.3.1.3).

Mineral dissolution and precipitation in fractures and in the rock matrix can modify the porosity, permeability, and unsaturated hydrologic properties of the potential repository host rock in the vicinity of the emplacement drifts. The extent of mineral-water reactions will be controlled by the surface area of each mineral phase that is exposed to the liquid water. Other factors that may control property changes are the distribution of liquid saturation in fractures, the proportion of fractures with actively flowing water, and the rate of evaporation or boiling, which can control crystal growth and nucleation (CRWMS M&O 2000a, Section 3.3.1.4). Rock-water interactions will affect the chemistry of the water that may seep into the emplacement drifts. The effect of rock-water interactions on hydrologic properties and seepage is evaluated in Section 4.2.2.3.3.

#### 4.2.2.1.3 Conceptual Basis of Thermal-Mechanical Process

The stress field in the rock mass surrounding emplacement drifts would be altered by excavation of drifts and by the heating/cooling cycle associated with emplacement of radioactive waste. The direction and magnitude of principal stresses will change significantly because of thermal loading and then will return to near-ambient values during cooldown—but not completely, since the rock mass will be changed permanently from deformations occurring from stress redistribution; however, the magnitude of changes in hydrologic properties will be limited (CRWMS M&O 2000a, Section 3.5). Compressive stress will build up rapidly in the host rock, especially after the end of the ventilation period. The stress field generally will gradually decay as the temperature in the rock decreases. Potential seismic effects on the repository system are discussed in *Drift Degradation*

*Analysis* (CRWMS M&O 2000e, Sections 6.3.4 and 7.1); potential effects of fault displacement on the repository system are discussed in *Disruptive Events Process Model Report* (CRWMS M&O 2000f).

The potential repository host rock is a fractured, densely welded, ash-flow tuff. These fractures are expected to deform as stress conditions evolve. Two types of fracture deformations will contribute to thermal-hydrologic-mechanical coupling: normal displacement perpendicular to a fracture plane and shear displacement parallel to a fracture plane.

Rock-mass permeability is an important thermal-hydrologic property for assessment of repository performance. Because the rock has low matrix permeability, the rock mass permeability is mainly associated with fractures, and large changes in rock mass permeability may result from fracture deformation.

The potential effect of fracture deformation on fracture permeability is discussed in Section 4.2.2.3.4. The potential for drift degradation to affect the drip shield (i.e., rockfall on the drip shield) is discussed in Section 4.2.3. The basis for screening these potential processes from the TSPA-SR model is referenced in the process and model and/or the TSPA abstraction sections.

#### 4.2.2.2 Summary State of Knowledge

This section presents a summary of the state of knowledge of properties (rock and fluid) and processes tested in the laboratory and in the field. Much of the information presented in this section is extracted from Hardin and Chesnut (1997).

##### 4.2.2.2.1 State of Knowledge of Laboratory Measured Properties

This section describes the available laboratory data for assessing matrix contributions to thermally coupled processes. Laboratory data for assessing fracture contributions are relatively limited and are described to a lesser extent. Because sample sizes are typically much smaller than the in situ fracture spacing, laboratory measurements generally provide properties of the rock matrix only and do

not directly show the effects of thermally coupled processes on rock-mass behavior. Laboratory data therefore provide only part of the input data required to investigate coupled processes. The properties of fracture networks are also needed and have been inferred from observations and measurements in the field.

##### 4.2.2.2.1.1 Thermal-Mechanical Properties

Variation of matrix thermal and thermal-mechanical properties with temperature is relatively well understood, and data are available. The dependence of matrix and fracture rheology on temperature, including deformation modulus and creep properties, is less well known, but some data at elevated temperature are available. These data do not indicate that rheology is important for prediction of long-term repository performance.

**Rock Creep**—Laboratory testing of the rock matrix showed that significant creep occurs only when samples are stressed to at least 50 percent, and in some cases more than 90 percent, of their ultimate strength (Martin et al. 1995). Such stress conditions may be uncommon in the host rock, occurring only at fracture asperity contacts. These results also indicate a tendency for fractures in the host rock to close in response to heating and open in response to cooling.

**Physical Properties (Porosity and Grain Density)**—For the TSw2 welded tuff, these properties change little from ambient temperature up to at least 180°C (356°F). Change in the welded tuff matrix near the emplacement drifts is expected to be minor and will probably be caused mainly by mineral phase transitions (e.g., a→b cristobalite) and dehydration of hydrous phases, such as clinoptilolite and smectites. Of these, dehydration of hydrous fracture-lining minerals has a greater potential to affect host rock performance (Hardin and Chesnut 1997, Section 2.2).

**Thermal Conductivity**—Laboratory measurements of thermal conductivity have been performed on samples from the Exploratory Studies Facility, in conjunction with field-scale thermal testing (Brodsky et al. 1997). There is a slight increase of thermal conductivity with

temperature for the Topopah Spring welded tuff. Water saturation apparently increases thermal conductivity of the TSw2 welded tuff by approximately 50 percent. A small pressure effect in other rock types, whereby conductivity increases with confining stress, has been observed and is probably caused by closing of microcracks. Pressure effects on thermal conductivity have not been examined for Yucca Mountain tuffs but are likely to be small or highly localized in the host rock.

**Heat Capacitance**—When measured on dried samples, the heat capacitance of the TSw2 welded tuff increases about 20 percent from ambient temperature to 200°C (392°F) (SNL 1996). Behavior at temperatures greater than 150°C (302°F) is affected by mineral phase transitions, notably that of cristobalite, which occurs at temperatures greater than 200°C (392°F). In polycrystalline rocks, the cristobalite transition apparently occurs over a temperature range of 20 to 50 C° (36 to 90 F°).

**Thermal Expansion**—The coefficient of thermal expansion for TSw2 welded tuff increases with temperature because of mineral-phase transitions and dilatancy caused by heterogeneous thermal expansion of different minerals. Linear unconfined expansion measurements have been reported for ambient pressure, temperatures to 300°C (572°F), and several saturation states (Brodsky et al. 1997, Table B-5) determined from samples that are somewhat heterogeneous and exhibit some variability between samples. Measured thermal expansion for samples of TSw2 welded tuff varies by a factor of about five. Thermal expansion is relatively insensitive to saturation. Hysteresis becomes apparent at temperatures greater than 200°C (392°F), probably because expansion produces irreversible changes in rock fabric.

**Mechanical Properties**—For the Topopah Spring welded tuff, long-term (3.5- to 6-month) changes in the mechanical properties of three samples were investigated at temperatures of 80°, 120°, and

180°C (176°, 248°, and 356°F) (Hardin and Chesnut 1997, Section 2.5.1). The results indicate that temperature effects on mechanical properties are smaller than the differences between the samples. More recently, a 0.5-m (1.6-ft) scale block of Topopah Spring welded tuff was subjected to uniaxial loading at temperatures as great as 85°C (185°F) (Hardin and Chesnut 1997, Section 3.8.1). The apparent Young's modulus for the tuff matrix at several locations in the block decreased significantly as temperature increased.

**Compressive Strength Versus Saturation**—It has been reported that a significant decrease in compressive strength could be associated with increased saturation (Nimick and Schwartz 1987, Section 3.4.2.2.1). This observation was based on early studies that may have been affected by different methods used to control sample saturation (Boyd et al. 1994, Section 4.3).

#### 4.2.2.2.1.2 Hydrologic Properties

Thermal-hydrologic processes in fractured rock have been investigated theoretically and experimentally since the early 1980s (Pruess, Tsang et al. 1984; Pruess, Wang et al. 1990; Buscheck and Nitao 1993; Pruess 1997; Tsang and Birkholzer 1999; Kneafsey and Pruess 1998). The laboratory work and early field studies are reported in *Synthesis Report on Thermally-Driven Coupled Processes* (Hardin and Chestnut 1997) and *Near-Field Environment Process Model Report* (CRWMS M&O 2000a, Sections 2.2 and 3). See also Section 4.2.1.2.5 of this document for hydrologic properties of fractures.

For matrix hydrologic properties, there are fundamental temperature-dependent responses that may be important to understanding the thermal-hydrologic process. These include the temperature effect on hysteresis of wetting and drying characteristic curves, Knudsen diffusion, and enhancement of vapor diffusion (CRWMS M&O 2000a, Section 3.6.3.1).

**Matrix Permeability**—Variations in matrix permeability of the Topopah Spring welded tuff that are associated with temperature changes have been found to be much less than natural variations between samples (CRWMS M&O 2000a, Section 3.6.3.1).

**Unsaturated Hydraulic Conductivity**—A limited number of measurements have been made of unsaturated matrix conductivity in Yucca Mountain tuffs. Changes in the properties of water at elevated temperature (viscosity and surface tension) suggest that unsaturated conductivity may increase by as much as an order of magnitude from 20° to 100°C (68° to 212°F). The viscosity effect is taken into account in current thermal-hydrologic simulations, but the surface-tension effect is not. In addition, changes in the water-rock-air contact angle at elevated temperature can also influence unsaturated conductivity (Hardin and Chesnut 1997, Section 2.10).

**Enhanced Vapor Diffusion**—No enhancement in vapor diffusion was observed in a limited investigation of the Topopah Spring welded tuff matrix (Wildenschild and Roberts 1999).

**Knudsen Diffusion**—Knudsen diffusion and its variation with temperature are possible mechanisms for transport of moisture in the host rock (Hardin and Chesnut 1997, Section 2.7.4). This is likely to be of little significance and has not been investigated experimentally.

#### 4.2.2.2.1.3 Chemical and Transport Properties

Chemical reactions are strongly temperature-dependent, and laboratory measurements of reaction rates and surface areas under controlled conditions are sparse. However, experimental kinetic data are not generally needed for reactions that can be modeled satisfactorily using qualified thermodynamic equilibrium and reaction-path models, such as EQ3/6 and its associated chemical databases. Determination of which chemical processes in the potential repository can be modeled in this manner rely on results from laboratory and field-scale testing.

Thermodynamic equilibrium data for many aqueous and mineral species have been measured or estimated, and reviewed for accuracy and consistency in preparation for use with qualified analyses. For certain other types of reactions (e.g., surface complexation), equilibrium conditions at elevated temperatures are relatively unknown.

**Seepage Water Compositions**—Two water compositions have been considered for use in TSPA-SR modeling for various purposes. One is referred to as chloride-sulfate-type water that is based on the chemical analyses of matrix pore waters from near the Drift Scale Test (CRWMS M&O 2000cg, Sections 6.5 and 6.7.4; BSC 2001o, Section 6.1.2). Another is referred to as bicarbonate-type water, based on the composition of J-13 well water (CRWMS M&O 2000cg, Section 6.5; see also Section 4.2.4). The chloride-sulfate-type water is more concentrated in total dissolved minerals and is selected for calculations that evaluate potential changes in fracture properties from precipitation of minerals and salts. The source of water and gas chemistry for use in the thermal-hydrologic-chemical model is based on the chemical composition of matrix pore water collected from Alcove 5 (BSC 2001o, Sections 4.1.3 and 6.1.2).

**Behavior of Radionuclides in J-13 Water**—Experimental data on the speciation and solubility of important radionuclides at elevated temperature are limited. However, the investigation of spiked J-13 water at temperatures as great as 100°C (212°F) indicates that plutonium solubility decreases, but uranium, neptunium, and americium remain soluble or become increasingly soluble at elevated temperatures (Nitsche 1991). Carbonate complexes appear to be important to the solubility of uranium, neptunium, and americium at elevated temperatures. Knowledge about complexation and solubility of nickel, zirconium, technetium, uranium, neptunium, plutonium, and americium in J-13 water at elevated temperatures was published in a recent review (Wruck and Palmer 1997).

**Hydrothermal Tuff Alteration**—Batch studies of hydrothermal alteration of wafers of Topopah Spring welded, devitrified tuff have been performed at temperatures from 90° to 250°C

(194° to 482°F) and for durations to 120 days (Knauss 1987; Knauss and Beiriger 1984; Knauss, Beiriger et al. 1987; Knauss, Delany et al. 1985; Knauss and Peifer 1986; Oversby 1984a; Oversby 1984b; Oversby 1985). They show that changes in the composition of water in contact with the tuff are moderate at temperatures as great as 150°C (302°F), with slight alteration of the tuff over a few months. At higher temperatures, similar alteration products are produced, but reaction rates increase significantly. Accelerated experiments on crushed tuff at temperatures greater than 150°C (302°F) have produced more extensive alteration, including metastable phases.

**Energetics of Zeolite Dehydration**—Zeolites could have a significant effect on the heat and water balance where they are abundant because zeolite dehydration is more energetic than evaporation of water on a molar basis (Bish 1995; Wilder 1996, Section 3.4.3; Hardin and Chesnut 1997, Section 2.6.2.1). Zeolite hydration is apparently reversible at dehydration temperatures as great as 215°C (419°F) for clinoptilolite, so complementary effects will occur during repository cooldown. Altered units above and below the repository horizon contain a large fraction of zeolites; the data produced by these studies indicate that dehydration will cause some amount of shrinkage, increasing porosity and probably also increasing permeability. This could affect the water-perching behavior at altered zones associated with the upper and lower Topopah Spring vitrophyres.

**Effect of Hydrothermal Alteration on Flow Paths**—Plug-flow reactor studies involving flow-through reaction of J-13 water with crushed tuff at 240°C (464°F) resulted in significant dissolution of alkali feldspar and cristobalite (DeLoach et al. 1997, p. 5). This experiment produced significantly different results from those of batch reactor studies at similar temperatures (i.e., predominantly dissolution instead of alteration). The two approaches span the range of conditions likely to exist in the host rock: stagnant vs. flowing water in the tuff matrix or along fractures. Dissolution and alteration behavior of the major minerals constituting the host rock are temperature-dependent and much slower at temperatures near the boiling point of water.

**Limitations of Available Kinetic Data**—The available kinetic data for dissolution of mineral phases that may be important to repository performance are limited reflecting the general sparseness of laboratory data on kinetic interactions involving rock. Different investigators have used various investigation and measurement strategies, and test results are sensitive to methodology (e.g., batch methods versus flow-through methods).

**Kinetics of Silica Dissolution and Precipitation**—Reaction rates for dissolution of quartz and silica polymorphs, and precipitation of amorphous silica, are key parameters in estimating the extent and magnitude of thermal-hydrologic-chemical coupled effects in the host rock. Dissolution will be expressed in heat pipe zones where refluxing water is at approximately 100°C (212°F). Mineral species like silica will then be deposited where the reflux water evaporates or boils. A boiling front will expand outward from each emplacement drift, but eventually reverse because of less heat generation. Depending on how fracture properties and connectivity are affected by precipitated minerals, seepage into the drift openings may become more or less likely during cooldown.

**Experimental Data for Silica Kinetics**—Dissolution rates are key parameters for estimating the extent and magnitude of thermal-hydrologic-chemical coupled effects in the host rock. In a classic study, the dissolution rate for silica polymorphs increased by 2 orders of magnitude for each 100 C° (180 F°) temperature increase, with a factor of 300 increase in the dissolution rate between 25° and 70°C (77° and 158°F) (Rimstidt and Barnes 1980, Figure 9). In addition, upon cooling a saturated silica solution, decreasing solubility caused supersaturation, while the rate constant for precipitation decreased, producing a maximum precipitation rate at a temperature 25 to 50 C° (45 to 90 F°) less than the saturation temperature. A more recent investigation of quartz dissolution kinetics at 70°C (158°F) (Knauss and Wolery 1988) produced dissolution rate data that were similar, at neutral to mildly alkaline pH, to rates predicted for quartz by the classic model.

**Interaction of Radionuclides with Alteration Products of Introduced Materials**—Surface

complexation reactions will be important for retardation of actinides, and possibly pertechnetate, in the host rock. Introduced materials, including structural steel, could be a source for potential high-affinity sorbents for radionuclides. If the sorbents are colloidal, the sorbed radionuclides may be transported. Limited test data for radionuclide sorption on these materials (e.g., goethite, clays, or silica polymorphs) are available, mainly for ambient temperature and simplified chemical systems (see, for example, Section 6.6 of *Engineered Barrier System: Physical and Chemical Environment Model* [CRWMS M&O 2000cg]).

**Matrix Diffusion Effects**—Diffusion of radionuclides into minerals and into the tuff matrix is an important temperature-dependent retardation mechanism. The tuff matrix has been shown to contain ubiquitous nanopores that support slow diffusion, plus a few connected paths through which diffusion is much faster but limited in overall effect. Effective diffusion coefficients have been estimated for uranium migration into polished wafers of Topopah Spring Tuff at ambient temperature (Wilder 1996, Section 7.4.1). Relative diffusivities of actinide and technetium species have been compared at 90°C (194°F) using “tuff cup” experiments (Hardin and Chesnut 1997, Section 2.10). Effective diffusion parameters for migration of strontium and cesium ions in clinoptilolite have been estimated (Hardin and Chesnut 1997, Section 2.6.5.1). These data generally indicate that the rate of diffusion in the tuff matrix and sorbent minerals is enhanced at elevated temperature.

#### 4.2.2.2.1.4 Other Properties

**Self-Potential**—Naturally occurring electrical potentials were observed in the Single Heater Test and in the Drift Scale Test and were large enough to be considered as a factor in waste package corrosion analyses, but the source of these potentials and the amount of current generated have not been investigated (Hardin and Chesnut 1997, Section 2.10).

**Microbial Activity**—Investigations have established that the natural microbes present in the unsaturated zone, plus those introduced by excava-

tion, include species that can survive exposure to desiccation and elevated temperature. Some species produce metabolic products that could be important in determining rates of corrosion and radionuclide transport in the near-field environment. There are few data that can be used to describe microbial activity at elevated temperatures (Hardin and Chesnut 1997, Section 2.10).

#### 4.2.2.2.2 Laboratory-Scale Process Investigations

Laboratory experiments have included comparison of vapor-phase and liquid-phase rewetting, fracture healing, fracture-matrix coupling with flow into heated tuff, fracture flow visualization, heat pipe formation, and rock-water interaction studies. These physical simulations of thermally coupled processes have advanced conceptual understanding and provided data for testing mathematical models.

**Rewetting Behavior**—Testing of wafers of welded tuff has indicated (Wilder 1996, Section 2.1.1) that water-retention hysteresis varies at elevated temperatures. Typical wetting/drying hysteresis at ambient temperature was nearly zero at 78°C (172°F) and reversed at 94°C (201°F). Rewetting behavior at elevated temperature is also summarized by Hardin and Chesnut (1997, Section 2.7.5). The effect is probably related to changes in surface tension and the rock-water-air contact angle at elevated temperatures. Hysteresis behavior is generally ignored, for computational expediency, in thermal-hydrologic models, and this appears to be defensible. The possible effects of negative hysteresis have not been considered.

**Vapor Resaturation**—Tuff matrix rewetting due to the presence of saturated water vapor (100 percent relative humidity) has a different result than rewetting by liquid at the same zero potential. Experimental data (Buscheck et al. 1992) show that rewetting of dry tuff in the presence of water vapor occurs much more slowly than does rewetting by imbibition of liquid water. This effect is incorporated in thermal-hydrologic models by adjusting the matric potential versus saturation relationship so that matrix saturation of 30 to 40 percent or greater corresponds to a relative humidity of nearly 100 percent. The vapor resatu-

ration effect strongly influences the timing of rewetting in the repository (Wilder 1996, Section 10.1) and tends to increase the relative humidity calculated at waste packages during cooldown.

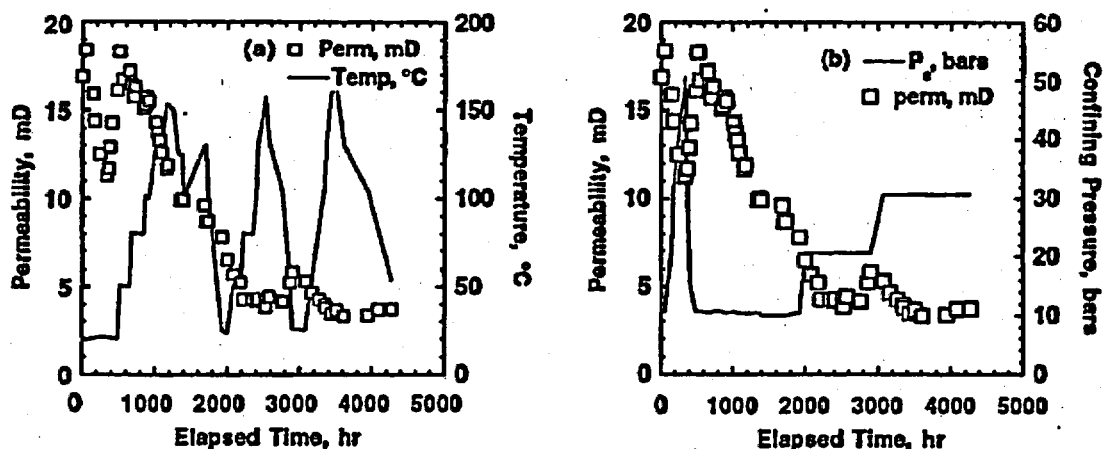
**Fracture Healing**—An understanding of fracture-permeability reduction has been developed, and observations reported in the literature can be explained by three mechanisms (CRWMS M&O 2000a, Section 3.6.3.3):

1. Dissolution of fracture asperities by flowing water and consequent aperture reduction under the influence of confining stress
2. Dissolution/precipitation reactions that clog porosity by redistributing silica or by creating alteration products with greater molar volume
3. Migration of heated pore water from the rock matrix, toward fractures, where the pressure is lower and evaporation or boiling occurs, clogging fractures or the matrix porosity.

Experiments have shown that flowing water or steam promotes permeability reduction, and the effect is strongest at temperatures greater than 90°C (194°F) (Hardin and Chesnut 1997, Section 3.10) (Figure 4-41). All these mechanisms can lead to changes in fracture porosity and permeability in the host rock where there is sufficient water.

**Fracture-Matrix Coupled-Flow Visualization**—Fracture flow studies in the laboratory (Hardin and Chesnut 1997, Section 3.3.1) have physically demonstrated fracture-matrix flow coupling in welded tuff, using x-ray imaging to visualize the flow (Figure 4-42). By varying the water injection pressure and the resulting flow velocity, the nonequilibrium nature of flow coupling was demonstrated. When the experiment was repeated with a thermal gradient, a different flow regime resulted, with localized precipitation of the solute tracer (Figure 4-42).

**Flow Channelization**—Visualization experiments (Hardin and Chesnut 1997, Section 3.4) showed, among other findings, that fracture transport in response to constant boundary conditions can be unsteady and produce intermittent rivulets that “snap off” and reform episodically. The authors related the average repetition rate for episodic flow



000500C\_ATP\_Z1642\_108.d

Figure 4-41. Permeability of a Single Fracture in a Core Sample of Topopah Spring Welded Tuff as a Function of Time and Exposure to Flowing Water

Temperature (left) and confining pressure (right) during the test series are plotted for comparison. Source: CRWMS M&O 2000a, Figure 3-101.

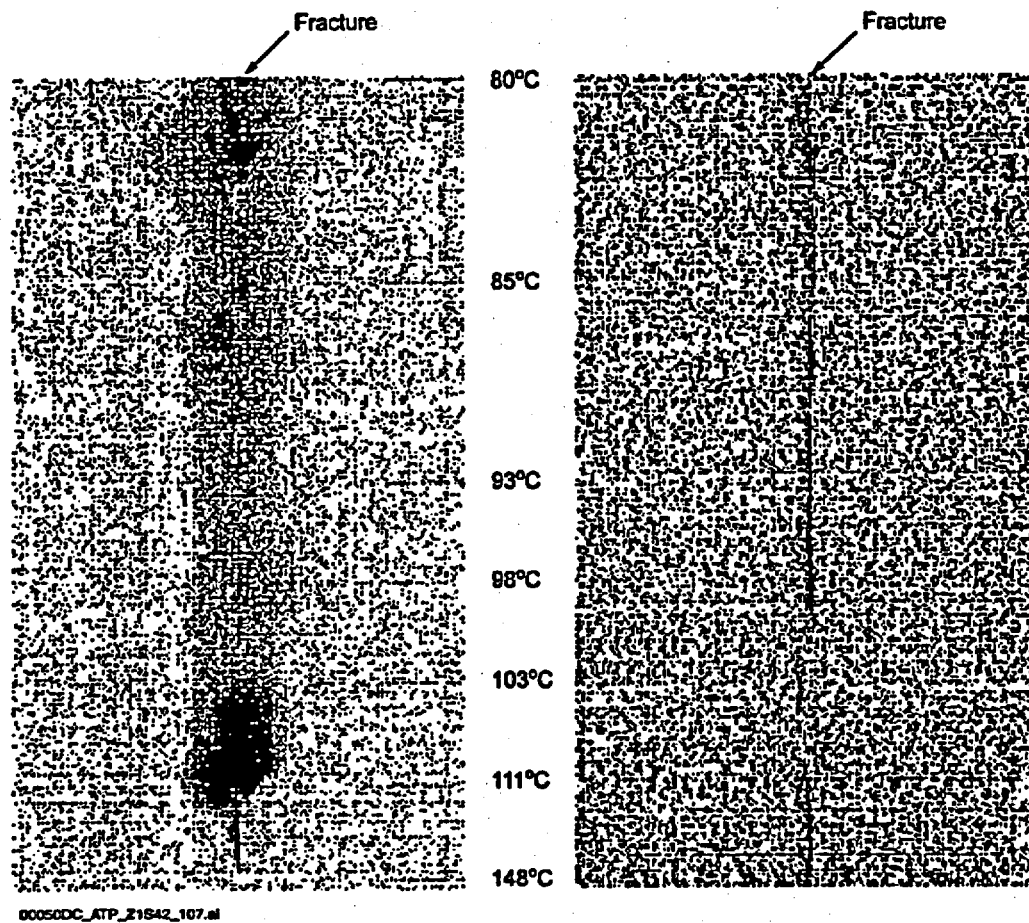


Figure 4-42. Difference X-Ray Radiography Images of 7.2 Hours (left) and 0.67 Hours (right) after Flow was Initiated

Left image 7.2 hours and right image 0.67 hours after flow was initiated. Thermal gradient is indicated between the figures. The difference between these two experiments was the height of the water column: 0.26 m (left) and 0.46 m (right), respectively. The difference in head was large enough to force flow through the boiling region in the right image. Source: CRWMS M&O 2000a, Figure 3-102.

with fracture aperture and wetting properties and the inclination of the models to gravity. These ambient-temperature experiments demonstrated that simple, simulated fractures can produce unsteady fracture flow in response to constant boundary conditions. Similar flow can be expected in the fractures of a heat pipe zone. These data have important implications for fracture-matrix interaction (i.e., there is limited contact time available for fracture-matrix interaction).

**Physical Models of Heat Pipes—Fracture thermal-hydrology visualization studies by Kneafsey and Pruess (1997) examined conditions**

(e.g., fracture saturation, temperature difference, and fracture dimensions) that support heat pipe development. Heat pipes were observed in parallel plate fractures containing obstacles, heat sources, and vents. Film flow as well as meniscal flow were observed to produce heat pipes (Figure 4-43). Unsteady rivulet-flow behavior, analogous to episodic fracture flow at ambient temperature, was observed (Hardin and Chesnut 1997, Section 3.5.1). Rapid evaporation events occurred when "islands" of fluid became superheated and suddenly boiled, constituting another mechanism for unsteady flow with the potential to rapidly disperse solute. A few of these observations were

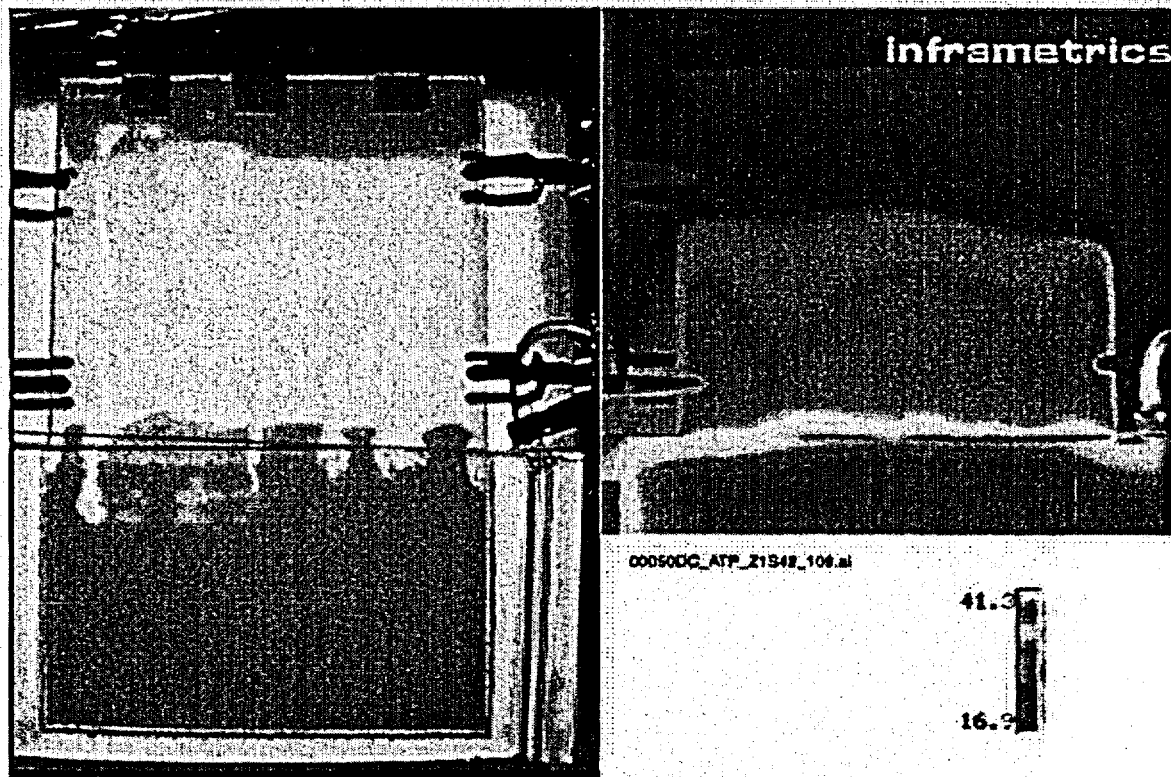


Figure 4-43. Pentane and Temperature Distribution Showing Heat Pipe  
Experiment 9:  $T_{\text{bath}} = 42.4^{\circ}\text{C}$ . Color scale indicates temperatures shown in the right image in  $^{\circ}\text{C}$ . The experiment was conducted by injecting a small amount of pentane liquid between panes of glass. The lower half of the apparatus (shown in the left image) was immersed in a temperature bath sufficiently warm to boil pentane. The upper part of the apparatus was warmed by migration and condensation of pentane vapor, as seen in the green region in the right image. This region, in which vapor moved up and liquid moved down, was a heat pipe zone. The temperature in this zone was maintained at nearly the boiling point of pentane by thermal reflux activity. Source: CRWMS M&O 2000a, Figure 3-104.

repeated with a half-cast model incorporating welded tuff as one fracture wall.

**Water-Rock Interaction**—Chemical analyses of effluent water from matrix flow and fracture flow experiments have indicated water-rock interaction. When J-13 water was flowed through an intact core sample, the concentration of most major anions and cations first increased, then approached influent concentrations (Hardin and Chesnut 1997, Section 3.6.2.2). Anions such as chloride and sulfate were leached in quantities that may be significant to the in-drift chemical environment. Other reported data for similar tests (Hardin and Chesnut 1997, Section 3.6.2.1) included chemical analyses of water that flowed through a healed, natural fracture at elevated temperatures.

**Fracture Flow in a Heated and Stressed Block**—Laboratory tests were conducted on 0.5-m (1.6-ft) scale blocks to monitor fracture flow and mechanical deformation properties under conditions that approximated the near-field environment expected in a repository at Yucca Mountain (Costantino et al. 1998). In this test, a rectangular block was bisected by an artificial fracture perpendicular to the fabric of the tuff. Water was supplied at a point source at the center of the fracture under various pressures. Both fluid flow and mechanical properties were found to be anisotropic and strongly correlated with the ash-flow fabric of the sample. Fluid flow measurements revealed that only minor imbibition of water occurred through the fracture surfaces, and that flow rates were independent of normal stress up to 14 MPa across the fracture, and at temperatures to  $140^{\circ}\text{C}$  ( $280^{\circ}\text{F}$ ). Flow through

the fracture occurred largely through uncorrelated porosity that intersected the fracture plane.

#### 4.2.2.2.3 Field-Scale Processes

This section briefly describes selected results from a number of field-scale tests and natural processes having some features in common with processes expected at Yucca Mountain. Emphasis is given to thermally driven coupled processes. The field-scale tests include those presented by Hardin and Chesnut (1997) and those presented in the *Near-Field Environment Process Model Report* (CRWMS M&O 2000a, Section 3.6.1). These tests are grouped into three groups: non-Yucca Mountain tests, Yucca Mountain tests, and natural analogues.

##### 4.2.2.2.3.1 Non-Yucca Mountain Tests

**Climax Spent Fuel Test** (Hardin and Chesnut 1997, Section 4.1.1; Wilder and Yow 1987)—Acoustic emissions responded to the rate of thermal energy production and may be useful for monitoring the stability of a repository. No significant changes in mineralogy or microfracturing occurred, as a result of heat or irradiation, near the electrical heaters or spent nuclear fuel canisters. Nitric acid formed by radiolysis of atmospheric nitrogen accelerated corrosion of the carbon steel emplacement hole liners. Corrosion was also observed in alloys such as stainless steel, Inconel 600, and super-Invar.

**Edgar Mine, Colorado School of Mines** (Hardin et al. 1982)—Heating of a fractured gneiss caused significant reductions in the loading and unloading moduli and reductions in the permeability of a test fracture. The largest permeability change occurred during excavation. Compressive loading reduced the permeability, but the permeability did not return to the preexcavation condition. Permeability reduction at elevated temperatures was smaller in magnitude than the effect of excavation.

**G-Tunnel Small-Diameter Heater Tests** (Zimmerman and Finley 1987)—For the first month of heating in the horizontal heater test in welded tuff, small amounts of water collected in the heater borehole and wetted a sensor located

immediately under the heater. Relative humidity approached saturation within hours after the start. Total pressures remained at ambient. Neutron-probe measurements of moisture content in the heated rock showed that significant changes occurred in the temperature range 70° to 120°C (158° to 248°F). Dewatering apparently began at temperatures less than boiling.

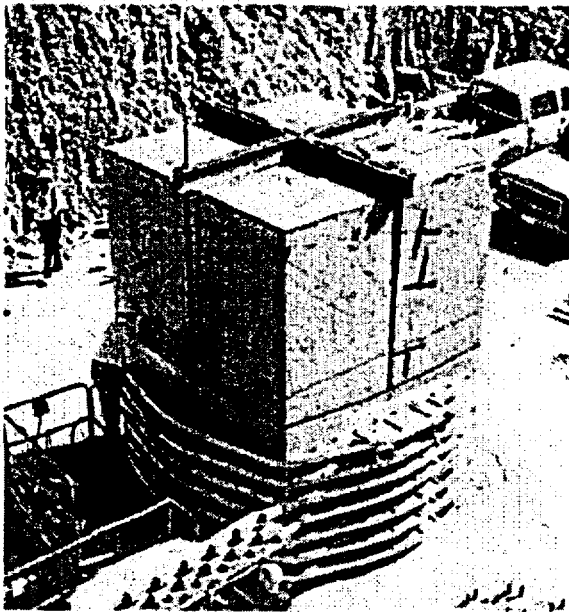
**G-Tunnel Heated Block Test** (Zimmerman et al. 1986)—A slight dependence of modulus on stress was indicated, but there was no significant temperature effect. Thermal expansion behavior of the heated block was well represented by measurements on intact rock samples. The largest changes in permeability of a test fracture were associated with excavation. Subsequent compressive loading and increased temperature lowered the apparent permeability of a test fracture. Saturation declined, in steps corresponding to successive cycles, from 60 to 80 percent and down to approximately 15 percent as a result of heating. Rehydration upon cooling was not significant on a time scale of weeks.

**G-Tunnel Prototype Engineered Barrier System Field Test** (Hardin and Chesnut 1997, Section 4.1.3; Ramirez et al. 1991; Lee and Ueng 1991)—The drying front penetrated most rapidly along fractures, and rewetting occurred most rapidly near fractures during the ramping down and cooling phases. Water vapor that condensed below the heater drained away from the boiling zone, and rock below the heater dried out more quickly than it did above the heater. During cooling, rewetting above the heater occurred slightly more quickly than it did below the heater. After heating and cooling back to ambient temperature, measured permeability in the heater borehole increased by 10 to 1,800 percent. The increase was greatest in intervals with the smaller values of preheating permeability. The boiling zone acted as an "umbrella," shielding rock below the heater from drainage of condensate generated above the heater.

**Underground Tests at Stripa, Sweden**—Fracture closure in response to heating was confirmed by observation of diminished water inflow to heater and instrument boreholes (Nelson et al. 1981).

#### 4.2.2.2.3.2 Yucca Mountain Tests

**Large Block Test**—The Large Block Test was described by Wilder et al. (1997). Figure 4-44 shows the Large Block Test during its construction, and a schematic of the test showing the instrument boreholes is given in Figure 4-45. One-dimensional heating geometry and moisture movement in the block were achieved as planned. Boiling of the pore water was indicated by temperatures measured near the heaters. Figure 4-46 shows the temperature measured at the TT1-14 and TT2-14 temperature sensors. Note that the boiling temperatures apparent from these two figures are slightly different, indicating heterogeneity in the pore pressure and/or concentration of chemicals in the pore water. Heat pipe activity was observed along the two vertical temperature holes in the block. Figure 4-47 illustrates one aspect of that heat pipe activity, whereby condensate drainage toward the heaters was most evident during the two thermal refluxing episodes of the Large Block Test. Figure 4-48 illustrates one of those refluxing episodes and the



000500C\_ATP\_Z1S42\_181.ai

Figure 4-44 Photograph of the Large Block Test Site

This photograph shows the Large Block Test during construction, with the block itself exposed as the exterior insulation is being constructed from the bottom to the top.

episodic water movement that followed its onset. Cooler liquid water apparently penetrated the heated interval, causing the temperature in a wider zone extending above and below the heaters to converge to near the boiling point. This was followed by episodic thermal refluxing, which caused the temperature to fluctuate. The redistribution of moisture was monitored by electrical resistivity tomography and neutron logging, as shown in Figure 4-49 and Figure 4-50, respectively. These refluxing events are believed to have been caused by rainstorms, which introduced water into the test.

Drying of the Large Block Test was also nearly one-dimensional. Neutron logging shows that localized dryout reached its maximum after about 334 days of heating. Subsequent heating extended the dryout zone but did not dry out the rock further. Mechanical displacement measurements on the block indicate that during the June 1997 thermal refluxing episode, a major near-horizontal fracture near the top of the block opened approximately 0.0094 to 0.011 cm (0.0037 to 0.0043 in.) at the northern and eastern sides, with a 0.0058 cm (0.0023 in.) shear displacement on the western side. Deformation data also indicate that during heating the block experienced horizontal expansion that increased linearly with height above the base. These deformations may have affected the hydrologic properties of the block. Simulation of the Large Block Test using the thermal-hydrology modeling code NUFT was used to capture the major characteristics of the measured temperatures of the Large Block Test (CRWMS M&O 2000a, Section 3.6.1.1) (see additional discussion below).

**Single Heater Test** (CRWMS M&O 2000a, Section 3.6.1.2)—The Single Heater Test was described in *Single Heater Test Final Report* (CRWMS M&O 1999m). A schematic of the Single Heater Test is shown in Figure 4-51. Measurement of mechanical displacements in the Single Heater Test showed expansion along the heater hole, with compressive movement at the beginning of the heating, followed by expansion perpendicular to the heater. These results were simulated by calculations using the continuum mechanical modeling code FLAC. Simulation using the thermal-hydrology modeling code

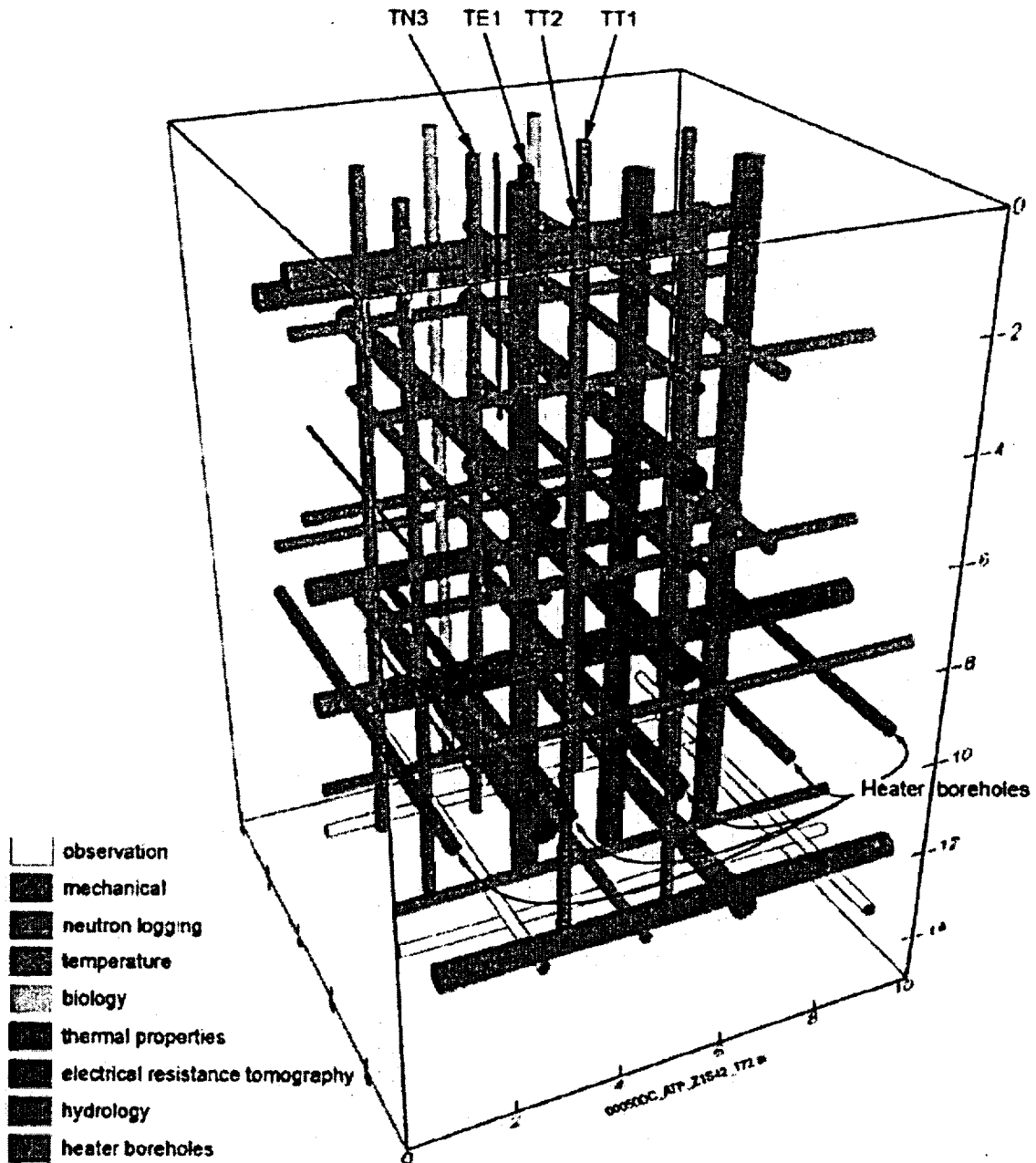


Figure 4-45. Schematic of the Large Block Test Instrument Boreholes. Borehole diameter is significantly exaggerated in the illustration. Only the heater boreholes and the instrument boreholes discussed in this section (i.e., TE1, TN3, TT1, and TT2) are labeled. Source: Modified from CRWMS M&O 2000a1, Figure 3-49.

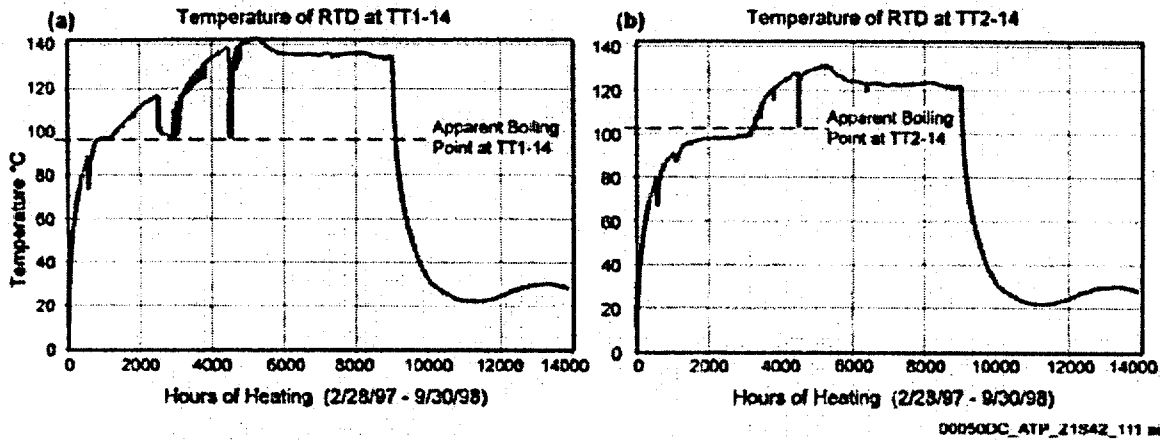
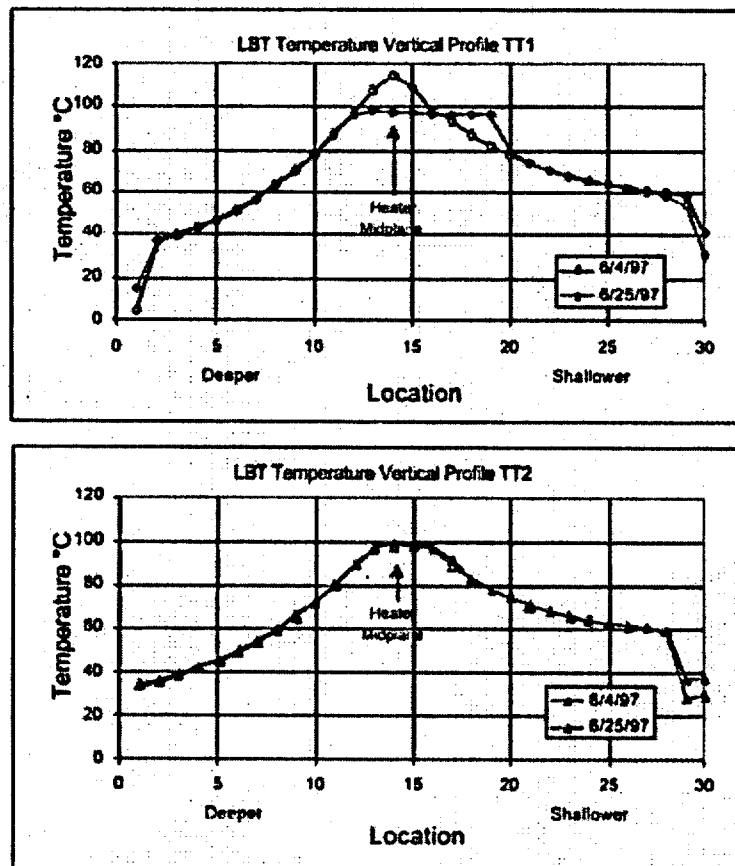


Figure 4-45 Temperatures Measured at (a) TT1-14 and (b) TT2-14 of the Large Block Test as a Function of Elapsed Time

See Figure 4-45 for the locations of Boreholes TT1 and TT2. RTD = resistance temperature detector. Source: CRWMS M&O 2000a, Figures 3-50 and 3-51.



00050DC\_ATP\_Z1542\_113 m

Figure 4-47. Vertical Temperature Profiles through the Large Block for June 4 and June 25, 1997, Showing Development of a Heat Pipe Zone

The heat pipe zone is indicated by the "flattening" of the temperature curve for TT1 on June 25, 1997, which shows boiling temperatures distributed over a greater length of the borehole. See Figure 4-45 for the locations of Boreholes TT1 and TT2. LBT = Large Block Test. Source: Modified from Hardin and Chesnut 1997, Figure 4-7.

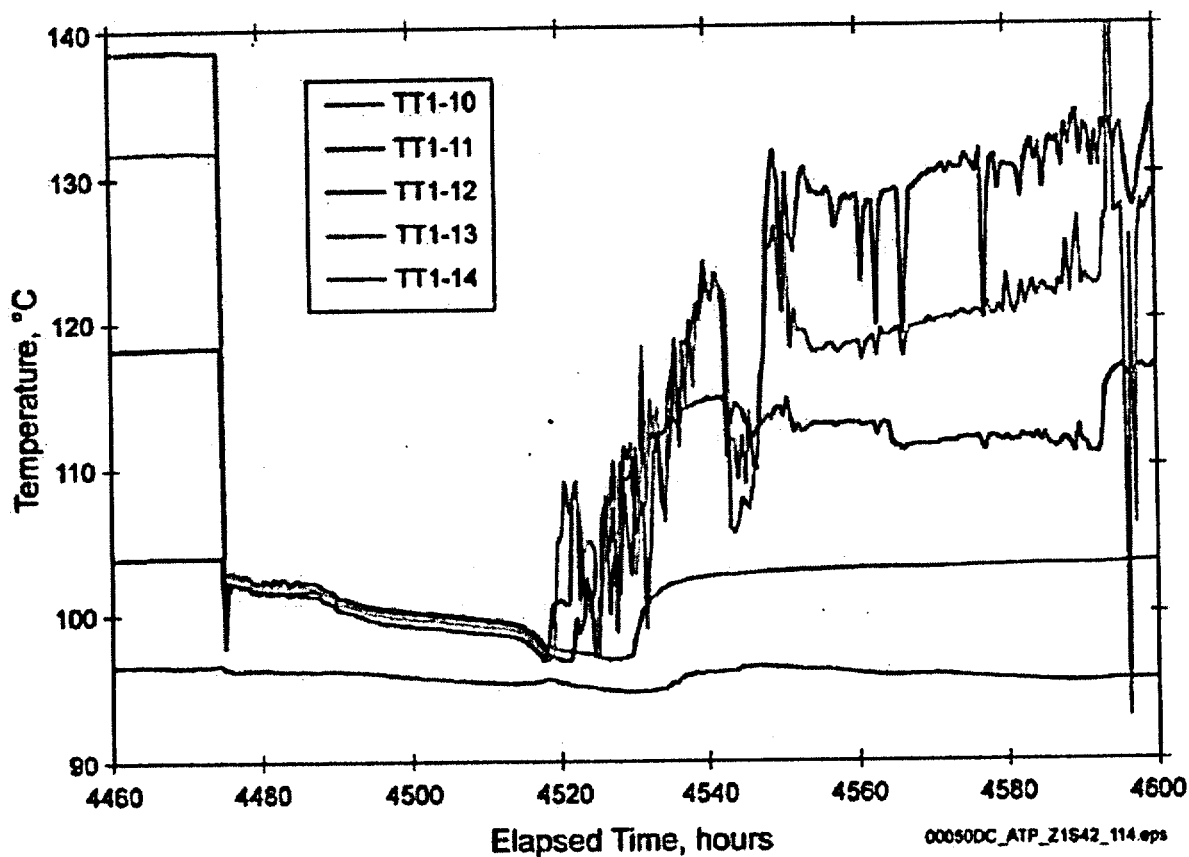
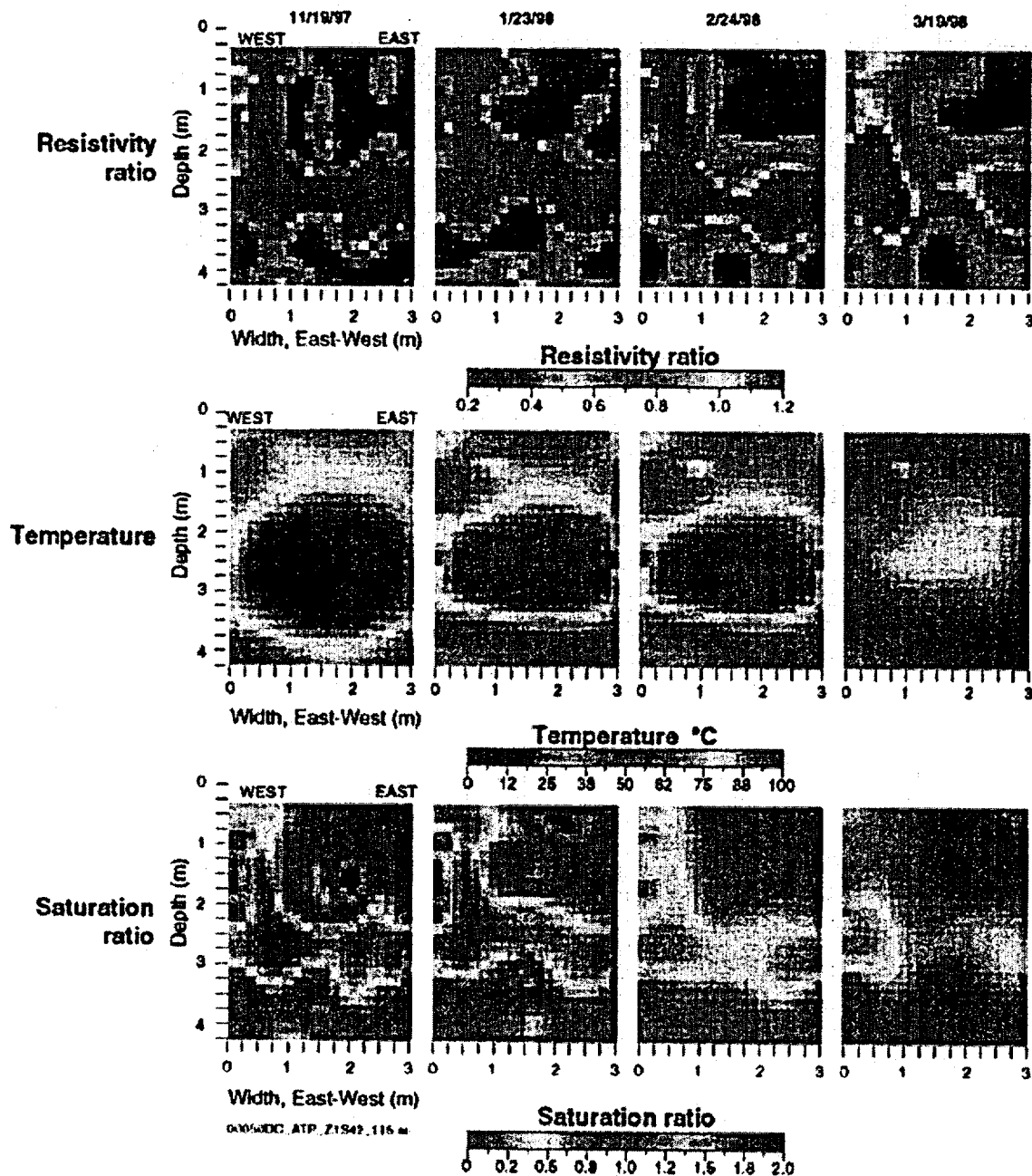


Figure 4-48. Temperatures at Several Resistance Temperature Detectors in TT1, Showing the Fluctuations Due to a Thermal-Hydrologic Event on September 2, 1997  
See Figure 4-45 for the location of Borehole TT1. The beginning of thermal reflux (heat pipe) activity is clearly indicated by the abrupt change in temperature at about 4.475 hours after the start of heating (i.e., September 2, 1997). Source: CRWMS M&O 2000a, Figure 3-55.

TOUGH2 was used to represent the evolution of measured temperatures. Modeling of this test provided important insights into the hydrologic properties and responses of the fractured tuff. The test confirmed that water moves away from heat sources as vapor, condenses where it is cooler, and tends to drain downward. Condensate was collected in a borehole, where it intersected a fracture drainage pathway. The apparent rapidity of drainage through fractures indicates that rock-water interaction between condensate and fracture surfaces is limited to relatively short residence times. The chemistry of sampled water was similar

to, but more dilute than, J-13 water. Solution equilibrium modeling indicates that the gas-phase carbon dioxide fugacity during the heated portion of the test was about two orders of magnitude greater than atmospheric.

**Drift Scale Test**—The Drift Scale Test, the largest thermal test conducted by the project to date, involves heating a drift that is approximately 48 m (157 ft) long. The rock mass being heated in this test will experience a thermal environment somewhat hotter than the repository design, with rock surface temperatures reaching a maximum of about



**Figure 4-49. Electrical Resistance Tomographs of an East-West Vertical Cross Section of the Large Block Test, Showing the Variation of the Moisture Distribution within the Imaging Plane**  
 The resistivity ratio and saturation ratio results for 2/24/98 and 3/19/98 are of lesser quality than the ratios for the previous dates because fewer measurements met the acceptance criteria for interpretive processing. This probably occurred because dryout of the block surface affected the electrical signal strength. The interpretation of the apparent rewetting in the central region of the block is, therefore, less reliable than the interpretation of dryout from the earlier results. Source: CRWMS M&O 2000a, Figure 3-56.

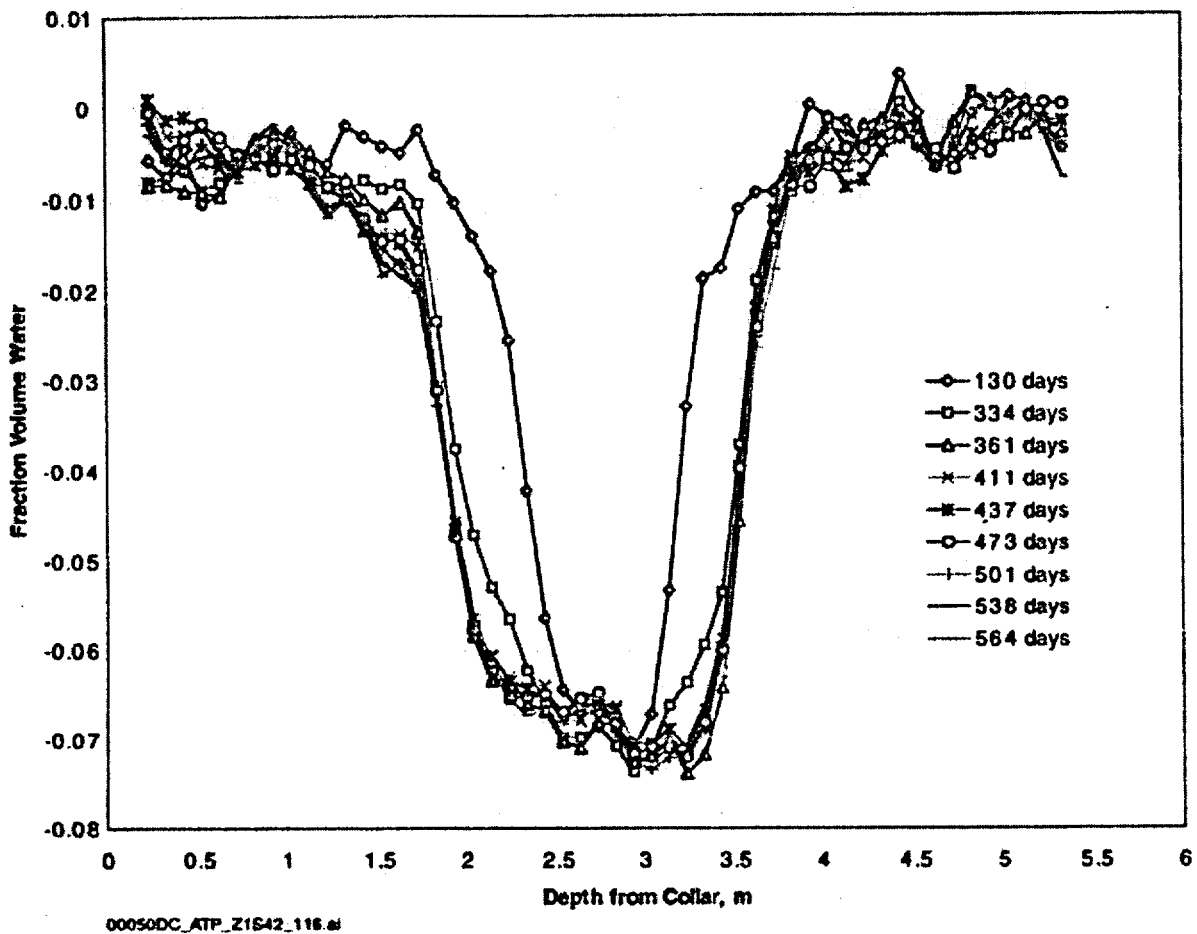


Figure 4-50. Difference Fraction Volume Water in Large Block Test Borehole TN3 as a Function of Depth, from 103 to 565 Days of Heating

See Figure 4-45 for the location of Borehole TN3. Difference fraction volume water is the change in volumetric water content. As shown by the measurements plotted here, decreased water content resulted from heating. Source: CRWMS M&O 2000a, Figure 3-58.

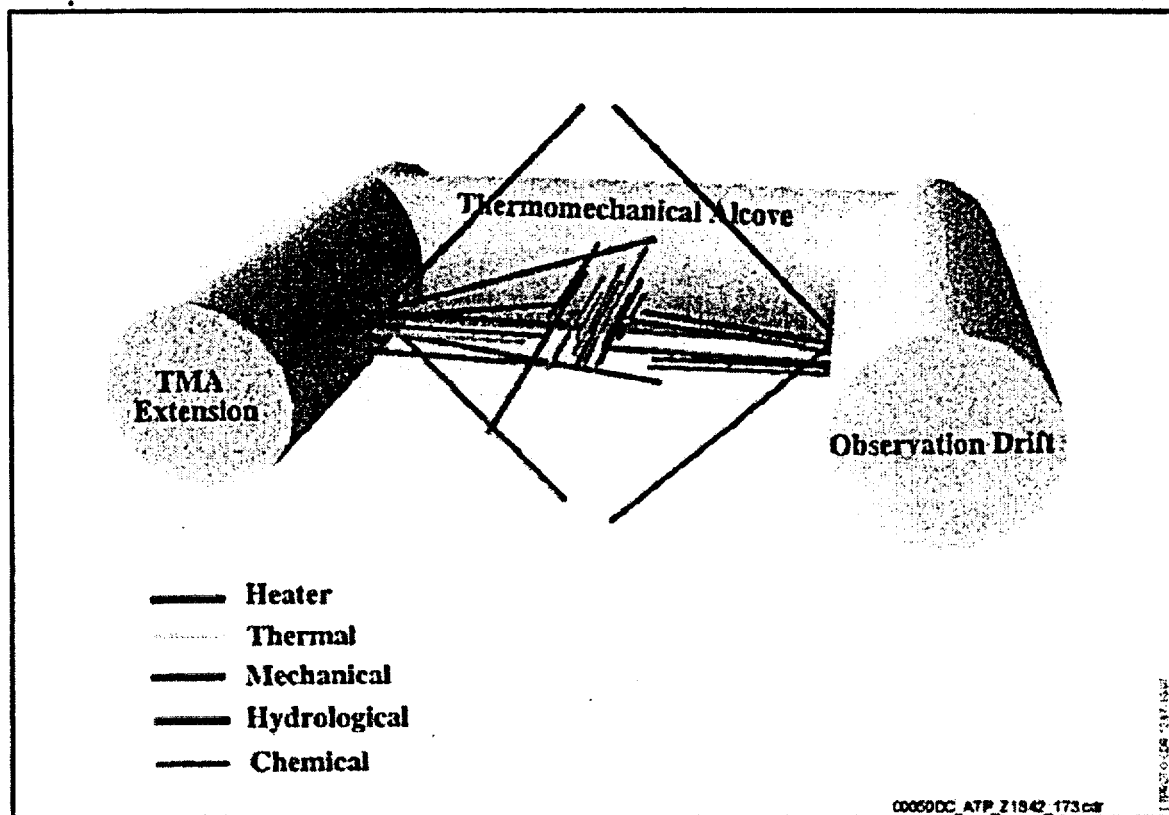
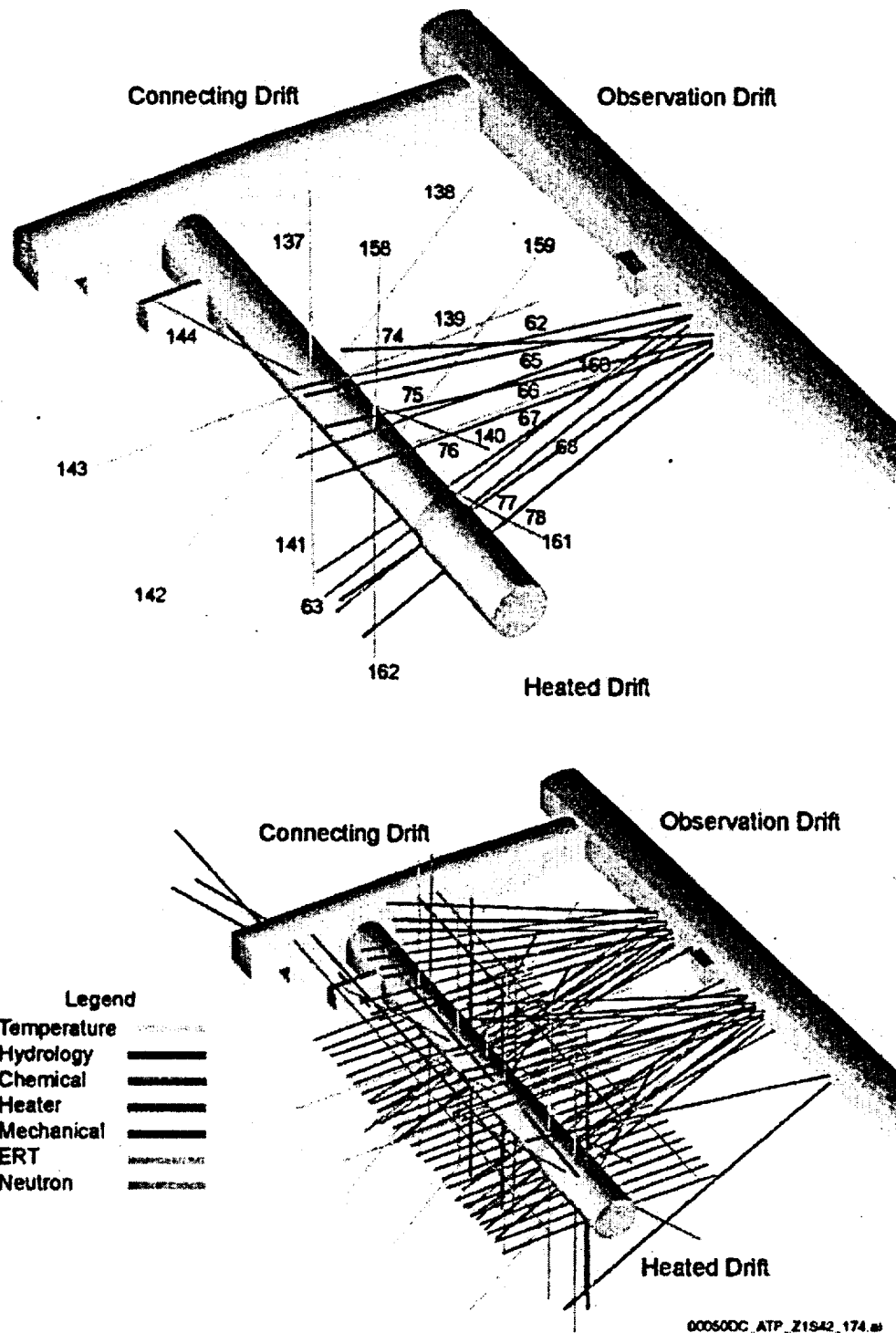


Figure 4-51. Schematic Illustration of the Single Heater Test in the Exploratory Studies Facility. Borehole diameter is significantly exaggerated in the illustration. The Single Heater Test is located near the Drift Scale Test (see Figure 2-78) at the Thermal Test Facility at Alcove 5. TMA = Thermomechanical Alcove. Source: CRWMS M&O 2000c, Figure 2.2-13; modified from CRWMS M&O 1999m, Figure 3-2 and Table 3-1.

200°C (390°F). This test is designed to produce above-boiling temperatures in about 10,000 m<sup>3</sup> of rock. The Drift Scale Test was described in *Near Field Environment Process Model Report* (CRWMS M&O 2000a1, Section 3.6.1.3). A schematic of the Drift Scale Test is shown in Figure 4-52. After 4 years of heating, the Drift Scale Test is to begin a 4-year cooling phase beginning in early 2002 (CRWMS M&O 2000ch Section 1; CRWMS M&O 2000a1, Section 3.6.1.3). The test results have provided and will continue to provide important insights into analyses of coupled processes, as described in this and following sections. Figure 4-53 shows the effect of boiling, as indicated by the temperature history at a single location. Boiling of pore water is represented by a

relatively flat region at about the boiling point of pore water in the temperature-time curves. Variations in heating rates are due to different distances between the sensors and the heaters. The duration of boiling is apparently affected by the availability of pore water to evaporate and the extent to which condensate flows back toward the heaters at each location.

Drying in regions near the heated drift and the wing heaters has been measured by electrical resistivity tomography, neutron logging, and ground-penetrating radar. Results obtained using these methods are shown in Figures 4-54, 4-55, and 4-56, respectively.



**Figure 4-52. Schematic Illustration of the Drift Scale Test in the Exploratory Studies Facility**  
Borehole diameter is significantly exaggerated in the illustration. For simplified identification of the boreholes discussed in this section, the top figure shows only those boreholes; the lower figure shows all the Drift Scale Test boreholes. See Figure 2-78 for the location of the Drift Scale Test at the Thermal Test Facility at Alcove 5. ERT = electrical resistance tomograph. Source: modified from CRWMS M&O 2000c, Figure 2.2-14, and CRWMS M&O 1998c, Table 4-1 and Figures 4-2 through 4-4.

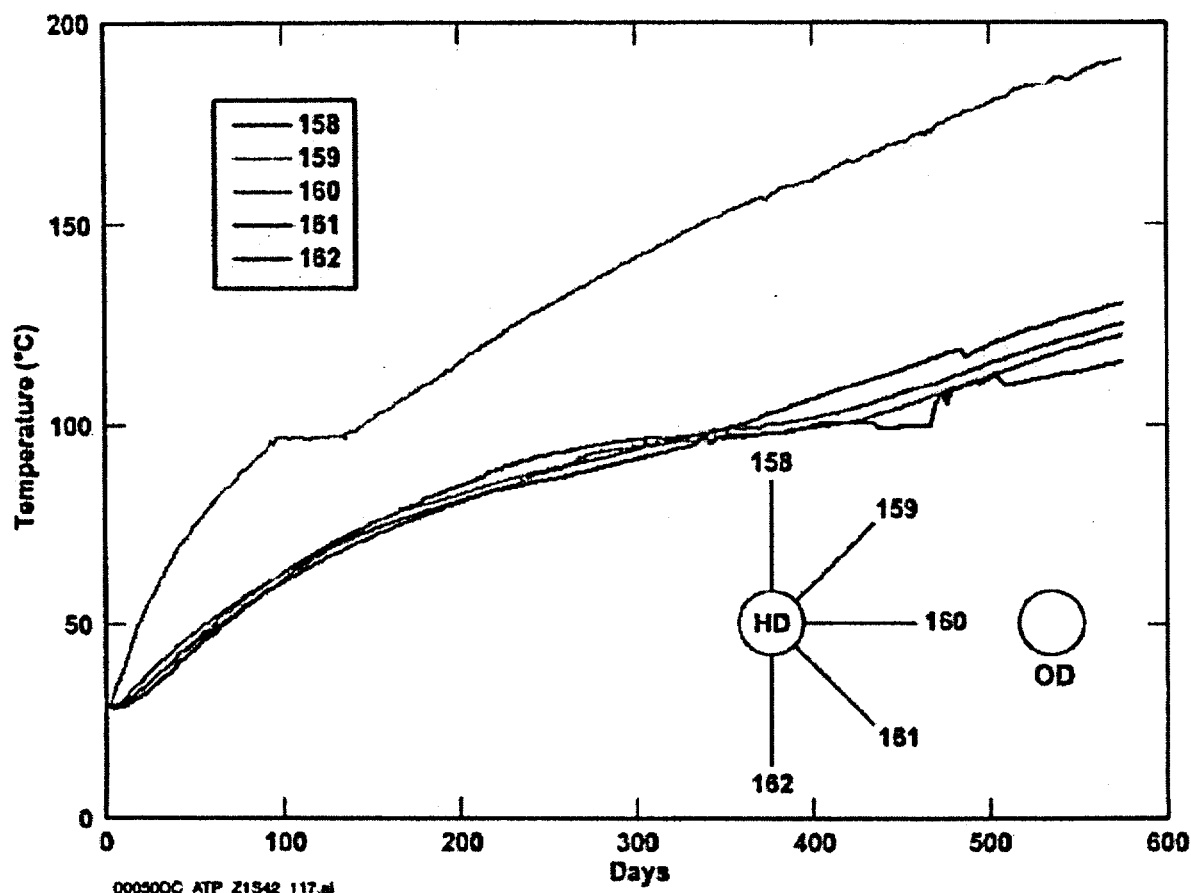


Figure 4-53. Temperature Measured at 2 m (6.6 ft) from the Collar of Boreholes 158 to 162 in the Drift Scale Test as a Function of Time, Showing the Spatial Variation of the Boiling of the Pore Water. Inset shows the location of the heated drift (HD) and Boreholes 158 to 162, where temperature measurements were taken, in relation to the observation drift (OD). See Figure 4-52 for the location of these boreholes. Source: CRWMS M&O 2000a1, Figure 3-79.

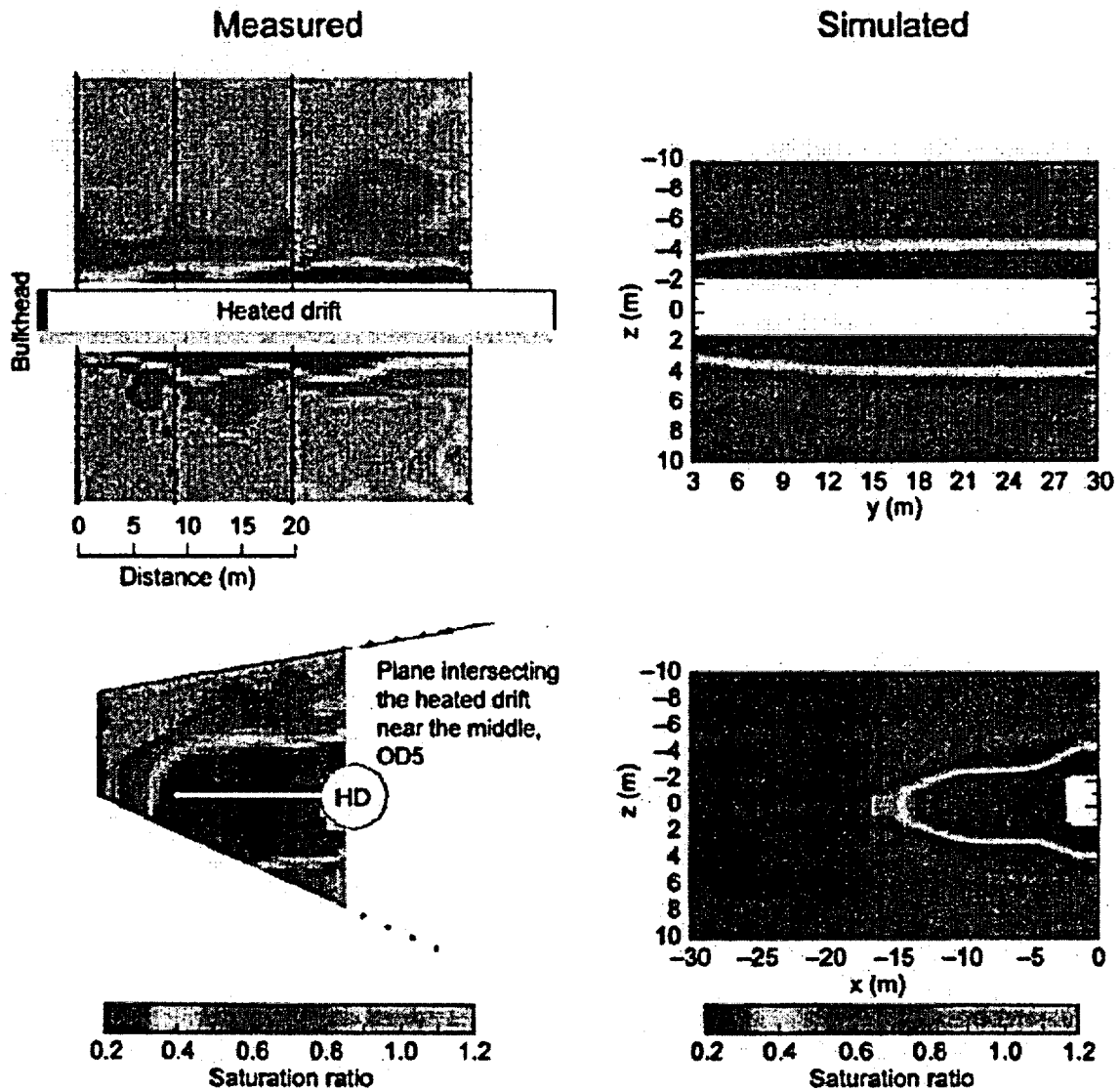
Heat pipe activity caused by thermal refluxing of condensate water has been observed at some temperature measurement locations, as shown in Figure 4-57.

*Thermal Tests Thermal-Hydrological Analyses/Model Report* (CRWMS M&O 2000ch) reports that both the TOUGH2 and NUFT modeling codes have predicted the temperature evolution and the dryout (liquid saturation) for the rock around the heated drift, consistently and with reasonable success. These thermal-hydrologic simulations support high confidence in using the thermal conductivity of rock mass to predict average temperature distributions. In addition, *Drift-Scale*

*Coupled Processes (DST and THC Seepage) Models* (BSC 2001o, Section 6.2.7) shows that the TOUGHREACT modeling code was able to produce reasonable predictions of the evolution of carbon dioxide and composition of collected water samples as affected by heating.

#### 4.2.2.2.3.3 Natural Analogues

Natural analogues related to the effects of heating on water movement and rock mass response were discussed by Hardin and Chesnut (1997) and in *Near Field Environment Process Model Report* (CRWMS M&O 2000a1, Section 3.6.2). Additional information on natural analogues is provided in



00050DC\_ATP\_21542\_118.ai

**Figure 4-54. Comparison of Distributions of Drift Scale Test Water Saturation Measured by Electrical Resistivity Tomography and Simulated by NUFT at 547 Days**

Measured saturation ratio was derived from electrical resistivity tomography after 558 days of heating. The top pair show the longitudinal cross section through the heated drift (HD) axis; the bottom pair show the transverse cross section at the plane of Boreholes 62 and 63. See Figure 4-52 for the location of these boreholes. OD = observation drift. Source: CRWMS M&O 2000ch, Figure 56.

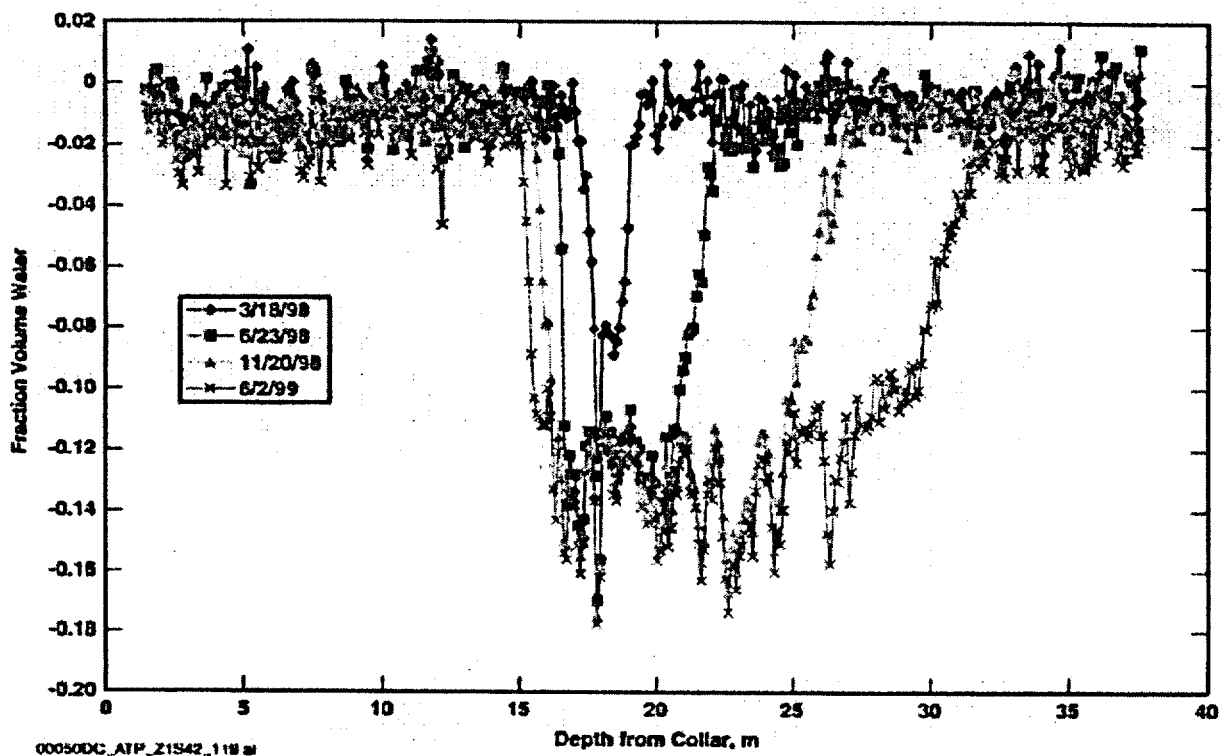


Figure 4-55. Difference Fraction Volume Water in Borehole 67 of the Drift Scale Test as a Function of Depth from Collar.

These measurements show the change in volumetric water content in the rock in comparison to ambient measurements taken in February 1998. See Figure 4-52 for the location of Borehole 67. Source: CRWMS M&O 2000a1, Figure 3-85.

*Natural Analogs for the Unsaturated Zone* (CRWMS M&O 2000bp) and in *Yucca Mountain Site Description* (CRWMS M&O 2000b, Section 13). Figure 4-58 illustrates selected examples of analogue information for heat induced and coupled processes. The information from geothermal studies can be used to demonstrate that the effects of decay heat on water movement can be evaluated. The available information ranges from core-scale and outcrop evaluations of fossil thermal-hydrologic-chemical coupled processes, understanding of efficient heat transfer mechanism with vapor-liquid counter flow phenomena (heat pipe), induced changes in operating geothermal fields, to dynamic or even disruptive processes with mechanical changes. Some of these phenomena are described in this section.

**Geothermal Fields**—Heat pipes in the repository will be short-lived, transient features compared to geothermal systems. Thermal-hydrologic characteristics of the repository host rock are similar to vapor-dominated geothermal systems (Hardin and Chesnut 1997; Simmons and Bodvarsson 1997), and similar modeling methods are applicable. Geothermal systems are apparently self-sealing, but conditions for development of a mineral cap above the emplacement drifts in a repository are different and less likely to result in sealing.

Table 4-15 lists selected geothermal systems evaluated in many countries. A photograph of a tuff core with indication of fracture sealing and opening from the Yellowstone geothermal field and a

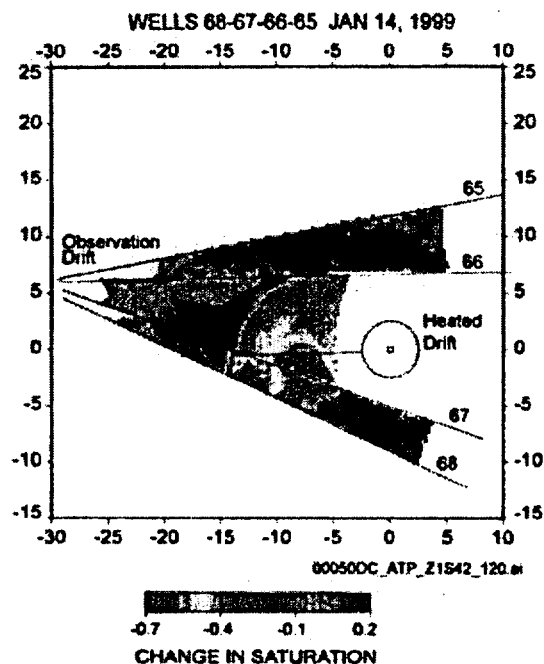


**Figure 4-56. Tomogram Showing Saturation Change from Preheat Ambient Values after Approximately 13 Months of Heating**  
Measurements taken January 14, 1999, from a cross-hole radar survey in the plane of Drift Scale Test Boreholes 64 to 68. See Figure 4-52 for the location of these boreholes. Source: CRWMS M&O 2000ch, Figure 33.

photograph of topographic deformations associated with the high-temperature geothermal field at Krafla, Iceland, are examples illustrated in Figure 4-58. Also included in Figure 4-58 is a photograph of the concrete-lined tunnel, subjected to heating by nuclear reactor processes, at the Krasnoyarsk-26 site in Russia. This is one example of the different kinds of site studies of anthropogenic (human-induced) analogues (CRWMS M&O 2000b, Section 13.3.6.3). Additional information on natural analogues and model calibration and validation for thermal-hydrologic applications is provided below in Section 4.2.2.3.6.

**The Geysers**—The Geysers is a geothermal field located about 65 km (45 miles) north of Santa Rosa, California. The pressure and temperature of

the vapor-dominated geothermal system at The Geysers plot along the liquid-vapor phase boundary for water, whereas the repository host rock will be free-draining, and the pressure of refluxing water will be constrained at about 1 atm (Hardin and Chesnut 1997, Section 4.3.1; Wilder 1996, Chapter 1). The maximum heat flux from the repository will be 50 to 70 times that calculated for The Geysers. Therefore, the calculated reflux magnitude at The Geysers, 4 to 5 mm/yr, does not imply that there will be no dryout zone above the repository. However, heat pipe activity is likely in the repository host rock and may be important for an extended period during cooldown.

**Taupo Volcanic Zone and Geothermal Fields, New Zealand**—The Taupo volcanic zone analogue was used to compare observed water composition and mineral occurrence in a geothermal well with chemical modeling calculations. In accordance with observations, major phases such as quartz and calcite were calculated to be at near-equilibrium. Other phases were predicted less accurately for several reasons: (1) uncertain kinetics, (2) completeness of thermodynamic data, (3) solid-solution effects (such as heterogeneity), and (4) the influence of boiling on precipitation (Glassley and Christenson 1992; Bruton et al. 1994). Differences were observed between precipitation rates measured in the laboratory and those measured in the field. Earlier studies by Rimstidt and Barnes (1980, p. 169) argued that precipitation rates for silica polymorphs are the same, but this approach does not explain certain natural analogue observations (Carroll et al. 1995, pp. 7 to 13).

Figure 4-58 includes an example of geothermal fields in New Zealand. At the Wairakei geothermal field illustrated in Figure 4-58, rates of amorphous silica precipitation measured in the field were 400 times faster than those obtained in the laboratory measurements. Similar rates are found at the Broadlands field. Both field data and model results indicate that stable mineral assemblages are sensitive to small differences in fluid chemistry, temperature, and pressure. Silica precipitation under potential repository conditions at Yucca Mountain could exhibit rate behavior somewhere in a range between the laboratory and field experiments (CRWMS M&O 2000b, Section 13.4.1.3).

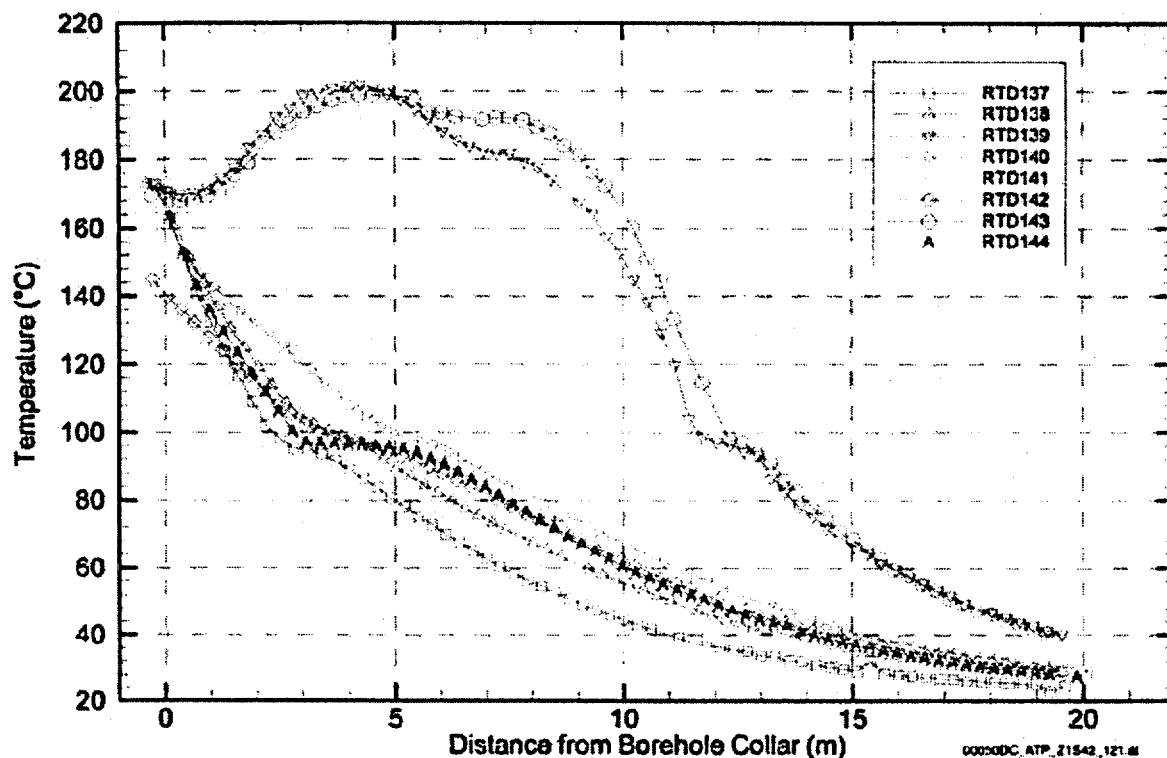


Figure 4-57. Measured Drift Scale Test Temperatures as a Function of Distance of Sensor Locations from Borehole Collars after 18 Months of Heating  
Data shown from resistance temperature detectors (RTDs) in Drift Scale Test Boreholes 137 to 144. See Figure 4-52 for the location of these boreholes. Source: CRWMS M&O 2000ch, Figure 21.

**Grants Ridge, New Mexico**—Despite the high-temperature basaltic intrusion, there was no evidence of pervasive hydrothermal circulation and alteration in the country rock that could have resulted from thermally driven liquid-phase convection (CRWMS M&O 2000al, Section 3.6.2.1).

**Yucca Mountain**—Conceptual models for mineral evolution at Yucca Mountain (Carey et al. 1997) suggest that the most likely mineralogical reactions caused by repository heating would include dissolution of volcanic glass and precipitation of clinoptilolite, clay, and opal-CT; dissolution and precipitation of silica polymorphs (cristobalite, opal-CT, tridymite, and quartz); alteration of feldspars to clays; and finally, reactions involving calcite and zeolites. Thermodynamic modeling results indicate that the stability of various zeolites

is a function of silica activity, temperature, aqueous sodium concentration, and the mineralogy of silica polymorphs. Increasing temperature or sodium concentration causes the alteration of zeolites to other phases. Kinetic data suggest that water saturation conditions are necessary for significant progress in these reactions. Therefore, under ambient conditions the reactions are likely to proceed more slowly in the Yucca Mountain unsaturated zone (excluding perched water zones) than below the water table. However, if prolonged boiling occurs in water-saturated tuffs, significant progress in such reactions can occur (CRWMS M&O 2000al, Section 3.6.2.2).

**Valles Caldera, New Mexico**—The contact between the Banco Bonito obsidian flow and underlying Battleship Rock tuff on the southwest rim of the caldera was studied by Krumhansl and

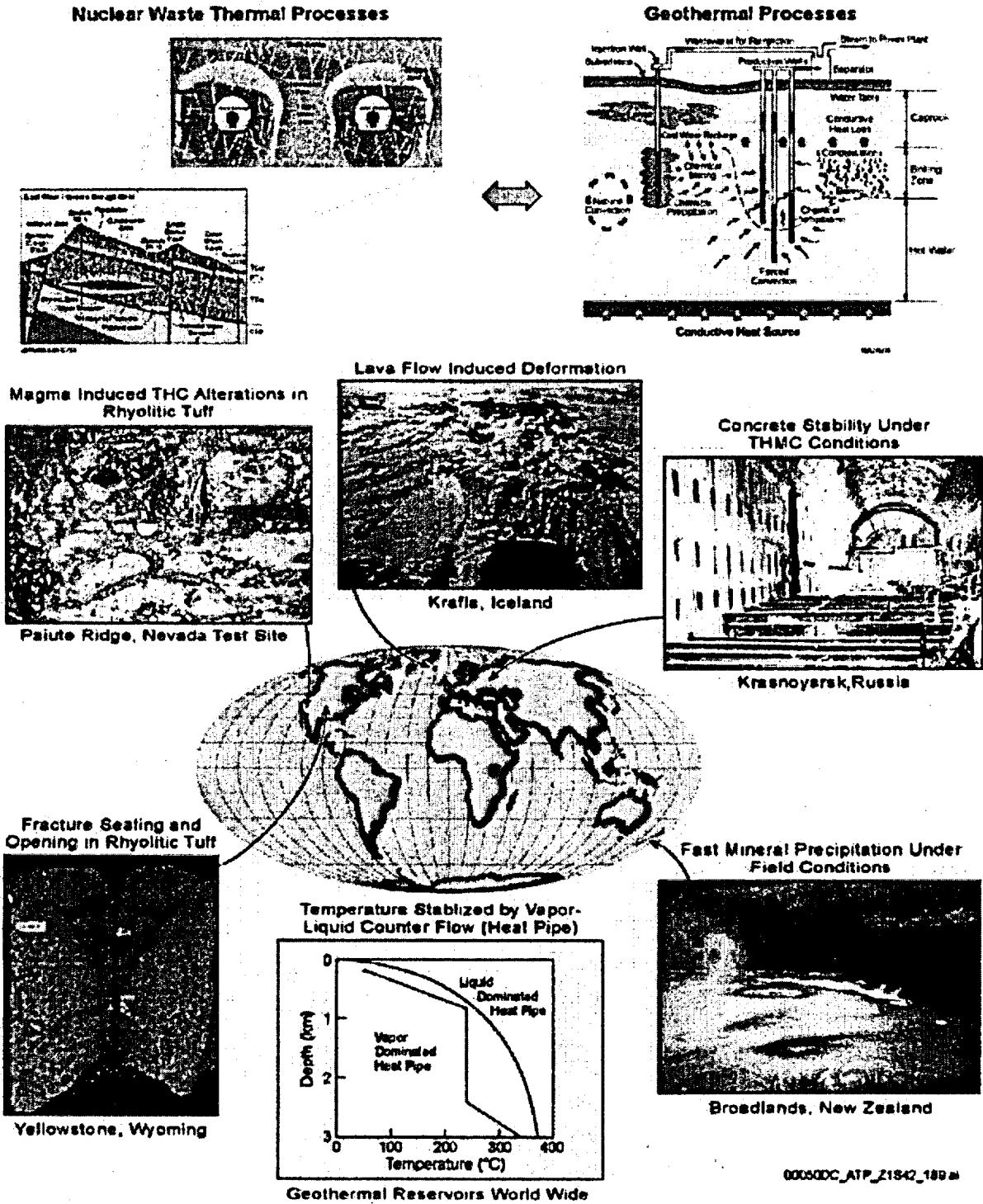


Figure 4-58. Analogue Studies for the Effects of Decay Heat and Thermal-Hydrologic-Chemical Coupled Processes

THC = thermal-hydrologic-chemical; THMC = thermal-hydrologic-mechanical-chemical.

Table 4-15. Geothermal Analogues for Process Evaluation

| Analogue  | Data and/or Process   |
|---|---|
| Yucca Mountain as self-analogue                           | Mineral reaction rates (Bish and Aronson 1993; Carey et al. 1997)   |
| Papoose Lake sill, Paiute Ridge, Nevada Test Site, Nevada | Magma intrusion, coupled thermal-hydrologic-chemical processes (Crowe, Seif et al. 1983; Matyskiela 1997; Lichtner et al. 1999)   |
| Dixie Valley, Nevada                                      | Geothermal, coupled thermal-hydrologic-chemical processes, preferential flow, fracture-matrix interaction, mineral precipitation and dissolution, mineral alteration  |
| Cerro Prieto, Mexico                                      | Geothermal, preferential flow, fracture network permeability, mineral reaction rates, self-sealing  |
| East Mesa, California                                     | Geothermal, preferential flow, mineral reaction rates   |
| Heber, California   | Geothermal (Lippmann and Bodvarsson 1985)   |
| Long Valley, California                                   | Geothermal, fracture-matrix interaction, mineral precipitation and dissolution  |
| The Geysers, California                                   | Geothermal, preferential flow, fracture network permeability, heat pipes, boiling and condensation, self-sealing  |
| Valles Caldera, New Mexico                                | Magma intrusion (Stockman et al. 1994, Sections 1.2 and 1.3)  |
| Grants Ridge, New Mexico                                  | Magma intrusion (VoldeGabriel et al. 1999)  |
| Fenton Hill, New Mexico                                   | Geothermal, mineral precipitation and dissolution   |
| Newberry Volcano, Oregon                                  | Geothermal (Sammel et al. 1988)   |
| Yellowstone, Wyoming                                      | Geothermal, fracture-matrix interaction, mineral alteration   |
| Eldora stock and Alamosa River stock, Colorado            | Deep hydrothermal intrusions (Brookins 1988; Wollenberg and Flexser 1986)   |
| Wairakei, New Zealand                                     | Geothermal, hydrologic properties, preferential flow, fracture network permeability, mineral precipitation and dissolution, mineral alteration, thermal-hydrologic-mechanical subsidence (Mercer and Faust 1979; Bruton et al. 1993; Glassley and Christenson 1992) |
| Broadlands, New Zealand                                   | Geothermal, mineral precipitation and dissolution, mineral alteration   |
| Kamojang, Indonesia                                       | Geothermal, hydrologic properties, fracture network permeability, heat pipes, boiling and condensation, self-sealing  |
| Bulalo, Philippines                                       | Geothermal, thermal-hydrologic-mechanical subsidence  |
| Tianjin, China  | Geothermal, hydrologic properties   |
| Sumikawa, Japan   | Geothermal, hydrologic properties, fracture network permeability  |
| Matsukawa, Japan  | Geothermal, fracture network permeability, heat pipes, boiling and condensation, self-sealing   |
| Larderello, Italy   | Geothermal, fracture network permeability, heat pipes, boiling and condensation, mineral precipitation and dissolution, self-sealing  |
| Krafla, Iceland   | Geothermal, fracture network permeability, thermal-hydrologic-mechanical subsidence (Bodvarsson, Benson et al. 1984)  |
| Reykjanes, Iceland  | Geothermal, self-sealing  |
| Olkaria, Kenya  | Geothermal, fracture network permeability, fracture-matrix interaction (Bodvarsson, Pruess et al. 1987)   |

Sources: Adapted from CRWMS M&O 2000c, Table 2.3-1; CRWMS M&O 2000bp, Table 6-13.

Stockman (1988) and Stockman et al. (1994). No evidence of hydrothermal alteration was noted, suggesting that the area was unsaturated at the time of contact. The effects of heating in this unsaturated environment appeared to have been slight and were limited to the tuff nearest the contact. The principal mineralogic change in tuff near the contact was the development of feldspar-silica

linings on voids in the pumiceous tuff matrix; no significant development of zeolites was found.

**Paiute Ridge, Nevada Test Site**—This characterization has been further developed as a distribution of “key blocks” that are defined by the fractures. An example of a sill observed on the outcrop of Paiute Ridge is illustrated in Figure 4-58.

Matyskiela's (1997) study of alteration surrounding one intrusion, the 50-m-wide (160-ft-wide) Papoose Lake sill, found alteration of glass shards to cristobalite and clinoptilolite within 60 m (200 ft) of the intrusion. He observed complete filling of pore spaces with silica at fracture-matrix interfaces, thus enhancing flow along fractures by inhibiting fracture-matrix interaction. Matyskiela (1997) estimated enhanced fracture flow to be as much as five times ambient conditions. A different kind of response to heating in the repository host rock (i.e., formation of a silica cap) was predicted by Nitao (reported in Hardin 1998, Section 5.6). Those simulations show that both the fractures and the adjacent matrix (at the fracture-matrix interface) could be plugged by dissolved solids transported into the boiling zone by fracture flow. This result depends on the total quantity of dissolved solids (e.g., silica) transported to the boiling zone and on the value of the fracture porosity (a smaller value of the fracture porosity makes plugging more likely). Another set of calculations reported in *Near Field Environment Process Model Report* (CRWMS M&O 2000a1, Section 3.2.5) indicates that only minor changes in fracture permeability would result from mineral precipitation during the thermal pulse, based on a larger estimate for fracture porosity and consideration of more complete ranges of minerals and chemical species.

Scoping analyses by Lichtner et al. (1999) provide additional perspective on the potential for plugging of porosity in the fractures and matrix. The approach considers the dissolved silica in the pore water present initially (before heating) in the tuff matrix. During heating, the matrix pore water will evaporate in a region proximal to the drift openings. If the silica contained in the pore water migrates to the fractures as evaporation occurs (ignoring evaporation in the matrix), then the degree of fracture plugging depends on the initial fracture porosity, as well as the particular silica polymorph produced. Based on this analysis, the fracture porosity used in Nitao's models (reported in Hardin 1998, Section 5.6) would be completely filled with amorphous silica for tsw33 and tsw34 units and about 50 percent filled in the tsw35 unit (CRWMS M&O 2000a1, Section 3.6.2.2).

#### 4.2.2.3 Process Model Development and Integration

Two models, namely the mountain-scale thermal-hydrologic model and multiscale thermal-hydrologic model, differing primarily in the spatial scales of interest, are used to model the effects of decay heat on water movement (CRWMS M&O 2000a1, Section 3.2.2). Both models solve heat and mass balance equations written for a fracture continuum interacting with a matrix continuum. The mountain-scale model evaluates changes in temperature and water movement at greater distance from the potential repository and is used for comparison to analogous geothermal sites. The multiscale thermal-hydrologic model provides detailed output describing temperature and moisture movement in the emplacement drifts and is abstracted directly for use in performance assessment. Both models rely on hydrogeologic properties developed for the unsaturated zone flow model.

Another model is used to calculate the drift-scale thermal-hydrologic-chemical processes and to address the change of chemistry of water entering drifts and the flow properties of the surrounding rock that control the seepage flux (CRWMS M&O 2000a1, Section 3.3). A final model is used to calculate the normal and shear displacement of distinct blocks of rock surrounding the heated emplacement drift and to address the consequent change in flow properties of the near-field rock that control the seepage flux (CRWMS M&O 2000a1, Section 3.5).

##### 4.2.2.3.1 Mountain-Scale Thermal-Hydrologic Model

The mountain-scale thermal-hydrologic model simulates the effects of repository heating on the unsaturated zone, including a representation of thermally driven processes occurring in regions far away from the potential repository (CRWMS M&O 2000ci, Section 7; CRWMS M&O 2000c, Section 3.12). This model is used to understand the mountain-scale effects of repository heating on water movement and to conclude that the mountain-scale effects of heating on water movement would not degrade the function of the host rock to

divert water from the engineered barriers and the waste form. Thus, the assessment of environmental conditions within the emplacement drifts can be focused on the drift-scale effects of heating on water movement.

The simulations provide predictions for thermally driven flow of liquid water and water vapor, and distributions for temperature and moisture in the unsaturated zone, for a period of 100,000 years. Approaches for simulation of the two-phase heat and mass transport processes in fractured systems are generally based on geothermal and petroleum reservoir simulation methods. Early multiphase modeling studies identified the importance of heat pipe effects in models that include heat sources. The heat pipe phenomenon is associated with boiling conditions and can occur if sufficient liquid is transported back toward the heat source (by gravity or capillarity) to sustain the boiling (Pruess, Wang et al. 1990, p. 1241). In the dryout zone, temperature variation is controlled by heat conduction and the thermal output of the heat source. In previous mountain-scale thermal-hydrology models, planar heat sources were used to represent closely spaced emplacement drifts, with the result that thick heat pipes and condensate zones were predicted (Buscheck and Nitao 1992). In the mountain-scale model, heat sources are more discrete, and drainage can occur through the pillars between emplacement drifts.

The mountain-scale thermal-hydrologic model uses the mathematical formulation employed in previous models (Pruess 1987, pp. 2 to 11; Pruess 1991, pp. 5 to 26). The approach involves volume averaging, the dual-permeability, continuum approach for modeling coupled fluid and heat flow, and fracture-matrix interaction (CRWMS M&O 2000br, Section 6.7; Liu et al. 1998). The model was developed from the unsaturated zone flow model and uses the mathematical formulations employed in the TOUGH2 code to describe flow under thermal-loading conditions (CRWMS M&O 2000c, Section 3.12.1). For the flow model, predictions of the three-dimensional ambient temperature distribution were calibrated against measured temperature profiles in boreholes (CRWMS M&O 2000ci, Section 6.1). The same thermal properties

are used in the mountain-scale thermal-hydrology model, and the ambient temperature distribution is used as the initial condition for modeling thermal effects.

Several numerical models were developed, including a three-dimensional mountain-scale model and two cross-sectional models. Plan views of the three-dimensional grid and the two-dimensional cross-sectional grids are shown in Figures 4-59 and 4-60, respectively. The three-dimensional model represents each emplacement drift and the adjacent pillars as one element, which does not resolve thermal-hydrologic processes in the vicinity of the potential repository. The two-dimensional models are more detailed and therefore allow drainage of condensed water through the pillars between drifts. The two-dimensional cross-sectional models are finer than the three-dimensional model but coarser than the drift-scale models described in Section 4.2.2.3 (see Figure 4-72 in Section 4.2.2.3.6 for a comparison). Accordingly, only the elements outside the drift elements are evaluated in the mountain-scale studies. More detailed discussion of these numerical models is presented in supporting documentation (CRWMS M&O 2000br, Section 6; CRWMS M&O 2000ci, Sections 6.2 and 6.3).

The mountain-scale thermal-hydrologic model uses input parameters that are fully consistent with the unsaturated zone flow model (CRWMS M&O 2000c, Section 3.6; CRWMS M&O 2000cj, Section 6), including hydrologic properties, the mean infiltration distribution, and the evolution of future climate states (CRWMS M&O 2000c, Section 3.5; USGS 2000b, Section 6). The simulations use an average initial thermal loading of 72.7 kW/acre (18.0 W/m<sup>2</sup>, equivalent to average areal mass loading of 60 MTHM per acre), based on a potential repository area of 1,050 acres (4,250,000 m<sup>2</sup>) (CRWMS M&O 2000c, Section 3.12.2.3; CRWMS M&O 2000ci, Section 5.1). The thermal load is scaled down by the natural decay curve over a total simulation period of 100,000 years. To account for ventilation, only 30 percent of this heat is used during the first 50 years (CRWMS M&O 2000c, Section 3.12; CRWMS M&O 2000ci, Sections 6.10 and 6.11). Figure 4-61

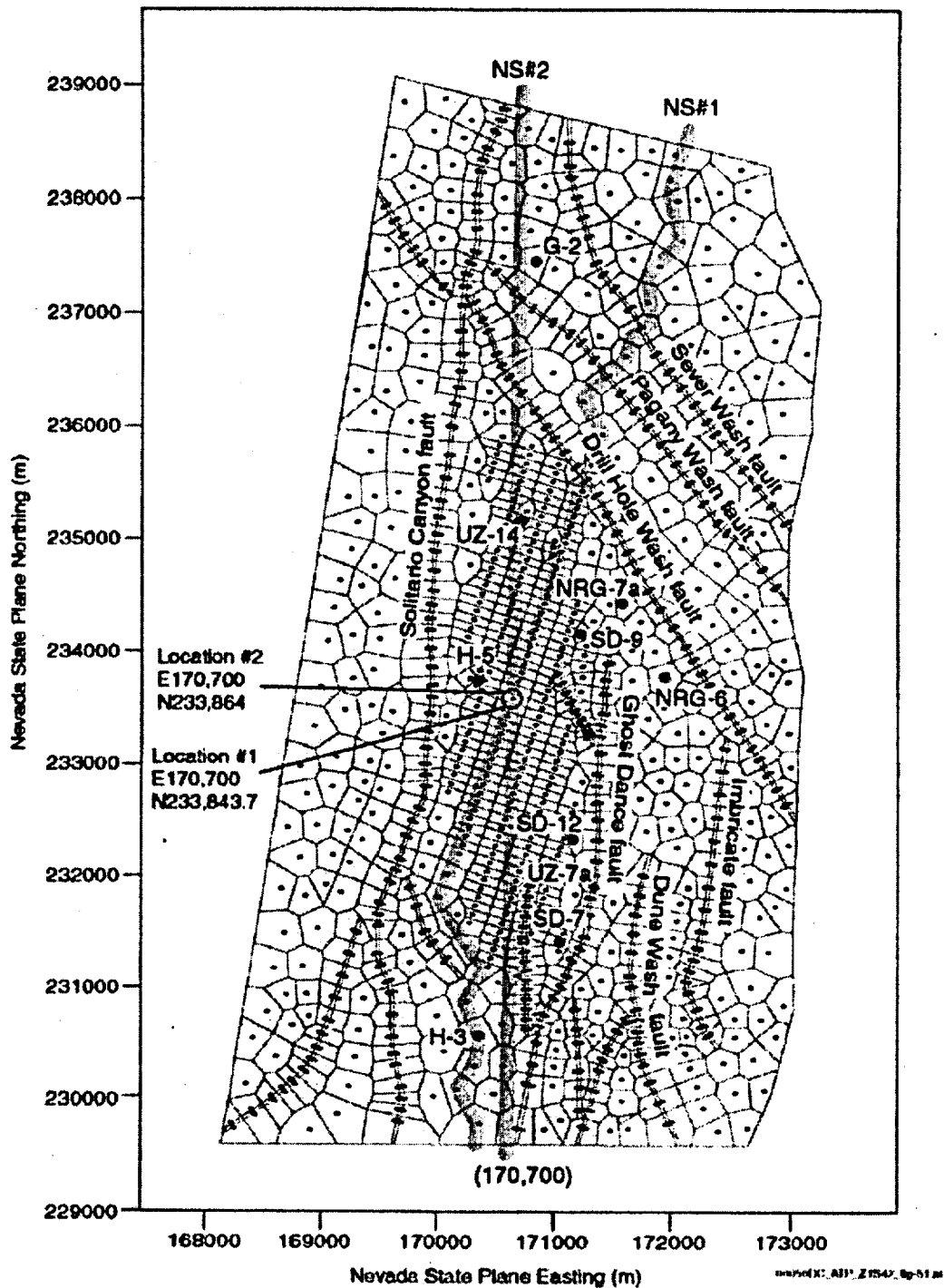


Figure 4-59. Plan View of the Three-Dimensional Grid Used for the Unsaturated Zone Flow Model and the Mountain-Scale Thermal-Hydrologic Model  
Locations #1 and #2 are used for detail plots. Large solid circles represent borehole locations; small circles represent grid column centers. The thick gray lines show the locations of cross sections NS#1 and NS#2. Source: CRWMS M&O 2000c, Figure 3.12-3.

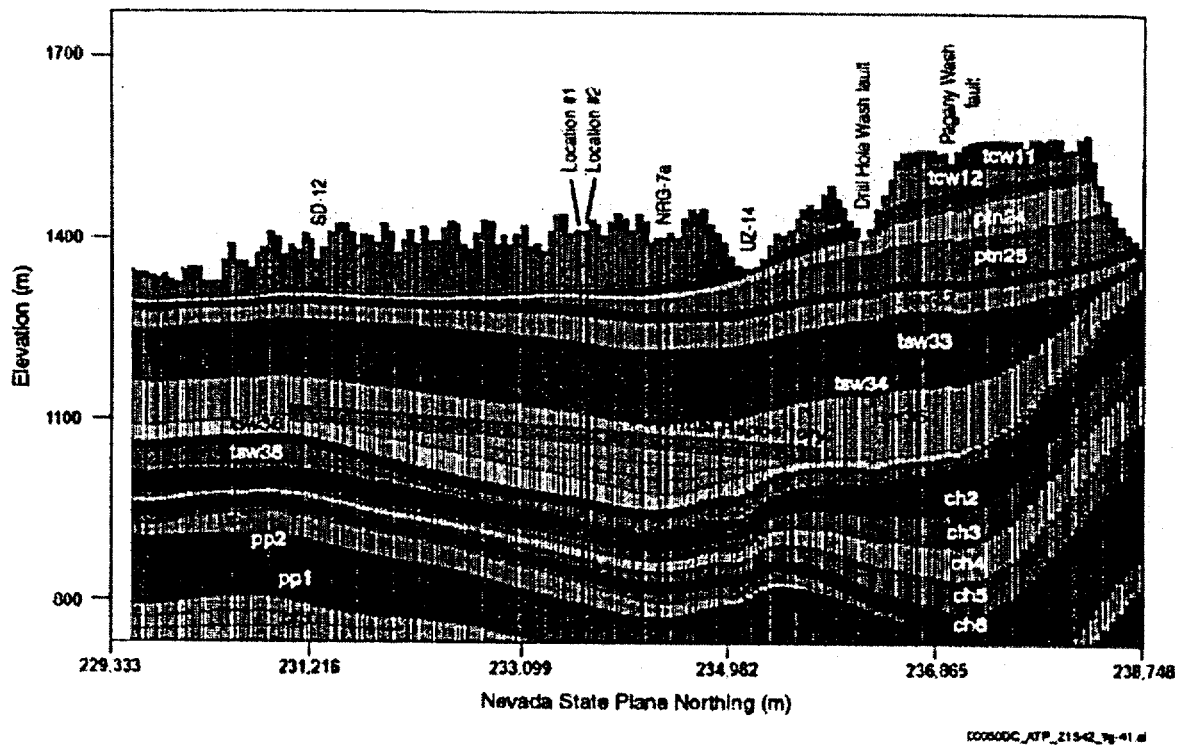


Figure 4-60. Lateral and Vertical Discretization at the NS#2 Cross Section Based on the Refined Numerical Grid

Plot shows the location of the potential repository and the unsaturated zone model layering. The figure has approximately 4½:1 vertical exaggeration. The location of this cross section is indicated on the plan view grid in Figure 4-59. Source: CRWMS M&O 2000c, Figure 3.12-4.

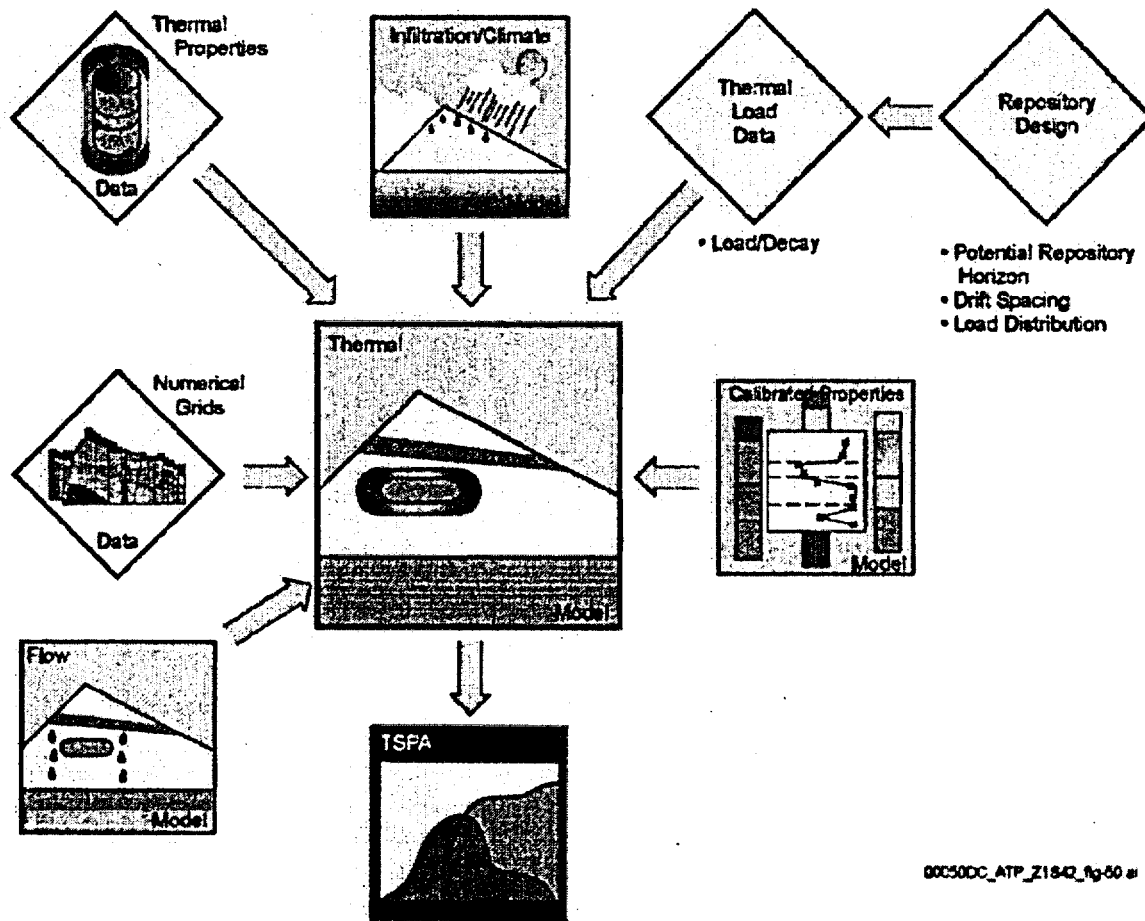
depicts the relationship between the thermal-hydrologic model, the input data, and supporting models.

Presented below are some of the results obtained for the two-dimensional cross-sectional models, focusing on the case with ventilation. Discussion of the other two-dimensional and three-dimensional cases is presented in supporting documentation (CRWMS M&O 2000ci, Sections 6.10 and 6.11). The results presented below are based on the higher-temperature operating mode.

**Temperature**—Figure 4-62 shows the distribution of temperature along cross section NS#2 after 1,000 years of thermal load (a) without ventilation and (b) with ventilation for the first 50 years. The variations in net infiltration across the model influence the evolution of temperature in both cases. Higher temperatures are predicted to occur in areas with less infiltration. The plots show dryout only in

the immediate vicinity of the potential repository. At a lateral distance of 100 m (330 ft) or more from the potential repository, no substantial increases in temperature are predicted, which suggests that buoyant, mountain-scale convection of the gas-phase, driven by production of water vapor and the heating of the gas-phase, will be important within or near the potential repository.

With or without ventilation, the predicted maximum temperatures at the centers of the pillars between emplacement drifts do not exceed boiling. Results also show that the long-term temperature response anywhere in the unsaturated zone is unaffected by 50 years of ventilation. Temperatures at the base of the PIn unit may increase to boiling conditions if the potential repository is not ventilated. Such temperatures could induce property changes in the PIn unit from mineral alteration, particularly in areas with less infiltration. With 50 years of ventilation as planned, temperatures in the



000500C\_ATP\_Z1842\_pg-50 #

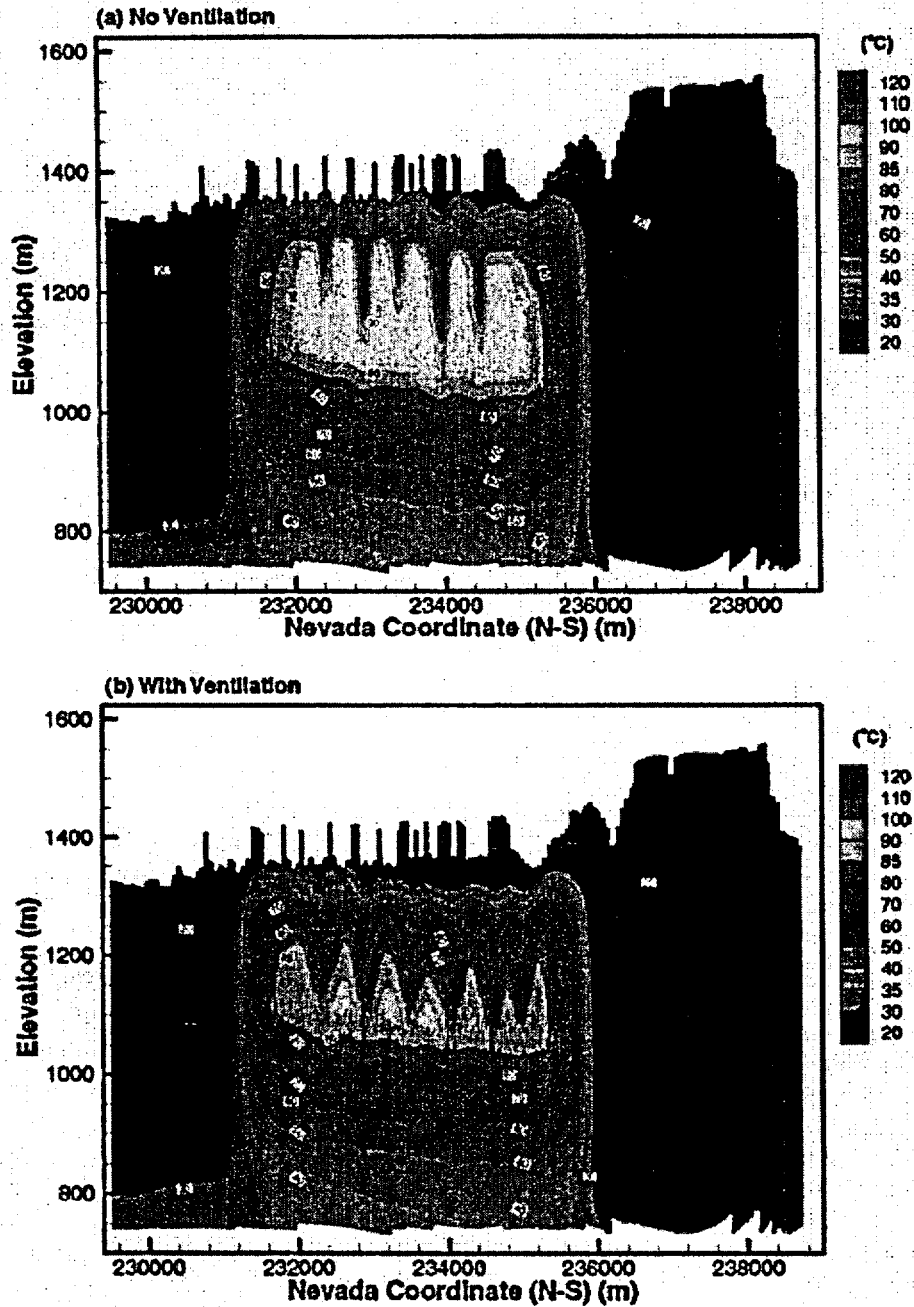
Figure 4-61. Schematic Showing Input Data and the Unsaturated Zone Models that Support the Development of the Thermal-Hydrologic Model  
Source: CRWMS M&O 2000c, Figure 3.12-2.

PTn unit are predicted to increase to an average of 40° to 45°C (104° to 113°F). At the top of the CHn unit, below the potential repository, the models predict a maximum temperature of 70° to 75°C (158° to 167°F), which will occur after 2,000 and 7,000 years, depending on location. This temperature range suggests minimal potential for thermally induced mineralogical degradation of zeolites in the CHn unit. At the water table, the models predict a maximum temperature of 65° to 70°C (149° to 158°F), compared to the average ambient temperature of 30°C (86°F).

**Saturation**—With or without ventilation, all fractures in the drifts at the potential repository horizon

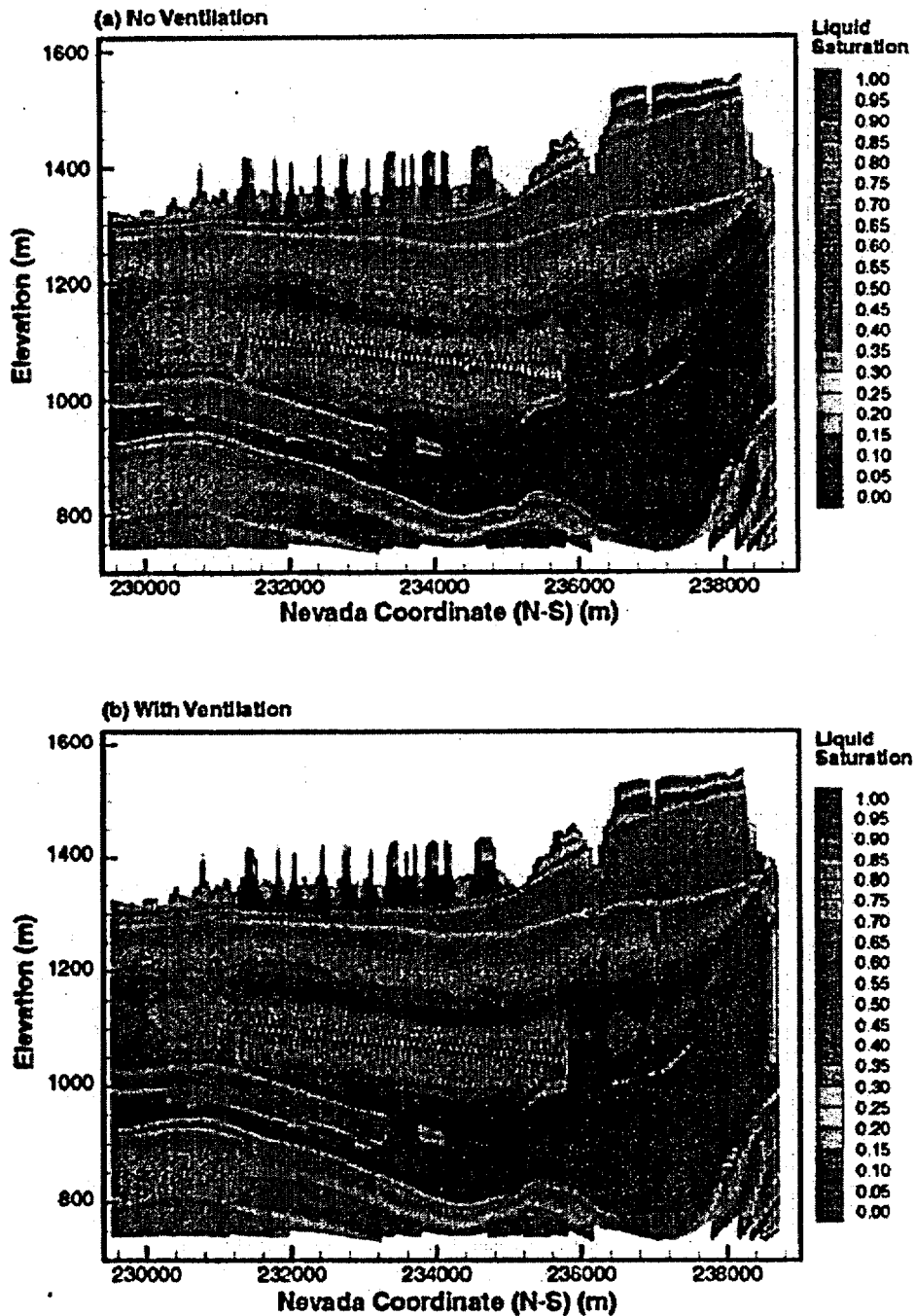
are completely dry within the first few years of thermal loading. The dryout zone expands and reaches a maximum thickness between 600 to 1,000 years after thermal loading (CRWMS M&O 2000c, Sections 3.10.5.2 and 3.12.3.2). Thereafter, the dryout zone contracts and persists for several thousand years (i.e., 1,000 to 3,000 years), well after cessation of above-boiling conditions (BSC 2001o, Section 6.3.5.1).

Figure 4-63 shows contour plots of matrix liquid saturation at 1,000 years (a) without ventilation and (b) with ventilation (CRWMS M&O 2000c, Section 3.12.3.2). The plots show large decreases in matrix liquid saturation only near the drifts.



0005000 ATP 21042 4p-42 m

Figure 4-52. Temperature Distribution at 1,000 Years along NS#2 Cross Section from the Mountain-Scale Thermal-Hydrologic Model  
 (a) No ventilation, removing 70 percent of heat during the 50-year preclosure period. The figure has approximately 8:1 vertical exaggeration. The lateral and vertical cross section used here is shown in Figure 4-60; the location of this cross section is indicated on the plan view grid in Figure 4-59. Source: CRWMS M&O 2000c, Figure 3.12-5.



00090DC\_ATP\_21542\_8p-43.epa

Figure 4-63. Matrix Liquid Saturation at 1,000 Years along NS#2 Cross Section from the Mountain-Scale Thermal-Hydrologic Model  
(a) No ventilation. (b) With ventilation, removing 70 percent of heat during the 50-year preclosure period. The figure has approximately 8:1 vertical exaggeration. The lateral and vertical cross section used here is shown in Figure 4-60, the location of this cross section is indicated on the plan view grid in Figure 4-59. Source: CRWMS M&O 2000c, Figure 3.12-8.

Liquid saturation at a lateral distance of more than 50 m (160 ft) away from the potential repository is predicted to remain at near-ambient conditions. A zone of decreased saturation extends to about 50 m (160 ft) above and below the emplacement drifts. After 5,000 years, the matrix liquid saturation is almost fully recovered to ambient conditions. The fracture and matrix liquid saturation within the pillars remain at near-ambient levels and are controlled primarily by changes in the climate state.

**Thermally Driven Changes in Percolation Flux**—Although ventilation lasts only 50 years, it results in changes in flux patterns that persist for hundreds of years. This is because the heat removed by ventilation will delay the onset of boiling conditions. The model results show that ventilation leads to lower thermally driven liquid and gas fluxes because the effective thermal load is only 30 percent of the total heat output during the early period in which the heat output of the emplaced waste is greatest. Figure 4-64 shows the calculated liquid flux through the potential repository horizon with ventilation.

With ventilation, thermal evolution is delayed because the temperature of the rock must rise to boiling conditions to maximize evaporation and heat pipe activity. At 100 years (50 years after closure), the liquid flux is 10 mm/yr (0.4 in./yr). However, flux recovers to more than 150 mm/yr (6 in./yr) at 500 years as a result of higher temperatures. Because of the decay in thermal output, and the increased infiltration imposed by climate change, the liquid flux in the fracture continuum at the potential repository horizon recovers to the ambient percolation flux after approximately 5,000 years. With ventilation, the fracture flux through the pillars between the drifts remains at or above ambient conditions and temperatures remain below boiling throughout the thermal pulse. Beyond approximately 500 years, the fracture liquid flux in the pillars returns to the ambient percolation levels, though these levels change in response to changes in climate state. The liquid saturation within the pillars remains at or above the ambient liquid satu-

ration because of vapor condensation and liquid flux being channeled through the pillars. This flux may be increased by condensate drainage for several hundred years.

Liquid flux through the pillars is the direct result of the counter-current vaporization and condensation (reflux) cycle associated with the development of heat pipe conditions predicted by the mountain-scale thermal-hydrologic model (CRWMS M&O 2000c, Section 3.12.3.3). At early times (less than 100 years), thermally induced liquid fluxes above the drift are up to two orders of magnitude larger than the ambient percolation flux. At around 1,000 years, model results show fracture liquid flux at several locations to be 20 to 50 mm/yr (0.8 to 2.0 in./yr). At around this time, mountain-scale thermal model results suggest liquid flux may occur downward into the drifts (CRWMS M&O 2000c, Section 3.12.3.3).

Mountain-scale thermal-hydrologic modeling shows that temperature increases at the base of the PTn unit and the top of the CHn unit are moderate (much less than boiling) and are not expected to cause mineralogical alteration of these units. Temperatures at a lateral distance of more than 100 m (330 ft) outside the potential repository are expected to remain near ambient conditions. The mountain-scale model predicts little impact on thermal-hydrologic conditions outside the potential repository layout, possibly because large-scale gas-phase buoyant convection promotes upward mass and heat transfer.

#### 4.2.2.3.2 Multiscale Thermal-Hydrologic Model

The multiscale thermal-hydrologic model (CRWMS M&O 2000cf) is used to model the effects of decay heat on water movement at the drift scale and within the emplacement drifts. Simulation results are used either directly or indirectly as input to other process models or abstractions for TSPA. The model uses the nonisothermal unsaturated-saturated flow and transport computer code to solve coupled heat and mass-transfer equations (CRWMS M&O 2000cf, Section 6).

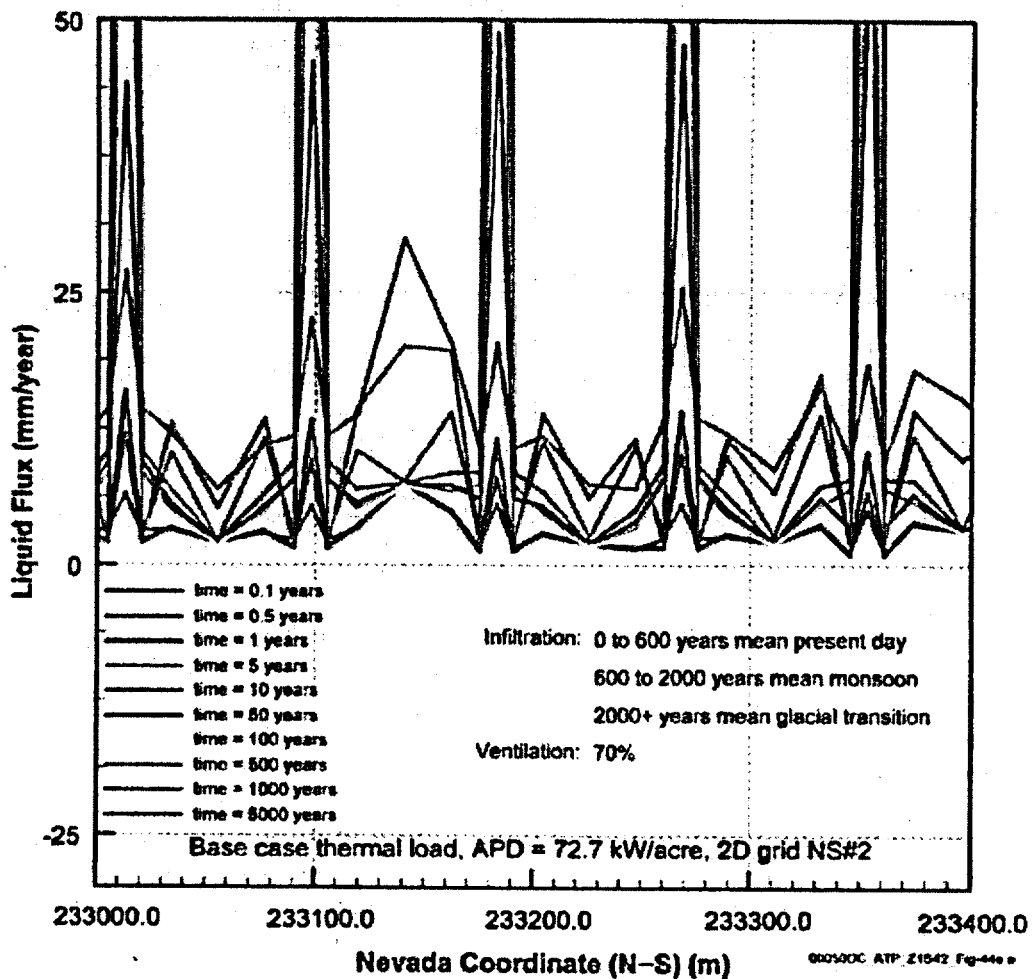


Figure 4-64. Fracture Liquid Flux along NS#2 Cross Section from the Mountain-Scale Thermal-Hydrologic Model

Case with ventilation, removing 70 percent of heat during the 50-year preclosure period. This figure shows the vertical liquid flux along a horizontal profile at the potential repository horizon in a two-dimensional model representing a north-south vertical cross section through the repository. The model is somewhat coarse, but it captures the behavior over multiple drifts at large scale. The maximum fluxes are located at the drifts in early time. This is caused by thermal reflux activity, whereby water evaporates, condenses above the drifts, and flows back down. As the thermal output declines with time, this type of activity diminishes. At later times (e.g., 1,000 years), the flux profile is much more uniform. At 10,000 years, the natural variability of flux conditions at Yucca Mountain, corresponding to predicted future climate conditions, controls the distribution of liquid flux. APD = areal power density. Source: based on CRWMS M&O 2000ci, Figure 69.

This model estimates thermal-hydrologic conditions within the emplacement drifts and the surrounding rock as functions of time, waste package type, and location in the potential repository. The multiscale thermal-hydrologic model is based on drift-scale thermal-hydrologic models of the types used to analyze the field-scale thermal tests, combined with three-dimensional thermal models that incorporate thermal interactions

between waste packages and mountain-scale heat transfer. The resulting multiscale model predicts fine-scale behavior within the emplacement drifts while including the effects of repository-scale heat transfer (CRWMS M&O 2000cf, Section 6).

The multiscale thermal-hydrologic model relates the results from different types of smaller models to capture the effects of key factors that can affect

thermal-hydrologic conditions in the emplacement drifts and surrounding rock (CRWMS M&O 2000cf, Section 6):

- Variability of the percolation flux on the scale of the potential repository
- Temporal variability of percolation flux (as influenced by climate change)
- Uncertainty in percolation flux (as represented by the mean, high, and low infiltration flux conditions described in Section 4.2.1.3.3)
- Variability in hydrologic properties (e.g., those properties which control fracture-matrix interaction and capillarity of fractures) on the scale of the potential repository
- Edge-cooling effect (cooling increases with proximity to the edge of the potential repository)
- Dimensions and properties of the engineered barrier system components, such as the drip shield and invert
- Waste-package-to-waste-package variability in heat generation rate
- Variability in overburden thickness on the scale of the potential repository
- Variability in rock thermal conductivity (emphasizing the host rock units) on the scale of the potential repository.

Table 4-16 lists the specific performance measures that are predicted using the multiscale thermal-hydrologic model. This model simulates time-varying thermodynamic conditions such as temperature, relative humidity, and evaporation and condensation. Thermal-hydrologic conditions are also predicted, such as liquid saturation, liquid-flux (percolation flux), gas-phase flux, and capillary pressure. These results are used in coupled models, in engineered barrier system performance analyses, and to describe the overall evolution of the thermodynamic and thermal-hydrologic environments in

the emplacement drifts and surrounding rock for TSPA (CRWMS M&O 2000a1, Sections 2.2.1 and 3.2; CRWMS M&O 2000cf, Sections 6.11 and 6.12).

The need for a multiscale modeling approach stems from the fact that the performance measures depend on thermal-hydrologic behavior within a few meters of the emplacement drifts and also on thermal and thermal-hydrologic behavior at the mountain scale. A single, explicit numerical model would require a large number (many millions) of grid blocks. The multiscale model is used to estimate results that would be obtained if such a single model were feasible. The multiscale thermal-hydrologic model also predicts the effects of different waste package types (e.g., different commercial spent nuclear fuel waste packages, codisposal of DOE high-level radioactive waste) on the various performance measures (CRWMS M&O 2000cf, Section 6.1).

The multiscale thermal-hydrologic model comprises four major models and includes multiple scales (mountain and drift), multiple dimensions (one-dimensional, two-dimensional, and three-dimensional), and different assumptions regarding the coupling of heat transfer to fluid flow (conduction-only and fully coupled thermal-hydrologic). The four types of models are (CRWMS M&O 2000cf, Section 6.1):

- Line-averaged-heat-source, drift-scale, thermal-hydrologic model
- Smeared-heat-source, mountain-scale, thermal-conduction model
- Smeared-heat-source, drift-scale, thermal-conduction model
- Discrete-heat-source, drift-scale thermal-conduction model.

It is useful to think of the line-averaged-heat-source, drift-scale, thermal-hydrologic model as the basis model. These two-dimensional drift-scale thermal-hydrologic models use hydrologic properties and other input data that are fully consistent with the unsaturated zone flow model. The models